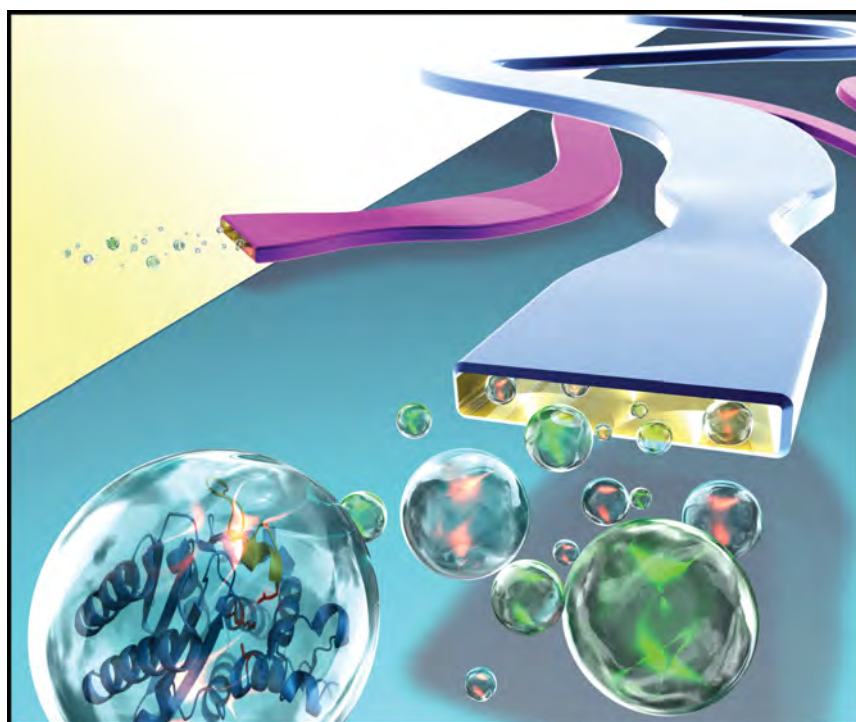


Thesis

Development, integration and application of modules for droplet-based microfluidics



Lucas Frenz

*Laboratoire de Biologie Chimique
Institut de Science et d'Ingénierie Supramoléculaire (ISIS)
Université de Strasbourg, France*

This dissertation is submitted for the degree of *Doctor of Philosophy*

October 2009

Thèse

Présentée à l'Université de Strasbourg
Ecole Doctorale des Sciences Chimiques

Pour obtenir le grade de

DOCTEUR DE L'UNIVERSITÉ DE STRASBOURG

Auteur (Author)

Lucas Frenz

Période de thèse (Thesis period)

1. Novembre 2006 – 31. Novembre 2009

Directeur de thèse (Supervisor)

Prof. A. D. Griffiths

*Institut de Science et d'Ingénierie Supramoléculaire (ISIS),
Université de Strasbourg, France*

Rapporteurs (Referees)

Prof. P. Dear

*MRC Laboratory of Molecular Biology,
Cambridge, United Kingdom*

Prof. W. Huck

*Department of Chemistry,
Cambridge University, United Kingdom*

Examineur (Examiner)

Prof. J. Haiech

*Ecole Supérieure de Biotechnologie de Strasbourg (ESBS)
Université de Strasbourg, France*

Abstract

Miniaturization has become a powerful concept influencing almost every scientific discipline. Initially revolutionizing electronics and computing, it has soon expanded into the microelectromechanical fields, where these systems are very successful especially for sensor technology and medical devices. It is therefore not surprising that expectations are similarly high for another field of miniaturization - microfluidics. Here, channels which are often thinner than a human hair are used to manipulate micro- to picoliter amounts of reagents to reduce costs and increase sensitivity and throughput by the novel mechanisms present within these size regimes. The highest level of sample and reaction miniaturization is probably achieved using single droplets. Especially when techniques evolved to form and manipulate these micro-reactors at speeds up to the kHz regime it became evident that droplet-based microfluidics might soon have a strong impact on fundamental and applied research such as combinatorial chemistry, material sciences, molecular biology, drug-screening and systems biology.

The work performed within this thesis touches the three main areas of investigation in droplet-based microfluidics: physics, material sciences and screening applications. Novel droplet manipulation modules and principles have been developed and characterized. One module enables to sort droplets by size differences rather than on its content. Another development concerns a novel droplet synchronization module which can create droplet pairs with an almost perfect accuracy. This system has been analyzed in detail and a general mathematical model has been evolved, describing and characterizing the module. Probably the most broadly useful module is the development of an on-chip incubation delay-line. Issues as back-pressure and dispersion of incubation times have been addressed and solutions have been developed, which are essential for a large number of biological assays. Due to these efforts it was therefore possible to integrate several droplet-based modules functionally with each other on a single chip, to create complex devices useful for the previously mentioned screening applications. Another development concerning screening applications is a dilution system enabling to ramp concentrations of a compound over several orders of magnitude, allowing to perform quantitative high-throughput screening with a statistical data quality far in excess of conventional methods. Additionally to these biological applications the microfluidic droplets have been used to synthesize superparamagnetic iron-oxide nano-particles in a very fast and controllable reaction.

Contents

Abstract	iii
List of Tables	ix
List of Figures	xi
Nomenclature	xv
1. Introduction	1
1.1. Overview (French)	2
1.2. Overview (English)	8
1.3. Technology	14
1.3.1. Device fabrication	14
1.3.2. Fluorescent optical setup	16
1.4. Fluidics	17
1.4.1. Navier-Stokes-equations	17
1.4.2. Viscosity	17
1.4.3. Laminar slit flow and fluidic resistance	18
1.4.4. Surface tension	20
1.4.5. Contact angle	21
1.4.6. Capillary pressure	22
1.5. Droplet-based microfluidics and its modules	23
1.5.1. Droplet creation	24
1.5.2. Mixing within droplets	25
1.5.3. Splitting of droplets	27
1.5.4. Droplet fusion	28
1.5.5. Droplet sorting	30
1.6. Applications of compartmentalization in emulsions	31
1.6.1. Emulsion PCR (ePCR)	31
1.6.2. Next generation sequencing methods	33
1.6.3. Directed evolution	34
1.6.4. Diagnostics	39
1.6.5. Proteomics and protein-protein interactions	40

2. Size dependent sorting of droplets	43
2.1. Introduction	44
2.2. Theory	45
2.3. Experiments	48
2.4. Chapter summary and conclusion	49
3. Droplet-based microreactors for the synthesis of magnetic iron oxide nanoparticles	51
3.1. Introduction	52
3.2. Synchronization of droplet production	53
3.3. Synthesis of iron oxide nanoparticles	55
3.4. Characterization of the synthesized nanoparticles	56
3.5. Materials and methods	56
3.6. Chapter summary, conclusion and outlook	57
4. Microfluidic production of droplet pairs	59
4.1. Introduction	60
4.2. Results and discussion	60
4.3. Chapter summary, conclusion and outlook	66
4.4. Materials and methods	66
5. Reliable microfluidic on-chip incubation of droplets in delay-lines	69
5.1. Introduction	70
5.2. Solutions to avoid pressure problems	70
5.3. Dispersion of incubation times	72
5.4. Reducing the dispersion of incubation times	74
5.4.1. Redistribution of droplets as a strategy to reduce dispersion	74
5.4.2. Multiple parallel channels as a strategy to reduce dispersion	76
5.5. Measurement of enzyme kinetics	78
5.6. Materials and methods	80
5.6.1. Cloning, expression and purification of β -lactamase	80
5.7. Chapter summary, conclusion and outlook	81
6. Integration and directed evolution	83
6.1. Introduction	84
6.2. Microfluidic improvements and device integration	84
6.2.1. Synchronization of reinjected emulsion	84
6.2.2. Improvements and recommendations for the sorting device	87
6.2.3. Device integration	89
6.3. Preliminary screening and enrichment results	91
6.4. Chapter summary and conclusion	92

7. Quantitative high-throughput screening using droplet-based microfluidics	95
7.1. Introduction	96
7.2. Description of the system	97
7.2.1. Dilution module	99
7.2.2. Calculation of the dilution network	100
7.2.3. Loading of the compounds	103
7.3. Results	105
7.3.1. Dilution module characterization	105
7.3.2. Dose-response curve determination	106
7.3.3. K_m determination	106
7.4. Materials and methods	108
7.4.1. Microfluidic chip fabrication and operation	108
7.4.2. Reagents	108
7.5. Chapter summary and conclusion	109
A. Co-authored work	111
A.0.1. Clausell-Tormos & Lieber <i>etal.</i> 2008	112
A.0.2. Baret & Miller <i>etal.</i> 2009	123
A.0.3. Mazutis & Fallah <i>etal.</i> 2009	132
B. Compounds and chemicals structures	141
B.0.4. Fluorophores	141
B.0.5. Substrates	143
B.0.6. Oils	144
B.0.7. Surfactants	145
C. Instrumentation	147
References	149

List of Tables

1.1. Fluidic resistance for different channel cress sections	20
3.1. Example of long term stability tests for droplet synchronization	54

List of Figures

1.1. Exemple de complexité réalisée avec des systèmes microfluidiques	3
1.2. Dispositif de microfluidique en gouttelettes intégré	5
1.3. Stratégie de criblage quantitatif haut débit par microfluidique en gouttelettes	6
1.4. Microfluidic Large Scale Integration	9
1.5. Integrated droplet-based microfluidic devices for screening applications	11
1.6. Work-flow for quantitative high throughput screening (qHTS) using droplet-based microfluidics	11
1.7. Soft-lithography	14
1.8. Electrode fabrication	14
1.9. Optical setup	16
1.10. Illustration of the internal friction in a fluid	17
1.11. Laminar slit flow	18
1.12. Illustration of surface tension and an experimental setup in order to measure it	20
1.13. Illustration for the derivation of the static contact angle θ	21
1.14. Two examples of the wetting behavior of liquids	22
1.15. Sketches for the derivation of the capillary pressure	22
1.16. Examples of more specialized droplet microfluidic modules	24
1.17. Droplet creation	24
1.18. Microfluidic approaches for mixing in continuous flow	25
1.19. Mixing within droplets	25
1.20. Illustration of the baker's transformation for mixing of droplets	26
1.21. Splitting of droplets	27
1.22. Fusion of droplets	28
1.23. Synchronization and fusion of droplets by electrical control	29
1.24. Sorting of droplets	30
1.25. Roche/454 sequencing method	32
1.26. Targeted sequencing workflow	34
1.27. Directed-evolution using gene-product linkage	35
1.28. Directed-evolution using SNAP display	35
1.29. Directed-evolution using double emulsions in combination with FACS	37
1.30. Directed-evolution using microbead display	38

1.31. Enzymatic amplification in droplets	39
1.32. Enzymatic amplification in droplets	41
1.33. Enzymatic amplification in droplets	41
2.1. Size sorting principle	45
2.2. Adjusting the droplet size sorter	46
2.3. Sorting droplets by size	47
2.4. Sorting droplets with small size differences	47
3.1. Synchronization of droplet production	53
3.2. Characterization of alternation	53
3.3. Mixing in droplets - co-flow vs in-line droplet fusion	54
3.4. Formation of iron oxide nanoparticles in droplets	55
3.5. Characterization of iron oxide particles generated in microfluidic droplets	56
4.1. Pairing module	61
4.2. Symmetrical actuation of the droplet synchronizer	62
4.3. Pairing frequencies at the droplet synchronizer	63
4.4. Decomposition of the asymmetric case for the synchronizer	64
4.5. Model and experiment comparison for the synchronizer	65
5.1. Layout of a two-depth device with a delay-line	71
5.2. Dispersion of droplets at different droplet densities	73
5.3. Reducing dispersion in delay-lines	75
5.4. Characteristics of different constriction designs	76
5.5. Multiple channel delay-line	77
5.6. A delay-line device designed for kinetic measurements	78
5.7. A delay-line device designed for kinetic measurements	79
6.1. Work-flow directed-evolution	85
6.2. Synchronize a reinjected emulsion	86
6.3. Sorting improvements	88
6.4. Sorting image sequence	88
6.5. Droplet-based microfluidics modules	89
6.6. Enrichment results	91
7.1. Comparison: current qHTS vs digital microfluidics qHTS	97
7.2. Inhibitor screening procedure	98
7.3. Inhibitor screening procedure	98
7.4. Inhibitor screening procedure	99
7.5. Illustration of resistor network to calculate the dilution gradient	101

List of Figures

7.6. Illustration of resistor network layout calculation	101
7.7. Compound loading procedure	104
7.8. Dilution module characterization	105
7.9. Measured dose-response curve	107
7.10. Measured results and fits for the IC ₅₀ and K _m of the model system	107
C.1. Detailed illustration for the optical setup	148

Nomenclature

Latin Characters

Variable	Meaning
A	Surface
a, b, c	Constants used in geometrical calculations
C	Concentration
d	Diameter
D	Diffusion coefficient
E	Electrical field
f	Frequency
F	Force
F	Percentage of high fluorescent droplets within packages of 100 droplets in chapter 5.
h, H	Height
H	Magnetic field strength
l, L	Length
M	Magnetization
P	Pressure
Q	Volumetric flow-rate
Q_o	Generally the oil volumetric flow-rate
Q_x, Q_y	Generally the aqueous volumetric flow-rate
r	Radius
R	Dispersion ratio (transition time/delay time ratio) in chapter 5
R	Fluidic resistance
R_{fl}	Fluidic resistance
t	Time
u	Velocity
U	Voltage
W	Work energy
V	Volume
w, W	Width

Variable	Meaning
x, y, z	Coordinate axes

Greek Characters

Variable	Meaning
α, β	Angles used in geometrical calculations
α, β	Fitting parameters in chapter 4
ε	Small number
ε	Indicates the fraction of the oil-flow in chapter 4
ε_0	Vacuum dielectric constant
ε_r	Electric permittivity of a dielectric
η	Viscosity
ω	Frequency of the AC voltage
σ	Surface tension
θ	contact angle
v	Velocity
ρ	Density

Short Cuts

Shortcuts	Meaning
AC	Alternating current
BSA	Bovine serum albumin
Ca	capillary number
CMC	Critical micelle concentration
DMSO	Dimethyl sulfoxide
DNA	Deoxyribonucleic acid
DC	Direct current
ELISA	Enzyme-linked immunosorbent assay
ePCR	Emulsion PCR
FACS	Fluorescence-activated cell sorter
FADS	Fluorescence-activated droplet sorter
FRET	Fuorescence resonance energy transfer
GFP	Green fuorescent protein
HPLC	High performance liquid chromatography

Shortcuts	Meaning
HRTEM	High resolution Transmission electron microscopy
HTS	High-throughput screening
IVC	<i>In vitro</i> compartmentalization
IVE	<i>In vitro</i> protein expression
IVTT	<i>In vitro</i> transcription and translation
LOC	Lab-on-a-chip
MEMS	Microelectromechanical systems
μ TAS	Micro total analysis systems
mLSI	Microfluidic large-scale integration devices
MRI	Magnetic resonance imaging
MS	Mass spectrometry
PBS	Phosphate buffered saline
PCA	Protein complementarily assay
PCR	Polymerase chain reaction
PDMS	Poly(dimethylsiloxane)
PEG	Polyethylene glycol
PE	Poly(ethylene)
PEEK	Poly(etheretherketone)
PFF	Pinched flow fractionation
PFPE	Perfluorinated polyether
PMT	Photomultiplier tube
POC	Point-of-care
qHTS	Quantitative high throughput screening
Re	Reynolds number
RNA	Ribonucleic acid
SDS-PAGE	Sodium dodecyl sulfate polyacrylamide gel electrophoresis
SEM	Scanning electron microscope
SQUID	Superconducting quantum interference device
TAP	Tandem affinity purification
TEM	Transmission electron microscopy
UV	Ultraviolet
w/o	Water-in-oil
w/o/w	Water-in-oil-in-water
Y2H	Yeast-two-hybrid
YFP	Yellow fluorescent protein

Chapter 1.

Introduction

Contents

1.1. Overview (French)	2
1.2. Overview (English)	8
1.3. Technology	14
1.3.1. Device fabrication	14
1.3.2. Fluorescent optical setup	16
1.4. Fluidics	17
1.4.1. Navier-Stokes-equations	17
1.4.2. Viscosity	17
1.4.3. Laminar slit flow and fluidic resistance	18
1.4.4. Surface tension	20
1.4.5. Contact angle	21
1.4.6. Capillary pressure	22
1.5. Droplet-based microfluidics and its modules	23
1.5.1. Droplet creation	24
1.5.2. Mixing within droplets	25
1.5.3. Splitting of droplets	27
1.5.4. Droplet fusion	28
1.5.5. Droplet sorting	30
1.6. Applications of compartmentalization in emulsions	31
1.6.1. Emulsion PCR (ePCR)	31
1.6.2. Next generation sequencing methods	33
1.6.3. Directed evolution	34
1.6.4. Diagnostics	39
1.6.5. Proteomics and protein-protein interactions	40

1.1. Overview (French)

Les pratiques modernes de laboratoires, plus particulièrement dans le domaine des sciences de la vie, sont demandeuses de systèmes d'analyse plus fiables, plus rapides et moins coûteux [1]. L'enjeu est non seulement de mettre en place des méthodologies permettant de réduire la consommation en réactifs, mais également d'augmenter les débits, de sorte à obtenir des informations englobant un plus grand nombre de paramètres. Ces systèmes haut-débits sont particulièrement intéressants pour des applications de criblage et de diagnostique, mais aussi pour des études dans les domaines de l'évolution dirigée, la protéomique, la chimie combinatoire et le développement de matériaux.

La compartimentation des analyses en puits a fait des plaques de microtitration la plateforme de criblage la flexible et la plus utilisée aujourd'hui. Cependant, la réduction des volumes en deçà de 1-2 μL est problématique et le débit maximum, même en utilisant des approches robotiques complexes (et coûteuses) de manipulation, est limité à un petit peu moins de un test par seconde. De plus, ces imposantes stations robotiques de manipulation de liquides occupent des laboratoires entiers et nécessitent de considérables investissements financiers, d'espace et de main d'œuvre. Une question naturelle consiste donc à demander s'il est possible d'automatiser et de miniaturiser les analyses chimiques et biologiques tels que cela a pu être fait en électronique par le biais des circuits intégrés.

La microfluidique est un domaine essentiellement dédié à la miniaturisation des manipulations de liquides et permet l'utilisation de faibles volumes de l'ordre du μL [2]. En plus de la réduction de volume de réactifs, la physique fondamentale des fluides change rapidement avec la réduction des échelles de tailles [3]. Un des exemples les plus significatifs est que le transport de masse en dispositifs microfluidiques est généralement dominé par la dissipation visqueuse, et que les effets inertiels sont généralement négligeables. En absence d'inertie, la non linéarité est perdue et les courants de liquides peuvent s'écouler les uns à côté des autres sans turbulence ni mélange. Ce phénomène est appelé écoulement laminaire et offre de nouvelles capacités fondamentales pour le contrôle des concentrations et des destinations de molécules dans l'espace et le temps. Une autre conséquence de la miniaturisation est l'augmentation du rapport surface/volume rendant les effets de surface plus dominant [4], ce qui se produit habituellement aux interfaces liquide-solide ou gaz-liquide, mais également entre différentes phases liquides au sein des microcanaux.

La microfluidique a bénéficié du développement rapide de nouvelles méthodes de fabrication, de nouveaux matériaux et applications au cours des dernières années, permettant aux laboratoires sur puce (lab-on-a-chip) et aux microsystèmes d'analyse totale (μTAS) [5] de faire leur route vers une production industrielle et une commercialisation [6]. Des systèmes impressionnant de part leur complexité, dénommés dispositifs à haut degré d'intégration (mLSI) [7, 8] ont été développés avec des milliers de valves micromécaniques et de composants intégrés (Figure 1.1). D'autre part, de simples dispositifs diagnostiques à bas coût [9, 10] pourraient changer les diagnostics dans le futur.

Ce travail est dédié à un domaine spécifique au sein de la microfluidique utilisant des gouttelettes d'eau dans l'huile [11–14]. L'huile fonctionne comme une barrière imperméable, permettant à chaque gouttelette de fonctionner comme un microréacteur indépendant avec un volume compris entre 1

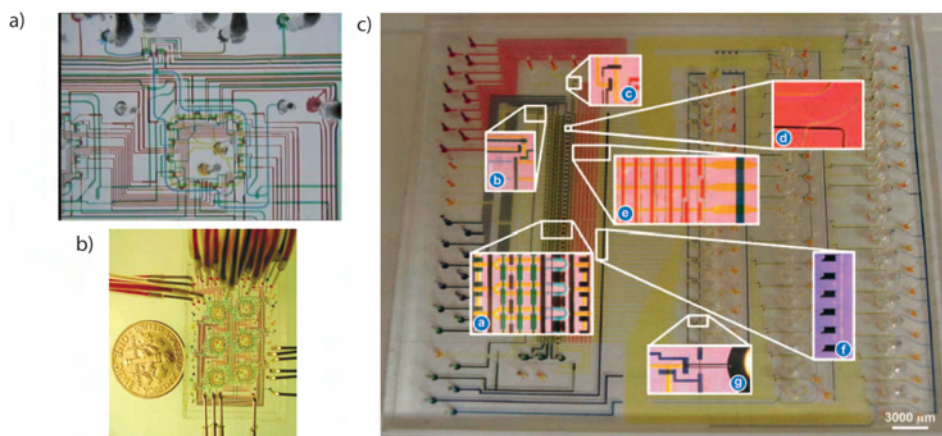


Figure 1.1.: Exemple de complexité réalisée avec des systèmes microfluidiques suivant les concepts de circuits largement intégrés en électronique. a) et b) d'après [8] et c) d'après [7].

nL et 1fL, ce qui est 10^3 à 10^9 fois plus petit que le plus petit volume utilisable dans le puit d'une plaque de microtitration. Contrairement aux émulsions conventionnelles générées par mélange ou homogénéisation mécanique [15], les gouttelettes créées en systèmes microfluidiques sont extrêmement monodisperses (moins de 3% de variation de volume) [16] et il est possible d'agir sur ces gouttelettes de façon indépendante après leur création. Cela signifie qu'il est possible d'y ajouter des réactifs en les fusionnant avec d'autres gouttelettes [17, 18], de diviser ces gouttes [17, 19], ou de les trier en fonction de leur contenu [20–22]. Toutes ces opérations peuvent être réalisées à des cadences dans des régimes de l'ordre de quelques kHz, permettant la réalisation d'un très grand nombre de réactions totalement automatisées en quelques heures. La microfluidique présente donc plusieurs des caractéristiques requises pour un système de criblage haut-débit.

Au début de ce travail (fin 2006), la microfluidique en goutte suscitait des intérêts croissants rapidement, plus particulièrement récemment, depuis que les premières applications, principalement en chimie, ont été publiées et que les preuves de principe des principaux concepts de la manipulation de gouttelettes comme la création de gouttelettes, leur division, leur fusion et leur tri ont été démontrés [11]. Il y avait néanmoins encore plusieurs difficultés à surmonter avant que ces systèmes de base ne puissent être utilisés pour des tests biologiques plus complexes. Le tensio-actif utilisé pour stabiliser les émulsions s'est révélé être un élément déterminant à la réalisation de réactions biologiques en gouttelettes [23]. De mauvaises formulations montraient des propriétés d'inhibition des activités enzymatiques ou à la fuite des composés fluorescents, utilisés dans la plupart des tests, abolissant ainsi le concept de compartimentation [24, 25]. De plus, certains concepts inhérents à la manipulation des gouttelettes, plus particulièrement la synchronisation des gouttelettes, leur fusion et leur tri n'étaient pas assez reproductibles pour une utilisation en routine et nécessitaient un développement plus approfondi et de nombreuses optimisations. Un autre élément faisant défaut pour de nombreux tests concernait un système d'incubation des gouttelettes. Des systèmes biologiques tels que, par exemple, l'expression de protéines par transcription/traduction *in vitro* (IVTT), nécessitent jusqu'à une heure

d'incubation. D'autre par, les cinétiques enzymatiques de conversion des substrats des protéines ainsi produites peuvent se faire dans des temps de l'ordre de la minute au contraire des systèmes modèles utilisés jusque là [26] et où les catalyses très efficaces étaient de l'ordre de la seconde à la milliseconde. Idéalement, l'incubation des gouttelettes devrait se réaliser sur puce pour faciliter et pouvoir automatiser l'expérimentation, ainsi que permettre la mise en place de tests biologiques sophistiqués dans des systèmes microfluidiques en gouttes.

Les travaux entrepris au cours de cette thèse ont concerné un certain nombre de ces problématiques et ont permis de proposer des méthodes pour y remédier. Une des premières méthodes développée a été la synchronisation des gouttelettes et leur fusion. Des stratégies telles que le contrôle actif de la libération de gouttes basé sur l'utilisation de champs électriques [27] ou le couplage hydrodynamique passif au niveau d'une buse unique ont été proposés [28, 29]. Néanmoins, ces approches ne permettaient pas encore une utilisation en routine, et leur automatisation était relativement compliquée. Plus particulièrement, la reproductibilité et l'efficacité d'appariement des gouttelettes ne pouvait excéder 70-80% et était compliqué à obtenir et à maintenir. Nous avons donc développé une méthode permettant de produire des paires de gouttelettes de façon extrêmement efficace et reproductible [30]. Celle-ci est basée sur le couplage hydrodynamique de deux buses spatialement distinctes. L'utilité de ce système a été démontrée en produisant par précipitation des particules d'oxyde de fer au travers d'une réaction très rapide (moins de 2 ms) et reproductible après fusion de paires de gouttelettes. La synthèse de précipité en systèmes microfluidiques est habituellement entravée par l'obstruction des canaux et la mélange des réactifs en une phase unique est contrôlé uniquement par la diffusion. L'utilisation de la microfluidique en gouttes permet d'éviter ces problèmes, et la méthode d'appariement nouvellement développée s'est révélée être idéale pour l'automatisation et la reproductibilité de réaction nécessitant un mélange rapide. Les réactifs entrent en contact uniquement lors de la fusion des paires de gouttelettes, compartimentant ainsi la réaction tout au long de la synthèse.

Du fait du comportement physique surprenant et très intéressant présenté par cette méthode d'appariement, nous en avons approfondie l'étude par la mise en place d'un modèle décrivant et prédisant les caractéristiques du système [31]. Il s'est avéré qu'il était possible de créer des paires de gouttelettes variant en combinaison de taille et de volume sans modifier le design du dispositif microfluidique. L'efficacité d'appariement de ce dispositif atteint des valeurs proches de 100% et fonctionne avec différence stœchiométrique de volume jusqu'à 1/5 (dans certains cas même jusqu'à 1/7) entre chaque gouttes d'une paire. Cela signifie que des modulations stœchiométriques de 1/25 (voire 1/49) peuvent facilement être entreprise, tout en maintenant la réaction compartimentée durée toute l'expérience. Le modèle mathématique produit une équation générale de la fréquence de la production des gouttelettes en fonction de différents débits permettant de prédire et de comprendre le comportement et les limites du système.

Une autre question importante abordée durant cette thèse a concerné l'incubation des gouttelettes. Au premier abord, cela peut paraître relativement simple à réaliser en utilisant un long canal, mais deux phénomènes physiques restreignent cette approche. L'allongement des canaux microfluidiques qui sont très fins et peu profond, s'accompagne d'une augmentation proportionnelle de la résistance

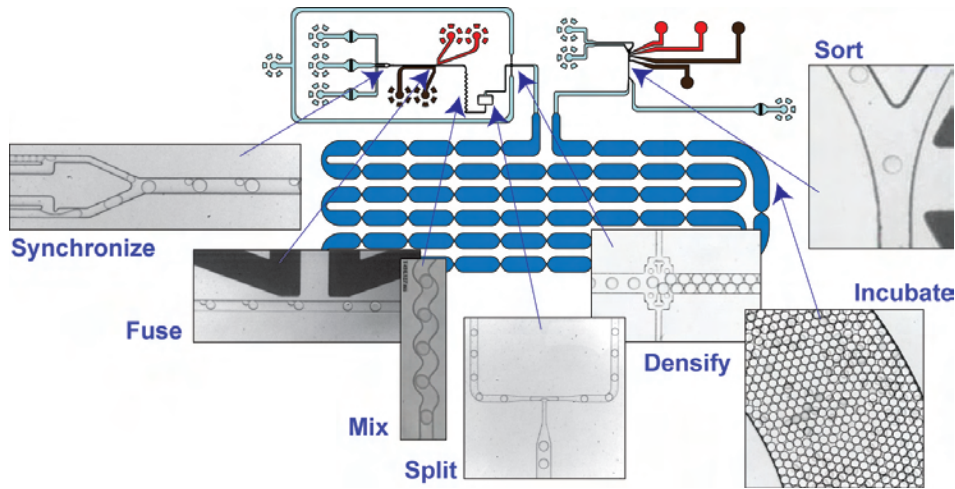


Figure 1.2.: Dispositif de microfluidique en gouttelettes intégré dédié aux applications de criblage telles que l'évolution dirigée d'enzymes.

fluidique conduisant à une contre-pression surpassant facilement les limites de travail des pompes et des puces. La simple augmentation de la largeur et de la profondeur des canaux permet d'éviter ce problème mais en soulève un autre. Alors que les gouttelettes restent ordonnées (fil indienne) dans les canaux fins et peu profonds, elles ont tendance à se dépasser et ainsi ne conservent plus leur ordre dans des canaux de dimensions plus importantes (canaux large et profonds). De plus, ce comportement est amplifié par phénomènes, connus sous le nom d'*écoulement de Poiseuille* et *dispersion de Taylor* [32], consistant en un écoulement plus rapide au centre d'un canal qu'en ses bords. Cela signifie que les gouttelettes situées au centre du canal peuvent circuler jusqu'à deux fois plus vite que celles situées sur les bords, créant ainsi une importante dispersion des temps d'incubation et rend toute sorte de mesure quantitative impossible. Ces limitations ont été étudiées en détail, leurs limites et leurs ampleurs ont été décrites et des stratégies pour y remédier ont été proposées et développées [33]. Ces efforts ont permis de réduire la dispersion des temps d'incubation sous la barre des 10%, rendant ainsi accessible des temps d'incubation de l'ordre de la minute à l'heure. Les premières applications ont consisté en suivis cinétiques de réactions enzymatiques sur les temps d'incubation nouvellement accessibles. Dans un premier temps, des mesures ont été réalisées à des temps espacés linéairement, permettant un suivi homogène du profil réactionnel. Dans un second temps, des dispositifs permettant des points de mesures à des temps séparés exponentiellement ont été développés en vue du suivi de changements cinétiques brusques et rapides (ms-s), tout couvrant l'intégralité de la réaction sur plusieurs minutes. Cette approche méthodologique est habituellement difficilement accessible avec le matériel de laboratoire conventionnel tel que les lecteurs de microplaques.

Cette possibilité d'incuber les gouttelettes sur puce a ensuite rendu possible l'intégration de plusieurs autres modules sur une puce unique, renforçant ainsi le concept d'automatisation et la facilité d'utilisation des systèmes. Comme montré sur la figure 1.2, il a été possible de fabriquer des dispositifs utilisant la plupart des principaux modules de manipulation de gouttelettes, ceux-ci étant utilisables pour des

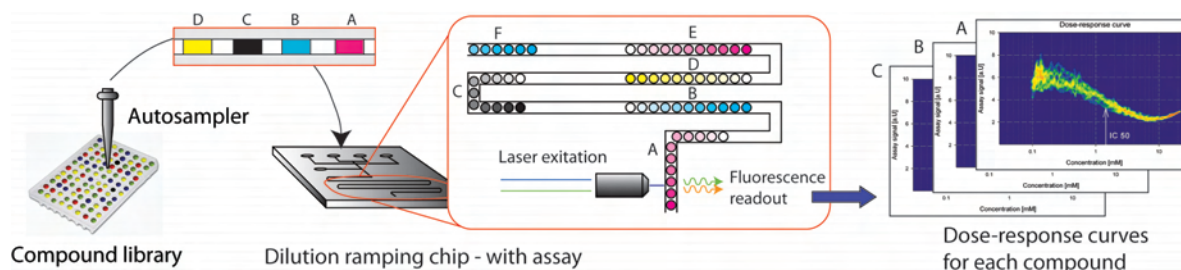


Figure 1.3.: Stratégie de criblage quantitatif haut débit par microfluidique en gouttelettes.

criblages complexes. En parallèle de ce travail, d'autres membres du groupe ainsi que des collaborateurs se sont consacrés aux problèmes liés au tensio-actif [23], à l'amplification de l'ADN et à l'expression des protéines dans les gouttelettes [34, 35]. Dans un effort commun, nous essayons à l'heure actuelle de combiner les différentes méthodes pour réalisation d'expériences d'évolution dirigée de protéines en dispositifs microfluidiques à gouttelettes en partant de variants de gènes individualisés en gouttelettes. Une fois mises en place, ces méthodes pourront être utilisées pour évoluer une vaste variété d'enzymes et d'ARN pour des propriétés d'association, de catalyse ou de régulation, mais également pour des études d'interaction protéines-protéines.

Une autre cible intéressante pour l'utilisation de la microfluidique en gouttes est l'industrie pharmaceutique [36, 37]. Les approches conventionnelles de criblage de médicaments nécessitent un effort important en termes d'instrumentation, de robotique, de temps et d'argent [38, 39]. Le développement d'une nouvelle plateforme de microfluidique en gouttelettes dédiée au criblage de médicaments (Figure 1.3) a débuté suite à la mise en place d'un projet impliquant plusieurs membres de notre laboratoire ainsi qu'un partenariat industriel avec Sanofi-Aventis et Raindance Technologies. Le but est de réaliser des criblages quantitatifs à haut débit (qHTS) de chimiothèques avec une réduction significative des quantités de réactifs utilisées et une augmentation de la qualité des données et du débit. Un des composants clé dans ce concept est le besoin d'injecter les composés l'un après l'autre dans la puce microfluidique et d'augmenter la concentration des composés sur gradient de 3 à 4 ordre de grandeur. Etant donné que les gouttelettes sont produites à des régimes de l'ordre du kHz, cela permet à chaque concentration d'être représentée plusieurs centaines de fois, augmentant ainsi significativement la valeur statistique des mesures réalisées, tout en permettant de couvrir toute la gamme de concentrations de façon presque continue au lieu de réaliser uniquement 5 à 7 points de mesure comme cela est fait dans les approches conventionnelles [39]. L'importante réduction des volumes des tests devrait permettre d'importantes économies financières (actuellement estimées à 1000 fois).

En résumé, ce travail a contribué à l'établissement de plusieurs nouveaux concepts et idées contribuant un domaine de recherche en pleine expansion avec un énorme potentiel futur dans le domaine des sciences de la vie. Il reste à voir si les avantages et promesses de la microfluidique en gouttelettes sont suffisamment forts pour atteindre le stade de la commercialisation et entrer dans les pratiques courantes en laboratoires. Il y a certaines indications, par exemple avec des sociétés comme Raindance

1.1. Overview (French)

Technologies qui commence à vendre ses premiers produits, que cette technologie a atteint un niveau de fiabilité suffisamment important pour convaincre de potentiels clients de ses potentiels. D'autre part, des start'ups de service sont en train de se développer et des produits tels que des criblages quantitatifs à haut débit pourraient devenir un jour une pratique commune dans le milieu de l'industrie pharmaceutique.

1.2. Overview (English)

Modern laboratory practice, especially in life sciences demands faster, cheaper and more reliable assay systems [1]. This is a quest aimed at finding methodologies to reduce sample consumption, but also increasing throughput to provide information on larger parameter spaces. These so-called high-throughput systems are especially useful for screening applications and diagnostics but also for studying evolution, proteomics, combinatorial chemistry and materials research.

The compartmentalization of assays in wells makes microtitre-plates the most flexible and most widely used screening platform in use today. However, reducing assay volumes to below 1-2 μL is problematic and the maximum throughput, even when using sophisticated (and expensive) robotic handling, is little more than one sample per second. Additionally these enormous robotic fluidic workstations take up entire laboratories and require considerable expense, space, and labor. Therefore, a natural question is, whether it is possible to automate and miniaturize biology and chemistry to an extent similar to what has been achieved in electronics in the form of integrated circuits. Microfluidics is a field dedicated to miniaturized fluidic manipulation and allows handling of small liquid volumes down to the pL range [2]. In addition to sample reduction, the fundamental physics of fluidics changes rapidly as the size scale is decreases [3]. One of the most significant examples is that mass transport in microfluidic devices is generally dominated by viscous dissipation, and inertial effects are generally negligible. Without inertia, non-linearities get lost and fluid streams can flow alongside without turbulence and mixing. This phenomenon is called laminar-flow and offers fundamentally new capabilities in the control of concentrations and destinations of molecules in space and time. Another consequence of miniaturization is the increased surface-to-volume ratio making surface effects more dominant [4], which occur usually at the liquid-solid or gas-solid interface but also between different phases within these microchannels.

The field of Microfluidics has experienced rapid development of new fabrication methods, novel materials and application during the last ten years and so-called lab-on-a-chip or micro-total-analysis-systems (μTAS) [5] are making their ways into industrial commercialization [6]. Very impressive and complex systems have evolved, referred to as microfluidic large-scale integration devices (mLSI) [7] with thousands of integrated micromechanical valves and control components (see figure 1.4). But also simple low-cost devices, serving the point-of-care market [9, 10] may change diagnostics in the future.

This work is dedicated to a specific field within microfluidics utilizing water-in-oil droplets [11–14]. Ideally the oil functions as an impenetrable barrier, meaning that each aqueous droplet functions as an independent microreactor with a volume between one nanoliter to one femtoliter, which is between 10^3 and 10^9 times smaller than the smallest working volumes in a microtitre plate well. In contrast to bulk emulsions, which are generated by mechanical homogenizers or mixers [15] the droplets created in microfluidic channels are extremely monodisperse ($< 3\%$ volume variation) [16] and it is possible to process droplets independently after their creation. This means it is feasible to add additional reagents by droplet-fusion [17, 18], they can be split [17, 19], or they can be sorted based on their

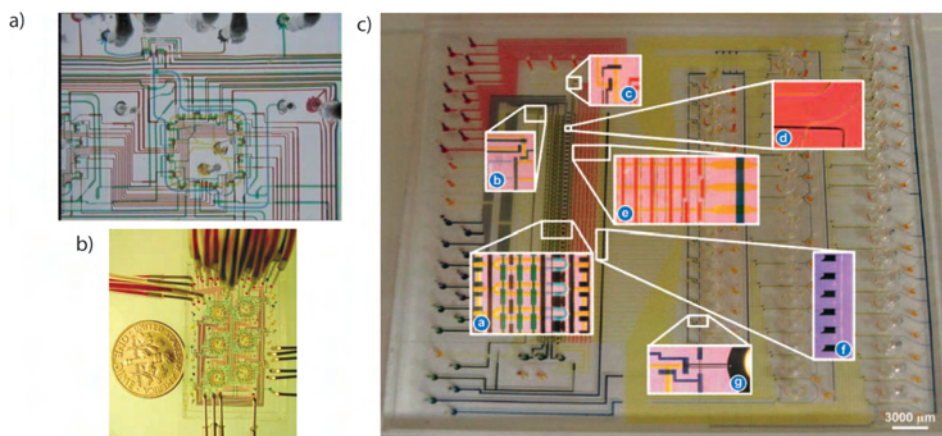


Figure 1.4.: Examples of complexity achieved in microfluidics - following the concepts of largely integrated circuits in electronics. a), b) reprinted from [8] and c) reprinted from [7].

content [20, 21]. All of these operations can be performed up into the kHz regime, allowing a huge amount of reactions to be handled in a completely automated fashion within a few hours. Therefore, droplet-based microfluidics shows many of the desired characteristics required as a high-throughput systems.

When this work began at the end of 2006, interest in droplet-based microfluidics was growing rapidly, especially since the first applications - mainly in chemistry - had recently been published and many of the main concepts of droplet-processing, such as droplet creation, splitting, fusion and sorting had been shown as proof of principle [11]. Nevertheless there were still several obstacles to overcome before these basic methods could be used for more complex and multi-step biological assays. Surfactant, used to stabilize emulsions appeared to be the key component to perform biological reactions in droplets [23]. Using the wrong formulations led to inhibited enzymatic activities, or the fluorescent products, used in many assays, could leak from one droplet to the other by micellar transport [24, 25], destroying the concept of compartmentalization. Furthermore, some of the concepts for droplet manipulation, especially synchronization, fusion and sorting of droplets were not yet reliable enough or routinely performed and needed further optimization and investigation. Another missing component for many assays was the incubation of droplets. Assays such as the *in vitro* transcription and translation of enzymes (IVTT) often require several minutes up to an hour to complete, and the enzyme concentrations reached by this method allow only substrate conversion kinetics, which typically lie in the minute range rather than in the millisecond to second regime, demonstrated previously [26]. Ideally this incubation of droplets should be performed on-chip in a run-through (continuous) fashion to facilitate and automate experimentation and allow one to perform sophisticated biochemical assays in droplet-based microfluidics.

The research within this thesis addresses many of these problems and proposes novel solution mechanisms. Along with every new concept, novel methods and assays became accessible. One of the first methods investigated was droplet synchronization and fusion. Strategies such as active control of

droplet release based on electric fields [27], or passive hydrodynamic coupling at a single nozzle had been proposed [28, 29]. Nevertheless, these approaches were still some steps away from being performed routinely, and automation was rather difficult. Particularly the reliability and pairing efficiency could only reach values of 70-80% and was labor intensive to achieve and maintain. Therefore, we have developed an extremely reliable method to create droplet pairs, based on hydrodynamic coupling of two spatially separated nozzles. The utility of this system has been demonstrated by precipitating iron oxide nanoparticles in a very fast (\sim ms kinetics) and reproducible reaction after fusion of droplet pairs. Synthesis of precipitates in microfluidics is usually hindered by clogging of channels, and mixing of reagents in single phase microfluidics is diffusion limited. These problems could be circumvented using droplet-based microfluidics and the novel droplet pairing method turned out to be ideal for reliable and automated reactions that require fast mixing and create particulate. Reagents only come in contact when the droplet-pairs fuse, compartmentalizing the reaction throughout the whole assay.

Since this pairing method also showed some very interesting and surprising physical behavior we investigated this issue further to evolve a model describing and predicting the characteristics of the system. We found that it is possible to create droplet pairs at various size- and volume combinations without altering the design. The pairing efficiency of this system reaches values close to 100% and works up to a stoichiometric volume difference of 1:5 (in some cases even up to 1:7) for the droplet pairs. This means stoichiometry modulations of 1:25 (or 1:49) can easily be achieved, still compartmentalizing the reaction throughout the whole experiment. The mathematical model derives a general equation of droplet frequencies as a function of the various flow-rates, allowing one to predict and understand the behavior and the limitations of the system.

Another key issue addressed during this work was the question of droplet incubation on-chip. At a first glance this might seem easily achievable by a long incubation channel but two physical phenomena restrict this solution. By simply increasing the length of these narrow and shallow channels the fluidic resistance increases proportional to the channel length resulting in a back-pressure easily surpassing the working limits of the pumps and chips. Increasing the channel dimensions in width and height does overcome this issue but also leads to an additional problem. Whereas droplets remain single filed in these thin and narrow channels, they can overtake and change order in wide/large channels. Unfortunately this is even enhanced by a phenomena called *Poiseuille flow* and *Taylor dispersion* [32] where the flow-rate in the center of a channel is higher than at the walls. This means that droplets traveling in the center of a channel can travel up to two times as fast as those at the channel walls, creating a huge dispersion of incubation time and usually making any kind of quantitative readout impossible. These limitations were investigated in detail, its limits and extent were described and solution strategies proposed and developed. Due to these efforts it was possible to reduce the dispersion of incubation times under 10% making the extremely interesting regime of incubation times in the minute to hour range accessible. As first application enzymatic reaction kinetics in this time range could be demonstrated. Initially with a linear distribution of measurement points over the time course, allowing homogenous monitoring of the reaction profile. Furthermore, devices with exponential distribution of

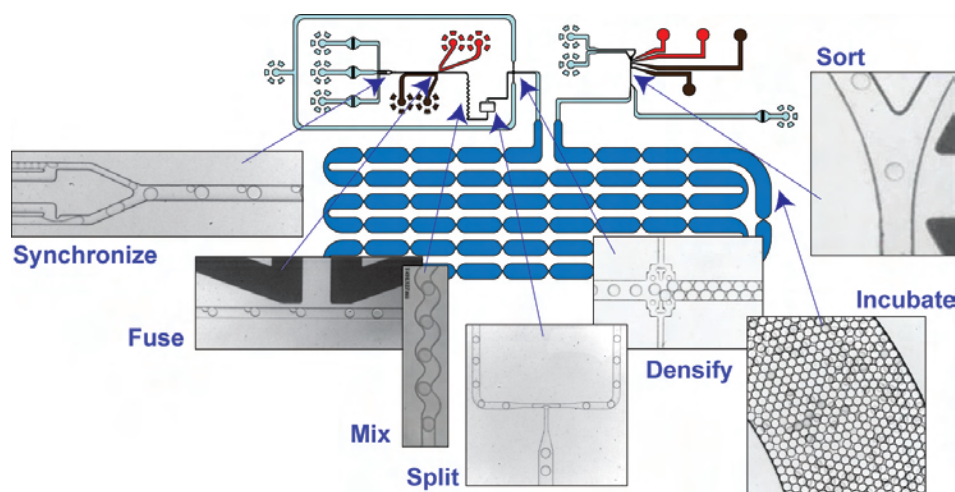


Figure 1.5.: Integrated droplet-based microfluidic devices for screening applications as e. g. directed evolution of enzymes.

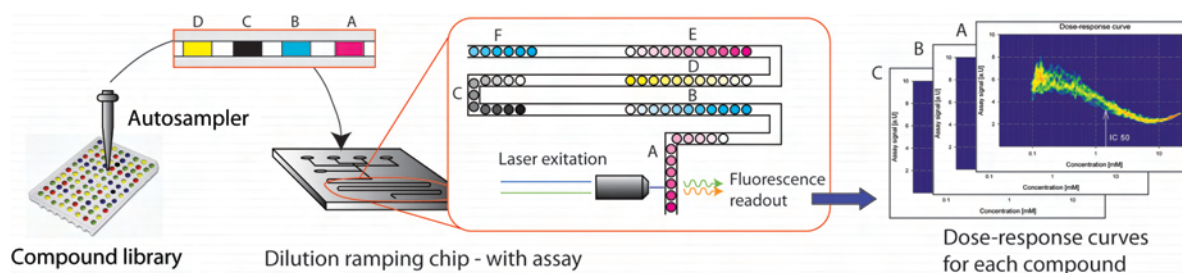


Figure 1.6.: Work-flow for quantitative high throughput screening (qHTS) using droplet-based microfluidics.

measurement points were developed to track down sudden and fast kinetic changes (ms-s), but still covering the full reaction of several minutes. This procedural method is usually not easily accessible with common laboratory instrumentation such as plate-readers.

With the ability to incubate droplets on-chip it was further possible to integrate several droplet modules onto a single chip, therefore enhancing the concept of automation and laboratory ease of usage. As shown in figure 1.5 devices could be fabricated which use most of the main droplet-modules and now enable sophisticated screening applications to be performed. In parallel to this work other investigators among our collaborators and within the group focussed on the issues of surfactant [23], DNA amplification and protein expression in droplets [34, 35]. In a shared effort we are currently trying to combine the results and methods to perform directed-evolution of enzymes in droplet-based microfluidics starting from single DNA strands. Once established these methods could be utilized to evolve a vast variety of enzymes and RNAs involved in binding, catalysis and regulation, but can be also used to study protein-protein interactions.

Another interesting target for the utility of droplet-based microfluidics is the pharmaceutical indus-

try [36, 37]. The common practice currently in drug-screening demands a huge effort in instrumentation, robotics, time and costs [38, 39]. In a project involving several members of our laboratory, as well as industrial partners/investors such as Sanofi-Aventis and RainDance Technologies, a novel drug-screening platform utilizing droplet-based microfluidics is being developed (see figure 1.6). The aim is to perform quantitative high-throughput screening (qHTS) of compound libraries with a significant reduction of sample consumption, along with an increased amount of quality data and throughput. One of the key components in this concept is the need to inject one compound after the other into a the microfluidic chip and ramp the concentration within the droplets over at least 3-4 orders of magnitude. Since droplets are created in the kHz regime this provides several hundreds of copies per concentration, improving the statistical significance of the data, but also covering the whole concentration range almost continuously instead of the typical 5-7 measuring points in current practice [39]. The massive reduction in the assay volume should result in big cost savings: estimations so far expect savings of more than 1000 fold.

In summary, this work has contributed several novel concepts and ideas to a massively growing research field with a lot of potential in life sciences in the future. Now it remains to be shown whether the advantages and promises of droplet-based microfluidics are strong enough to also find their way into commercialization and common laboratory practice. There are some indications with companies such as RainDance Technologies selling their first products now, that this technology has reached a level of reliability strong enough to convince customers of its potentials. Also other service providing start-ups are evolving and products such as the qHTS in micro-droplets might one day be the common practice in the pharmaceutical industry.

In detail the thesis is structured as follows:

Chapter 2 describes the theory and method of sorting droplets by size rather than their content.

Chapter 3 describes a novel nozzle design enabling the creation of droplet-pairs for fusion with a reliability in pairing efficiency reaching almost 100% . This device enabled fast reactions, forming particulate to be performed and its utility was demonstrated by synthesizing superparamagnetic iron-oxide nano-particles in microfluidics.

Chapter 4 describes the derivation of a mathematical model for the droplet pairing nozzle. It leads to a general equation of droplet frequencies as a function of the various flow-rates allowing one to prediction and understanding of the behavior and the limitations of the system.

Chapter 5 describes the problems involved with droplet incubation on chip in delay-lines. The limitations and hindrances are analyzed and the proposed solution strategies enabled the usage of delay-lines as a novel module in droplet-based microfluidics and made a variety of new applications accessible.

Chapter 6 describes how the microfluidic modules have been evolved and improved in order to integrate them into easy and robust devices for screening applications such as the directed evolution of enzymes.

Chapter 7 describes the concept of a novel qHTS system utilizing droplet-based microfluidics. The advantage of this technique is the great amount of data and the statistical significance of the screening results.

The Appendix includes the publications co-authored during this work. Additionally it describes many of the typical reagents and the instrumentations involved with droplet-based microfluidics.

1.3. Technology

1.3.1. Device fabrication

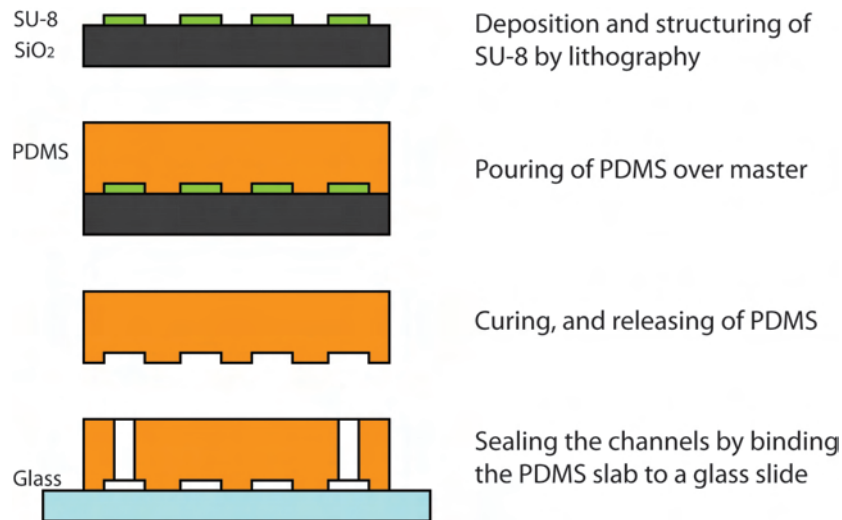


Figure 1.7.: Schematic illustration of the procedure for fabricating PDMS microfluidic devices. The first step is to create a master (mold) by SU-8 lithographic structuring on a silicon wafer. After replicating this master in PDMS, the fluidic connection inlets are punched and the PDMS slab is bound to a glass slide.

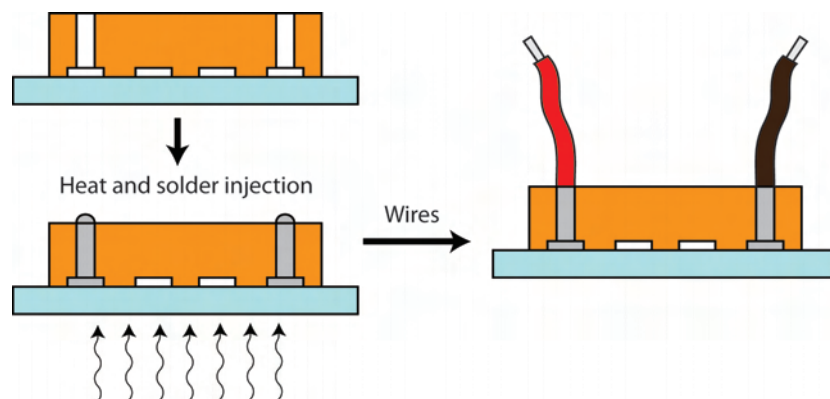


Figure 1.8.: Schematic illustration of the procedure for fabricating electrodes in the micro-structured chip. The device is placed on a hotplate at 90° and the solder is injected through one of the inlets. For electrical contact wires are inserted into the still liquid solder.

Microfabrication uses a variety of patterning techniques, and one of the most powerful being photolithography. Most integrated circuits are fabricated using this technology [40]. Projection photolithography is a parallel process wherein the entire pattern of the photomask can be projected onto a thin film of photoresist all at once. For MEMS applications with no need of submicron structures, SU-8 as a photoresist has become popular as it provides the ability to create features with aspect ratios greater than 1:18 and vertical sidewalls into the millimeter range [41]. Furthermore, SU-8 has

beneficial chemical and mechanical properties which allow structured SU-8 to be used as molds for micro-molding techniques [42].

Figure 1.7 illustrates the procedure of this casting technique. First, a master is fabricated by photolithographically structuring SU-8 on a silicon wafer. Then, a prepolymer of an elastomer (Poly(dimethylsiloxanes) (PDMS)) is poured over the master. It consists of a mixture of a liquid silicon rubber base (i. e. a vinyl-terminated PDMS) and a catalyst or curing agent (i. e. a mixture of a platinum complex and copolymers of methylhydrosiloxane and dimethylsiloxane). Once mixed, degassed, poured over the master, and heated to elevated temperatures, the liquid mixture becomes a solid, cross-linked elastomer via the hydrosilylation reaction between vinyl ($\text{SiCH}=\text{CH}_2$) groups and hydrosilane (SiH) groups within a few hours [43]. In order to use these PDMS slabs as microfluidic devices, inlet holes need to be punched and the channels need to be sealed by another PDMS slab or a glass slide. Although different techniques have been reported for PDMS-PDMS or PDMS-glass bonding [44] surface activation by an oxygen plasma is the most commonly used technique.

Elastomers such as PDMS are used because they create a conformal contact with surfaces (even those that are nonplanar on the μm scale) over relatively large areas and because these elastomers can be easily released from rigid masters or from complex, quasi-three-dimensional structures that are being molded. In addition to its elasticity, the PDMS elastomer also has other properties that make it extremely useful [43, 45]. These include (i) that the PDMS provides a surface that has a low interfacial free energy ($\sim 21.6 \text{ dyn cm}^{-1}$) and good chemical stability (most molecules do not adhere irreversibly to, or react with the surface of PDMS), (ii) that the PDMS elastomer is optically transparent down to $\sim 300 \text{ nm}$, (iii) that PDMS is hydrophobic with a contact angle of $\sim 110^\circ$, (iv) that PDMS is an excellent sealant and encapsulant for high voltage applications ($\epsilon_r = 2.75$; dielectric strength of 21 kV mm^{-1}), (v) that PDMS is not hygroscopic; it does not swell with humidity, (vi) that the PDMS membrane passes gas easily and (vii) that the PDMS elastomer has good thermal stability (up to $\sim 186^\circ \text{ C}$ in air).

In addition to fluid handling, some applications also require electrical control and it is favorable if the electrodes can be fabricated in close proximity to and well-aligned with the fluidic channels. The easiest and fastest method currently is to pattern additional channels for the electrodes into the same mold and to fill them with a low-temperature solder [46]. This procedure is illustrated in figure 1.8. After placing the device on a hotplate at 90° , a low-temperature solder (51In/32.5Bi/16.5Sn) is introduced into the channels, filling them completely, and wires are placed into the inlet holes for electrical contact.

The last step for obtaining functional devices for droplet-based microfluidics is a surface treatment. The channel surfaces should be wetted by the continuous phase - meaning hydrophilic for oil-in-water droplets [47] or hydrophobic for water-in-oil droplets. This is necessary to avoid the droplets wetting the surface and to reduce cross-contamination. PDMS is naturally hydrophobic but since for some applications a fluorinated oil is used, it is necessary to treat the channel walls fluorophilic. A typical surface treatment is either to use a commercial surface coating agent (Aquaapel, PPG Industries) or to silanize the surfaces.

1.3.2. Fluorescent optical setup

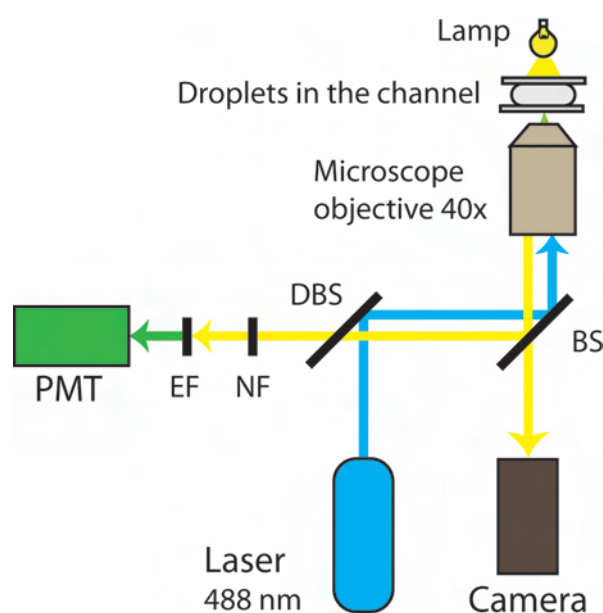


Figure 1.9.: Schematic representation of the optical setup. The 488 nm laser is reflected by a dichroic beamsplitter (DBS) into the microscope. Inside the microscope the laser is reflected at a beamsplitter (BS) and focused into the microfluidic channel by a 40× objective. The emitted fluorescent light and the light of the lamp pass back through the microscope and reach either the highspeed camera or pass through the filters (Notch filter NF and emission filter EF). The emission filter is a bandpass filter transmitting 504 ± 20 nm to the PMT which records the light intensity.

Optical detection methods have the advantage that they are fast, that no physical contact to the probe is needed and that a broad spectrum of already existing biological assays is available. Therefore, the microfluidic devices are usually placed onto a setup which allows to detect droplets optically. An example of such a setup is illustrated in Figure 1.9. It consists of a laser source which excites the fluorophores within the droplets. The laser is focused into the channels through a microscope objective and the fluorescence emission is filtered with an appropriate set of filters. A photomultiplier tube (PMT) collects these signals and passes the data to a data-acquisition and analysis software. Additionally, a high speed camera records sequences of images of the droplet movement in the channels. These techniques enable one to obtain information about microfluidic behavior of the droplets as well as information on the content of a droplet. Automated control and data analysis can then be implemented into the evaluation software.

1.4. Fluidics

1.4.1. Navier-Stokes-equations

The *Navier-Stokes-equations* are the basic equations for the continuum description of fluid dynamics. They are valid for stationary as well as for transient problems and can be derived using the principles of conservation of mass and momentum [48]:

$$\rho \left(\frac{\partial \mathbf{u}}{\partial t} + (\mathbf{u} \cdot \nabla) \mathbf{u} \right) = -\nabla P + \eta \Delta \mathbf{u} + \mathbf{F}_{vol}, \quad (1.1)$$

$$\nabla \cdot \mathbf{u} = 0. \quad (1.2)$$

where ρ is the density, \mathbf{u} the velocity vector, P the pressure, η the viscosity and \mathbf{F}_{vol} the body forces.

Equation 1.1 forms the momentum equation for a infinitesimal continuum element according to Newton's second law for an incompressible fluid. The left hand side describes the total change in momentum of a continuum element, whereas the expression $\rho \partial \mathbf{u} / \partial t$ describes the change in momentum for an unsteady flow and $\rho (\mathbf{u} \cdot \nabla) \mathbf{u}$ the change in momentum caused by convection. The terms on the right hand side describe the driving forces for the change in momentum, i. e. the pressure gradient $-\nabla P$, friction forces $\eta \Delta \mathbf{u}$ and the resulting body forces \mathbf{F}_{vol} on the considered continuum element. An example of a body force is the gravity. \mathbf{F}_{vol} becomes in this case $\rho \mathbf{g}$.

Equation 1.2 is the continuity equation. Together with equation 1.1 they form the *Navier-Stokes-equations*. Other differential equations might be added according to the problem, such as the energy-equation in the case of compressible fluids.

1.4.2. Viscosity

The dynamic viscosity η of a fluid is a measure for the energy dissipation in a fluid due to internal friction [48].

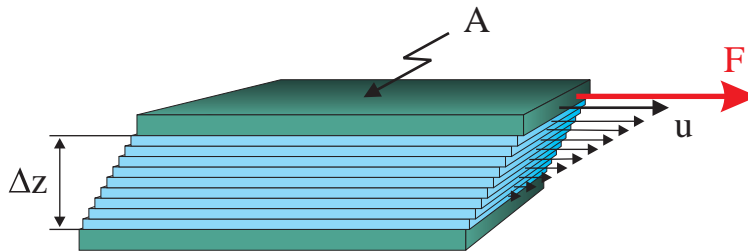


Figure 1.10.: Illustration of the internal friction in a fluid. The force F is needed to overcome this friction, to achieve a steady movement of the upper plate with the velocity u relatively to the lower plate.

To define the viscosity η , a fluid between two plates with a surface area A may be considered and assume the separating distance between these two plates is Δz . The upper plate is moved steadily by

a force F with the velocity u relative to the lower plate, as illustrated in figure 1.10. At the surface, the fluid sticks to the plate; consequently the fluid lamella at the upper plate has the velocity u and the lamella at the lower plate remains at rest. Each fluid lamella exerts a force on the next lamella, due to internal friction. To keep the movement of the upper plate steady, the force F needs to compensate for the internal friction forces. This force is proportional to the surface area A and the velocity difference Δu , but it is inversely proportional to the separating distance Δz :

$$F = \eta A \frac{\Delta u}{\Delta z}. \quad (1.3)$$

The proportionality factor is the dynamic viscosity η . For a constant velocity gradient, equation 1.3 becomes:

$$F = \eta A \frac{du}{dz}. \quad (1.4)$$

This force only depends on the friction between the molecules in the fluid. Fluids, where η is independent from the velocity are called *Newtonian fluids*.

1.4.3. Laminar slit flow and fluidic resistance

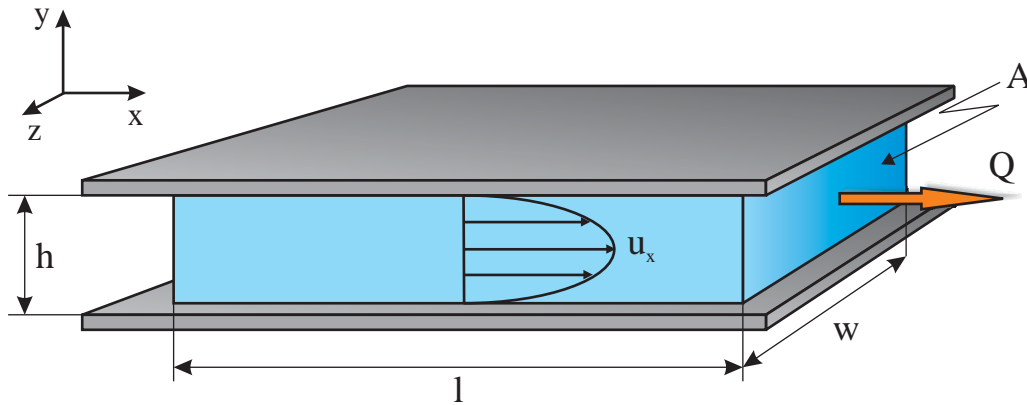


Figure 1.11.: Illustration of the laminar slit flow.

Figure 1.11 shows a fluid flowing through a narrow slit, driven by a pressure gradient in the x -direction. To derive the velocity, the Navier-Stokes-equations (equation 1.1 and 1.2) need to be solved for this problem.

For a fully developed slit flow, all velocity components in the y - and z -directions vanish,

$$u_y = u_z = 0 \quad (1.5)$$

since

$$-\frac{\partial P}{\partial y} = -\frac{\partial P}{\partial z} = 0. \quad (1.6)$$

Equation 1.1 can therefore be simplified:

$$\rho \left(\frac{\partial u_x}{\partial t} + u_x \frac{\partial u_x}{\partial x} \right) = -\frac{\partial P}{\partial x} + \eta \left(\frac{\partial^2 u_x}{\partial x^2} + \frac{\partial^2 u_x}{\partial y^2} + \frac{\partial^2 u_x}{\partial z^2} \right) + \mathbf{F}_{vol}. \quad (1.7)$$

The velocity u_x is constant in the z -direction, since there are no constraints in this direction. Additionally, it is constant in the x -direction, since it is considered to be a fully developed flow, i. e. there is no acceleration in the x -direction.

Since gravity has only a very small effect on microfluidic dynamics [48], the body force term, i. e. the gravity, can be neglected. By considering the constant velocities and $\mathbf{F}_{vol} = 0$, equation 1.7 can be further simplified:

$$\eta \left(\frac{\partial^2 u_x}{\partial y^2} \right) = \frac{\partial P}{\partial x}. \quad (1.8)$$

The solution of this differential equation is:

$$u_x(y) = \frac{1}{2\eta} \frac{\partial P}{\partial x} y(y-h). \quad (1.9)$$

In order to calculate the fluidic resistance of the laminar slit flow, the volumetric flow Q must be derived. The gradient $\partial P/\partial x$ is replaced by $-\Delta P/l$, where l is the length of the slit. The volumetric flow through an area element $dA = w dy$ is:

$$dQ = (w dy) u_x(y), \quad (1.10)$$

where w is the width of the slit. The volumetric flow through the slit is therefore:

$$\begin{aligned} Q &= \int_0^h w u_x(y) dy \\ &= -w \int_0^h \frac{1}{2\eta} \frac{\Delta P}{l} y(y-h) dy \\ &= \frac{wh^3}{12l\eta} \Delta P. \end{aligned} \quad (1.11)$$

The fluidic resistance is the ratio of the pressure loss to the volumetric flow. By inserting equation 1.11 the fluidic resistance for laminar slit flow results in:

$$R_{fl} = \frac{\Delta P}{Q} \Leftrightarrow \boxed{R_{fl} = 12\eta \frac{l}{h^3 w}}. \quad (1.12)$$

By similar methods it is possible to derive the fluidic resistance for other types of channel geometries. Some of them are summarized in table 1.1. Especially the fluidic resistance for rectangular channels is important for many problems in microfluidics, since this geometry is often used by micro-

structuring methods as described in section 1.3.1.




Cross section	Description	Fluidic resistance R_{fl}
	Rectangular	$R_{fl} = c\eta \frac{l}{h^3 w}$ $c = 12 \left[1 - \frac{192}{\pi^5} \frac{h}{w} \tanh\left(\frac{\pi w}{2h}\right) \right]^{-1}$
	Circular	$R_{fl} = 8\eta \frac{l}{r^2}$
	Slit	$R_{fl} = 12\eta \frac{l}{h^3 w},$ <p>for $w \gg h$</p>

Table 1.1.: Fluidic resistance for different channel cross sections. l , w , h are the channel length, width and height, r is the channel radius and η is the viscosity.

1.4.4. Surface tension

Surface tension plays an important role in micro scale channels, due to the high surface-to-volume ration in these dimensions. Consequently, surface forces usually dominate volume forces [48].

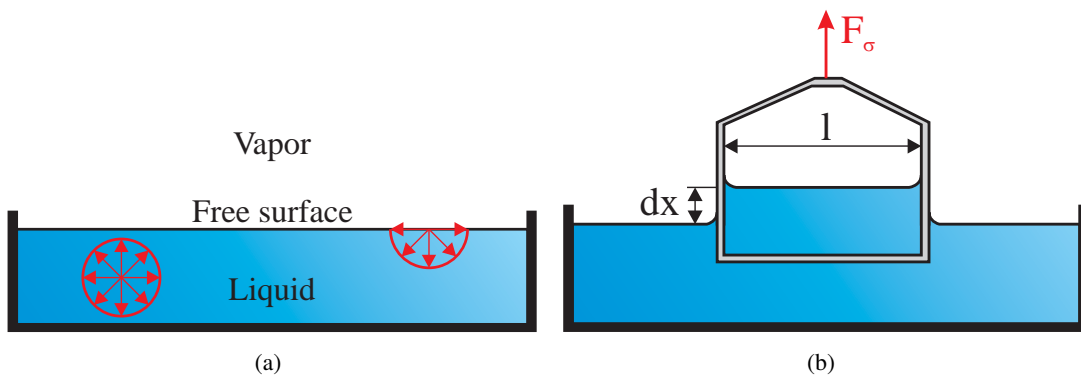


Figure 1.12.: a) Illustration showing that surface tension arises as an imbalance of forces among liquid molecules. b) An experimental setup to measure the surface tension. A wire frame is pulled slowly out of the fluid and the necessary force is a measure for the surface tension.

Surface tension results from attractive cohesion forces between the molecules in a fluid. A molecule within a fluid is surrounded by other molecules and the resulting force in all directions is isotropic (compare figure 1.12a. However, molecules at the surface are only subjected to forces acting on them from the 'sides' and from 'below'. Work has to be applied to increase the surface of a fluid. Consequently, a liquid always tries to minimize its surface and to reduce its free energy [49].

$$\sigma = \frac{dW}{dA}, \quad (1.13)$$

An experiment, as illustrated in figure 1.12b, can be used to measure the surface tension. The applied work is $dW = F_{\sigma} dx$, and the increase of the surface is $dA = 2l dx$. The factor two has to be added, since two surfaces need to be created, one in the front and one in the back.

Equation 1.13 needs to be rewritten for this experiment as:

$$\sigma = \frac{dW}{dA} = \frac{F_{\sigma} dx}{2l dx} = \frac{F_{\sigma}}{2l}. \quad (1.14)$$

1.4.5. Contact angle

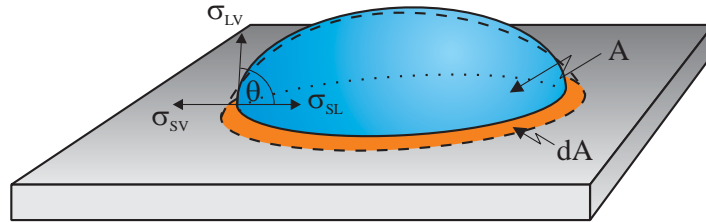


Figure 1.13.: Illustration for the derivation of the static contact angle θ . The droplet wets the area A on a surface. An energy minimum is reached when $dW/dA = 0$. The surface area remains stable at this minimum.

The attractive forces between the molecules in a fluid are called cohesion forces and the ones between molecules of a liquid and a solid surface adhesive forces. The wettability of a surface depends on these two forces. For example, if the adhesive forces dominate the cohesive forces, the surface is wetted, whereas it de-wets in the opposite case.

A droplet sitting on a substrate has three different phase boundaries: the solid-liquid interface with the interfacial energy σ_{SL} , the solid-vapor interface with the interfacial energy σ_{SV} and the liquid-vapor interface with the interfacial energy σ_{LV} . Figure 1.13 illustrates the derivation of the contact angle θ .

The virtual displacement of the contact line and its resulting variation of the free energy W is [49]:

$$dW = \sigma_{SL} dA - \sigma_{SV} dA + \sigma_{LV} \cos \theta dA. \quad (1.15)$$

The energy minimum is reached when $dW/dA = 0$. Solving this equation for $\cos \theta$ leads to the

Young equation:

$$\cos \theta = \frac{\sigma_{SV} - \sigma_{SL}}{\sigma_{LV}} \quad (1.16)$$

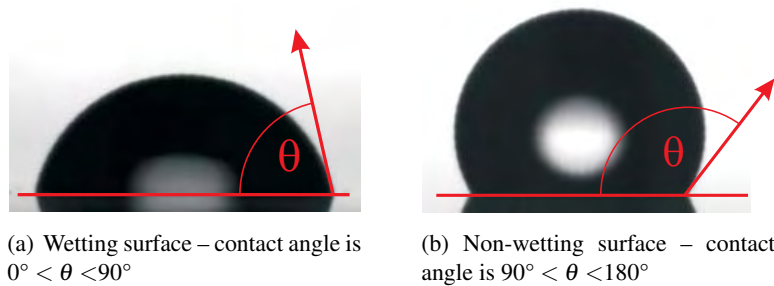


Figure 1.14.: Two examples of the wetting behavior of liquids (wetting vs non-wetting surfaces).

The contact angle θ at a solid-liquid interface is a measure of the degree of wettability. If the angle lies between 0° and 90° , the surface is partially wetted by the fluid (see figure 1.14a). If it is between 90° and 180° it is called non-wetting (figure 1.14b).

1.4.6. Capillary pressure

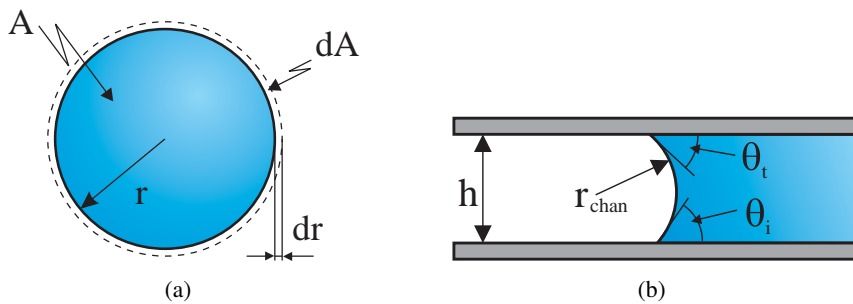


Figure 1.15.: Sketches for the derivation of the capillary pressure. a) for a circular droplet and b) in a slit, with the contact angles θ_t to the upper wall and θ_i to the lower wall.

Since no additional driving forces are needed, capillary effects are very useful in microfluidic devices with its typically small channel dimensions. A curved interface between the liquid and the vapor phase causes a pressure perpendicular to this interface, due to surface tension.

The internal pressure P of a circular fluidic droplet, as illustrated in figure 1.15a can be calculated

by using equation 1.13. The work dW , which has to be applied to increase the surface area by dA is:

$$\begin{aligned} dW &= \sigma dA \\ &= \sigma h(2\pi(r + dr) - 2\pi r) \\ &= 2\pi\sigma h dr. \end{aligned} \quad (1.17)$$

On the other hand $dW = P_{\text{cap}} dV$ or:

$$dW = P_{\text{cap}} A dr = P_{\text{cap}} 2\pi h r dr. \quad (1.18)$$

Equation 1.17 and (1.18) have to be equal and therefore P_{cap} results in:

$$P_{\text{cap}} = \frac{\sigma}{r}. \quad (1.19)$$

For a surface with two different radii (one in the x -direction and the other one in the y -direction) equation 1.19 becomes the *Young-Laplace-Equation*:

$$P_{\text{cap}} = \sigma \left(\frac{1}{r_x} + \frac{1}{r_y} \right). \quad (1.20)$$

A consequence of this equation is that the capillary pressure or *laplacepressure* increases for smaller radii r_x and r_y .

In a slit with a contact angle θ_t to the top wall and a contact angle θ_i to the lower wall, as illustrated in figure 1.15b, the radius of the curvature in the slit r_{slit} is given by:

$$r_{\text{slit}} = -\frac{h}{\cos \theta_t + \cos \theta_i}. \quad (1.21)$$

The resulting pressure of this curvature is therefore:

$$P_{\text{slit}} = -\sigma \frac{\cos \theta_t + \cos \theta_i}{h}. \quad (1.22)$$

1.5. Droplet-based microfluidics and its modules

This section aims at presenting the basic modules for droplet-based microfluidics. To discuss all of the techniques developed so far in this field would exceed the scope of this brief review. Nevertheless, a large number of diverse and fascinating techniques have been developed within the past 6-7 years [52–56, 51, 57–61]. Two examples, which can be very useful, but which are not discussed in detail are shown in figure 1.16. The main intention in this section is to focus on the droplet-based modules

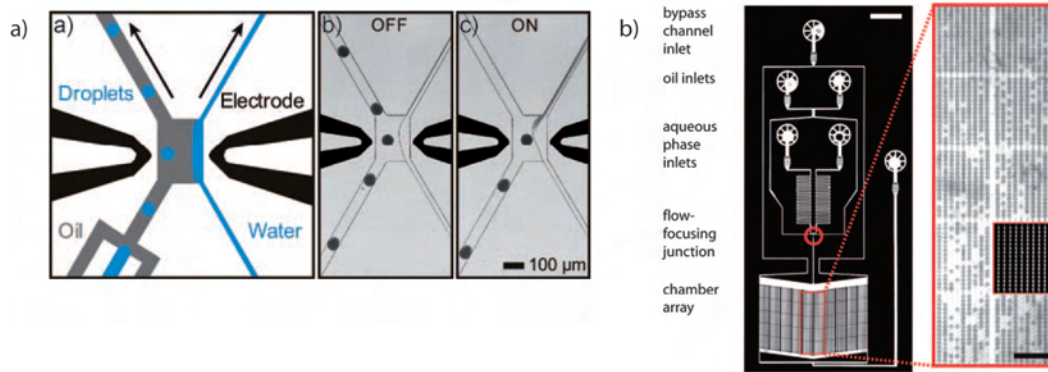


Figure 1.16.: Examples of more specialized droplet microfluidic modules. a) This module allows to fuse droplets into an aqueous stream, giving the opportunity to connect the multiphase droplet world to single phase microfluidics. b) Is a droplet park and observation module. Thousands of droplets can be stored, fixated and monitored in parallel. a) Reprinted from [50] and b) from [51].

that are applicable to the majority of applications.

1.5.1. Droplet creation

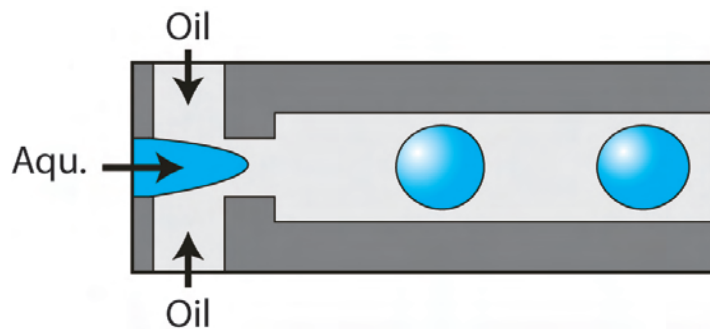


Figure 1.17.: Droplet creation at a flow focussing nozzle.

Generally, instability and nonlinearity are not present in microfluidics since inertial effects can be neglected [48]. As most microfluidic devices operate at low Reynolds numbers, the *Navier-Stokes-equation* (equation 1.1) becomes linear and the flow is laminar. In contrary, by interaction of two immiscible fluids it is possible to introduce nonlinearity and instability, which leads to droplet formation [62, 63]. It is achieved by high shear forces generated at the leading edge of the water perpendicular to the oil flow [64]. The two important effects are non-static boundary is and that the motion of one fluid can entrain the other. The common understanding is that droplet generation in flow focusing designs (as shown in figure 1.17) is the result of a competition between surface tension and shear forces [62, 65, 64].

By operating such a flow focusing device, droplets with a narrow size distribution can be created

(< 3%) [16]. It depends thereby on the surface coating and the type of surfactant whether it creates water-in-oil or oil-in-water droplets. In general, the inner fluid almost completely fills the width of the neck and the second phase exerts a drag on the thread. A neck forms due to the shear stress and brakes on finite time scale since the equilibrium of the interfacial tension and the hydrostatic pressure occurs much slower. In addition, the usage of surfactant reduces the surface tension thus favoring droplet breakup.

1.5.2. Mixing within droplets

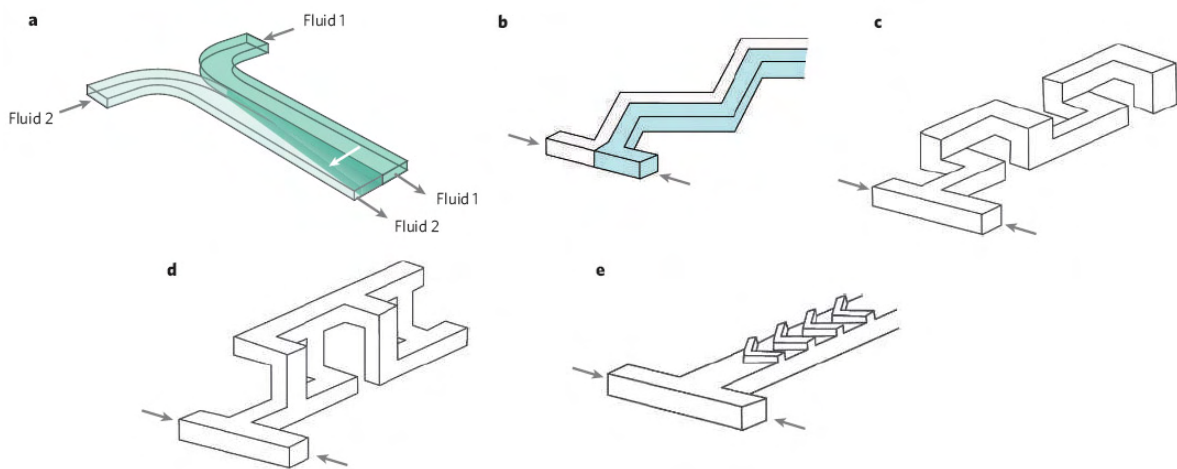


Figure 1.18.: Microfluidic approaches for mixing in continuous flow. a) Mixing of two miscible fluid streams under laminar flow conditions. The component streams mix only by diffusion, creating a dynamic diffusive interface with predictable geometry. b) Zigzag-shaped channel for chaotic mixing at high Reynolds numbers [66]. c) Three-dimensional L-shaped channel for chaotic mixing at intermediate Reynolds numbers [67]. d) Three-dimensional, connected out-of-plane channel for chaotic mixing at intermediate Reynolds numbers. e) Staggered-herringbone grooves for chaotic mixing at low Reynolds numbers [68]. Reprinted from [69].

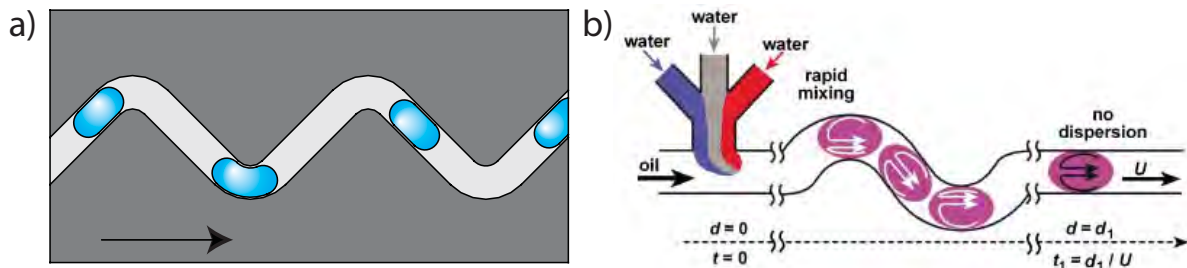


Figure 1.19.: Mixing within droplets. a) A winding channels accelerates mixing within droplets. b) Illustration of the mixing mechanism. By changing the direction of the droplet also its internal circulation pattern changes. This increases the mixing efficiency. Part b) reprinted from [17].

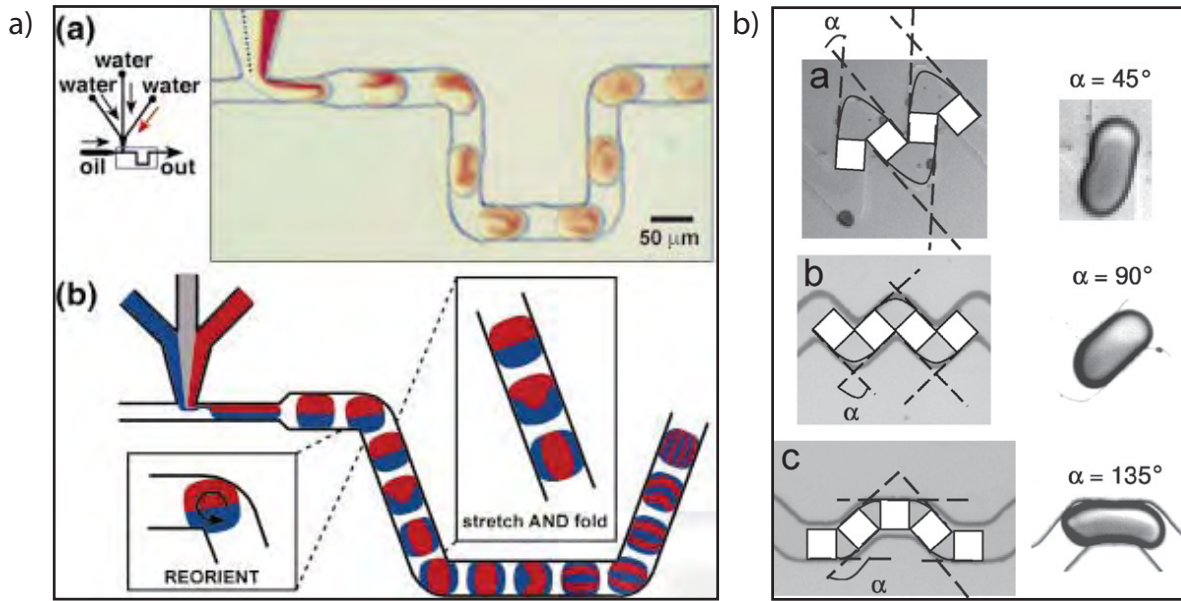


Figure 1.20.: a) Mixing by the baker's transformation in droplets moving through winding microfluidic channels shown (i) experimentally and (ii) schematically. b) Illustration of different angel geometries for the winding channel. Part a) reprinted from [70] and part b) from [71].

The mixing of reagents in microfluidic devices is an essential process and typically it is slow in such microscale systems, since the streams of reagents flow laminarly at low Reynolds numbers. In the absence of advection, diffusive mixing (see figure 1.18a) is the dominant mechanism. In this type of process the mixing time t_{diff} is proportional to the square of the initial striation length s_l - the distance over which the mixing occurs by diffusion with a diffusion coefficient D [70]:

$$t_{\text{diff}} \propto \frac{s_l^2}{2D} \quad (1.23)$$

Mixing that occurs solely by diffusion is often too slow for some applications within microfluidic systems, including high-throughput analysis and kinetic measurements. Consequently, some efforts have been directed towards addressing this issue. Figure 1.18b,c,d,e show some of these attempts in single phase systems.

For droplet-based microfluidics, it has been shown that droplets moving in a straight channel generate a steady, recirculating flow in each hemisphere [72, 73]. This flow mixes the fluid only within the two hemispheres of the plug, but not across the centerline. A droplet moving through a winding channel (see figure 1.19a) sequentially undergoes different internal circulation direction changes [17] and thereby moves the centerline back and forth into the two mixing hemispheres as illustrated in figure 1.19b. Another explanation of the effect these winding channels have, is shown in figure 1.20a. Chaotic flow in droplets moving through winding channels may be represented by the baker's transformation [70]. The baker's transformation can be described as a series of stretches, folds, and reorien-

tations that decrease the striation length. By this method the mixing times in droplets can be reduced into the order of only a few milliseconds [17, 70, 74].

Further detailed studies on the geometries of the winding channels revealed that the angle plays a crucial rule for the mixing efficiency [71] as shown in figure 1.20b. Whereas the 45° and 90° bend configurations show efficient mixing properties, the 135° configuration does not seem to have great improvements compared to the straight channel. It appears that this design cannot force the inner fluid to reorientate and the mixing time is about one order of magnitude higher [71] than for the other configurations.

1.5.3. Splitting of droplets

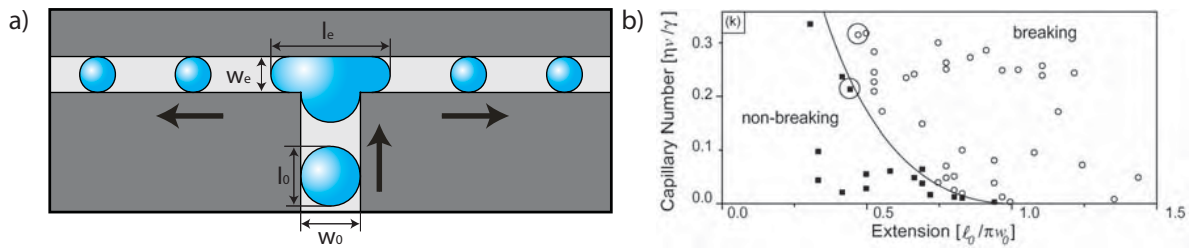


Figure 1.21.: *Splitting of droplets. a) Illustration. b) Plot showing droplets which break (open circles) and those who do not (squares) for various droplet velocities (v or Ca) and initial extensions l_0 . A function for the critical capillary number (equation 1.25) separates the two regimes. Part b) was Reprinted from [19].*

A methodology for passively breaking droplets into smaller daughter droplets [17] is illustrated in figure 1.21a. The sizes of these daughter droplets depend upon the ratio of flow-rates running through the two outlet channels. The volume relation is given by:

$$V_1/V_2 = Q_1/Q_2, \quad (1.24)$$

whereby V_1, V_2 are the volumes of the two daughter droplets and Q_1, Q_2 are the flow-rates in the two channels. Especially the case of equal flow-rates in both channels may be useful because droplets can be repeatedly split without increasing the polydispersity of the droplet population [19].

Whether or not droplets divide at a junction depends on the initial extension a_0 (ratio of droplet length l_0 to circumference πw_0) and the droplet velocity v . When a droplet enters a junction it becomes elongated up to a maximum extension $a_e = l_e/\pi w_e$ and splits only if $a_e \geq 1$ [19]. This limit is consistent with the classical *Rayleigh-Plateau instability* in which a cylindrical liquid thread can reduce its total surface area by breaking up when its length exceeds its circumference.

Practically, these findings mean that droplets with an initial extension of ≥ 1 will always split at the junction at all flow-rates. In order to split smaller droplets additional force must be applied by increasing the droplet velocity. The limit is usually expressed by the critical capillary number $Ca = \eta u/\sigma$. Using various flow conditions, the Ca as a function of the measured initial extension a_0

was measured and the results are plotted in figure 1.21b. Droplets that break are represented by open circles, those which do not split are represented by solid squares. Consistent with the expectations, droplets whose initial extension values are larger than one, always break, while the critical capillary number Ca_{cr} separates regions of breaking and non-breaking droplets. It has been determined to be:

$$Ca_{cr} = \alpha a_0 (1/a_0^{2/3} - 1)^2, \quad (1.25)$$

where α is a dimensionless constant that is a function of the viscosity contrast of the two fluids and the geometry of the channel [19]. This relationship between Ca_{cr} and l_0 is shown in figure 1.21b with a fitted constant of proportionality $\alpha = 1$. The predicted criteria for breakup is in excellent agreement with the experimentally observed transition.

1.5.4. Droplet fusion

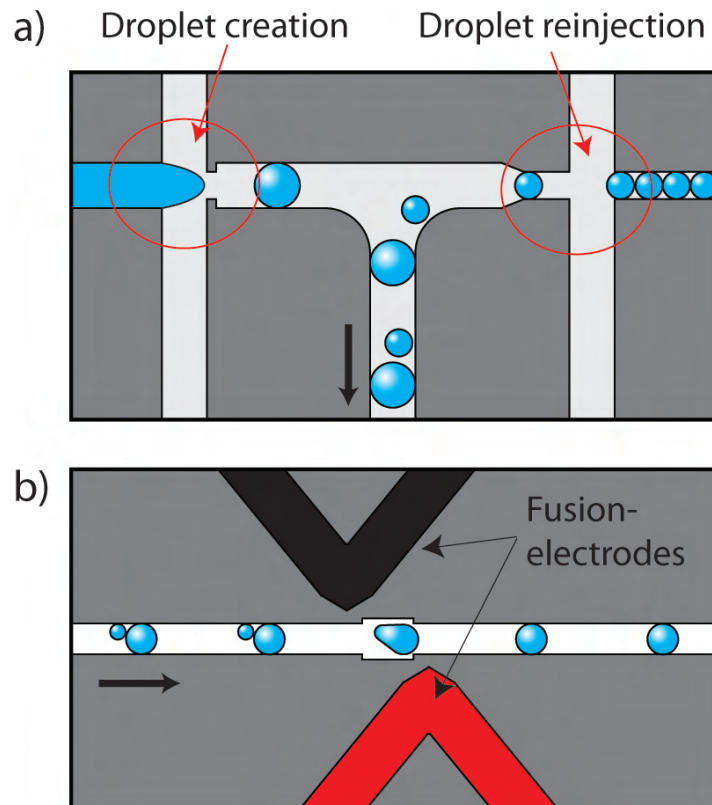


Figure 1.22.: The process of pairwise droplet fusion is divided into two parts. a) Two nozzles need to be synchronized, whereby usually one nozzle reinjects droplets and the other one creates droplets. The droplets then pair-up while exiting through the outlet channel. b) By applying an electrical field over the two electrodes droplet-pairs can be coalesced.

The purpose of this module is to fuse two independent droplets with each other. Usually this method is used to add a compound or a mixture of reagents to an already preformed emulsion. An emulsion is

reinjected into the module and a second stream of droplets is created at another nozzle (see figure 1.22). The whole process consists out of two independent operations. First it is necessary to pair the droplets one-by-one (see figure 1.22a) and next, these droplet pairs are coalesced (see figure 1.22b).

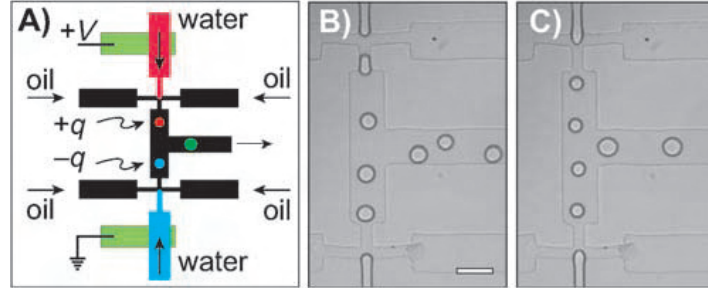


Figure 1.23.: (a) Droplets having opposite sign of electrostatic charge can be generated by applying a voltage across the two aqueous streams. (b) In the absence of an electric field the frequency and timing of droplet formation at the two nozzles are independent and each nozzle produces a different-sized droplet at a different frequency; the infusion rates are the same at both nozzles. After the confluence of the two streams, the droplets from the upper and lower nozzles stay in their respective halves of the stream and, owing to the presence of surfactant, do not coalesce even in the case of large droplets that fill the width of the channel (scale bar: $100\ \mu\text{m}$). (c) With an applied voltage of 200 V across the 500-micron separation of the nozzles, the droplets simultaneously break off from the two nozzles and are identical; simultaneous droplet formation can be achieved for unequal infusion rates of the aqueous streams even up to a factor of two difference in volumes. Reprinted from [20].

Synchronization can be achieved by adjusting the flow-rates of the two nozzles. The reinjected emulsion arrives with a selected flow-rate Q , determining the droplet frequency f :

$$f \approx Q/V_d, \quad (1.26)$$

where V_d is the droplet volume. The oil flow at this nozzle has the sole purpose of spacing the droplets before they enter the synchronization channel. At the second nozzle the flow-rates of the aqueous and the oil phase need to be adjusted in order to achieve approximately the same frequency as the reinjected emulsion. The two emulsions meet in the synchronization channel and droplets pair due to different traveling speeds of differently sized droplets [17, 18]. Usually small droplets travel faster than larger droplets since they only travel in the faster streamlines in the center of the channel. Larger droplets travel with a speed averaged over all *Poiseuille flow* flow-lines [18]. Due to these different traveling speeds the small droplets catch up to the larger ones and form droplet pairs. Nevertheless depending on the system there have also been reports of the opposite behavior where larger droplets catch up to the smaller ones [17, 30]. Hydrodynamic chromatography [75] has been claimed to be the reason for this [17].

After the droplets have paired they can be coalesced, either passively (usually in the absence of surfactants) [17, 55] or actively by introducing hydrophilic patches on the channel walls [76] or by electrical fields [18, 77, 30]. For this purpose electrodes on both sides of the channel polarizes the droplets and due to the electrical force the droplets merge.

An alternative method to this strategy has been proposed by Link *et al.* [20], where two nozzles create droplets synchronized by electrical fields. The emitted droplets are charged and fuse in the moment of contact (see figure 1.23). This method can only be used when both nozzles create droplets - it is not applicable for a reinjected emulsion and its longterm stability still needs to be shown.

1.5.5. Droplet sorting

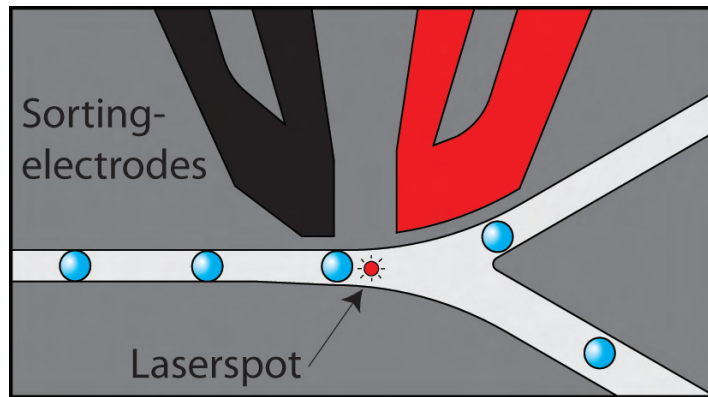


Figure 1.24.: *Sorting of droplets. Without applying an electrical field, droplets move into the lower channel. Only if an electrical field is applied over the electrodes droplets are pulled into the upper channel. The decision whether a droplet is selected is usually based on the fluorescent emission signal activated by the laser spot.*

Usually a sorter is designed as a channel-junction with electrodes on one side of the channel [20, 21] (figure 1.24). In the absence of an electrical field, droplets follow the path of the larger flux into one of the two arms of the junction. By either decreasing the fluidic resistance or externally forcing a higher flow-rate into the lower channel in figure 1.24 (i. e. by connecting the outlet to a syringe pump) all droplets can be directed into this direction. When the voltage is on, the electrical field elongates and displaces the droplets towards the electrodes and the droplets get pulled into the upper channel. If this voltage is triggered based on the content of a droplet, it is possible to sort the droplets into these two channels. A fast and convenient way to differentiate the droplet content, is using fluorescence and there are a variety of chemical and biological assays using fluorophores which can be used for such a purpose. Droplets flowing down the channel pass a laser spot which excites the fluorophores. The emission is recorded by an optical setup (see section 1.3.2) and processed by an appropriate software. Depending on the emission intensity, the voltage can be switched on and the droplets can be sorted.

The velocity v with which droplets get directed towards the electrodes is determined by the dielectrophoretic force F_d acting on a droplet:

$$\mathbf{F}_d = \mathbf{m} \cdot \nabla \mathbf{E}, \quad (1.27)$$

where \mathbf{m} is the dipole moment of the droplet and \mathbf{E} is the electric field. For a spherical droplet of

radius r , in an oil of dielectric permittivity ϵ_{oil} , the induced dipole moment is given by:

$$\mathbf{m} = 4\pi\epsilon_{\text{oil}}\text{Re}[CM(\omega)]r^3\mathbf{E}, \quad (1.28)$$

where $\text{Re}[CM(\omega)]$ is the *Claussius-Mossotti factor*. For water droplets in oil and for frequencies from DC to several MHz $\text{Re}[CM(\omega)] = 1$. The dielectrophoretic force on the droplets is balanced by the viscous or *Stokes drag*:

$$\mathbf{F}_s = 6\pi\eta_{\text{oil}}r\mathbf{u} \quad (1.29)$$

Thus, the velocity of the droplet is:

$$\mathbf{u} = \eta_{\text{oil}} \frac{r^2 \nabla \mathbf{E}^2}{3\eta_{\text{oil}}} \quad (1.30)$$

$$\Rightarrow \mathbf{u} = \epsilon_{\text{oil}} \frac{r^2 k U^2}{3\eta_{\text{oil}}} \quad (1.31)$$

where U is the applied voltage and k is a geometric factor determined by electrode shape and location.

1.6. Applications of compartmentalization in emulsions

1.6.1. Emulsion PCR (ePCR)

One of the most important biotechnological advances made in the 20th century involved methods that converted single DNA molecules into populations of identical DNA molecules. The first wave of techniques used cells (cloning) [78] and the second used PCR [79]. Therefore, it is not surprising that so far, in the commercial sense one of the most successful applications of compartmentalization is emulsion polymerase-chain-reaction (ePCR) [15, 80].

With ePCR, it is possible to clonally amplify templates from complex mixtures in a bias-free manner. The DNA molecules are segregated in droplets, such that each droplet contains no more than a single template, i. e. the droplets are monoclonal. The advantage of this is that each template is amplified in isolation avoiding competition between multiple amplicons. Isolation of individual PCR reactions prevents preferential amplification of one template over another due to differences in amplification efficiencies caused, for example, by different lengths and G/C contents. Amplification in isolation also prevents generation of artifactual fragments by recombination between homologous regions of different DNA templates [81]. Thus, amplification by ePCR reflects the original composition of complex mixtures of genes, such as encountered in genomic and cDNA libraries, much better than conventional PCR and a homolog amplification can be realized.

For many applications, it is favorable to recover the DNA from the emulsion and preserve the monoclonal nature. This is not possible by simply breaking the emulsion and pooling the content of all droplets. A method to overcome this problematic is called BEAMing (beads, emulsions, amplification and magnetics) [80, 83] (see figure 1.25b). It is a process built on ePCR that (i) includes beads within

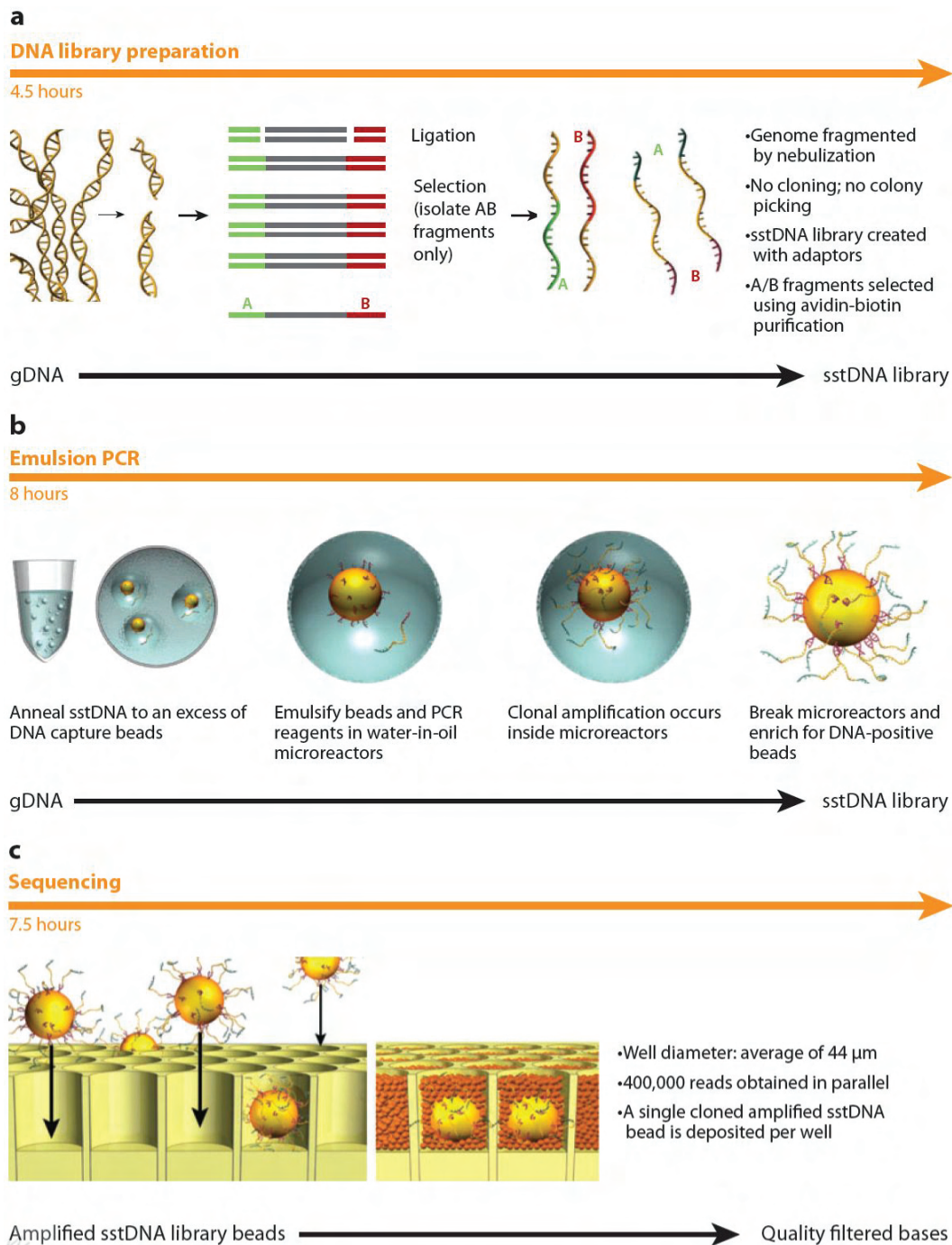


Figure 1.25.: The method used by the Roche/454 sequencer to amplify single-stranded DNA copies from a fragment library on agarose beads. A mixture of DNA fragments with agarose beads containing complementary oligonucleotides to the adaptors at the fragment ends are mixed in an approximately 1:1 ratio. The mixture is encapsulated by vigorous vortexing into aqueous micelles that contain PCR reactants surrounded by oil, and pipetted into a 96-well microtiter plate for PCR amplification. The resulting beads are decorated with approximately 1 million copies of the original single-stranded fragment, which provides sufficient signal strength during the pyrosequencing reaction that follows to detect and record nucleotide incorporation events. Reprinted from [82].

the compartments and (ii) ensures that one strand of the PCR product is bound to the beads. Millions of these monoclonal beads, carrying several thousands copies of the single DNA molecule originally present in the droplet, can be analyzed within minutes using flow cytometry or optical scanning instruments. The signal-to-noise ratio obtained by hybridization or enzymatic assays is extremely high since each bead contains thousands of molecules of the identical sequence and DNA bound to beads provides excellent templates for other applications.

Currently a potential draw-back of this technology might be that the efficient amplification on beads is limited to relatively short amplicons (<250 bp) [83]. Nevertheless, it has already proven to be useful for detection and quantification of rare genetic variations [84, 80, 85], high-throughput screening of transcription-factor targets [86], directed evolution of DNA polymerases [87, 88], single-molecule reverse-transcription PCR [89], haplotyping [90] and amplification of complex gene libraries [81].

Some of the methods described above are now being transferred into microfluidic droplets [91, 92, 34, 93], thus allowing direct integration with other droplet unit operations, such as fluorescence-based monitoring of the amplification. In some newer systems, the PCR can be carried out in a continuous fashion by guiding the droplets through different heat zones allowing for denaturation, annealing and extension [94, 95]. Amplification in these droplets is efficient enough to start from a single gene per droplet making so call 'digital PCR' [96, 97] feasible. It is a method to detect and quantify minute amounts of DNA, e. g. in medical diagnostics or in analytical applications. The analysis of a 'digital PCR' experiment is based on a count of the total number of droplets and droplets in which amplification was successful (corresponding to the presence of template DNA in these droplets) [94]. Thus 'digital PCR' transforms exponential analog data from conventional PCR to more reliable linear digital signals [96, 97].

Although thermocycling is the most common DNA amplification strategy, it is not the only one. Several isothermal DNA amplification methods exist, which do not require thermocycling [98]. This makes integration with other droplet operations and biochemical experiments convenient, since no equipment for heat control of the droplets is necessary. This strategy has been applied in one of the co-authored works [35] (see section A.0.3).

1.6.2. Next generation sequencing methods

Most notably among all applications of ePCR on microbeads, this technology is a key step for some of the high-throughput second generation sequencing platforms, as e. g. 454 [99] (see figure 1.25), SOLiD [100] and Polonator [100] where in vitro clonal arrays are sequenced, avoiding the potential bias and the bottlenecks of transformation and colony picking that bacterial cloning introduces [101, 82]. Next-generation DNA sequencing has the potential to dramatically accelerate biological and biomedical research, by enabling the comprehensive analysis of genomes, transcriptomes and interactomes to become inexpensive, routine and widespread, rather than requiring significant production-scale efforts [101].

Many of the techniques described so far do not necessarily include microfluidics yet. These bulk

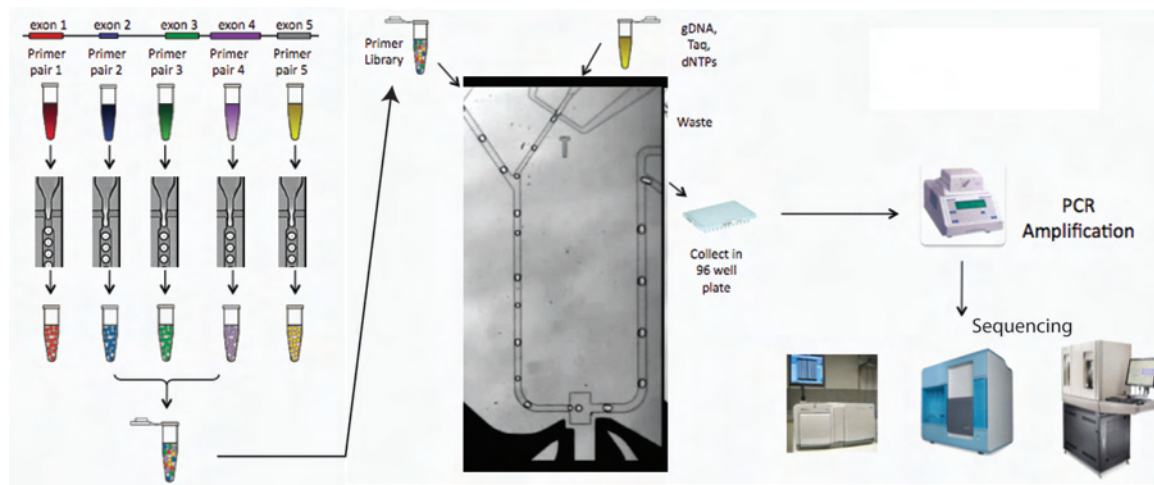


Figure 1.26.: Targeted sequencing workflow.

emulsions have the advantage of being easily and quickly generated and do not need a great technological effort. Nevertheless, by using microfluidics and in particular droplet-based microfluidics, applications can benefit from at least two great advantages: the monodispersity of the droplets and the ability to add reagents to individual droplets (see section 1.5.4). A specific example is an approach to targeted sequencing developed by RainDance Technologies [102] - the first commercially available platform using microfluidic droplets. The platform shown in figure 1.26 enables target enrichment for targeted sequencing for numerous biomedical applications, including genomics research, gene expression analysis, drug development, and key marker detection of diseases for personalized medicine. For the latter application, a collection of primer pairs corresponding to selected genomic targets are encapsulated in microfluidic droplets, collected, pooled, shipped to the customers and then merged with droplets containing the genomic sample DNA and the PCR reaction mixture, followed by off-chip thermo-cycling. The amplification products of enriched sequences are recovered by breaking the emulsion, purified and processed for second generation sequencing using standard sequencing library preparation methods. Here, microfluidics enables controlled droplet fusion, allowing easy combination of the primer library with the genomic DNA. In turn, the use of monodisperse droplets improves target enrichment uniformity, reducing the amount of oversampling necessary for the reliable detection of rare alleles and thus saving sequencer capacity.

1.6.3. Directed evolution

The key practical consideration in directed evolution of functional biomolecules is the linkage of genotype and phenotype [104]. 'Phenotype' means the functional trait, such as binding or catalytic activity, and 'genotype' the nucleic acid that can be replicated. Nature links genotype and phenotype by compartmentalizing genes in cells. Successful directed evolution experiments have generally employed colony screening, auxotrophic selections or cell surface display [105, 106]. However, probably the

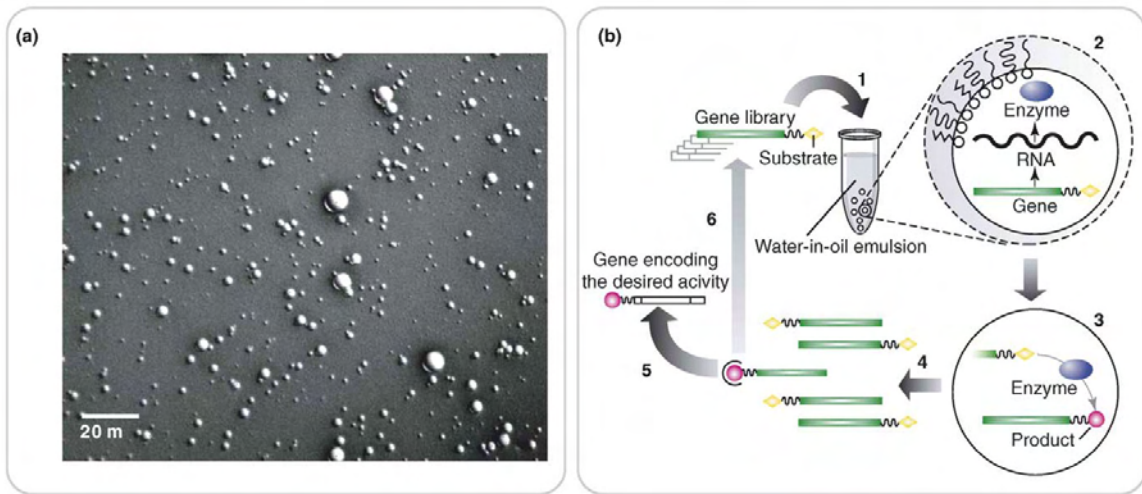


Figure 1.27.: Directed-evolution using gene-product linkage. (a) Optical microscopy of a typical w/o emulsion. (b) Schematic representation of IVC selection by physical gene-product linkage in droplets. 1: An IVT reaction mixture containing a library of genes linked to a substrate is dispersed to form a w/o emulsion with typically one gene per aqueous compartment. 2,3: After transcription/translation, proteins (or RNAs) with enzymatic activities convert the substrate into a product that remains linked to the gene. 4: Next, the emulsion is broken. 5,6: Genes linked to the product are selectively enriched, then amplified and either characterized or linked to the substrate and compartmentalized for further rounds of selection. Reprinted from [12].

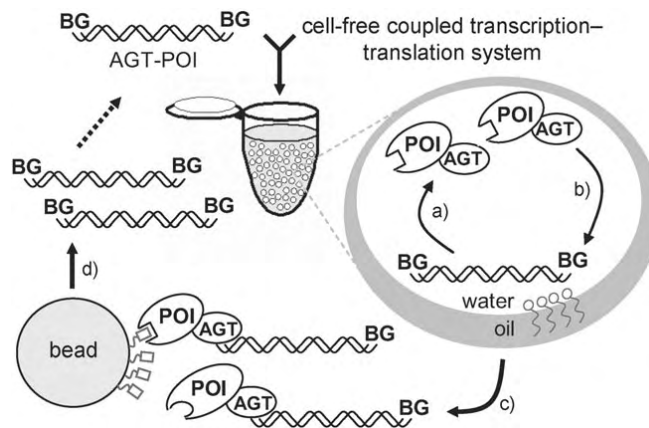


Figure 1.28.: Directed-evolution using SNAP display. (a) A fusion protein of AGT and the protein of interest is expressed in emulsion compartments by IVT. The coding DNA is labelled with BG. (b) A covalent link between genotype and phenotype is created through treatment of the AGT fusion protein with BG attached to its own coding DNA. (c) The emulsion is broken, and magnetic beads carrying immobilized ligands bind cognate protein tags. (d) PCR amplification of enriched DNA. Reprinted from [103].

best-established technology is phage display [107], wherein the selected protein is fused to a phage coat protein, providing the link to the viral DNA. Phage display can be regarded as an *in vivo* method, as the proteins are expressed by cells, although selections take place under *in vitro* conditions and it is possible to routinely select from large libraries ($<10^{12}$, although typically closer to 10^8) [108].

Such *in vivo* methods are hampered by one or more of the following factors: the inability to select under conditions different from the cellular environment problems with the selection of proteins that are toxic, a low dynamic range, cells circumventing selection pressure and low transformation efficiency (generally limiting the library size typically to below 10^8) [109]. Even the scope of phage display is limited: proteins toxic to *Escherichia coli* and proteins whose (largely unpredictable) export is suboptimal may be prevented from displaying on phage.

New *in vitro* techniques could bypass these problems. Their main potential advantage is that, by cutting out transformation and cloning, library sizes can be much larger (up to the physical limit of DNA in solution that fits in a tube - depending on the size of the gene, well above 10^{15} molecules), enabling the exploration of a larger fraction of sequence space. In addition, selections can be performed under more stringent control - with non-natural amino acids, extremes of pH or temperature, and under desired non-physiological conditions. However, all of this will only be possible if the genotype-phenotype link is robust enough to survive these conditions, because only protein molecules coupled to their encoding nucleic acid can be selected.

Much of the cell-free work has been made possible by the commercial availability of *in vitro* translation [110], or transcription and translation systems from *E. coli*, as well as from yeast and wheat germ [111]. These extracts (or 'purer' versions [112] with designed functionality) contain all the necessary ingredients for *in vitro* protein expression (IVE). Proteins larger than 160 kDa have been expressed by IVE [113] and a large fraction of a given proteome can be expressed [114].

In vitro compartmentalisation (IVC) [15] mimics natural cell compartments by creating, in effect, cells that perform only the one reaction to be selected. In a typical procedure, members of the nucleic acid library are partitioned into microscopic compartments, so that, on average, one copy exists per droplet. Using IVE, multiple copies of the corresponding protein are synthesized in the compartment. The small size of the droplets enables large library sizes to be handled. For example, a 50 μ L reaction mixture can be dispersed into $\sim 10^{10}$ compartments (see figure 1.27a). These bulk emulsion methods have been applied to evolve catalytic properties of enzymes and RNAs, binding of peptides and proteins as well as regulatory activities [12, 115, 116].

The selection strategies pursued can be grouped into three main categories:

(i) The substrate and the subsequent product of the selected enzymatic activity are physically linked to the gene (see figure 1.27b). Enzyme-encoding genes, with the product attached, can be separated e. g. by affinity purification using a product-specific ligand. The simplest applications of this strategy lie in the selection of DNA-modifying enzymes, where the gene and substrate comprise the same molecule; indeed, IVC was first applied for the selection of DNA-methyltransferases [15]. Selection was performed by extracting the genes from the emulsion and subjecting them to digestion by a cognate restriction enzyme that cleaves the nonmethylated DNA. Other examples in this category

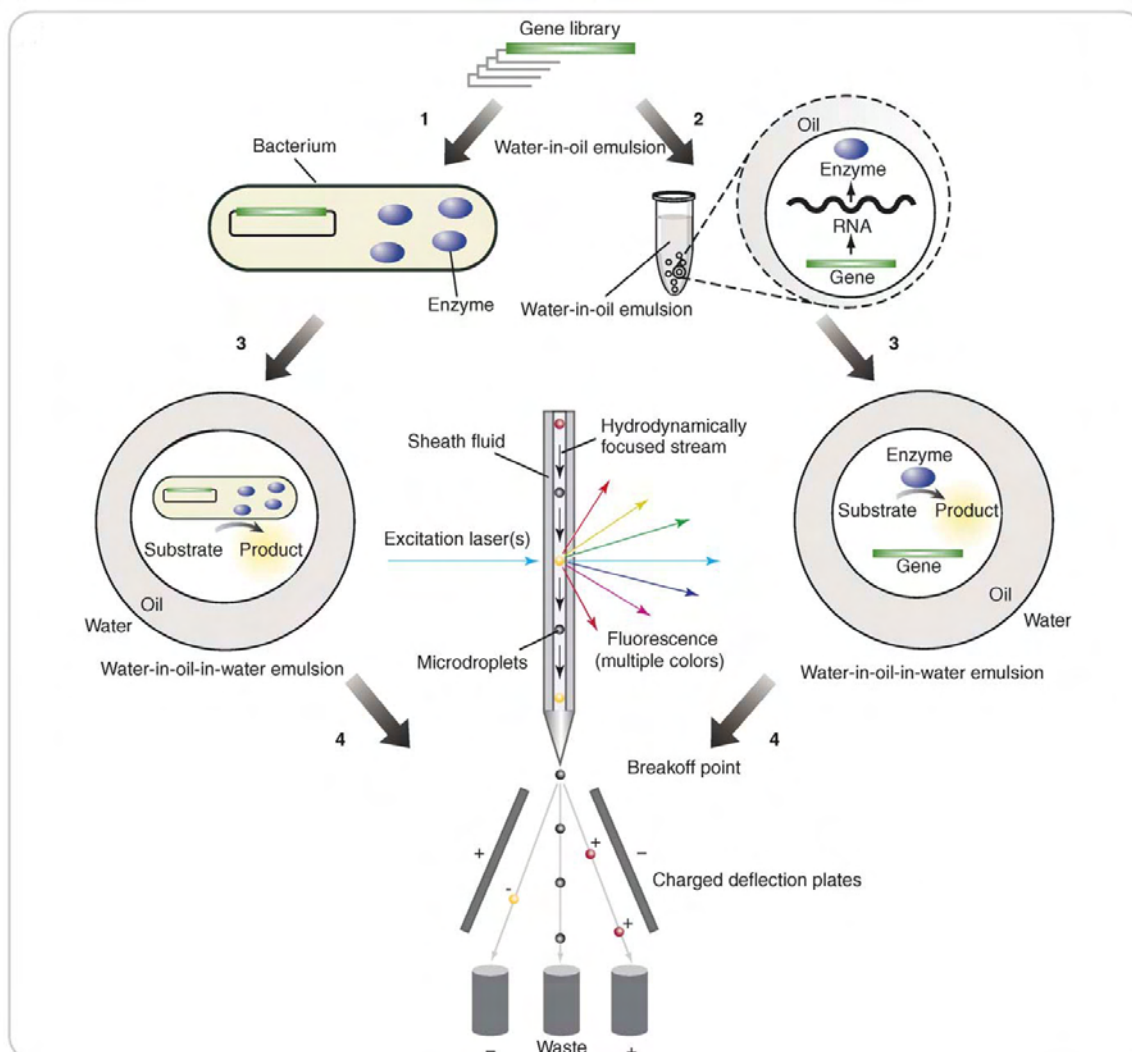


Figure 1.29.: Selections by fluorescence-activated cell sorter (FACS) sorting of double emulsion droplets. 1: A gene library is transformed into bacteria, and the encoded proteins expressed in the cytoplasm, periplasm or the surface of the cells. The bacteria are dispersed to form a w/o emulsion, with typically one cell per aqueous microdroplet. 2: Alternatively, an IVT reaction mixture containing a library of genes is dispersed to form a w/o emulsion, with typically one gene per aqueous microdroplet, and the genes are expressed within the microdroplets. 3: Proteins with enzymatic activity convert the non-fluorescent substrate into a fluorescent product, and the w/o emulsion is converted into a w/o/w emulsion. 4: Fluorescent microdroplets are sorted using FACS. The genes encoding the active enzymes are recovered either by propagating the bacteria or amplifying the DNA from the fluorescent droplets. Reprinted from [12].

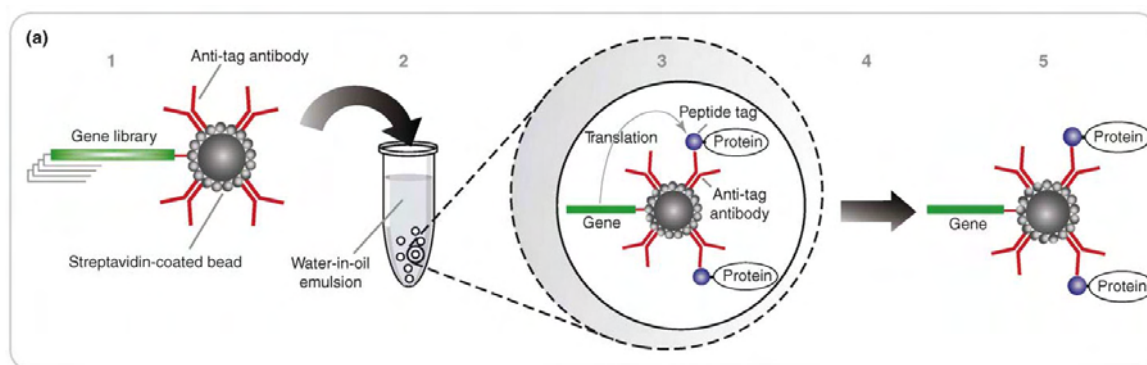


Figure 1.30.: Creation of protein and DNA microbead-display libraries. 1: A single gene of a repertoire of genes encoding protein variants, each with a common epitope tag, is linked to 1-2 μm streptavidin-coated beads carrying antibodies that bind the epitope tag. 2: The beads are compartmentalized in droplets. 3: After transcription and translation the proteins become attached to the bead and by means as well to the gene that encodes it. 4,5: The emulsion is broken, and the microbeads carrying the display library are isolated. Reprinted from [12].

are the evolution of polymerases with new properties such as increased thermostability or an altered substrate range [87, 117, 88]. The strategy of selecting for gene-product conjugates, with non-DNA substrates was e. g. demonstrated by selecting Diels-Alderase ribozymes for intermolecular catalysis and multiple turnovers [118].

(ii) In the second selection category, a stable DNA-protein linkage is formed in the droplet which persists after the emulsion is broken. In affinity selections for binding by 'panning' against a target molecule, binders are enriched and can be decoded via the attached DNA. The link between protein and DNA can be made in a number of ways. In STABLE, [119] the expressed proteins are fused to streptavidin and become non-covalently attached to its biotinylated coding DNA. In M.Hae III display [120], the conjugation is covalent and occurs via a DNA-methyltransferase (M.Hae III) fused to the protein of interest, which reacts irreversibly with a fluorocytidine analogue present at one end of the coding DNA fragment. Likewise, a covalent linkage is formed in the SNAP-display [103] (see figure 1.28) where a SNAP-tag (O6-alkylguanine-DNA alkyltransferase) reacts covalently with its suicide-substrate O6-benzylguanine (BG) incorporated into the linear coding DNA templates. The latter systems with covalent linkages should allow selections under distinctly non-natural conditions.

(iii) The third selection strategy is based on sorting of fluorescent droplets or beads. The biochemical product produced by the encapsulated enzymes or cells remains compartmentalized within the droplet and is therefore linked to the genotype. Droplets containing an active catalyst can be distinguished by the fluorescent signal. For bulk emulsions an additional emulsification step is required, since the water-in-oil (w/o) emulsions have a continuous oil phase that is not compatible with fluorescent-activated-cell-sorting (FACS). These compartmentalization systems are based on double emulsions (w/o/w) that enable an external aqueous phase, without the alteration of the aqueous droplets embedded in the primary w/o emulsion [121–123] (see figure 1.29). Microbead display is an

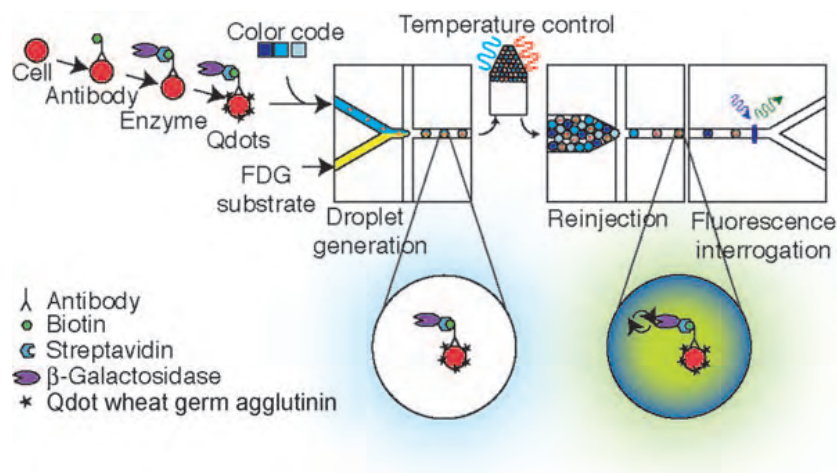


Figure 1.31.: Schematic depiction of the complete assay. Cells were labeled for a specific cell-surface protein with an antibody-coupled enzyme and a quantum dot wheat germ agglutinin (WGA) stain for visualization. Cells were then encapsulated in droplets on the microfluidic chip with a sample-specific color code and a fluorogenic enzyme substrate. After incubation to let the signal develop, each droplet's fluorescence was analyzed. FDG=fluorescein-di- β -d-galactopyranoside. Reprinted from [128].

other strategy that takes advantage of sorting by fluorescence [124–126]. As illustrated in figure 1.30, the coding gene and its protein become attached to a microbead within the droplets. The emulsion is then broken, and the gene-protein complexes recovered; those with the desired activity are enriched by affinity purification using the target-ligand-complex or by FACS of the gene-bead-protein-ligand complexes. A more recent strategy is fluorescent-activated-droplet-sorting (FADS) [22] (see also section A.0.2). As previously discussed in section 1.5.1 and 1.5.5, microfluidic w/o droplets are monodisperse, thus enabling better quantitative selection of activity, and droplets can be directly sorted without the need of w/o/w double emulsions as opposed to FACS.

As already introduced, one of the main objectives of this work was to enable the last introduced method of microfluidic droplet-based directed evolution. The challenge here was integration of the physical droplet processing steps with standard biological operations that are part of an integrated device for directed evolution. A first method using bacteria [22] (see section A.0.2) was developed within our group and a second system using a surface-protein display strategy with yeast was developed by our collaborators Agresti *et al.* [127]. But the cell-free system by IVTT especially needs several technical steps upon realization, as e. g. the development of bio-compatible surfactant [23], the *in vitro* protein expression [24, 35] (see section A.0.3) and the overall integration of microfluidic modules with each other and the biology.

1.6.4. Diagnostics

High expectations towards microfluidics have always been present in order to address the need for either (i) low cost portable point-of-care (POC) diagnostic devices or (ii) improved assay characteris-

tics helping to increase the sensitivity and/or lower the costs. The first point is especially important for the developing world, which does not have access to many of the best medical diagnostic technologies. These have been usually designed for air-conditioned laboratories, refrigerated storage of chemicals, a constant supply of calibrators and reagents, stable electrical power, highly trained personnel and rapid transportation of samples. Microfluidic systems allow miniaturization and integration of complex functions, which could move sophisticated diagnostic tools out of the developed-world laboratory. These systems must be inexpensive, but also accurate, reliable, rugged and well suited to the medical and social contexts of the developing world [129, 9, 130–132].

Droplet-based microfluidics have not yet been applied to this field since it is usually necessary to run these systems with syringe pumps or constant pressure devices, making them large and laboratory bound. An attempt to make droplet-microfluidics also available for POC devices utilizes centrifugal forces to pump the liquids and generate droplets [133]. Nevertheless, it is more likely that droplet-based microfluidics will be helpful for diagnostics to increase sensitivity, improve throughput and thereby reduce the costs. For example, it has been already shown that low-abundance cell-surface biomarkers can be detected by enzymatic amplification in a droplet version of an ELISA assay [128] (see figure 1.31). It has a significantly higher signal resolution above background than can be achieved using a standard fluorescence-activated cell sorter (FACS). Furthermore, DNA methylation analysis using methylation-specific PCR in microfluidic droplets has been performed [134]. Many cell-based assays could also be adapted for clinical purposes. For example, the hydrodynamic self-sorting of rare disease-causing bacterial cells present in a background of non-pathogenic bacterial cells has been demonstrated [135]. Another example is the detection of bacteria in a sample of human blood plasma, where the sensitivity of bacterial strains to different antibiotics was tested and their minimum inhibitory concentration was determined [136]. In contrast to flow cytometry, cell-based assays in droplets allow a much greater control over the environmental conditions and intracellular components secreted from the cells cannot escape the droplet compartment [22]. Typical for these cell-assays in droplet is the intention of encapsulating single cells in droplets. It is therefore either necessary to consider the poisson distribution of cell encapsulation [137, 138] or the usage of techniques specialized on single-cell encapsulation [135, 139, 140]

1.6.5. Proteomics and protein-protein interactions

Protein-protein interactions are key mediators of functions of life in the cell. They play crucial roles in the regulation of enzyme action, in signal transduction and inter-cellular communication. As interactions between proteins are central transmitters of function, the identification and prediction of protein interactions is the basis for understanding the intriguing complexity of cellular networks. Knowledge of such networks is central to fundamental research in cell and developmental biology, but also in molecular medicine, where the characterization of disease phenotypes at the level of the 'interactome' is an attractive route to identify new drug targets.

Proteome-wide or large-scale experimental characterization of protein-protein interactions has re-

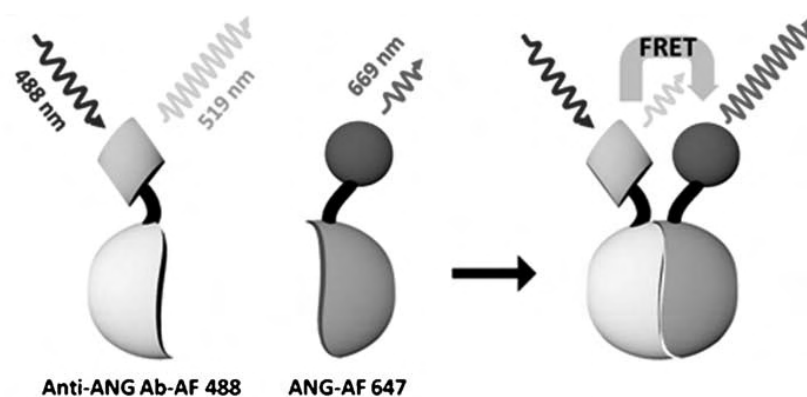


Figure 1.32.: Schematic of detecting protein-protein interaction by FRET. Reprinted from [141].

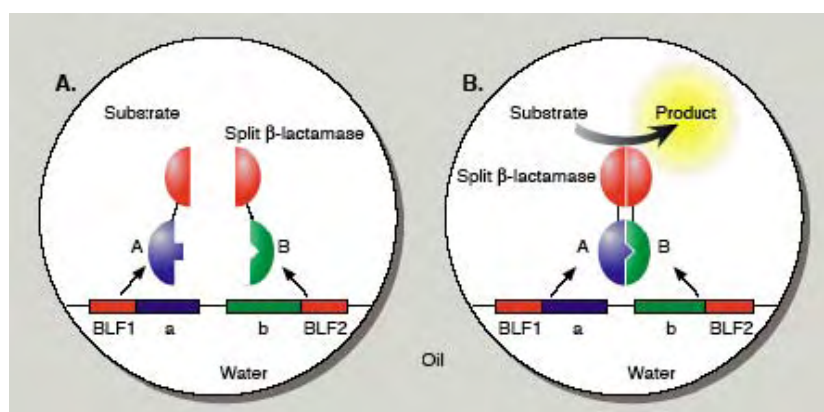


Figure 1.33.: Anticipated screening procedure for protein-protein interactions by recombination of a split enzyme. The split β -lactamase is inactive (microdroplet A) unless polypeptides A and B bind to each other driving the association of the two halves of the β -lactamase to form an active enzyme, which converts the non-fluorescent substrate into a fluorescent product (microdroplet B). Reprinted from [144].

lied largely on two techniques: (i) yeast-two-hybrid system [142] (Y2H) and (ii) tandem affinity purification [143] with subsequent mass-spectrometric identification of the interaction partners (TAP/MS). Y2H and TAP/MS are amenable to automation and allow genome-wide sampling. They have distinct systematic advantages and problems: The Y2H datasets are estimated to have relatively high rates of false positives (50%) and false negatives (90%). Moreover, the system is limited to protein interactions in the nucleus. The TAP/MS data is more accurate with an estimated 30% false positives. However, transient and weak interactions are unlikely to be detected. Most importantly, none of these methods provides any information on the stoichiometry of the component subunits in large protein assemblies.

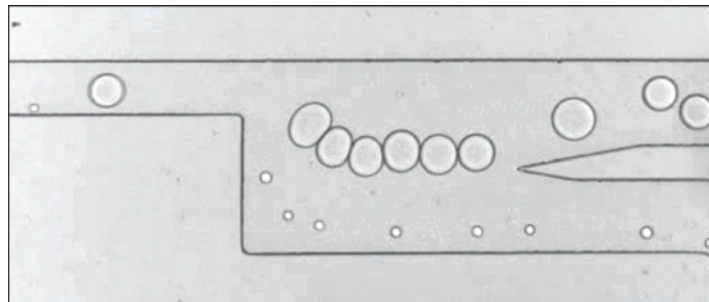
In order to address the need for high-throughput protein analysis, protein-microarray technology has been developed, addressing some of the above mentioned limitations. These microarrays allow the simultaneous analysis of thousands of different binding events including DNA-protein [145], protein-protein [146], receptor-ligand [147], enzyme-substrate [148–150] and protein-drug [151] interactions

within a single experiment. Nevertheless, in array-based systems, capture proteins must be immobilized onto a surface. This can lead to obstruction or deformation of the protein binding sites through interaction with the solid surface and therefore significantly interfere with specific protein-protein interactions.

Microfluidic droplets might allow more physiological conditions but still accounting for high-throughput. Approaches to measure protein-protein interactions could then either utilize FRET [152, 141] (see figure 1.32) or a protein complementarily assays (PCA), in which a reporter protein is split into two inactive fragments [153–155] (see figure 1.33). Each fragment is then fused to one of the interacting partner-proteins. If there is an interaction between both proteins, the function of the reporter is restored by complementation of its fragments. In order to monitor protein interactions in living cells, enzymes have been used as reporter, like the β -galactosidase [156], the dihydrofolate reductase [157] and the β -lactamase [158, 159]. They convert chromogenic or fluorogenic substrates into detectable products. Another strategy that has also been investigated is using as reporter a protein that is fluorescent by itself, like the green or yellow fluorescent protein (GFP, YFP) [160, 161]. Conducting these kind of experiments in droplets provides its *in vitro* equivalent.

Chapter 2.

Size dependent sorting of droplets



Contents

2.1. Introduction	44
2.2. Theory	45
2.3. Experiments	48
2.4. Chapter summary and conclusion	49

This chapter presents the theory and experimental results obtained to sort emulsions or droplets by size independent of their content. This passive sorting mechanism utilizes microscale hydrodynamics and can be used to purify polydisperse emulsions or select droplets which have a different size compared to the rest of the emulsion.

2.1. Introduction

Emulsions and the concept of compartmentalization have already been widely used for chemical and biological applications (see section 1.6), since every droplet within the emulsion can function as an independent micro-reactor. It is therefore possible to perform millions of reaction in parallel with little sample consumption. Initial polydisperse emulsions, created by mechanical homogenizers or mixers [15], can usually only be used if the reaction within each droplet alters the content and the readout or product is recovered after breaking the emulsion afterwards [115, 116]. In order to directly use the droplets and be quantitative on their content it is necessary to work with monodisperse emulsions. This need has been addressed by droplet-based microfluidics [11, 14, 13], which allow droplets to be created with a very narrow size distribution ($<3\%$) [62, 65].

Although it is now possible to create and handle monodisperse emulsions by microfluidics, there are still processes within complex assays which create polydispersity within initially monodisperse emulsions. Undesired coalescence for example is one source for this problematic and can be encountered during collection and reinjection of emulsion [35]. Another typical source is when droplet fusion was part of the work-flow. Since it is not always possible to have 100% pairing efficiency [30], the emulsion will later contain fused and unfused droplets with different sizes. It would be therefore advantageous if it is possible to purify these emulsions and regain the monodisperse emulsion.

Although it is possible to actively sort the droplets by electrical fields [20, 21], passive size dependent sorting of droplets holds a greater potential, especially since such a technique is independent of its content and no fluorescence within the droplets is necessary. It has been shown that it is possible to passively sort satellite droplets ($\sim 0.5 - 2.5\mu\text{m}$) from their parent droplets ($\sim 50 - 75\mu\text{m}$) [162], or even sort droplets with a size difference as low as $4\mu\text{m}$ [163]. Nevertheless, it has not been evaluated how reliable the method is and how well the purification efficiency is. The mentioned principle and recorded data indicates only a weak size dependency. In contrary a principle referred to as 'pinched flow fractionation (PFF)', developed for the size-dependent separation of solid particles, such as polymer microparticles or cells [164–166], can theoretically sort any size difference. As a first application it has been used to recover emulsions with a smaller size distribution from a polydisperse bulk emulsion [167].

This work aimed to use the PFF principle to characterize the important parameters and create devices to recover a monodisperse emulsion after undesired coalescence during re-injection and discrimination between fused and unfused droplets after droplet-fusion (see section 1.5.4).

2.2. Theory

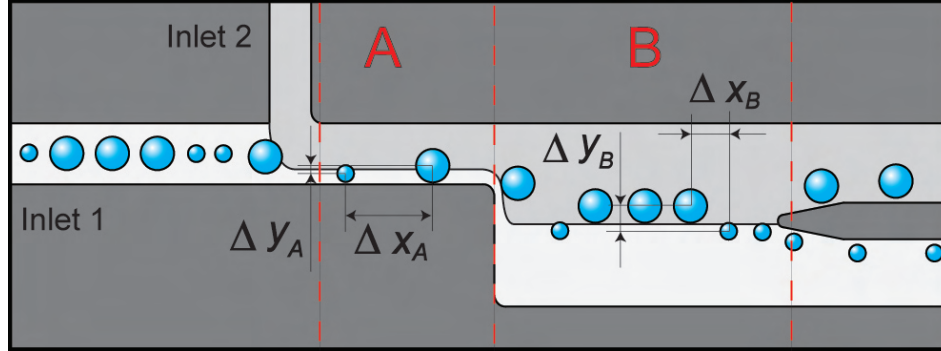


Figure 2.1.: Principle of passively sorting droplets by size. In region 'A' droplet get align to the wall by the second oil stream introduced by inlet 2. In region 'B' the channel and the stream-lines expands, increasing the separation distance $y_B > y_A$. Droplets follow their stream-lines and get sorted according to size.

The principle of PFF is shown in figure 2.1. An oil stream containing the droplets arriving from inlet 1 is focussed on one sidewall by a second oil stream introduced by inlet 2. By this operation the droplets align along the wall, with slight differences of their center position y_A depending on their size. Smaller droplets are spatially able to travel closer to the wall than larger ones. As the channel widens the stream-lines extend and droplets following their streamlines get further separated in the y -direction. Further downstream the channel branches into several arms sorting the droplets rapidly and continuously by size.

The sorting efficiency depends mainly on the separation capability at the channel expansion. The center of a droplet traveling along the sidewall in region 'A' has a distance of $y_A = d/2$ to the wall. After the channel expands in region 'B' by a factor of $\xi = w_B/w_A$ (w being the channel width) the position changes to:

$$y_B = \xi y_A \quad (2.1)$$

This means that droplets with a size difference of Δd , will increase their separation distance from $\Delta y_A = y_{A1} - y_{A2} = \Delta d/2$ to $\Delta y_B = y_{B1} - y_{B2}$ after the expansion:

$$\begin{aligned} y_{B1} - y_{B2} &= \xi y_{A1} - \xi y_{A2} \\ \Leftrightarrow \Delta y_B &= \xi \Delta y_A = \xi \frac{\Delta d}{2} \end{aligned} \quad (2.2)$$

In theory this means that any droplet size difference could be sorted by sufficiently amplifying the separation distance. Practically this is hindered by the spacing, therefore the amount of oil, between the droplets when they enter the extension. If the spacing is not sufficiently large, droplets would bump into each other, change their y -position by these interactions and create errors during sorting. By considering the mass and volume conservation the x -spacing between the droplets after the extension

2. Size dependent sorting of droplets

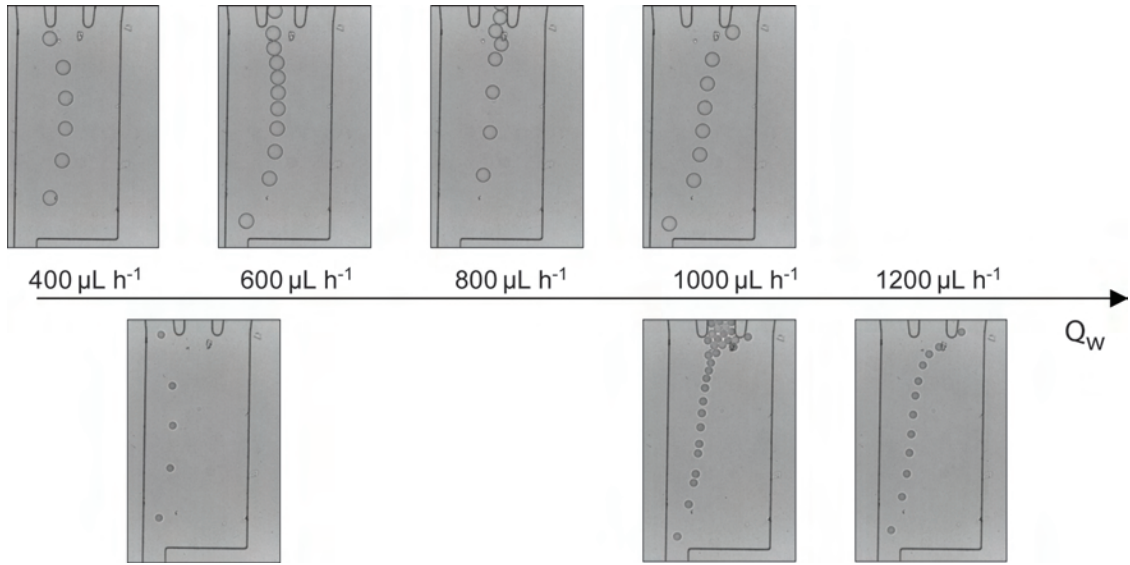


Figure 2.2.: Adjusting the droplet size sorter. Q_w is the flow-rate extracted through the upper right channel. Since the droplets have been aligned towards the left wall, a higher flow-rate Q_w is necessary to pull the smaller droplets to the right than the larger ones.

Δx_B can be calculated:

$$\begin{aligned} \Delta x_A w_A &= \Delta x_B w_B \\ \Leftrightarrow \Delta x_B &= \frac{\Delta x_A}{\xi} \end{aligned} \quad (2.3)$$

To ensure that droplets do not touch each other after the expansion the distance Δx_B must be greater than the sum of the two radii $R_1 + R_2$, forming an expression for the minimal spacing before the expansion Δx_{Am} .

$$\begin{aligned} \Delta x_B &\geq R_1 + R_2 \\ \Leftrightarrow \frac{\Delta x_A}{\xi} &\geq R_1 + R_2 \\ \Rightarrow \Delta x_{Am} &= \xi (R_1 + R_2) \end{aligned} \quad (2.4)$$

Technically it is not necessarily easy to realize a sufficient spacing between the droplets to fulfill this requirement, especially if small size difference need to be resolved and large expansions (large ξ) are necessary.

2.3. Experiments

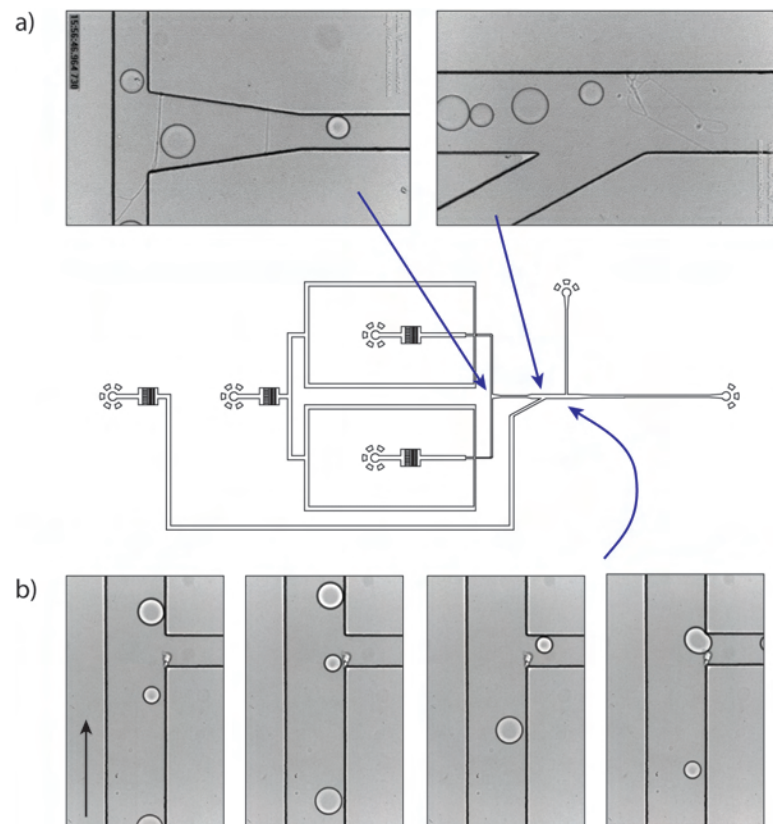


Figure 2.3.: a) Illustration of an initial design to sort droplets by size. Two independent nozzles create the different sized droplets. After combining the two streams at a junction the droplets are spaced by an oil stream and are sorted at the downstream junction which is tuned by a syringe pump in withdraw mode. b) Shows a series of picture when sorting droplets by size.

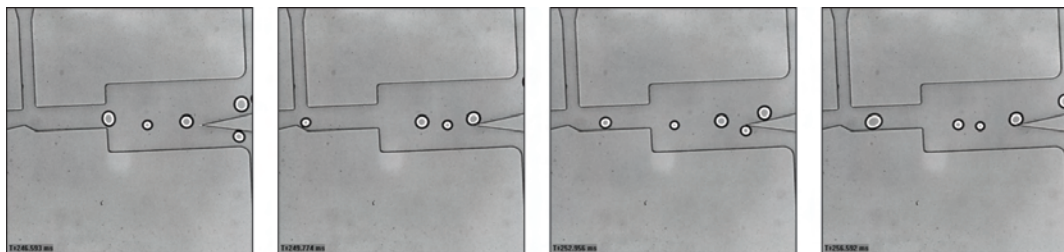


Figure 2.4.: a) Shows an easy case scenario when sorting droplets with a large size difference. b) Shows a series of pictures when sorting droplets with small size differences.

2.3. Experiments

As explained in the previous section the different sized droplet will follow different streamlines after they have been aligned towards one wall. After the expansion it is therefore possible to guide the droplets into different outlet channels. It is therefore either necessary to carefully calculate and design the device, or another possibility is to use a syringe pump in withdraw mode on one of the outlets. By this method it is possible to adjust and chose the amount of flow running through one of the channels. Figure 2.2 illustrates this principle. A withdraw pump has been connected to the outlet at the top-right corner. By increasing the flow-rate through this channel more and more stream-lines are captured. Therefore, first the droplets following the streamlines further to the right (larger ones in this case) will enter this channel, whereas higher flow-rates are necessary to capture also the smaller droplets. By choosing a flow-rate according to this graph the system can be adjusted on the sizes of droplets and furthermore ensures that droplets do not change the fluidic resistance and consequently the flow-rate through a channel depending on its droplet occupancy.

Another initial design tested to demonstrate the sorting capabilities is illustrated in figure 2.3. Different sizes of droplets are created at the two independent nozzles and further downstream the two droplet streams are combined to mimic a polydisperse emulsion. The droplets are spaced by an additional oil stream which additionally aligns the droplets towards one side wall (see figure 2.3a. At the sorting junction again one outlet channel has been connected to a withdraw pump. By changing the flow-rate through this channel the junction could be adjusted in order to only guide the small droplets through one outlet whereas the larger ones follow the other channel. In this case no expansion has been utilized. It shows that it is principally possible to just extract the amount of oil necessary to capture a droplet stream. The advantage of choosing a design like this is that it is less demanding for the minimal droplet spacing before the expansion Δx_{Am} . On the other hand the sorting was hard to maintain since any small fluctuations led to sorting errors. This reconfirms that a design like this would only be favorable if larger droplet size differences need to be sorted.

Figure 2.4 shows a device tested to sort droplets with small size differences. This case should mimic the scenario of having a fusion device further upstream and due to unperfect droplet pairing, two size populations can be expected. The slightly larger droplets (50 μm) would be the result of successful pairing and fusion events. The smaller ones (30 μm) would correspond to unfused droplets. In order to increase the sorting efficiency, the channel has been expanded $3\times$ and a high oil flow-rate (2000 $\mu\text{L h}^{-1}$) was necessary to space the droplets sufficiently. The position of the separation junction has been calculated and placed accordingly into the design. Nevertheless, as in the experiments before a withdraw pump has been connected to one of the outlets to finetune the sorting.

Although the sorting was successful for a majority of droplets ($\sim 80\%$) it was hard to achieve higher values. The reason for this are the difficulties in spacing all of the droplets sufficiently. The sorting errors occurred only when droplets where too close together and touched each other in the expanded region. Attempts to solve this issue by increasing the oil flow further were unsuccessful since it led to ripping of the droplets.

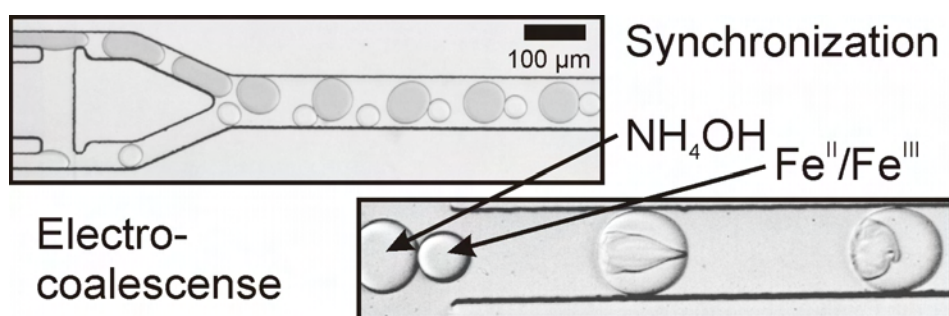
2.4. Chapter summary and conclusion

In summary the presented principle of sorting droplets by size works according to the theory. Furthermore, it was possible to demonstrate different successful designs and methods to perform sorts like this. It was possible to demonstrate that droplets with size differences of only 20 μm could be separated although in all cases the spacing of the droplets was the critical factor. A single oil stream might not always be sufficient for the droplet spacing. The sorting results are expected to be even more robust and more accurate if several oil stream are utilized to ensure the droplet spacing. It might be interesting for further applications to continue this project and use the principles discussed here to make the sorting more reliable and useable for applications.

2. Size dependent sorting of droplets

Chapter 3.

Droplet-based microreactors for the synthesis of magnetic iron oxide nanoparticles



L. Frenz, A. El Harrak, M. Pauly, S. Bégin-Colin, A. D. Griffiths and J.-C. Baret, *Angew. Chem. Int. Ed.*, 2008, **47**, 6817–6820. [30]

Contents

3.1. Introduction	52
3.2. Synchronization of droplet production	53
3.3. Synthesis of iron oxide nanoparticles	55
3.4. Characterization of the synthesized nanoparticles	56
3.5. Materials and methods	56
3.6. Chapter summary, conclusion and outlook	57

This chapter presents the concept of compartmentalization of fast reactions. An extremely reliable method to create droplet pairs, based on hydrodynamic coupling of two spatially separated nozzles has been developed. Droplets containing the reagents for the precipitation of iron oxide are electrocoalesced in order to synthesize iron oxide nanoparticles in a very fast (\sim ms kinetics) and reproducible reaction.

3.1. Introduction

Microfluidic systems are a powerful tool to study and optimize a wide range of biological and chemical reactions [2], and their use for the synthesis of nanoparticles is attracting more and more attention. Compared to conventional bulk synthesis strategies microfluidic systems allow more precise control of the reaction conditions which can lead to reductions in particle size and polydispersity [168]. A range of different nanoparticles have been synthesized in microfluidic systems: CdSe, CdS, TiO₂, Boehmite, Au, Co, Ag, Pd, Cu, BaSO₄, and CdSe-ZnS core-shell nanoparticles [169, 168]. Although there are preliminary results on the synthesis of iron oxide nanoparticles in a millifluidic system [170], so far microfluidic synthesis of magnetic iron oxide nanoparticles has not been demonstrated. Spinel iron oxide nanocrystals have attracted attention for their use as high density data storage media [171], or in biomedical applications, such as contrast enhancement agents for magnetic resonance imaging (MRI) and for drug delivery [172, 173]. Controlling the synthesis conditions of these particles is critical since this determines their physical properties [174]. While single-phase microfluidic systems are subjected to diffusion-limited mixing and reagent dispersion, droplet-based microfluidic systems overcome these limitations by fast mixing in spatially isolated microreactors (droplets) containing well defined quantities of materials [175, 71, 115], and therefore provide a high-level of control of the synthesis conditions [176, 14]. In droplet-based microfluidic systems reagents are generally brought together in a co-flowing stream just before droplet formation, the reaction occurring later in the microdroplet [175]. However, this method is unsuitable for aggressive or fast reactants which generate precipitates. To study and control such reactions, it is necessary to initiate the reaction by fusion of two droplets, each containing different reagents. The main limitation is then the accurate pairing of these droplets which is hindered by small variations in the channel depths or flow-rates [18]. There have been intensive studies on droplet coordination based on fluidic ladder networks [54], but the most promising approach is to use a synchronization mechanism directly at the production nozzle. Therefore, strategies such as active control of droplet release based on electric fields [27], or passive hydrodynamic coupling at a single nozzle have been proposed [28, 29]. Nevertheless, these approaches lack the control of droplet volume ratios required to optimize reaction stoichiometry and undesired coalescence occurs for certain flow-rate regimes.

Therefore, we have developed an extremely reliable method to create droplet pairs, based on hydrodynamic coupling of two spatially separated nozzles. The utility of this system has been demonstrated by precipitating iron oxide nanoparticles in a very fast (\sim ms kinetics) and reproducible reaction after fusion of droplet pairs by electrocoalescence [18].

3.2. Synchronization of droplet production

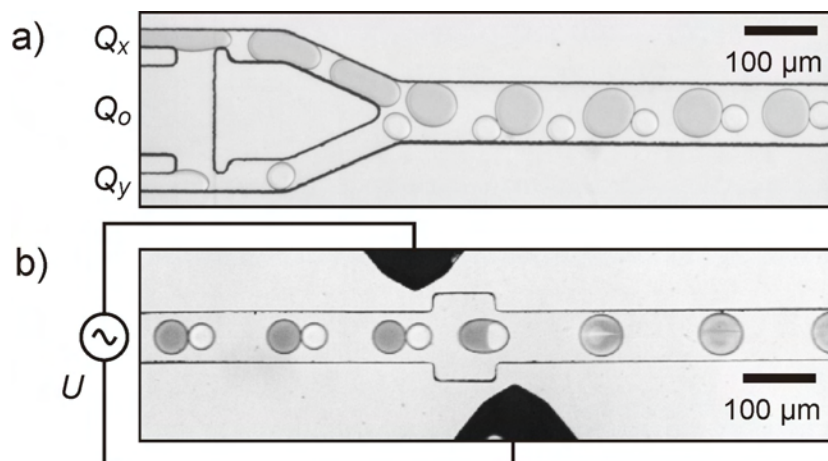


Figure 3.1.: a) Pairing module. Two aqueous phases (phosphate buffered saline with or without bromophenol blue) are injected by the outer channels and are synchronously emulsified by the central oil channel. The flow-rates are $Q_o = 800 \mu\text{L h}^{-1}$ for the oil and $Q_x = 400 \mu\text{L h}^{-1}$, $Q_y = 100 \mu\text{L h}^{-1}$ for the aqueous phases. b) Fusion module. Paired droplets can be coalesced by applying an electrical voltage U between the two electrodes. $Q_o = 650 \mu\text{L h}^{-1}$, $Q_x = 100 \mu\text{L h}^{-1}$, $Q_y = 60 \mu\text{L h}^{-1}$.

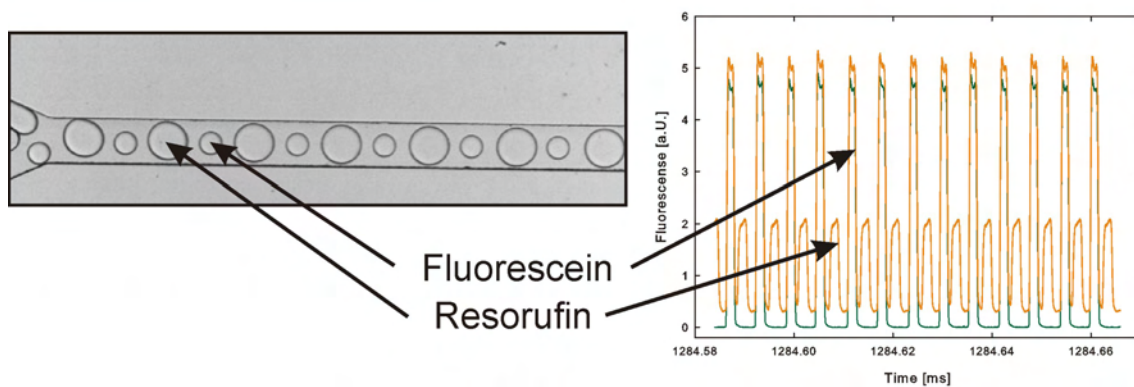


Figure 3.2.: Characterization of alternation: Two different photomultiplier tubes measure the fluorescent signals at 495-520 nm (green) and 578-657 nm (orange) respectively. Droplets containing fluorescein produce a peak on the green and orange channel; resorufin only on the orange channel. The content of each droplet is therefore easily distinguishable and pairing can be evaluated. For correct alternation a droplet pair contains a fluorescein and a resorufin droplet. An alternation error results in droplet pairs of identical fluorescence.

The microfluidic device (figure 3.1a) consists of two nozzles which are hydrodynamically coupled. During droplet formation in one of the two nozzles, the aqueous stream blocks the oil coming from the central channel, leading to an increased oil flow through the second nozzle. Once the droplet is released the oil flow switches back to the first channel allowing droplet formation at the second

Q_o [$\mu\text{L h}^{-1}$]	Q_x [$\mu\text{L h}^{-1}$]	Q_y [$\mu\text{L h}^{-1}$]	n_{droplets}	t [min]	f [s^{-1}]	unpaired	error
400	50	30	226 800	15.7	120.22	10	4×10^{-5}
500	100	60	4 019 100	124.7	268.58	22	5×10^{-6}
800	200	100	1 224 300	15.1	675.72	4	3×10^{-6}
800	250	200	2 252 501	23.3	806.11	3	1×10^{-6}
800	500	100	3 711 800	30.7	1007.62	39	1×10^{-5}

Table 3.1.: Examples of long term stability tests at different flow-rate combinations. Q_o is the oil flow-rate and Q_x, Q_y the aqueous flow-rates. The module can reliably pair millions of droplets n_{droplets} over a time t , with only a few unpaired events: the error is the ratio of unpaired events to the total number of drops. f is the droplet generation frequency at each nozzle.

nozzle. This alternation of the oil flow leads to perfect one-by-one droplet pairing at various flow-rates. Quantitative analysis was performed by labeling the droplets with different fluorophores in the two aqueous streams (see figure 3.2). One nozzle created droplets containing $10 \mu\text{M}$ fluorescein, the other created droplets containing $50 \mu\text{M}$ resorufin. By monitoring and evaluating the fluorescent signals the reliability of pairing was measured to be $\geq 99.99\%$ over millions of droplets (see table 3.1). Furthermore, droplet pairing is not only stable at equal aqueous flow-rates, but also at flow-rate ratios up to 1:5. Stoichiometry modulations (1:25) can therefore easily be achieved since the flow-rate ratio is equal to the droplet volume ratio in this system.

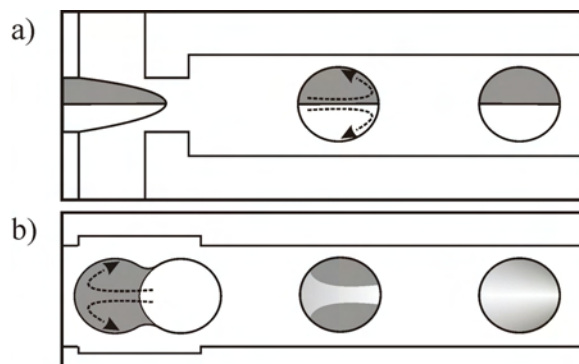


Figure 3.3.: Mixing in droplets. a) Reagents are brought together by a co-flow and then emulsified. Mixing occurs across the central line by diffusion only ($\sim 100\text{-}1000$ ms). b) In-line droplet fusion. Compounds are injected into both droplet hemispheres, mixing is enhanced by convection which results in faster mixing times (~ 2 ms)

In order to start a reaction the droplet pairs can be coalesced by applying an electrical field between the two on-chip electrodes (figure 3.1b). As illustrated in figure 3.3a using a co-flow system, mixing in droplets is limited to each droplet hemisphere [177], which makes additional mixing modules necessary [175]. In-line droplet fusion (figure 3.1b and 3.3b) overcomes this limitation, since the second

compound is injected homogenously into each hemisphere. In addition the dynamical rupture of the interface and the formation of the new droplet assists the mixing [71].

3.3. Synthesis of iron oxide nanoparticles

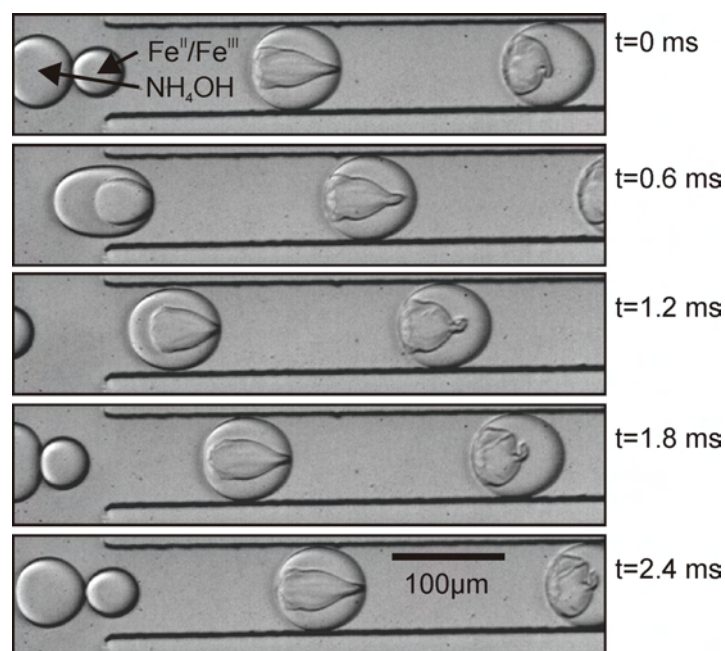


Figure 3.4.: Formation of iron oxide precipitates after coalescing pairs of droplets. $Q_o = 650 \mu\text{L h}^{-1}$ for the oil, $Q_x = 60 \mu\text{L h}^{-1}$ for the iron chloride solution (S1) and $Q_y = 120 \mu\text{L h}^{-1}$ for the ammonium hydroxide.

We have used this system to synthesize magnetic spinel iron oxide nanoparticles by co-precipitation of Fe^{II}/Fe^{III} salt solutions by the addition of a base. It is known that this leads first to magnetite (Fe₃O₄) which oxidizes readily subsequently to maghemite (γ -Fe₂O₃) when in contact with air [174, 173]. The co-precipitation is so fast that it immediately forms particles and blocks the channels in a co-flow system especially at higher concentrations (data not shown). Droplet fusion can potentially overcome this problem [29], but in the absence of surfactant [29], it is extremely difficult to achieve controlled pairwise droplet fusion [178]. In our system the two aqueous components never mix unintentionally, not even during the startup of the system, as the nozzles are spatially separated and the droplets are stabilized by surfactant.

Controlled pairwise droplet-fusion is achieved by electrocoalescence. This approach enabled us to increase the compound concentration by 2-3 orders of magnitude compared to earlier droplet-based microfluidic methods for the synthesis of nanoparticles [29, 179]. In detail, iron chloride solution was flushed into one arm of the nozzle and ammonium hydroxide into the second arm, which led to droplet pairs containing the two reagents. After electrocoalescence a precipitate of iron oxide nanoparticles appeared within ~ 2 ms (see figure 3.4). Due to identical reaction conditions in all droplets, the ki-

netics of precipitation and its morphology was extremely similar in all droplets throughout the whole experiment.

3.4. Characterization of the synthesized nanoparticles

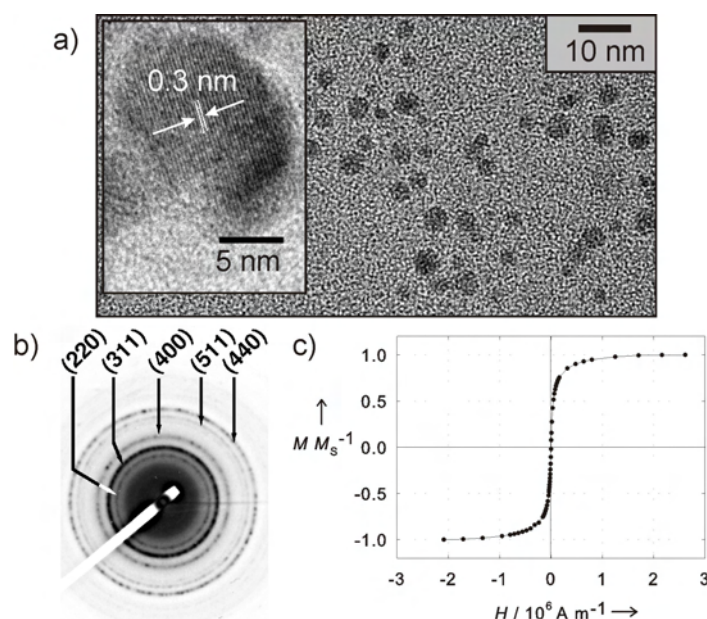


Figure 3.5.: Characterization of the iron oxide particles produced with solution (S2) on-chip. a) TEM image of the nanoparticles. Inset: HRTEM image of a particle showing (220) spinel planes. b) Electron diffraction pattern indicating different planes of the spinel structure. c) Magnetization MM_s^{-1} (M_s being the saturation magnetization) as a function of the magnetic field H .

Particle size measurements by transmission electron microscopy (TEM) (figure 3.5a) show that the average particle diameter is smaller for the fast microfluidic compound mixing (4 ± 1 nm) compared to bulk mixing (9 ± 3 nm). In addition, high resolution TEM (HRTEM) measurements (inset figure 3.5a) show that the nanoparticles are monocrystalline, no stacking faults being visible. They exhibit planes with interplanar distances of about 0.3 nm characteristic of (220) spinel planes. The electron diffraction pattern measured from a large zone (figure 3.5b) confirms the iron oxide spinel structure. Finally, the absence of hysteresis in the magnetization curve (figure 3.5c) of the nanoparticles synthesized, indicates that they are superparamagnetic, which is characteristic of spinel iron oxide nanoparticles smaller than 15 nm.

3.5. Materials and methods

The 25 μm deep structures used for fluid channels and electrodes were patterned into poly(dimethylsiloxane) (PDMS) using soft-lithography (see chapter 1.3.1). Electrodes used for fusion were patterned into

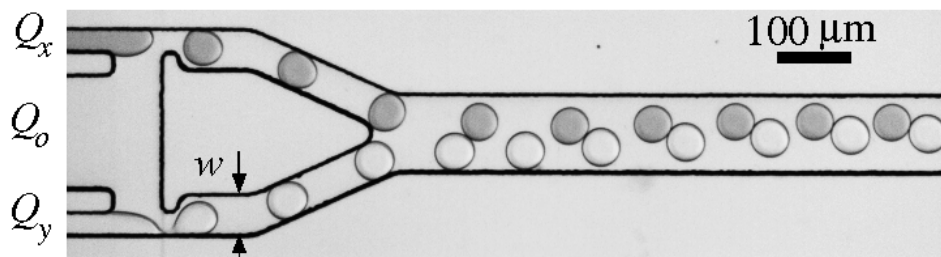
the same layer and in close vicinity to the fluidic channels [180]. A commercial surface coating agent (Aquapel, PPG Industries) was used to coat the channels. Harvard Apparatus syringe pumps (PHD2000) controlled the flow-rates. The continuous oil phase was a perfluorocarbon oil FC40 (3M) with 2.5% (w/w) of surfactant, made of the ammonium salt of a perfluorinated polyether (PFPE) (Krytox FSL - Dupont) [181], stabilizing droplets against coalescence. As starting materials for the precipitation of iron oxide nanoparticles we used $\text{FeCl}_2 \cdot 4\text{H}_2\text{O}$ (Sigma-Aldrich) and $\text{FeCl}_3 \cdot 6\text{H}_2\text{O}$ (Acros Organics); ammonium hydroxide solution (28% NH_3 -Fluka) and hydrochloric acid (37% HCl-Acros Organics) of analytical grade. After degassing 0.5 M HCl in Milli-Q water with an argon flux for 1 h we added the iron chloride salts and kept this solution under argon. Two different solutions with $\text{Fe}^{\text{III}}/\text{Fe}^{\text{II}}=2$ ratio were tested: (S1) 480 mM FeCl_3 + 240 mM FeCl_2 and (S2) 60 mM FeCl_3 + 30 mM FeCl_2 . As a base we used a 2 M ammonium hydroxide solution - also prepared using degassed Milli-Q water. In order to avoid oxidation of the Fe^{II} during the reaction process, the PDMS device was kept in a vacuum chamber over night before use, the oil was degassed with a nitrogen flux for 1 h, we used gas-impermeable polyethylene tubing (Becton Dickinson) and collected the sample into a nitrogen atmosphere. Electrocoalescence was achieved by an ac-voltage of $U=200$ V (Peak to peak) at 30 kHz, which was applied across the two electrodes positioned on each side of the microfluidics channel. TEM and HRTEM images were recorded with a TOPCON 002B transmission electron microscope, operating at 200 kV, with a point to point resolution of 0.18 nm. Magnetic measurements were performed using a Superconducting Quantum Interference Device (SQUID) magnetometer (Quantum Design MPMS-XL) at 200 K.

3.6. Chapter summery, conclusion and outlook

In summary, we have demonstrated for the first time the synthesis of spinel magnetic iron oxide nanoparticles in a microfluidic system. The novelty of this approach lies in the fact that the reaction is compartmentalized in microdroplets, which function as independent microreactors. We have designed a robust and flexible microfluidic module for the controlled production of droplet pairs based on hydrodynamic coupling, with errors of pairing in the order of only 10^{-5} . The reagents in the droplet pairs are brought together on demand by in-line electrocoalescence resulting in fast mixing (~ 2 ms). Various chemical strategies have been developed to obtain magnetic iron oxide particles, sometimes with high monodispersity [173]. The size of nanoparticles synthesized in microfluidics (4 nm) is equal to that of the smallest particles synthesized in bulk using other techniques. Furthermore, such on-chip synthesized particles could potentially be functionalized by an additional droplet-fusion step to synthesize core-shell particles optimized for bio-compatibility, drug anchoring, and cell targeting.[182] For iron oxide this is of special interest, since magnetite (Fe_3O_4), which displays a higher saturation magnetization than maghemite ($\gamma\text{-Fe}_2\text{O}_3$), could then be preserved without oxidation to maghemite. Besides these applications we believe that this system can be used to control and study a wide range of millisecond kinetic reactions in chemistry and biology and is therefore an additional tool that complements the other pre-existing microfluidic modules for droplet manipulation.

Chapter 4.

Microfluidic production of droplet pairs



L. Frenz, J. Blouwolff, A. D. Griffiths and J.-C. Baret, *Langmuir*, 2008, **24**, 12073–12076. [31]

Contents

4.1. Introduction	60
4.2. Results and discussion	60
4.3. Chapter summery, conclusion and outlook	66
4.4. Materials and methods	66

This chapter presents a study on a microfluidic dual nozzle for the production of water-in-oil droplet pairs. Droplets are paired by the hydrodynamic coupling of two nozzles over a wide range of aqueous and oil flow-rates. The droplet production frequencies and volumes are related to the flow-rates through a single, experimentally determined power-law. The data is in good agreement with a model based on a geometrical decomposition of the dual nozzle leading to a general equation of droplet frequencies as a function of the various flow-rates.

4.1. Introduction

In vitro compartmentalization (IVC) techniques [15], in which water-in-oil droplets are used as femtoliter to nanoliter reactors, allow as many as 10^{10} reactions to be performed in parallel in only one milliliter of emulsion. The small volumes of the reaction compartments enables the study of reactions at the single molecule, single gene, or single cell level [12, 116]. Combining IVC and microfluidics techniques [3, 2] promises to give an unprecedented level of control for high-throughput screening of chemical and biochemical processes [115]. Indeed, recent progress in the field of two-phase-flow microfluidic systems [11, 14] has enabled controlled operations on bubbles and droplets in microchannels, such as the production of monodisperse emulsions [65, 183–185] or foams [186], splitting of droplets [19], fusion of pairs of droplets [18, 27, 187, 188, 184], and sorting [21, 50]. Most of the studies on droplet generation in microfluidics focussed on a single nozzle and only a few papers investigated the effect of the coupling between two nozzles [28, 189, 185]. In this article, we discuss and analyze the design of a versatile nozzle used to produce droplet pairs, based on hydrodynamic coupling of two spatially separated nozzles. The design allows the production of droplets with a typical volume of $\sim 50 - 250$ pL and volume ratios between the two droplets ranging from 1:1 up to 1:5. The stability has been measured over a wide range of flow-rates with only a few mistakes over $\sim 10^5$ droplet pairs [30]. The droplet pairs can subsequently be electrocoalesced to combine reagents and initiate reactions [30]. Here, the experimental analysis of the droplet production frequencies results in a power-law behavior governed by a single exponent β . A model based on symmetry decomposition is derived for a detailed understanding of droplet pairing and its limitations.

4.2. Results and discussion

Qualitatively the idea behind the design presented in figure 4.1 is that the synchronization is promoted by the formation and presence of a droplet in one of the two nozzle arms forcing the oil through the second arm. Above a certain size limit the influence of the droplet on the fluidic resistance [190] is strong enough to force droplet breakup in the opposite channel leading to an alternating oil flow.

Quantitative analysis was performed by measuring droplet production frequencies for various oil flow-rates Q_o and equal aqueous flow-rates $Q_x = Q_y$ (symmetric case). A typical snapshot is displayed in figure 4.1a. Droplet pairing was obtained successfully until a flow-rate limit Q_o dependent on

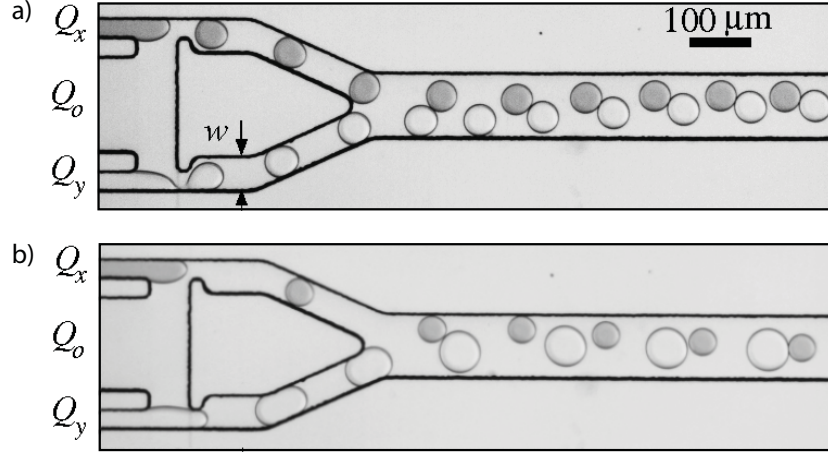


Figure 4.1.: Pairing module. Two aqueous phases are injected by the outer channels and synchronously emulsified by the central oil channel. The channel depth is $h=25\ \mu\text{m}$ and the channel width $w=50\ \mu\text{m}$ after the nozzle. a) Symmetric case: the flow-rates are $Q_o = 220\ \text{nL s}^{-1}$ for the oil and $Q_x = Q_y = 28\ \text{nL s}^{-1}$, for the aqueous phases. b) Asymmetric case: $Q_o = 140\ \text{nL s}^{-1}$, $Q_x = 16\ \text{nL s}^{-1}$, $Q_y = 50\ \text{nL s}^{-1}$.

the aqueous flow-rate (figure 4.2). Above this limit (i. e. beyond the points marked with a star in figure 4.2), the droplet production became irregular and lead to the creation of unpaired droplets. In the pairing regime the droplet frequency f_{xx} displays a linear relationship with the oil flow-rate Q_o (see figure 4.2) and a power law behavior with the aqueous flow-rate Q_x (see inset of figure 4.2) resulting in equation 4.1:

$$f_{xx} = \alpha Q_o Q_x^\beta \quad (4.1)$$

where $\beta \approx 0.82$ is characteristic of the system and $\alpha = 0.17$ for flow-rates expressed in nL s^{-1} and frequencies in s^{-1} .

In order to understand the flow-rate limit it is necessary to consider the volume V of the produced droplet. By inserting the mass conservation relationship $V = Q_x/f_{xx}$ into equation 4.1 the droplet production frequency reads:

$$f_{xx} = V^{\beta/(1-\beta)} (\alpha Q_o)^{1/(1-\beta)} \quad (4.2)$$

The experimental limit of regular droplet pairing (stars in figure 4.2) corresponds to the line of constant volume $V = 40\ \text{pL}$ (solid line of figure 4.2) for pancake-shaped droplets of height $h = 25\ \mu\text{m}$ and diameter $d = 45\ \mu\text{m}$. This means, when the droplets become smaller than the channel width ($w \sim 50\ \mu\text{m}$) they are too small to significantly alter the oil flow [189, 190]: the hydrodynamic coupling between the two nozzles vanishes and the droplets stop alternating. This result supports the qualitative argument that droplet pairing is promoted by the interplay of droplet size and channel dimensions leading to an alternating oil flow between the two nozzle arms.

The asymmetric case ($Q_x < Q_y$) was studied using the same method and as before the droplet

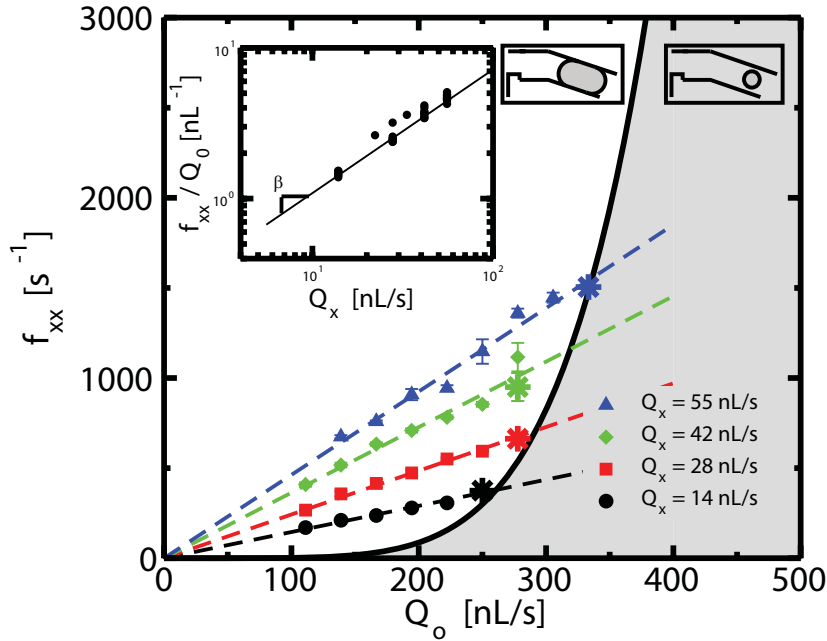


Figure 4.2.: Measurement of droplet frequency f_{xx} when $Q_x = Q_y \in \{14, 28, 42, 55\} \text{ nL s}^{-1}$ as a function of the oil flow-rate Q_o . The frequency is given by a linear relationship with Q_o (equation 4.1). The alternation occurs until the points marked with a star (until this point droplet pairing is stable) – beyond, droplet production became irregular. The solid line corresponds to a constant droplet volume of 40 pL (flat pancakes of 45 μm diameter) separating the two regimes of droplets larger than channel width (white - pairing) or smaller (gray - no pairing). Inset: Power-law behavior of the frequency with the flow-rate Q_x : $\beta \approx 0.82$.

production frequency was equal in both nozzle arms (figure 4.1b). The aqueous flow-rate ratio can reliably be varied between 5:1 and 1:5 leading to a volume ratio of $V_x/V_y = Q_x/Q_y$ due to mass conservation $V_{x,y} = Q_{x,y}f_{xy}$. By ramping up the oil flow-rate at different Q_x, Q_y combinations the frequency presents a similar linear behavior as a function of Q_o . The measured frequencies lie in between the frequencies obtained in the symmetric case with the corresponding aqueous flow-rates (see figure 4.3). However, deriving an equivalent of the power-law of equation 4.1 for the asymmetric case is not straight-forward.

In order to explain the experimental data and generalize the power-law behavior with the aqueous flow-rates to the asymmetric case, a model for the droplet alternation has been derived. In general, hydrodynamics calculations in the presence of droplets in channels is a complex problem [190], beyond the scope of the present paper. Here, understanding the symmetric case is sufficient to predict the frequencies obtained in the asymmetric case, on the basis of geometrical arguments. At the nozzle the oil flow splits into the two nozzle arms. In the symmetric case the flow-rate in each arm is on average $Q_o/2$ – average should be understood as the mean oil flow-rate over one period of droplet production – (see figure 4.4a), $\varepsilon = 1/2$ by symmetry).

In the asymmetric case, the oil flow splits unequally into two fractions of the total oil flow-rate (εQ_o and $(1 - \varepsilon)Q_o$, $0 \leq \varepsilon \leq 1/2$ (see figure 4.4b,c). The asymmetric case can be modeled as a

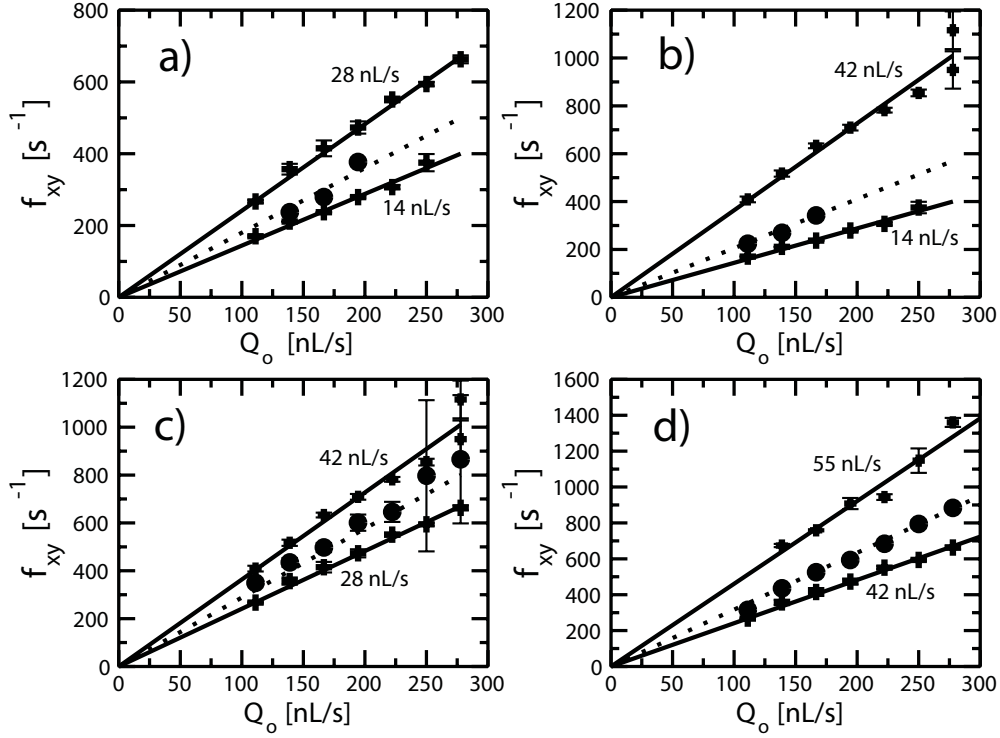


Figure 4.3.: Measurement of the droplet production frequencies for the symmetric case (+) and the asymmetric case (●). The dotted line corresponds to the construction of figure 4.4d and lies in-between the solid lines for the symmetric cases expressed by equation 4.1. In each plot the flow-rates are indicated in the graph.

combination of two symmetric cases: each side of the device behaves as a symmetric nozzle with oil flow-rates $2\epsilon Q_o$ and $2(1 - \epsilon)Q_o$ respectively. The frequency $f_{xy}(Q_o)$ is then solution of equation 4.3:

$$f_{xy}(Q_o) = f_{xx}(2\epsilon Q_o) = f_{yy}(2(1 - \epsilon)Q_o) \quad (4.3)$$

Figure 4.4d illustrates the geometrical interpretation of equation 4.3 leading to frequency determination: the distances BA_{xx} and BA_{yy} are equal. This construction has been applied to the experimental data of figure 4.3. In all studied cases the geometrical construction predicts accurately the frequencies of the asymmetric case. In addition, an analytical expression for ϵ is obtained by replacing Q_o in equation 4.1 by the new oil flow-rates and solving the right hand side of equation 4.3:

$$\epsilon = \frac{Q_y^\beta}{Q_x^\beta + Q_y^\beta} \quad (4.4)$$

The combination of equation 4.1, 4.3 and 4.4 leads to the general expression for the droplet production frequencies as a function of oil and aqueous flow-rates:

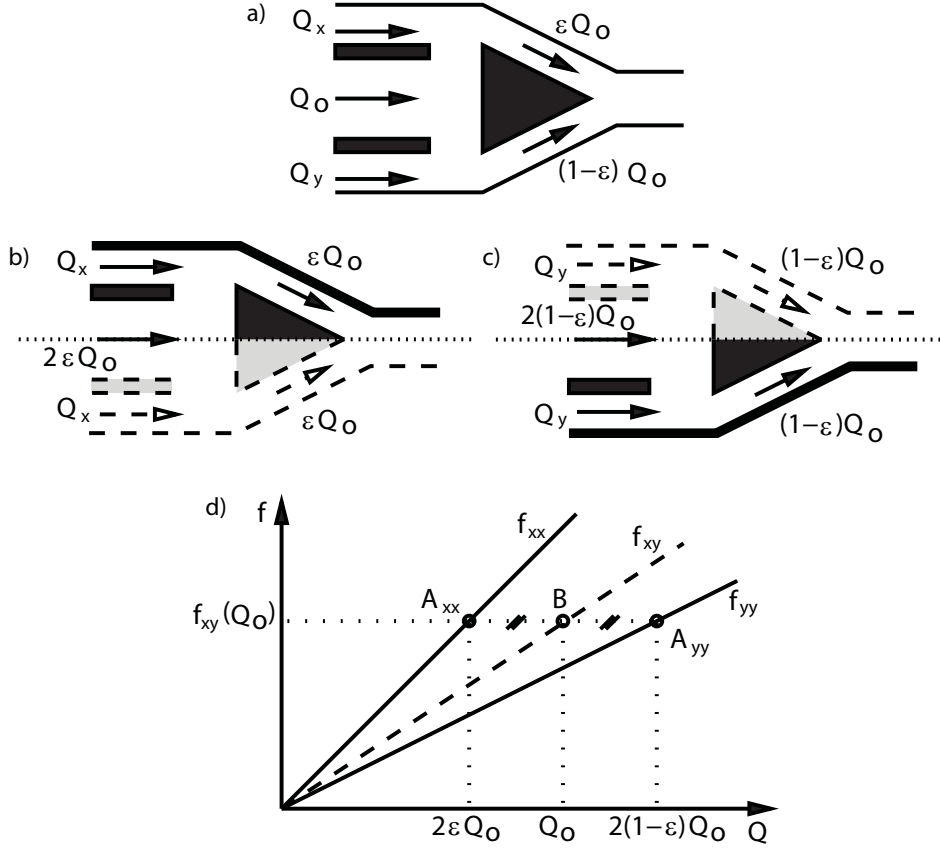


Figure 4.4.: Decomposition of the asymmetric case. a) Splitting of the oil flow in the asymmetric case. b,c) Decomposition of the asymmetric case into two symmetric cases. d) Geometrical determination of the droplet production frequency in the asymmetric case (point B). This point is obtained as the middle of the segment A_{xx}, A_{yy} corresponding to the symmetric cases with the decomposed oil flow-rates.

$$f_{xy} = 2\alpha \frac{Q_o Q_x^\beta Q_y^\beta}{Q_x^\beta + Q_y^\beta}, \quad (4.5)$$

The relationship between f_{xy} and the parameter $Q_o Q_x^\beta Q_y^\beta / (Q_x^\beta + Q_y^\beta)$ has been compared to all experimental results obtained at various oil and aqueous flow-rates in figure 4.5. The frequencies obtained experimentally collapse on a single master curve with an exponent of 1, as predicted by equation 4.5 without any additional fitting parameters. The exponent β is that obtained experimentally in the symmetric case.

Both the values of the symmetric and asymmetric case are overlaid in figure 4.5. Therefore, equation 4.5 is the generalized form of the power-law in equation 4.1 accounting for both the symmetric and the asymmetric case. In addition, equation 4.5 allows the frequency in the asymmetric case f_{xy} to be described as the harmonic mean value of the frequencies in the symmetric cases f_{xx} and f_{yy} :

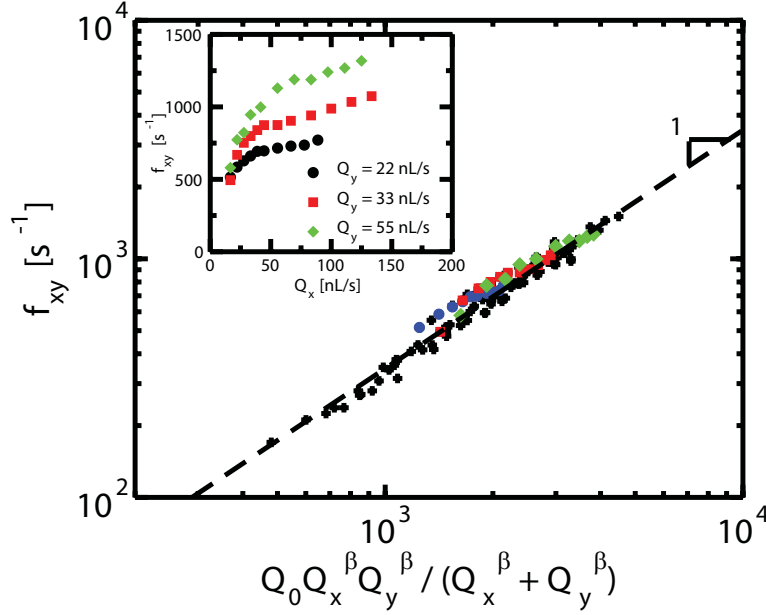


Figure 4.5.: Frequencies measured for various oil flow-rates (from ~ 110 to 400 nL s^{-1}) and aqueous phase (from ~ 10 to 60 nL s^{-1}). The data collapse on a single master curve predicted by equation 4.5. The exponent $\beta = 0.82$ is the one obtained experimentally from the symmetric case. inset: dependence of frequency as a function of Q_x for a fixed value of $Q_o = 220 \text{ nL s}^{-1}$ and for 3 values of Q_y . The data points are reported on the main graph with the same symbols.

$$f_{xy} = \frac{2}{1/f_{xx} + 1/f_{yy}} \quad (4.6)$$

According to figure 4.4d, there are an infinite number of ε solutions that guarantee a split of the oil between the two arms, each of these solutions corresponding to different frequencies f_{yy} and f_{xx} ; only one ε solution corresponds to the same frequency for both arms. It should be noted that pressure calculations based on Poiseuille flow in both arms of the nozzle do not explain these values of ε , since the presence of a droplet in the channel influences the pressure distribution in the channels [190]. This point confirms the previous conclusions: the mechanism of alternation between the two nozzles is the result of the modification of the oil flow by droplets wider than the channel.

Besides the possibility to accurately predict droplet production frequencies by equation 4.5 there is another important practical consequence from this theoretical analysis. We have shown that the dual nozzle is capable of producing droplet pairs over a large range of different flow-rate combinations. Nevertheless, this pairing accuracy can be only obtained for two continuous aqueous phases on both arms of the nozzle. When replacing a continuous stream by an emulsion of monodisperse droplets, both the flow-rate Q_x and the frequency f_{xy} are fixed. Under these conditions, according to figure 4.4d, for a fixed Q_y , there is only one flow-rate Q_o that guarantees that $BA_{xx} = BA_{yy}$: the coupling will occur only when the flow-rates are properly tuned, coming back to the initial limitations of pumping rate

and device depth heterogeneities. This conclusion is supported by experimental observations that no coupling occurred with reinjected emulsions (data not shown). Unless additional coupling strategies are applied, the presented analysis proves that it is not possible to obtain a self-triggered pairing device for a reinjected emulsion based on this coupling mechanism. However, the level of control and the accuracy in producing droplet pairs from continuous aqueous phases allows the realization of highly sensitive and reproducible experiments in microreactors, initiated by electrocoalescence of droplet pairs containing different reagents, that are not feasible in co-flow systems [30]. This design is therefore an additional tool for the control of (bio-)chemical reactions that complements the other pre-existing microfluidic modules for droplet manipulation.

4.3. Chapter summary, conclusion and outlook

In terms of fundamental studies, this work should be extended to determine the universality of the exponent β . Indeed, while we have shown here that in the case of alternating droplets, the system exhibits a power-law behavior which reduces the analysis of the system to a single power-law exponent, the nature of this exponent has not been determined. It might differ from the one expected from simple drop production due to a feedback effect similar to the one described recently by Sullivan and Stone [191]. Further studies should therefore focus on this point and on the determination of β as a function of device dimensions, fluid viscosities and interfacial tensions in order to test the universality of the exponent.

In summary, we have designed and characterized a microfluidic module for the controlled production of droplet pairs. The size ratio between paired droplets is directly controlled by the flow-rates of the aqueous streams. We determined a well-defined regime of flow-rates corresponding to droplet pairing which is achieved when the droplets are wider than the channel width. In this pairing regime, droplet production frequencies (and volumes) display a power-law behavior with the flow-rates – determined experimentally in the symmetric case and generalized to the asymmetric case – which enable the prediction of frequencies and droplet volumes.

4.4. Materials and methods

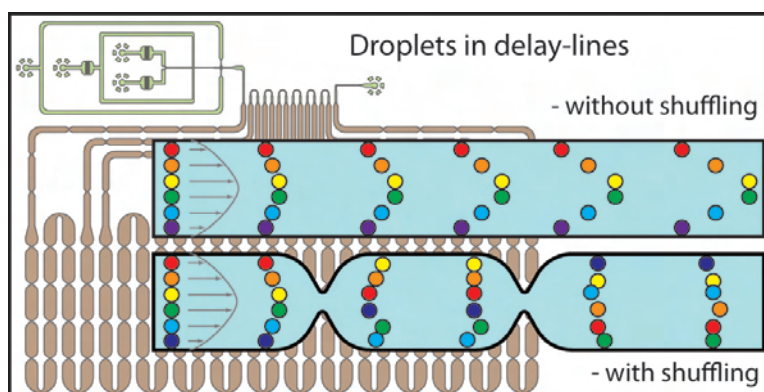
Microfluidic devices with $h=25\ \mu\text{m}$ deep channels were prepared by standard soft-lithography techniques in poly(dimethylsiloxane) (PDMS, Sylgard 184, Dow Corning) (see chapter 1.3.1). The PDMS was bound to a glass slide after treatment in an oxygen plasma. The channels were coated with a commercial surface coating agent (Aquapel, PPG Industries) to increase hydrophobicity and subsequently dried with N_2 . Volumetric flow-rates were controlled by syringe pumps (PHD2000, Harvard Apparatus). The microfluidic device consists of two adjacent nozzles coupled together by the use of a single central oil stream (figure 4.1).

The oil stream comprised a perfluorocarbon oil FC40 (3M) with 2.5% (w/w) of surfactant, made of the ammonium salt of a perfluorinated polyether (PFPE) (Krytox FSL, Dupont) [181] and flowing

at a rate Q_o . Two aqueous phases – a mixture of phosphate buffered saline solution (PBS; Sigma) containing either $50\ \mu\text{M}$ resorufin or $10\ \mu\text{M}$ fluorescein – are dispensed through the lateral channels x and y at volumetric flow-rate rates Q_x and Q_y . A 488 nm laser source focussed in the channels through a $\times 40$ microscope objective (Leica) excited the droplets. Fluorescent emission intensities were measured simultaneously on two photomultiplier tubes (Hamamatsu) in the range of 495-520 nm (green, fluorescein detection) and 578-657 nm (orange, resorufin detection) respectively. Fluorescent detection coupled to a data-acquisition device (Labview - National Instruments) allowed signal processing for droplet frequency measurements and statistical analysis. Additionally, sequences of images were recorded with a high speed camera (Phantom V4.2 at $2 - 10 \times 10^3$ frames per second).

Chapter 5.

Reliable microfluidic on-chip incubation of droplets in delay-lines



L. Frenz, K. Blank, E. Brouzes and A. D. Griffiths, *Lab Chip*, 2009, **9**, 1344–1348. [33]

Contents

5.1. Introduction	70
5.2. Solutions to avoid pressure problems	70
5.3. Dispersion of incubation times	72
5.4. Reducing the dispersion of incubation times	74
5.4.1. Redistribution of droplets as a strategy to reduce dispersion	74
5.4.2. Multiple parallel channels as a strategy to reduce dispersion	76
5.5. Measurement of enzyme kinetics	78
5.6. Materials and methods	80
5.6.1. Cloning, expression and purification of β -lactamase	80
5.7. Chapter summery, conclusion and outlook	81

Together with droplet creation, fusion and sorting, the incubation of droplets is one of the most important and essential operations for droplet-based microfluidic assays. This chapter concerns the development of delay-lines, which are necessary to allow incubation of reactions for precise time periods. We analyze the problems associated with creating delay-lines for incubation in the minute to hour time range, which arise from back-pressure and from the dispersion in the incubation time due to the unequal speeds with which droplets pass through the delay-line. We describe delay-line systems which resolve these problems and demonstrate their use to measure reaction kinetics over several minutes in droplets.

5.1. Introduction

Microfluidic modules have been described which allow highly monodisperse droplets to be created (chapter 1.5.1); split (chapter 1.5.3); fused (chapter 1.5.4); sorted (chapter 1.5.5); and the contents of the droplets mixed on ms timescales (chapter 1.5.2): all at high throughput (typically \geq kHz). Based on these developments a range of applications has already been transferred to microfluidic systems such as protein crystallisation [192], the measurement of chemical kinetics [17], enzymatic assays [26], cell based assays [137, 193], the synthesis of monodisperse polymer beads/particles [194, 185], the synthesis of organic molecules [195, 196], and the synthesis of nanoparticles [179, 30]. Multiple modules can potentially be integrated into single microfluidic chips, allowing sophisticated multi-step procedures to be executed on-chip.

This chapter describes the development of another essential module for performing reactions in integrated microfluidic systems - the delay-line - which is necessary to allow incubation of reactions for precise time periods. For long reaction times (>1 -2h) the droplets can be incubated within an on- or off-chip reservoir and reinjected into the microfluidic device for analysis [137, 193]. But this method is not practical for shorter incubation times. For very short reaction times (<1 min) short and narrow microfluidic channels (delay-lines) have been used in which the droplets remain in single-file [26, 197]. However, to date, it has not been possible to create a reliable delay-line for incubation times in the (extremely useful) range of 1 min to 1 hour. The ideal on-chip incubation system should have very low back-pressure, very low dispersion of incubation times and enough flexibility so that a range of different incubation times would be accessible for a given design.

5.2. Solutions to avoid pressure problems

Two simple equations are necessary to characterize the behavior of delay-lines. Equation 5.1 estimates the delay time t , whereby Q is the flow-rate and l , w and h represent the length, width and height of the channel. Equation 5.2 estimates the pressure drop P along a channel, whereby c is a constant depending on the w/h ratio (equation 5.3) and η is the viscosity. Equation 5.2 is accurate to within 0.26% for any rectangular channel with $w/h > 1$, provided that the Reynolds number is below ~ 1000

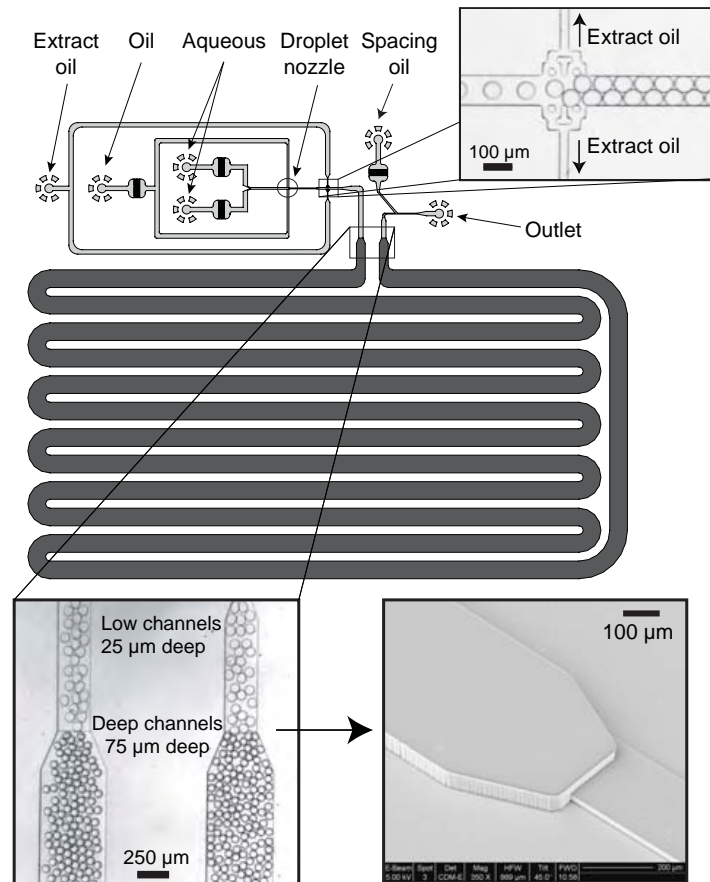


Figure 5.1.: Layout of a two-depth device with a delay-line. The $50\ \mu\text{m}$ wide nozzle for droplet generation and the fluorescent read-out channel after the delay-line have a channel depth of $25\ \mu\text{m}$ (light grey). In addition, this part contains two fork-like structures shortly after the nozzle which allow for the extraction of oil (top right image). The delay-line itself (dark grey) consists of channels with a depth of $75\ \mu\text{m}$, length of $40\ \text{cm}$ and a width of $1000\ \mu\text{m}$. The droplets pass from a $25\ \mu\text{m}$ to a $75\ \mu\text{m}$ deep channel at the connection point (bottom left image). The SEM image of the connection point (bottom right image) shows the robustness of this fabrication technique. Even if the channels are not perfectly aligned and overlap, the fluidic connection remains intact and no lifting of the structures occurs.

and no bubbles, droplets or obstructions are present [190]. It remains difficult to calculate P exactly for two phase microfluidic flow [190]. However, the estimate of the pressure drop given by equation 5.2 is sufficient to guide the design of delay-lines. The following example shows that the pressure over long channels can easily surpass the working limits of the pumps ($\sim 33\ \text{bar}$) and of the device (delamination at $\sim 3\ \text{bar}$) [44]. To obtain $10\ \text{s}$ of delay at a total flow-rate of $500\ \mu\text{L h}^{-1}$ in a channel of width $w = 50\ \mu\text{m}$ and height $h = 25\ \mu\text{m}$ (suitable for $30\text{-}50\ \mu\text{m}$ droplets in single-file) a channel length of $l = 1.1\ \text{m}$ is necessary.

$$t = \frac{lwh}{Q} \quad (5.1)$$

$$R_{fl} = c\eta \frac{l}{h^3w} \quad (5.2)$$

$$c = 12 \left[1 - \frac{192}{\pi^5} \frac{h}{w} \tanh\left(\frac{\pi w}{2h}\right) \right]^{-1} \quad (5.3)$$

According to equation 5.2 this leads to a back-pressure of over 100 bar ($\eta = 0.0034$ Pa s for the oil and $c = 17.5$). A solution to the pressure problem can be found by inspecting equation 5.2. All the parameters affect the pressure drop linearly except for the smallest channel dimension (usually the channel height), where the pressure drop is inversely proportional to the cube of the channel height. This means that increasing the channel height will significantly reduce the pressure drop.

Therefore, the use of delay-lines with deep, wide channels allows longer droplet incubation times without any back-pressure problems. However, to create and manipulate picoliter volume droplets the channels need to have dimensions similar to the droplet size (20-50 μm). A solution to satisfy both criteria is to create a device with narrow, shallow channels where the droplets are created, split, fused, analyzed and sorted, followed by a second part to incubate droplets with deep, wide channels to avoid pressure problems and to increase delay times. An example of such a device is presented in figure 5.1 and its fabrication is described in the materials and methods section 5.6.

An additional approach to increase delay times and to reduce the pressure drop is to decrease the total flow-rate Q . However, the aqueous flow-rate can not be reduced since it determines the throughput (droplets/second) and an oil flow-rate of at least the same magnitude as the aqueous is also necessary to create well defined droplets [64]. A solution is to extract oil after the droplets have been formed. The device shown in figure 5.1 allows the creation of droplets at any flow-rate and the subsequent oil extraction (of up to 92% of the oil) leads to a reduction of the total flow-rate. With this approach the delay time increases proportionally with the volume of oil extracted and delay times of 12 min are easily achievable even with the relatively short ($l = 40$ cm, $w = 1$ mm, $h = 75$ μm) delay-line shown in figure 5.1. By further increasing the channel dimensions, even longer delay times were achieved; the longest tested ($l = 1$ m, $w = 1$ mm, $h = 150$ μm) reached incubation times of up to 69 min without any back-pressure problems.

5.3. Dispersion of incubation times

Whereas wider and deeper channels resolve the pressure problem, the order of droplets is not necessarily maintained in these channels. A well known phenomenon in microfluidic channels is the so-called Taylor dispersion of reagents due to the parabolic flow profile within the channels (*Poiseuille flow*) [32]. As a consequence, the flow-rate in the center of the channel is higher than the flow-rate close to the walls. Therefore, as soon as a channel is wide enough for droplets to overtake each other these

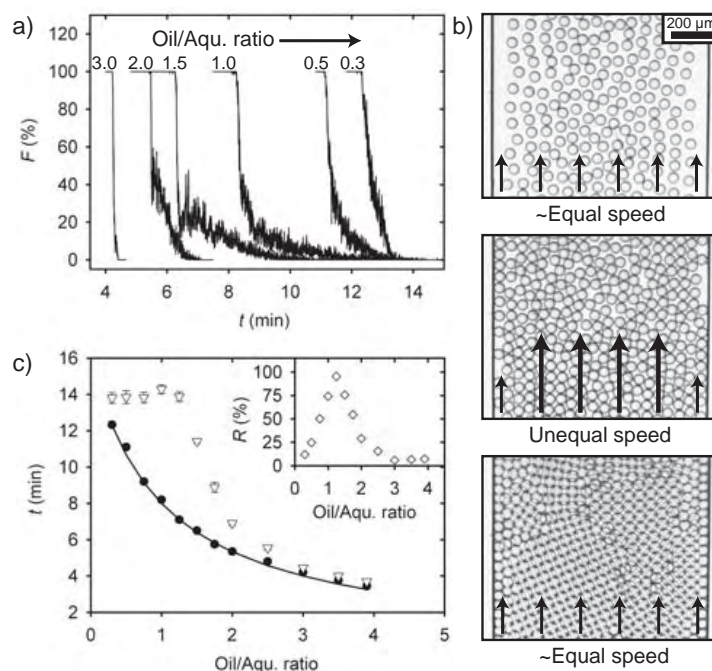


Figure 5.2.: Dispersion of droplets at different droplet densities (oil/aqu. ratio). a) The delay-line is filled with highly fluorescent droplets ($F = 100\%$), followed by a second population of droplets with lower fluorescence ($F = 0\%$) with an initially sharp transition time (~ 10 s) at the beginning of the delay-line. At the end of the delay-line the spreading of this transition is an indicator for the dispersion at different droplet densities (oil/aqu. ratios). b) At low densities (top; oil/aqu. > 3) the droplets do not have contact with the channel walls and all flow at roughly equal speed. At medium droplet densities (middle; oil/aqu. ratio of ~ 0.7 -3) some droplets travel in the slow flow lines close to the walls and are overtaken by droplets following the faster more central streamlines. At very high densities (bottom; oil/aqu. ratio < 0.7) this effect is reduced, due to the dense packing. c) Measurements of the transition parameters for different droplet densities. The transition time is defined as the difference between the start (\bullet) and the end (∇) of the transition. A fit to the start of the transition (\bullet), which corresponds to the delay time, returns the volume of the delay-line ($26.6 \mu\text{L}$) in good agreement with the calculated value ($28.2 \mu\text{L}$). The inset shows the relative dispersion ratio R defined as the transition time/delay time ratio.

different flow-rates over the cross section affect the droplet flow. The central droplet stream can flow faster than the streams close to the walls, thereby leading to significant differences in the incubation times of individual droplets.

Using the device in figure 5.1 we investigated the dispersion of droplets in a delay-line. For this purpose we used a stream of highly fluorescent droplets followed by a stream of low fluorescent droplets. We achieved this by co-flowing two streams of phosphate buffered saline (PBS) with and without $20 \mu\text{M}$ fluorescein into the nozzle. By switching the co-flow ratio from 4:1 to 1:4 two droplet populations containing different fluorescein concentrations were created directly after each other with a transition time of about 10 s. The transition time is defined as the time between the arrival of the first droplet with low fluorescence and the arrival of the last droplet with high fluorescence (followed by a continuous sequence of at least 10^6 low fluorescence droplets). A LabView program controlled the

flow-rates, and recorded the fluorescence intensity of individual droplets at the end of the delay-line. The recording was started when the ratio of the co-flow was switched so that the start of the transition corresponds to the delay time and the duration of this transition is the transition time. The percentage of high fluorescent droplets F was evaluated in packages of 100 droplets. The corresponding values were plotted into a time trace (see figure 5.2a) and no dispersion could be assumed if the transition time was still within 10 s at the end of the delay-line.

However, under many conditions much longer transition times were observed (see figure 5.2a). A systematic analysis showed that the droplet density has a strong effect on the dispersion. For this analysis, droplets were generated under identical conditions (resulting in a constant droplet volume of 78 pL and a diameter of 53 μm) while changing the droplet density by extracting different volumes of oil (figure 5.2a). At low droplet densities (oil/aqueous ratio of 3) a sharp transition (no dispersion) was observed. With increasing droplet density the transition became longer. In this regime, typically about 50-60% of the highly fluorescent droplets population passed through almost at the same time while the rest was significantly retarded. For example at an oil/aqueous ratio of 1.25 some droplets needed 6 min to pass the delay-line while others needed up to 11 min. Finally, at very high droplet densities the transition time decreased again.

These observations can be explained by inspecting figure 5.2b. At low droplet densities most of the droplets remain in the fastest streamlines in the middle of the channel and flow at almost equal speeds. At medium densities droplets get pushed outwards to the walls where they experience lower flow-rates and are overtaken by the more central droplets. At very high densities the droplets adopt a crystal-like packing, making overtaking almost impossible, and move as one block through the channel.

Figure 5.2c summarizes the dispersion ratio R (transition time/delay time ratio) of the droplets at different oil/aqueous ratios. The dispersion is very important for the mid-range of oil/aqueous ratios with values of R as high as $>90\%$. In this regime any quantitative analysis of reaction kinetics becomes impossible since the incubation times vary almost over a 2-fold range. In the low density regime (right part of the graph) the dispersion is low ($R \leq 10\%$), but the delay time may not be sufficiently long. Therefore, the high density regime would be desirable since both the delay time is long and the dispersion low ($R \leq 15\%$). However, it remains difficult to run the system in this regime. The slope of the curve is very steep and small changes in the volume fraction of the extracted oil can increase the dispersion by minutes. Furthermore, the system is not very flexible, since only the lowest oil/aqueous ratio can be used, limiting the spectrum of accessible delay times for a given design.

5.4. Reducing the dispersion of incubation times

5.4.1. Redistribution of droplets as a strategy to reduce dispersion

To address the problem of dispersion we tested two different approaches. The first approach consisted of preventing the droplets from overtaking each other by dividing the channel into multiple narrow channels (see section 5.4.2). This design did not reduce the dispersion sufficiently to enable reliable

5.4. Reducing the dispersion of incubation times

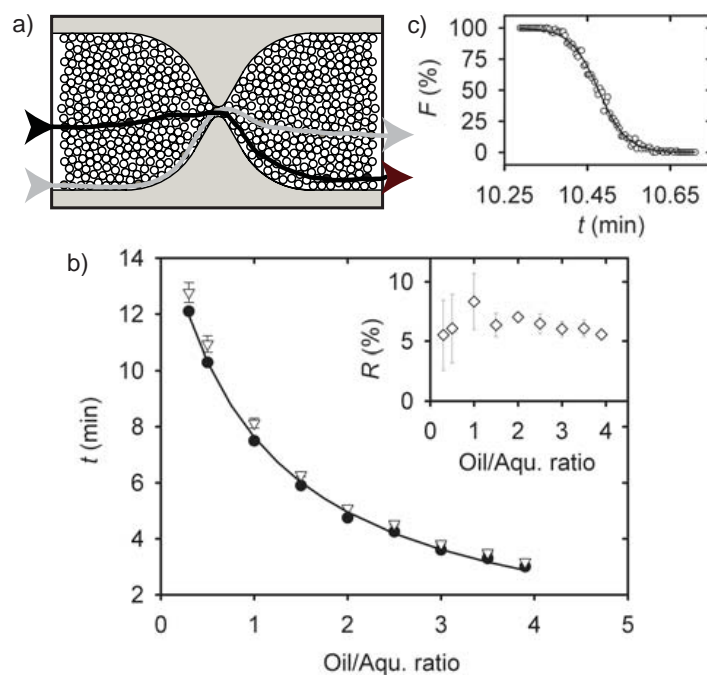


Figure 5.3.: Reducing dispersion in delay-lines. a) Droplets are stochastically redistributed (mixed) at each constriction, preventing the same droplets from remaining in the same (faster or slower) streamlines. b) Results of the dispersion measurements. The constrictions significantly reduce the dispersion (compared to figure 5.2c) for all droplet densities. The transition time is never higher than 45 s corresponding to relative dispersion ratio R lower than 10%. c) Due to the mixing effect the shape of the transition becomes logistic, corresponding to a Gaussian distribution for the incubation times.

kinetic experiments (R still reaches values of over 50%). The second strategy consisted of repeatedly shuffling droplets by introducing constrictions every 3 cm along the delay-line (figure 5.3a). These constrictions reduce the channel width to the dimension of a droplet and result in a repeated mixing of the droplets over the channel cross section, preventing the same droplets from remaining in the same (faster or slower) flow lines. This random re-distribution was verified by analyzing high speed movies.

Indeed, after testing several different constriction designs (see optimization section below), a significantly reduced dispersion ($R \leq 10\%$) was found (figure 5.3b) compared to the delay-line without constrictions (figure 5.2c). Furthermore, the shape of the transition changed. For a delay-line without constrictions the slow droplets lead to a long 'tail' as can be seen in figure 5.2a (e. g. oil/aqueous ratio of 1.5 or 1.0) and the transition is non-symmetrical. In contrast, for the delay-line with constrictions the shape of the transition becomes symmetrical (figure 5.3c). The incubation times of individual droplets in the delay-line are equally distributed around a mean value and the transition can be perfectly fitted with a logistic function, which corresponds to a Gaussian distribution of the incubation time. This Gaussian distribution is obtained at all droplet densities and the width of the distribution (which is a measure for the dispersion) scales proportionally with the incubation time of the droplets in the delay-line. With this improvement, the whole system becomes more stable and reproducible and opens up an important range of new applications.

Optimizations of the constriction designs

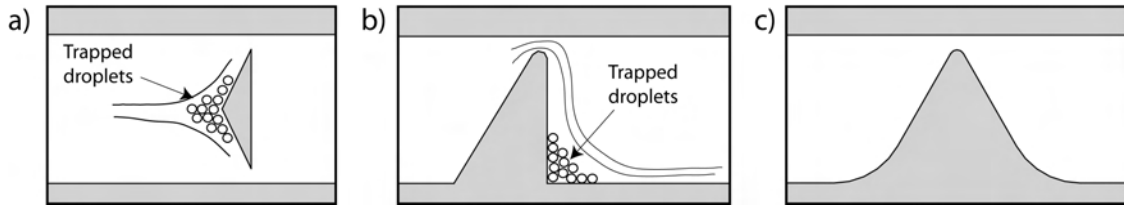


Figure 5.4: Characteristics of different constriction designs. In all cases the width of the main channel is $1000\ \mu\text{m}$ wide and is reduced to $60\text{-}100\ \mu\text{m}$ at the constriction. Droplets flow from left to right. a) Obstacles in the channel split the stream and trap droplets temporary. b) Sharp corners, especially after a constriction lead to dead volumes with low flow-rates. Droplets get temporary caught in the corner. c) Design avoiding any possibilities for droplets to get trapped.

In general, all tested layouts with constrictions in the delay-line proved to be useful in reducing dispersion. However, we extracted certain design rules which improved the system. Figure 5.4a shows a design with posts inside the channel. In this case, droplets are forced to pass the obstacle on either side. We observed that droplets can get temporary trapped at the tip of the obstacle where the stream splits, and that the droplet stream would confine them to this spot (see figure 5.4a). The second design depicted in figure 5.4b is an asymmetric constriction with a corner. The flow-rates in this corner are low and droplets get pushed and trapped into this spot especially at high droplet densities.

It is therefore favorable to avoid designs, which split the stream - meaning that obstacles in the middle of the channel should be avoided. Furthermore sharp corners, especially after a constriction should be rounded out. These findings led to two designs, which resulted in very low dispersion values. The first design is shown in figure 5.4c and the second design in figure 5.3a.

Additionally to the here presented mixing strategies by constrictions it might be also possible to use other methods to mix the droplets. Any of the illustrated methods from figure 1.18 could be used in principle, although one of the most interesting ones would be probably the usage of the heringbone-mixers throughout the entire channel [68].

5.4.2. Multiple parallel channels as a strategy to reduce dispersion

In addition to the delay-line with constrictions presented in section 5.4.1 we tested an alternative layout. The strategy was not to reduce dispersion but to prevent dispersion from occurring by removing the possibility for droplets to overtake each other. The design consists of multiple parallel narrow channels (see figure 5.5a), that are not wider than twice the droplet diameter. As a result, there can not be any fast central stream of droplets within these channels. Provided that the flow-rates in the different channels are equal, the expectation is that there would not be any dispersion.

Initial designs allowed an exchange of flow between the narrow channels only at the beginning and at the end of the delay-line. As a consequence, any irregularity (dirt, channel depth fluctuations, etc.) present in one of the channels completely destabilized the system. In order to reduce this problem

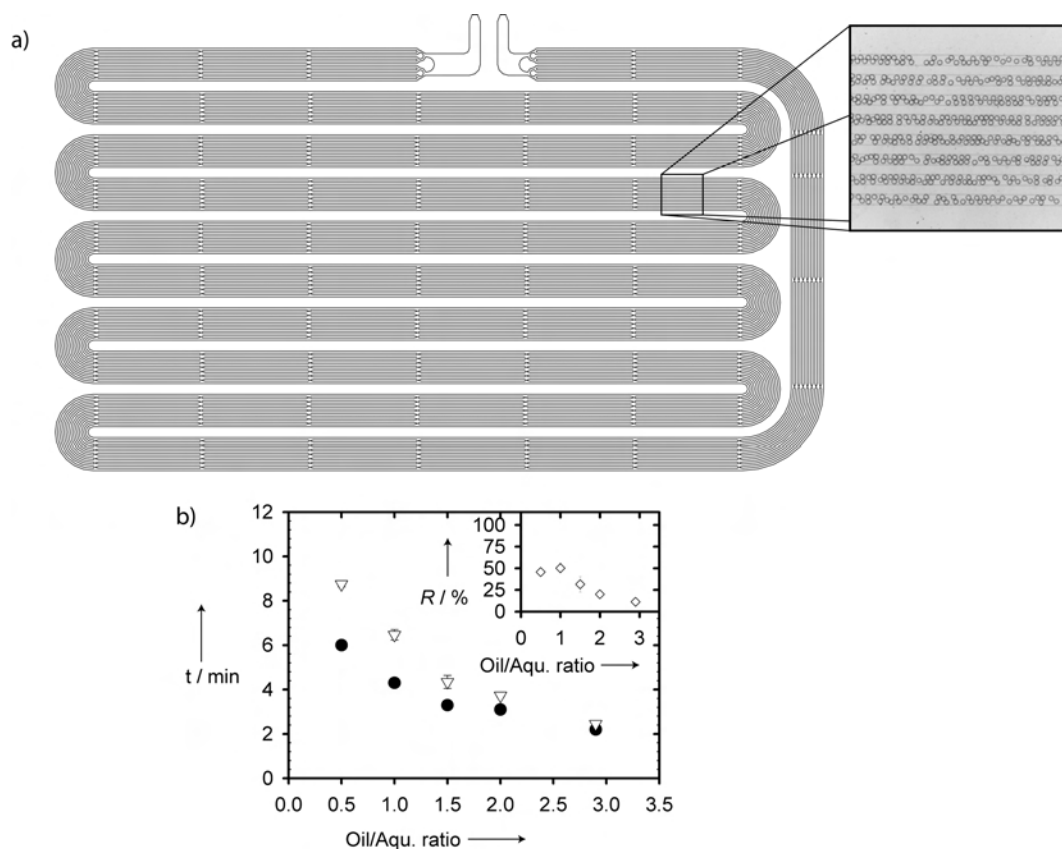


Figure 5.5.: Multiple channel delay-line. a) The wide channel which forms the delay-line is divided into eight parallel channels of $100\ \mu\text{m}$ width and $75\ \mu\text{m}$ depth. The design includes connections between the channels every 3 cm. Since the width of these channels is slightly smaller than twice the droplet diameter the droplets cannot overtake each other and all droplets have contact with the walls. b) Result of the dispersion measurements analogous to figure 5.2c.

we added bridges between the channels every 3 cm. This strategy improved the system but a completely homogenous flow across all the channels could not be achieved. For this reason the relative dispersion ratio, as seen in figure 5.5b, still reaches values above 50%. Although it is a clear reduction of the dispersion compared to the conventional delay-line (figure 5.2c - max $R > 90\%$), this layout is outperformed by the delay-line with constrictions (figure 5.3b - $R < 10\%$). Additionally, this multiple channel approach requires more real-estate on the chip to get the same volume as a single wide channel of the same length. Furthermore, the fluidic resistance is higher for multiple channels (equation 5.2), which limits the practical length of the delay-line (hence the maximum incubation time). In summary, the multiple channels approach has the potential to prevent dispersion, but further investigation is required to understand the factors at play in this system.

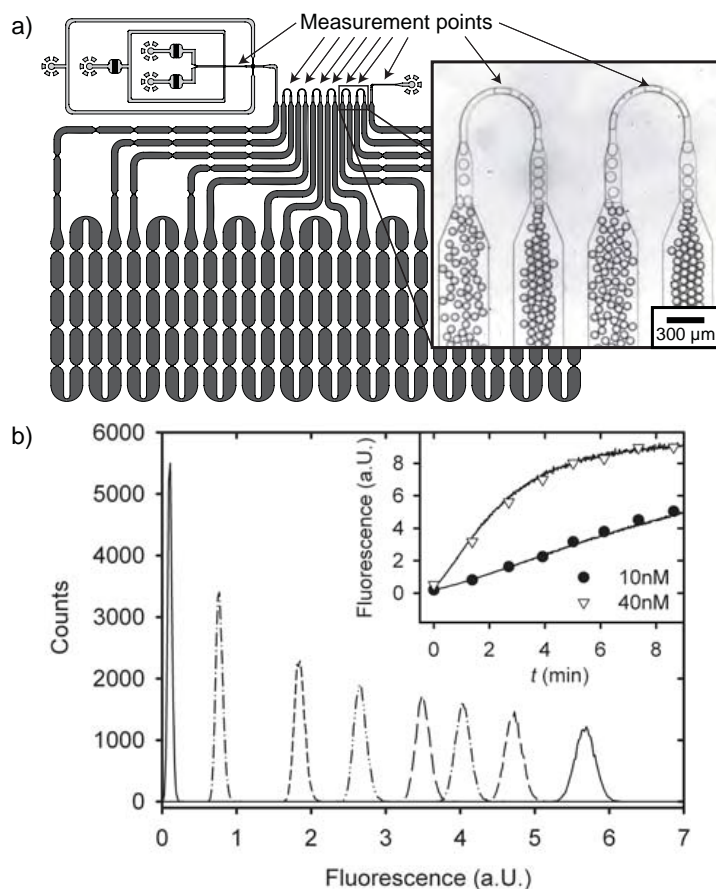


Figure 5.6: a) Layout of a device designed for kinetic measurements including eight measurement points within the shallow channels ($50\ \mu\text{m}$ wide, $25\ \mu\text{m}$ deep; light grey). The first point is located just after the droplet creation, followed by six loops (shown in the microscope image) and one last measurement point before the outlet. The deep channels ($1000\ \mu\text{m}$ wide, $75\ \mu\text{m}$ deep; dark gray) contain constrictions every $3\ \text{cm}$. b) Enzyme kinetics of β -lactamase. Histograms of fluorescence intensities of droplets containing $10\ \text{nM}$ β -lactamase and $10\ \mu\text{M}$ Fluorocillin were collected at the 8 measurement points (time points) in the delay-line. As expected for a delay-line with constrictions all the distributions (each containing 20,000 droplets) appear to be Gaussian. The inset shows the mean droplet fluorescence values plotted against the corresponding times for each measurement point. At an enzyme concentration of $10\ \text{nM}$ the reaction remains linear whereas it starts to saturate at $40\ \text{nM}$. Both measurements are in good agreement with the cuvette-based measurements (solid lines).

5.5. Measurement of enzyme kinetics

As a first demonstration of the delay-line reliability, we measured the kinetic of an enzymatic reaction. The turnover of the fluorogenic substrate Fluorocillin by the enzyme β -lactamase was detected over a range of several minutes in the delay-line. For this purpose, we introduced an additional feature into the layout of the delay-line. Whereas the geometry of the delay-line in figure 5.1 only allowed a single measurement at the end of the delay-line, now several additional measurement points were introduced between the inlet and the outlet (figure 5.6a). These measurement points were designed within the

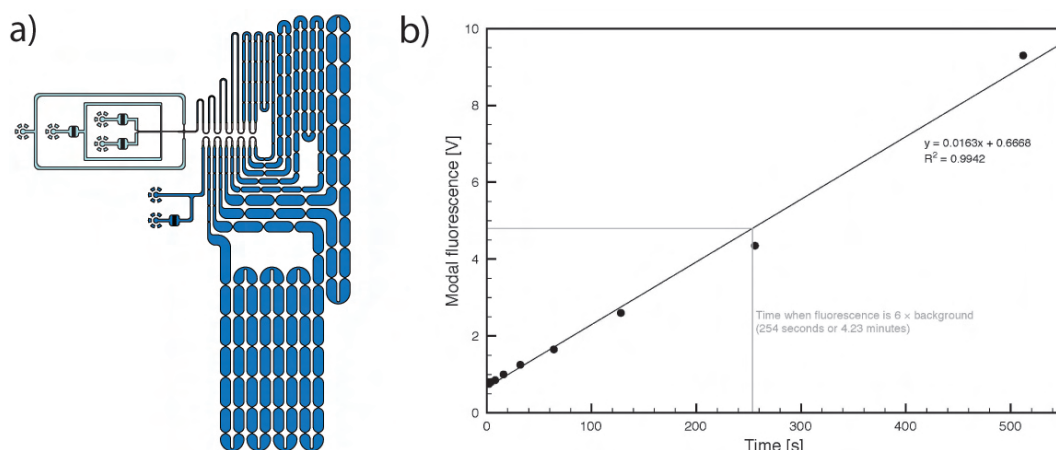


Figure 5.7.: a) Layout of a delay-line system to measure reaction kinetics with a higher sample density in the fast reaction region, while still covering the long reaction region. In this case the measurements were taken after 1,2,4,8,16... 512 s.

narrow and shallow channels to obtain sufficient spacing between the droplets and also to confine them laterally for the fluorescence detection. Droplets therefore moved back and forth between the deep channels for incubation and the narrow channels for measurements.

When performing measurements at several points along the delay-line the droplet density is an important factor. If the droplets are packed too densely the fluorescence signal of individual droplets cannot be resolved anymore. Therefore, these experiments need to be carried out at an oil/aqueous ratio that provides a good compromise between delay times and droplet spacing. This ratio corresponds exactly to the intermediate regime where the dispersion in a delay-line without constrictions is the highest. In contrast, for the delay-line with constrictions this medium packed regime is practically accessible without dispersion. Furthermore, since the dispersion is no longer influenced by the droplet density a whole range of incubation times can be reached by varying the amount of oil extracted.

Figure 5.6b shows the fluorescence signal of the β -lactamase reaction measured at different time points. At each point the distribution is Gaussian as expected and the standard deviation is directly proportional to the mean fluorescence (data not shown). Furthermore, the measured kinetics follows exactly the same trend as in the assay performed in a cuvette (Inset, figure 5.6b), showing that the system is fully biocompatible and accurate.

In some cases it can be useful to measure initial, fast reaction kinetics in the ms-s range, without losing the information of the overall kinetics. For this purpose it is easily feasible to modify the design in figure 5.6 and place the measurement points initially close to each other, and increase the distance between them further down the channel. An example is shown in figure 5.7a, where the measurement points have been placed with logarithmically increasing separation. Consequently, also the time points in figure 5.7b have a logarithmical spacing and the fast reaction region is densely sampled but still the overall profile is obtained.

These results clearly show that the improved delay-line layout is a very well-suited system to ana-

lyze enzymatic reactions in a fast, convenient and reliable way.

5.6. Materials and methods

Soft-lithography in poly(dimethylsiloxane) (PDMS, Sylgard 184, Dow Corning) was used to prepare the devices (see chapter 1.3.1). The molds consisted of SU-8 (Microchem) with two different heights [198]. We therefore used the following procedure: First we spin coated the thinner SU-8 layer (25 μm) and exposed it with a mask which covers the part of the wafer designated to the deeper structures. After fully developing and baking the structures we spin coated a second higher layer of SU-8 onto the same wafer. This second layer was exposed and structured by a second mask (delay-line), which was aligned to the lower structures in a mask aligner. Designing the connectors (figure 5.1) in close proximity to each other facilitated the alignment and made it less prone to angle misalignments.

After casting the mold in PDMS and binding it to a glass side (after activation in an oxygen plasma) the channels were made hydrophobic using a commercial surface coating agent (Aquapel, PPG Industries). The flow-rates were controlled by syringe pumps (PHD2000; Harvard Apparatus). In all experiments flow-rates of 400 $\mu\text{L h}^{-1}$ for the oil phase and 100 $\mu\text{L h}^{-1}$ in total for the aqueous phases were used to create 53 μm droplets (78 pL) at a 50 μm nozzle.

For the dispersion characterization experiments the oil phase consisted of a perfluorocarbon oil (FC40 - 3M) containing 2.5% (w/w) of a surfactant, made of the ammonium salt of a perfluorinated polyether (PFPE) (Krytox FSL - Dupont) [181]. For the kinetic measurements with β -lactamase the oil phase consisted of 'R' oil with 1% (w/w) 'EA' surfactant (both from Raindance Technologies). One aqueous phase for the co-flow consisted of PBS with 0.1% BSA, 20 μM Fluorocillin and 10% DMSO. The other aqueous phase consisted of PBS with 0.1% BSA and 20 nM (80 nM) β -lactamase. At a flow-rate ratio of 1:1 this led to a final concentration in each droplet of 10 nM (40 nM) β -lactamase, 10 μM Fluorocillin, 0.1% BSA, 5% DMSO in PBS.

5.6.1. Cloning, expression and purification of β -lactamase

In order to produce purified β -lactamase for the enzymatic assay, His-tagged β -lactamase was expressed in the periplasm of *E. coli* and subsequently purified from periplasmic extracts using a Ni^{2+} -NTA column.

The plasmid used is a derivative of the plasmid pAK400 [199], which already codes for a C-terminal His-tag. The plasmid contains the strong RBS T7G10 and a *pelB* signal peptide for periplasmic expression, which is flanked by an upstream *XbaI* and a downstream *NcoI* site. In contrast to pAK400, which possesses a *lac* promoter, the derivative used here contains the arabinose inducible promoter of the pBAD series of plasmids (Invitrogen, Cergy Pontoise, France). To obtain this new plasmid the *lac* promoter region had been replaced with a DNA fragment coding for the *araC* repressor and the *araBAD* promoter. Furthermore, an *EcoRI* site had been introduced before the C-terminal His-tag. For the cloning of β -lactamase a pUC based plasmid having ampicillin resistance (pIVEX series;

Roche Applied Science, Meylan, France) was used as the PCR template. β -lactamase was amplified together with its signal peptide using the primers bla_forw_Xba 5'-GCTCTAGAGAAGGAGATA-TACATATGAGTATTCAACATTTCCGTG-3' and bla_rev_EcoRI 5'-GGAATTCCTCAATGCTTAA-TCAGTGAGG-3'. The PCR fragment was purified, cut with *Xba*I and *Eco*RI and cloned into the pAK400 derivative thereby replacing the pelB signal sequence. The new plasmid was verified by sequencing.

The plasmid was transformed into the *E. coli* K12 strain TB1 (New England Biolabs, Frankfurt, Germany). The cultures for the purification were grown at 25° C in 400 ml of SB medium (20 g L⁻¹ tryptone, 10 g L⁻¹ yeast extract, 5 g L⁻¹ NaCl, 50 mM K₂HPO₄) containing 30 µg mL⁻¹ chloramphenicol. This culture was inoculated from a 20 ml preculture to OD₆₀₀ = 0.1. Expression was induced with 0.02% arabinose at an OD₆₀₀ between 1.0 and 1.5. The cells were harvested 3 h after induction by centrifugation at 5000 g and 4° C for 10 min.

Periplasmic extracts were prepared according to a protocol included in the manual for the Ni²⁺-NTA columns (Qiagen, Courtaboeuf, France). The extracts were dialyzed against loading buffer (50 mM sodium phosphate pH 8.0, 300 mM NaCl, 10 mM imidazole) and loaded onto the Ni²⁺-NTA column equilibrated with loading buffer. The column was washed with 30 column volumes of loading buffer and 5 column volumes of a washing buffer (50 mM sodium phosphate pH 8.0, 300 mM NaCl, 30 mM imidazole). Elution was achieved by adding 5 column volumes of elution buffer (50 mM sodium phosphate pH 8.0, 300 mM NaCl, 200 mM imidazole). The eluted material was dialyzed against phosphate buffered saline (PBS; 10 mM Na phosphate, pH 7.4, 137 mM NaCl, 2.7 mM KCl) and concentrated using Ultrafree-4 (Millipore, Molsheim, France). The purity was confirmed by SDS-PAGE. The concentration of β -lactamase was determined by measuring the absorbance at 280 nm. The extinction coefficient was calculated using the program Vector NTI (Invitrogen). Finally, the concentration was adjusted to 1 mg ml⁻¹ (corresponding to 32.6 µM) and the protein was stored in aliquots at -80° C.

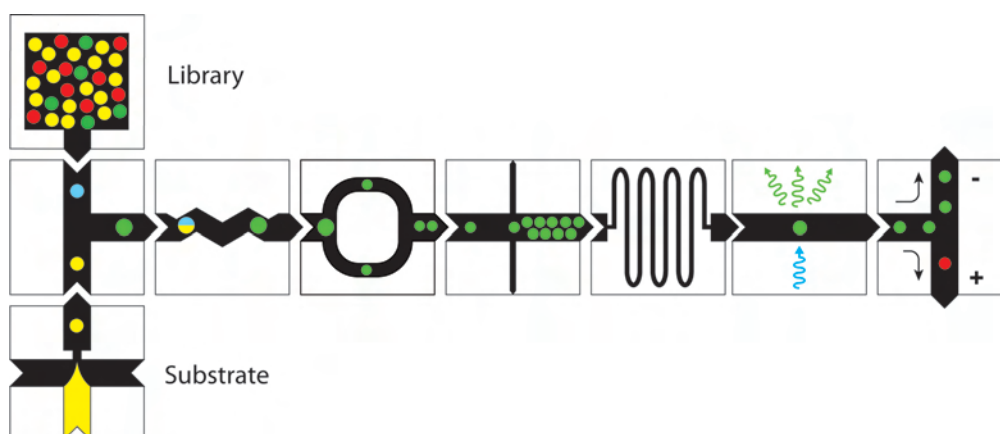
5.7. Chapter summery, conclusion and outlook

In summary, this chapter describes the problems associated with designing delay-lines to allow on-chip incubation time ≥ 1 minute for droplet-based microfluidics systems. Moreover, solutions to two fundamental problems are provided, namely the problems of pressure and unequal incubation times of droplets in the delay-lines (dispersion). The back pressure of the system can be reduced by using a two depth device with wide, deep channels for droplet incubation and narrow, shallow channels for the generation and manipulation of droplets. The extraction of oil directly after droplet generation further reduces the back pressure and facilitates even longer incubation times, which may easily reach the hour range. In addition, the extraction of oil broadens the range of incubation times, accessible for a given delay-line design. A general solution to the dispersion problem is the use of constrictions that redistribute the droplets repeatedly along the delay-line. This repeated shuffling of droplets leads to a significant reduction in the dispersion of incubation times and distributes these times equally

(Gaussian) around a mean value. These improvements allow the creation of integrated droplet-based microfluidic systems for a wide range of (bio)chemical reactions, containing multiple modules, including delay-lines which allow reaction times of 1 min to >1 hour. Finally, we validated our delay-line system by measuring the reaction kinetics of the enzyme β -lactamase on-chip: the reactions kinetics were identical to a conventional cuvette-based assay.

Chapter 6.

Integration and directed evolution



Contents

6.1. Introduction	84
6.2. Microfluidic improvements and device integration	84
6.2.1. Synchronization of reinjected emulsion	84
6.2.2. Improvements and recommendations for the sorting device	87
6.2.3. Device integration	89
6.3. Preliminary screening and enrichment results	91
6.4. Chapter summary and conclusion	92

This chapter describes a project concerning directed-evolution in droplet-based microfluidics. As outlined during the introduction 1.6.3, the purpose of this technique is to evolve improved functional biomolecules. The work described here outlines the strategies that have been developed, especially the microfluidic devices and functionalities that are necessary for these kind of assays.

6.1. Introduction

One of the main applications envisioned for droplet-based microfluidics is high-throughput screening. The ability to manipulate and sort droplets at speeds up into the kHz range makes this technology so interesting and attracts so much attention. Nevertheless, real screening applications have only recently begun to become accessible. All previous results have utilized cells [22, 127], since single molecule reactions usually do not reach signals strong enough for detection. Especially when working with DNA, amplification steps have been found to be mandatory, since no detectable enzyme activity could be observed when trying to express enzymes by *in vitro* translation/transcription (IVTT) systems from single DNA molecules per droplet [35]. On the other hand it has been demonstrated that it is possible to express smaller proteins, such as GFP, from a single DNA strand in droplets with gains exceeding the typical values for these IVTT systems ($\sim 30,000$ instead of ~ 300 proteins per gene) [24]. Nevertheless, it is believed that encapsulating single genes per droplet, amplification and IVTT is the most universal approach for a greater class of proteins. Therefore, when encapsulating single mutant genes of an enzyme into droplets, where each droplet potentially contains a different gene, mutant libraries can be created where each droplet contains a different mutant (see figure 6.1a).

The objective of this project is to develop a screening system designed to be as general and universal as possible. In the following sections, improvements to the traditional techniques of synchronizations/fusion and sorting are discussed. Furthermore, these modules are then integrated together with others to form the necessary screening chip (figure 6.1b).

6.2. Microfluidic improvements and device integration

6.2.1. Synchronization of reinjected emulsion

The synchronization system described in chapter 3 [33] can achieve almost 100% synchronization efficiency. Meaning that this system pairs all of the droplets almost perfectly. On the other hand the theory and calculations presented in chapter 4 suggest that this principle can only work when creating two emulsions, as opposed to reinjecting one through one of the two nozzle arms. Experiments confirmed this theory and it was not possible to achieve a coupling (synchronization) between the two nozzles when trying to run the system with a reinjected emulsion.

While this lack of perfect synchronization may appear to be a disadvantage, triggering droplet-breakup on the reinjected emulsion would lead to polydispersity within the newly created emulsion. For instance, assuming the breakup of the newly formed droplets (lower aqueous channel in fig-

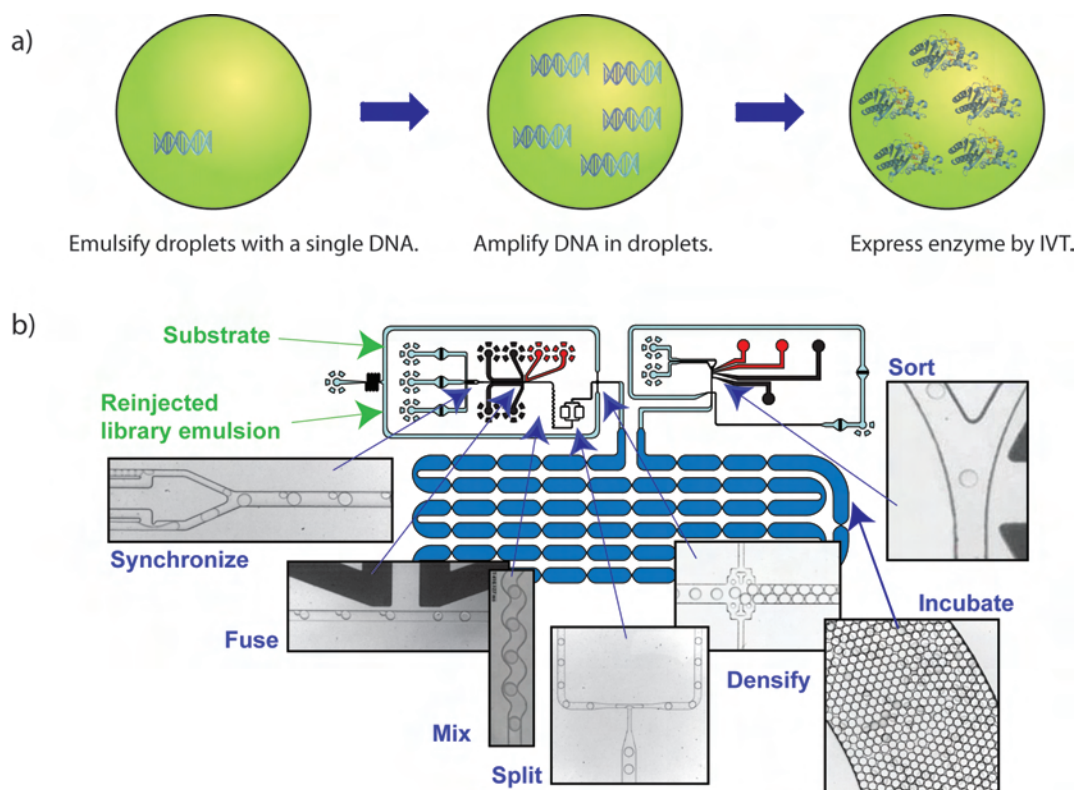


Figure 6.1.: Work-flow strategy for directed-evolution in droplet-based microfluidics. a) Library creation: One gene/mutant of the enzyme is encapsulated per droplet and is translated/transcribed into the protein it codes for. The workflow for this process is described in [35]. b) Library sorting: The emulsion containing the different mutants is reinjected into the integrated device. Here each library droplet is fused to a substrate droplet, incubated for an equal amount of time and sorted based on the activity.

ure 6.1a) would always 'wait' for a reinjected droplet passing the second nozzle (upper aqueous channel) and the reinjection frequency is not always perfectly homogenous, leading occasionally to more spacing between droplets. In these cases the newly created droplet would continue growing (constant flow-rate Q_y) and after the breakup this droplet would be larger than the previously formed droplets. In the worst case of random timing between the reinjected droplets, the newly created droplets would have a very broad size/volume distribution.

Following this logic, it is necessary to uncouple the two nozzles completely, ensuring that the creation of droplets at the lower nozzle is always constant - leading to a monodisperse emulsion from this arm. To minimize the crosstalk between the two nozzle arms, the oil stream coming from the center is already split further upstream, increasing the fluidic resistance between the two arms and therefore also reducing any crosstalk. The module can now be compared to two independent nozzles in close proximity to each other and fed by the same oil-stream. While this module cannot achieve higher synchronization efficiencies than the traditional method described in section 1.5.4, the design provides two advantages in comparison. First, instead of using four syringe pumps (2 for the oil- and 2 for the aqueous-phases) this system only requires three pumps. Consequently it is also easier to adjust the

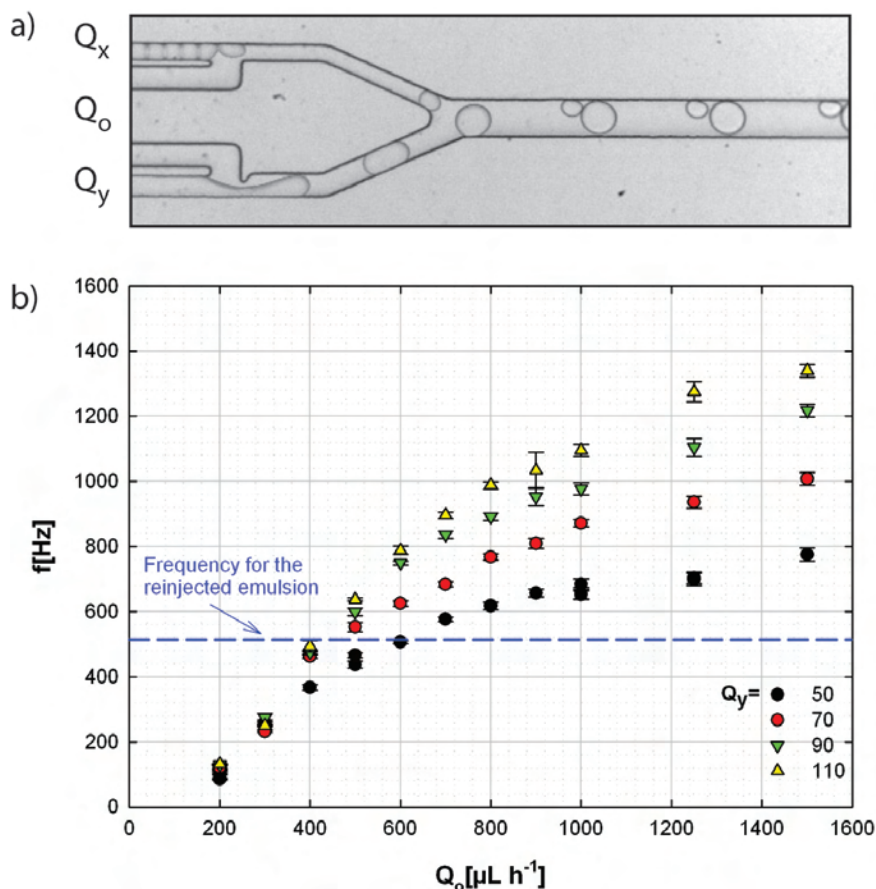


Figure 6.2.: Synchronize a reinjected emulsion. a) Shows the synchronization module. The emulsion is reinjected through the upper arm of the module, the oil enters through the central channel and the aqueous stream forming the newly made emulsion enters through the lower channel. b) Characterization of the module. The flow-rate of the reinjection Q_x is kept constant resulting in the constant frequency indicated by the blue line. The frequency of the newly created emulsion is dependent on both flow-rates Q_o and Q_y .

synchronization since only 3 instead of 4 parameters need to be considered. (ii) Additionally, the design is usually more compact and requires less space on the chip, making it useful for densely packed and highly integrated chips.

Figure 6.2b illustrates and characterizes the synchronization system. The frequency of the reinjected emulsion f_x is directly proportional to its flow-rate Q_x . The frequency of the newly formed droplets on the other hand is dependent on both the aqueous flow-rate and the oil flow-rate. The curves suggest that this frequency follows a stronger dependency on the aqueous than on the oil flow-rate. Consequently minor changes of the aqueous flow-rate result in large frequency changes, whereas oil flow-rate changes only affect this frequency minimally.

In practice these findings are very useful for adjusting and fine-tuning the nozzle. The following strategy leads to an optimally adjusted synchronization within only a few minutes.

1. Choose a flow-rate for the reinjection Q_x and define therefore the throughput.

2. Start with a random but reasonable flow-rate combination for the two remaining flow-rates.
3. Adjust the pairing efficiency roughly by the aqueous flow-rate Q_y with large frequency steps.
4. Fine-tune the synchronization with the oil flow-rate Q_o with small frequency steps.

Usually this strategy leads to a synchronization efficiency of 70-90%, depending on pump fluctuations and the homogeneity of the reinjected emulsion.

6.2.2. Improvements and recommendations for the sorting device

Sorting of droplets is probably the most sensitive and critical operation amongst the different droplet-manipulation techniques. False negatives and especially false positives can ruin the results of the entire screen. It is therefore critical to improve this step and make it as reliable as possible.

A basic requirement of a good sorting design and principle is that all droplets are required to move into the negative arm when the electrical field is switched off. It is therefore necessary to create a certain asymmetry or destabilization at the sorting junction. Initially this has been achieved by different lengths and fluidic resistances of the channels after the junction [20, 21]; droplets following the channel with the higher flux. Similarly it is possible to impose this higher flow-rate in the negative channel by connecting the outlet to a syringe pump in withdraw mode and adjusting the flow-rate manually to a value of 60-70% of the total flow-rate entering the sorting junction. This has the advantage that the system is constant, regardless of anything affecting the fluidic resistance in the two sorting arms (accumulation of droplets, tubing length differences, etc.). On the other hand the system needs time to start and syringe pump fluctuations can affect the sorting performance. A slightly different concept has been proposed recently [22], where the sorting junction itself is designed asymmetrically and therefore avoids using the extra syringe pump. On the other hand a disadvantage of this design is the increased volume of the sorting junction, demanding a larger spacing between the droplets entering the junction. The most stable and reliable system to date was recently developed by Agresti *et al.* [127]. Instead of increasing the fluidic resistance on the entire positive arm of the sorter, this sorter increases the fluidic resistance of this one arm only locally at the junction and restores the balance immediately afterwards by the ridges illustrated in figure 6.3. This has the advantage that the junction has the necessary imbalance to send all the droplets to the negative channel, while remaining resistant to anything happening further downstream. This sorting design appears to be more robust than the previous ones and also needs lower starting times than techniques that utilize withdrawing syringe pumps.

Another crucial point for sorting performance is the spacing between droplets entering the sorting junction. An increased number of false positives or negatives can be expected if the droplets are not properly spaced. This can cause droplets to come into contact with each other at the junction, potentially directing each other into the wrong channel. It is therefore necessary to use high oil flow-rates to space the emulsion. This value for the oil flow-rate reaches an upper limit at which the droplets start ripping apart by the strong shear forces and the design of the emulsion spacing region

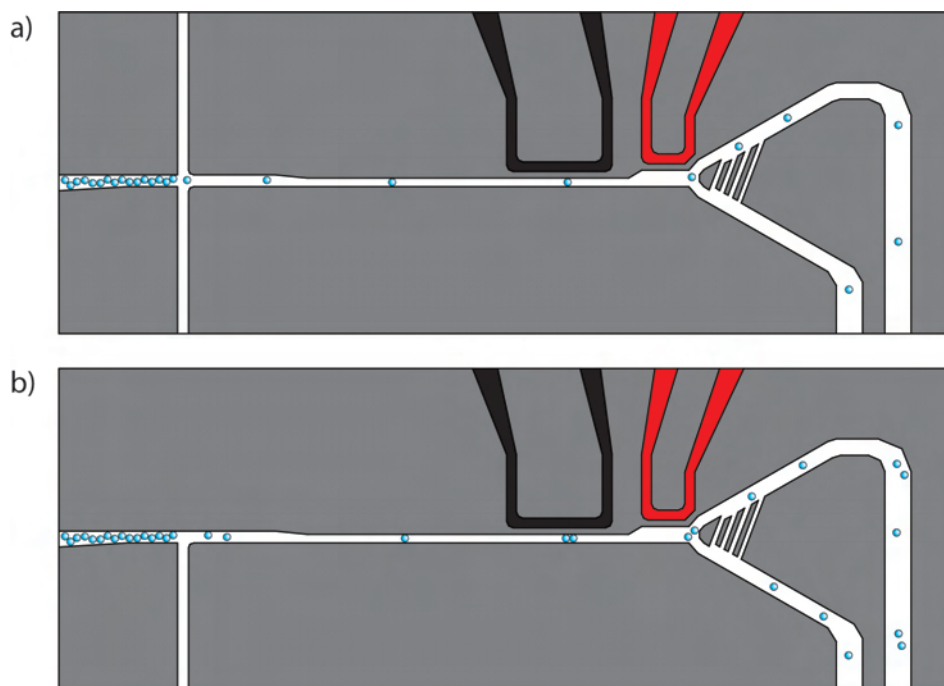


Figure 6.3: Sorting improvements. The design with the ridges after the sorting junction was developed by Agresti et al. [] and improves the stability of the sorter. A flow-focussing oil inlet to space the emulsion (a) is more efficient than a T-junction design (b). Here droplets sometimes travel as pairs leading to false positives or negatives.

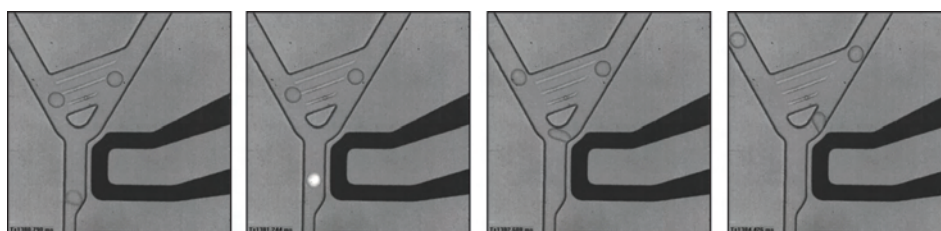


Figure 6.4: Sequence of images captured during droplet sorting.

has a strong influence on the spacing efficiency. The best spacing can be achieved by using a flow-focussing oil addition (figure 6.3a) instead of a T-junction design (figure 6.3b). When utilizing the T-junction design occasionally droplet pairs as opposed to single droplets arrive at the sorting junction leading to the previously mentioned problems of droplets bumping into each other. The flow-focusing design is more robust in this sense and usually results in better sorting performance. A sequence of pictures of successful sorting is shown in figure 6.4.

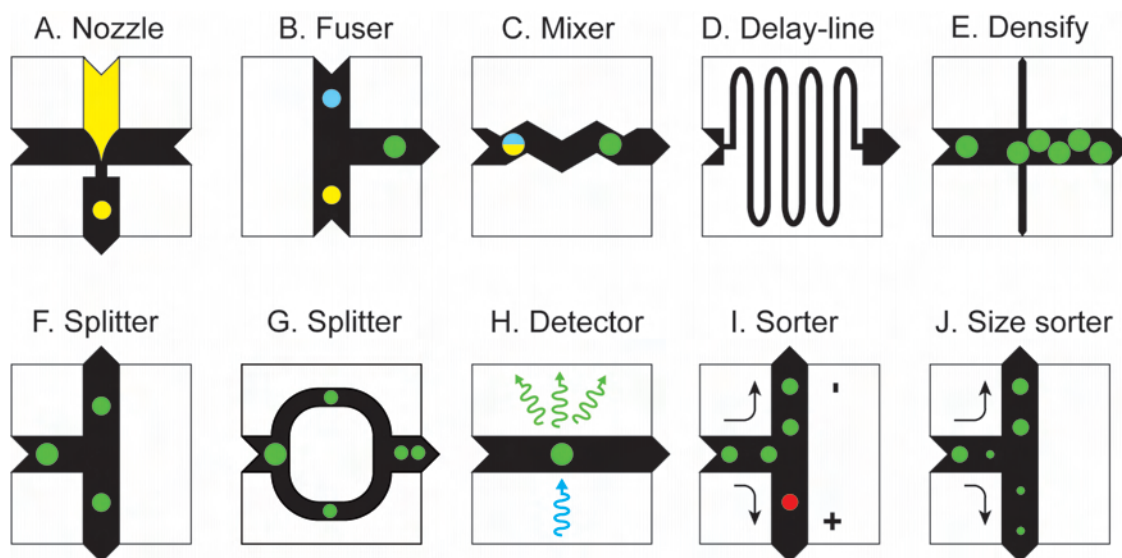


Figure 6.5.: Illustration of a selection of different droplet-based microfluidics modules. These modules can be combined and integrated according to the necessary application.

6.2.3. Device integration

The different droplet-based modules presented so far were usually only utilized as single chips, one by one, making it almost impossible to carry out multi-step assays in droplet-based microfluidics. This is especially true in cases where medium incubation times of several minutes were needed. The development of the delay-lines from chapter 5 was the first requirement for integrating several droplet-based modules functionally onto a single chip. Devices like this can be used as run-through systems as opposed to off-chip incubation [137, 35] or incubation in large on-chip storage chambers [24] and therefore avoid stopping the flow and off-chip handling. Consequently they can access large amounts of droplets and account for high-throughput with large libraries.

A great advantage for integrating several modules is the usage of flow-controlled actuation (syringe pumps) instead of pressure driven flow. In most instances all the calculations on the fluidic resistance and the resulting effects can be avoided.

Figure 6.5 shows some of the available modules and the following points describe what needs to be considered when trying to integrate them with others.

- Droplet creation is usually a starting module and can be easily followed by any other module.
- Mixing is unproblematic as well, since it is passive and in principle it is just a single channel with one inlet and one outlet.
- Incubation in a delay-line is also well integrable, since it is a linear device as well.
- Increasing the emulsion density is a linear device as well, although it must be considered

whether the oil extraction is passive or active by a pump. In the passive case the fluidic resistances need to be calculated in order to adjust the correct extraction volume.

- Splitting of droplets can be simple as well if the outlet channels recombine again. Such a system is required when the application demands to split the droplets to smaller sizes and send them through the same outlet channel. On the other hand if the droplets need to exit through different outlets, the flow-rate through each outlet is dependent on whatever follows.
- Fusion requires considerations of how the droplets arrive at the synchronization point. If the emulsion is dense and arriving with a low flow-rate (up to $\sim 200\text{-}500 \mu\text{L h}^{-1}$) it is comparable to the usual usage as a single module. If this is no longer the case, high oil flow-rates have to be used to space the arriving droplets reliably and it might be impossible to run the system accurately. Therefore, the use of droplet fusion as a subsequent module should be always considered with care.
- Sorting is probably the most sensitive of all the modules and is usually used at the end of a process. It is crucial to ensure the spacing between the droplets and furthermore droplets could break at the junction if the flow-rates exceed a certain limit. This limit depends on the design, the fluids/surfactants and the droplet size.

In general it is useful to have everything as constant as possible and flow-rate fluctuations e. g. from the pumps should be avoided or minimized. A helpful trick to dampen the fluctuations from a pump is to increase the resistance leading to a pump, which can be accomplished by inserting a fluidic resistor after the in- or outlet. This strategy is especially important for the oil-extraction since it is possible to increase the maximum extraction limit when dampening the syringe pump noise. This is also important for modules such as the synchronization/fusion as well as for the sorting. These modules can be used more easily when the flow-rates are reduced before entering them, and the emulsion is packed and homogenously spaced again.

Keeping these points in mind, it was possible to integrate 7 individual droplet-modules in order to build a universal screening chip (figure 6.1b). A library emulsion is reinjected into the chip, fused to droplets containing the fluorogenic substrate, incubated and sorted based on the activity. This procedural method is similar for most droplet libraries, no matter how they were created. The only factors that can potentially vary are the droplet sizes and the incubation time. In principle the chip will remain functionally the same - the reinjected emulsion is synchronized to droplets containing the substrate and fused to initiate the reaction. The next step within the assay would be to incubate the reaction. Nevertheless, as already mentioned, the sorting at the end of the chip is the most sensitive module and can not handle large droplets as efficient as smaller ones. Since the droplets are well spaced and well controlled after the synchronization/fusion, it is favorable to split them down to smaller droplets at this point. This is of course only possible if the content is homogenous, which makes a mixing step necessary before the splitting module. Before entering the incubation in delay-lines it might be favorable to extract the oil in order to increase the incubation time. As already mentioned the last step

6.3. Preliminary screening and enrichment results

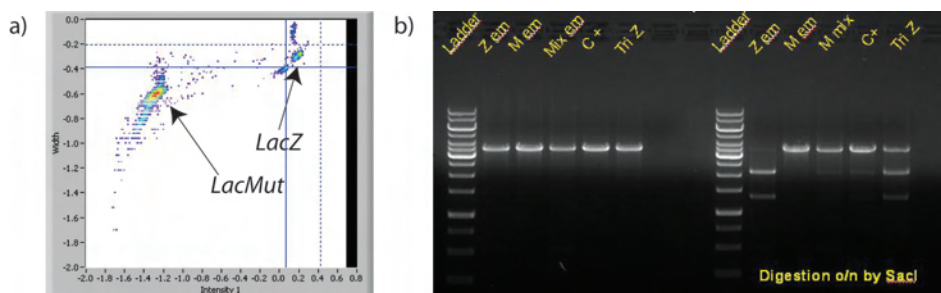


Figure 6.6.: Enrichment results. a) The histogram obtained during the sorting experiment of the mixed emulsion. The x-axis represents the fluorescent intensity, whereas the y-axis indicates the droplet width. The two populations are indicated in the figure. b) A gel showing the DNA fragments obtained from the different emulsions. Of primary interest for the enrichment of *LacZ* is the Tri Z column on the right gel, which shows two more pronounced bands compared to the C+ column next to it.

on this chip is the sorting after incubating the reaction. Therefore, the droplets need to be re-spaced and directed towards the sorting junction.

In some cases the incubation between the fusion and the sorting needs to be so large that an on-chip incubation is insufficient and therefore unnecessary. In this case the delay-line can be replaced by an outlet and the emulsion can be collected in a capillary and reinjected into the sorter after incubation. This method can no longer be considered as an integrated run-through chip but the methodical procedure of the screening remains the same.

6.3. Preliminary screening and enrichment results

In parallel to this work a team of colleagues worked on the biology for a model selection involving the enzyme β -galactosidase, with the fluorogenic substrate FDG (fluorescein di- β -D-galactopyranoside). The experimental procedures, protocols and techniques developed for compartmentalization of single genes, amplification and *in vitro* protein expression for this model system are described in Mazutis *et al.* [35] (see also section A.0.3). Now the aim is to use this system to demonstrate directed evolution in droplet-based microfluidics, ideally with several cycles of mutations and selections. Prior to this, it was necessary to demonstrate that it is possible to use the developed techniques (on the biological, as well as the microfluidics part) to enrich a more active enzyme population from a mixture. Therefore, two emulsions were prepared, one containing the genes ($\sim 10,000$ DNA strands per droplet) for the active variant *LacZ* of β -galactosidase and one for the inactive mutant *LacMut*. During the encapsulations step also the IVTT mixture as well as the substrate were added to the aqueous stream forming the droplets. Then the two emulsions were pooled together and collected in a capillary. Thereby, the two emulsions were mixed in a proportion of 19:1 *LacMut* to *LacZ*. In a subsequent step the emulsions were incubated for 2 hours at 37°C to express the enzymes. Afterwards the emulsion was reinjected into the sorting device and screened for the more active *LacZ* variants. Figure 6.6a shows the corresponding histogram obtained during this sorting experiment. The two populations of interest are indicated in

the histogram, whereby the one with the higher fluorescein signal (released by the conversion of the substrate FDG) corresponds to *LacZ* and the one to the left corresponds to *LacMut*. About 10,000 higher fluorescent droplets were collected after the sort. Subsequently the emulsion was broken, the DNA recovered and amplified by PCR.

In order to analyze the results the following set of DNAs was recovered from emulsions, amplified and loaded onto agarose gels, as illustrated in figure 6.6b.

Z em Is the DNA recovered from a emulsion containing only *LacZ* genes.

M em Is the DNA recovered from a emulsion containing only *LacMut* genes.

Mix em Is the DNA recovered from a emulsion containing a mixture of *LacZ* and *LacMut* genes.

C+ Is the DNA recovered from a emulsion (only 10,000 droplets) containing a mixture of *LacZ* and *LacMut* genes.

Tri Z Is the DNA of interest, recovered from a sorted emulsion (10,000 droplets) triggered on the more active droplets.

Negative control No DNA was co-encapsulated with the IVTT mixture and the substrate.

An advantage of using *LacZ* and *LacMut* for comparison is that both genes are equally long and therefore avoid any PCR biases. Consequently, also the bands on the gel appear at the same position for all emulsions. In order to differentiate between these two variants a restriction enzyme *SacI* is used. It cleaves a restriction site present in the *LacZ* gene, whereas *LacMut* is not affected by this digestion. Consequently an emulsion shows two bands of shorter DNA fragments on the gels after digestion if *LacZ* was present whereas only a single band of a longer DNA strand indicates *LacMut*. This can be also seen in the DNA recovered from the emulsions. The DNA from the emulsion containing only *LacZ* shows the characteristic two bands, the DNA from the emulsion containing only *LacMut* shows the one band and the mixture of both shows all three bands whereby the *LacMut* band is more pronounced since it was encapsulated in excess of 19:1. The next lanes shows that the same results can be obtain for smaller amounts of recovered droplets (10,000 compared to ~100,000). The Tri Z lane shows the results from the sort. Ideally it should only show the two bands corresponding to the more active *LacZ*, but it still also contains some DNA from *LacMut*. This is the result of occasional false positives during the sorting. Nevertheless, a clear enrichment compared to C+ can be observed, indicating a successful sorting result. Further optimizations and more experience with the sorting procedure can probably further improve these results.

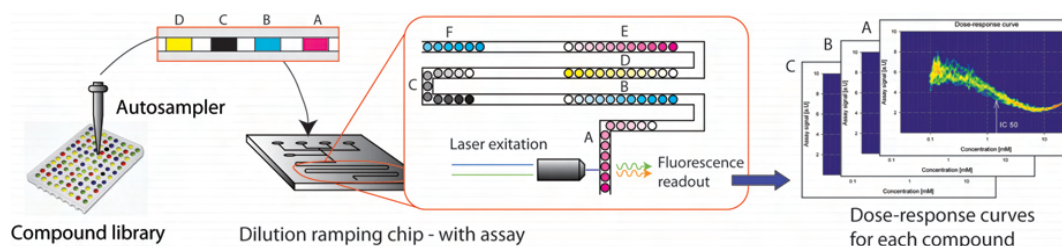
6.4. Chapter summary and conclusion

In summary it has been possible to improve and facilitate the use of the two most critical droplet modules - droplet fusion and droplet sorting. Furthermore, these modules have been integrated with

a set of other modules to form an integrated screening chip. The results are now being applied for the first screening application - i. e. directed evolution of β -galactosidase. The aim here is to use a cell-free system, meaning that all steps including amplification and enzyme expression are performed *in vitro*. First demonstrations indicate that it is possible to create the necessary libraries and that the sorting can be utilized to differentiate between enzymes with different activities and enrich DNA from more active variants. Nevertheless, the presented sorting results are not yet a real screen and did not utilize the final integrated screening chip yet. These tests are just preliminary results showing the progress of the still on-going project. Further optimizations might still be necessary on the biological side as well as the microfluidic side, but all of these preceding tests were successful and show the expected results it is very likely that this project will lead to successful end results.

Chapter 7.

Quantitative high-throughput screening using droplet-based microfluidics



Contents

7.1. Introduction	96
7.2. Description of the system	97
7.2.1. Dilution module	99
7.2.2. Calculation of the dilution network	100
7.2.3. Loading of the compounds	103
7.3. Results	105
7.3.1. Dilution module characterization	105
7.3.2. Dose-response curve determination	106
7.3.3. K_m determination	106
7.4. Materials and methods	108
7.4.1. Microfluidic chip fabrication and operation	108
7.4.2. Reagents	108
7.5. Chapter summary and conclusion	109

This chapter describes the progress in developing a novel high-throughput drug-screening platform. It takes advantage of the low measurement volumes (80 pL) and high measurement rates (several kHz) possible using droplet-based microfluidics, coupled with a novel on-chip dilution system, to determine the IC₅₀ of an enzyme inhibitor within minutes. The technology should be applicable to purified targets and to cell-based assays, wherever a fluorescence read-out is available. The gains in productivity and knowledge expected from the development and implementation of this technology are significant and should accelerate the process of lead-finding and chemical optimization in drug development.

7.1. Introduction

Historically, new therapeutic compounds were discovered by laborious one-by-one testing using low-throughput assays. However, in the early 1990's high-throughput screening (HTS) was developed to allow screening of very large compound libraries resulting from consolidation of small molecule collections and the use of combinatorial chemistry. The development of HTS was enabled by the advancement of techniques to produce recombinant proteins and engineered cell lines and the development of sophisticated robotic handling systems. Today, screening programs may process up to 100,000 compounds a day (~1 per second), a thousand times as many as were processed in an entire week in 1990 [201].

However, usually just a single measurement at a single concentration (typically 10 μ M) is obtained for each compound in the initial primary screen. Whereas the biological effects of chemical compounds are concentration-dependent [202], and the concentration-effect relationships can be complex, varying in potency, efficacy, and steepness of response. This approach, therefore, is characterized by high numbers of false positives and false negatives [38] as well as the inability to identify subtle complex pharmacology, such as partial agonism or antagonism.

Many of the limitations of traditional HTS can be overcome by the use of quantitative HTS (qHTS) [39]. By robotic plating of compounds at seven or more concentrations in 1,536-well plates, concentration-response profiles can be created for each compound in libraries of >200,000 compounds [203]. This allows for a more accurate assessment of biological activity, reducing the number of false positives and false negatives compared to single-point screening [39].

Further reducing test volumes for qHTS below the 1-2 μ L capacity of 1536-well plates would create both significant cost savings and would enable higher throughput, allowing the screening of larger compound collections and the collection of more data points for each compound. However, using microtitre plate technology further miniaturization is problematic: for example, evaporation becomes significant in microliter volumes and capillary action causes 'wicking' and bridging of liquid between wells [201].

The ability to convert a sample into discrete, picoliter compartments, droplet-based microfluidics increases the number of reactions that can be performed from thousands of reactions per day to millions per hour, offering great advantages in terms of reagent savings, and reduces time-costly manual

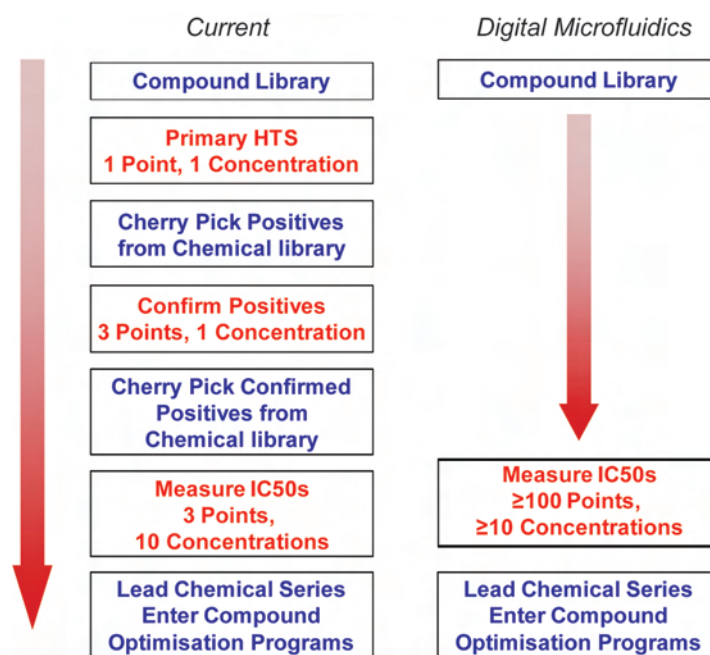


Figure 7.1.: Comparison: current qHTS vs digital microfluidics qHTS. Digital microfluidics is hoped to avoid some of the cherry picking steps and directly provide the necessary data for lead finding, which therefore increases throughput and cost-savings.

or robotical preparation steps. Applications so far are usually run at constant reagent concentration. Therefore one of the main challenges in this work was to develop a system which can reliably ramp the compound concentration over 3-4 orders of magnitude within a few seconds. This system is interfaced with a sampling robot allowing to measure the IC₅₀s for every compound in a compound library during the 'first-pass' HTS. Figure 7.1 compares the current screening approach versus the anticipated droplet (digital) microfluidics approach. It should enable a new era of quantitative high-throughput screening, characterized by rapidity of execution, reduced requirements for reagents and biological materials, and above all by a statistical quality far in excess of conventional methods.

7.2. Description of the system

Figure 7.2 illustrates the compound screening procedure and how the desired dose-response curves for each compound are obtained. A sampling robot sequentially loads each compound into the tubing leading to the microfluidic chip (see section 7.2.3). PBS buffer is loaded in-between the compounds to avoid cross-contamination. In the microfluidic chip these compounds are co-flowed with a stream of enzyme and a stream of the fluorogenic substrate and are compartmentalized into droplets. But before actually combining these three streams, the chip constantly ramps the dilution of these compounds up and down in order to obtain different compound concentrations in the different droplets. The aim hereby is to have a constant concentration of enzyme and substrate in the droplets but a varying com-

7. Quantitative high-throughput screening using droplet-based microfluidics

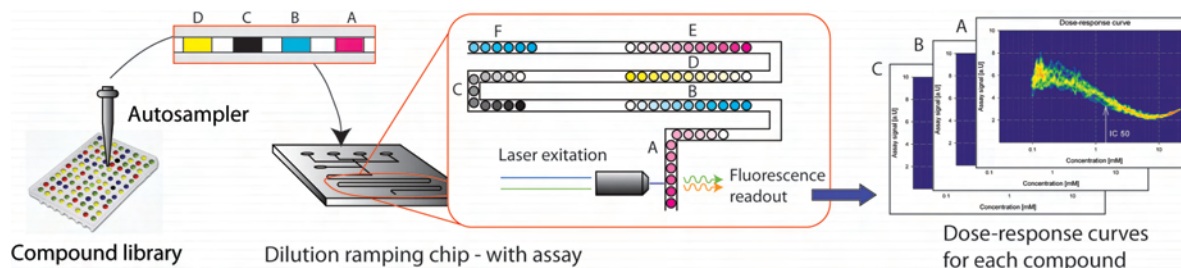


Figure 7.2.: Inhibitor screening procedure. An auto sampler sequentially sucks in compounds from an inhibitor library (separated by buffer) and feeds them into the dilution ramping chip. This chip constantly ramps the dilution of these compounds up and down (3-4 orders of magnitude) and compartmentalizes these together with an enzyme and a fluorogenic substrate into water-in-oil droplets. After incubating these droplets for a fixed time on-chip a fluorescent detection system reads out the inhibition and the software calculates the dose-response curves for each compound.

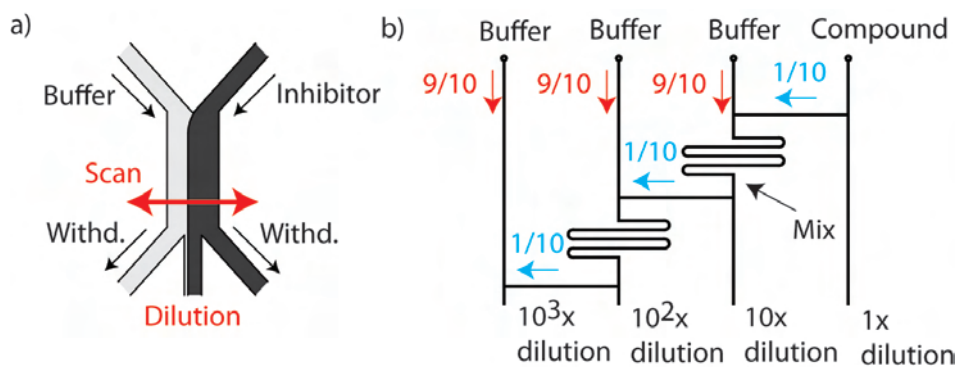


Figure 7.3.: a) A basic solution strategy for the dilution module. Two withdraw pumps shift the interface between the two aqueous phases from one side to the other, selecting therefore the percentage of compound entering the dilution/output channel. b) Serial dilution network. The compound stream is sequentially split, diluted and directed to the different outputs. The fluidic network ensures that always 1/10 of the compound stream is combined with 9/10 of the dilution buffer to achieve a logarithmically decreasing concentration at each output.

compound concentration, as illustrated by the droplet colors in figure 7.2. The droplets are then incubated for a fixed time in an on-chip delay-line before they reach the readout point for the fluorescence. Here the information of the compound concentration and level of inhibition is acquired for each droplet. A reference fluorophore which was diluted alongside with the compound encodes for the inhibitor concentration and the level of inhibition is measured by the second fluorophore which is the product of the enzymatic reaction. The software then plots these two fluorescent intensities against each other for each droplet and thereby composes the desired dose-response curves. In addition the software also tracks down the beginning and end of each compound and is therefore capable of recording the data for each compound arriving sequentially.

7.2. Description of the system

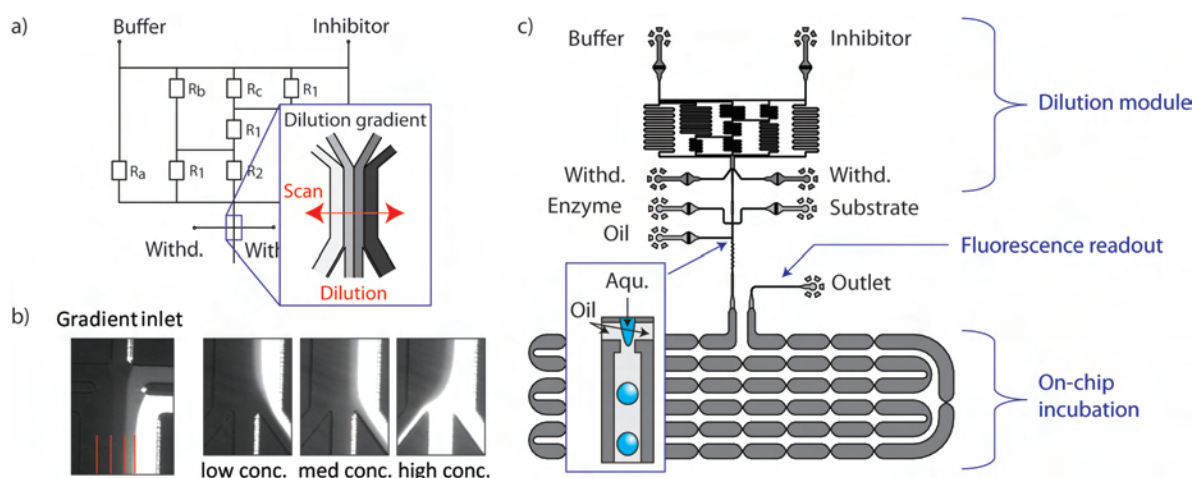


Figure 7.4.: Dilution ramping chip. a) A microfluidic resistor network creates different (logarithmic) dilution streams and combines these into a dilution gradient which feeds into the scanning region. b) Fluorescent photographs showing the inlet of the gradient region, as well as a series of outlet pictures at different configuration. For low output concentrations almost all compound stream are extracted towards the right, whereas high output concentrations require almost no dilution buffer. c) The integrated dilution ramping chip for inhibition screening assays. The dilution module at the top ramps the inhibitor concentration and combines this stream with a constant stream of enzyme and substrate. At a droplet nozzle the oil compartmentalizes these assays into droplets and runs them through an incubation delay-line, before they reach the fluorescent read-out.

7.2.1. Dilution module

A key component in this system is the dilution module, which should be able to constantly and precisely ramp the concentration over at least 3-4 orders of magnitude. Additionally it should work with a constant input flow-rate from the sampling robot and possibly also with a constant output flow-rate for the next modules following on the chip. A first, very simple approach is shown in figure 7.3a. The compound stream and a dilution buffer stream co-flow into a channel forming a constant laminar flow frontier between them. This channel then splits up into three outlet channels whereby the two outer ones are connected to aspirating syringe pumps (withdraw pumps). It is therefore possible to select what percentage of the flow travels through which channel and since everything is laminar this system can shift the frontier from left to right; consequently selecting the dilution of the compound. While changing these withdraw flow-rates it is important to maintain a constant flow-rate through the output (dilution) channel.

Although this system can theoretically cover the whole dilution range, practically it is very limited. In order to reach small compound concentrations it is necessary to shift the frontier precisely and with minimal step sizes towards the side wall. E. g. for a $1000\times$ dilution the compound stream would need to be $0.1\ \mu\text{m}$ wide in a $100\ \mu\text{m}$ wide channel, which is hard to maintain and obviously is not very precise. Serial dilution (see figure 7.3b) is therefore the logical consequence and microfluidics offers this opportunity passively. Analogue to electrical resistor networks it is possible to design the channel

residences and interconnections in a fashion that the different streams mix and split until several different output channels are obtained, each one with a $10\times$ dilution of the previous one (details on the calculation are described in section 7.2.2 and [204]). These different dilution streams are then recombined and laminarily fed into the scanning chamber as a logarithmic dilution gradient (figure 7.4a,b). This approach changes the characteristics significantly. For example: by moving the dilution gradient towards the high dilution end (low concentration in figure 7.4b) more high concentration streams will be directed to the right waste channel and consequently it is only necessary to dilute one of the other pre-diluted streams. Any fluctuations, e. g. by the pumps leads only to small dilution errors since everything is already pre-diluted.

The microfluidic design is shown in figure 7.4c. The upper part represents the dilution module with its two channels leading to the withdraw pumps. Then central dilution stream combines with the enzyme and substrate stream before reaching the droplet nozzle with the oil inlet. The lowest part represents the dispersion reduced delay-line for incubation [33] before the droplets reach the outlet with the fluorescence detection.

7.2.2. Calculation of the dilution network

In order to calculate the dilution gradient a generalized resistor-network was used [204, 205]. It is based on the analogy between fluidic circuits and electrical circuits and every channel can be represented by a fluidic resistance. The concept to create such a resistor network is illustrated in figure 7.5. The dilution buffer is injected through the input to the left with a flow-rate Q_B and the compound to be diluted enters to the right with Q_C . The compound stream then splits up and one part flows down through the last channel to the right with the number N and the second part branches out to the left, co-flows with the dilution buffer, mixes within the mixing channel (resistance R_M) and reaches the next branching point. According to this concept it is possible to choose a set of desired output concentrations $\{0\% = C_0 < C_i < C_N = 100\%\}$ and output flow-rates $\{Q_0, Q_1, Q_2, \dots, Q_i, \dots, Q_N\}$ and calculate the fluidic resistor network.

The first step to layout the network is to determine the flow-rates entering into each branching point to achieve the desired concentration C_i at the outlet channel i . The flow-rate entering such a branching point from the buffer side is $Q_{L,i}$ and the flow-rate entering from the compound side is $Q_{R,i}$. Using *Kirchhoff's* current law the following equations can be determined.

$$Q_{L,i} = \frac{C_{i+1} - C_i}{C_{i+1} - C_0} (Q_{R,i-1} + Q_i) \quad (7.1)$$

$$Q_{R,i} = \frac{C_i - C_0}{C_{i+1} - C_0} (Q_{R,i-1} + Q_i) \quad (7.2)$$

$$\text{where } Q_{R,0} = 0$$

7.2. Description of the system

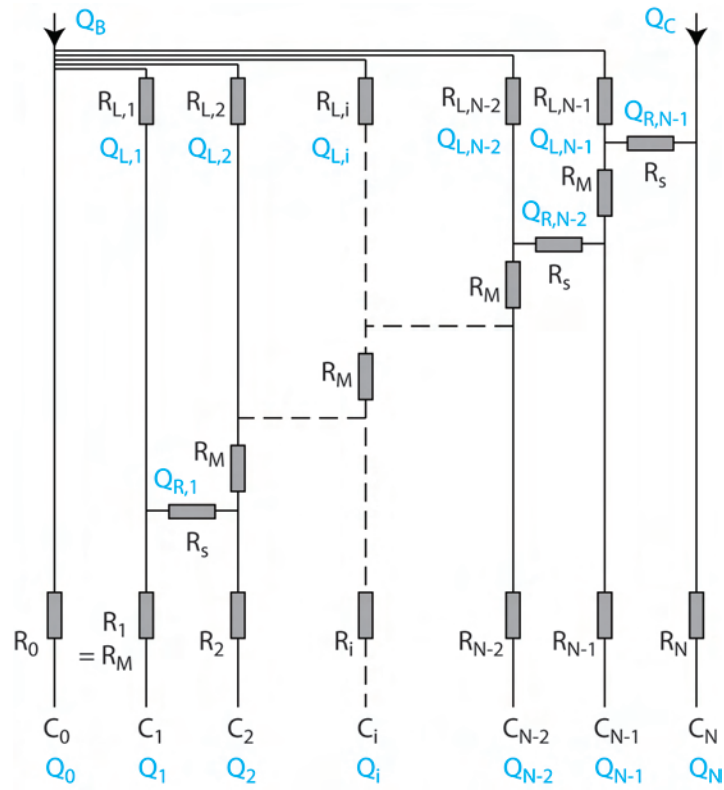


Figure 7.5.: Illustration of resistor network to calculate the dilution gradient.

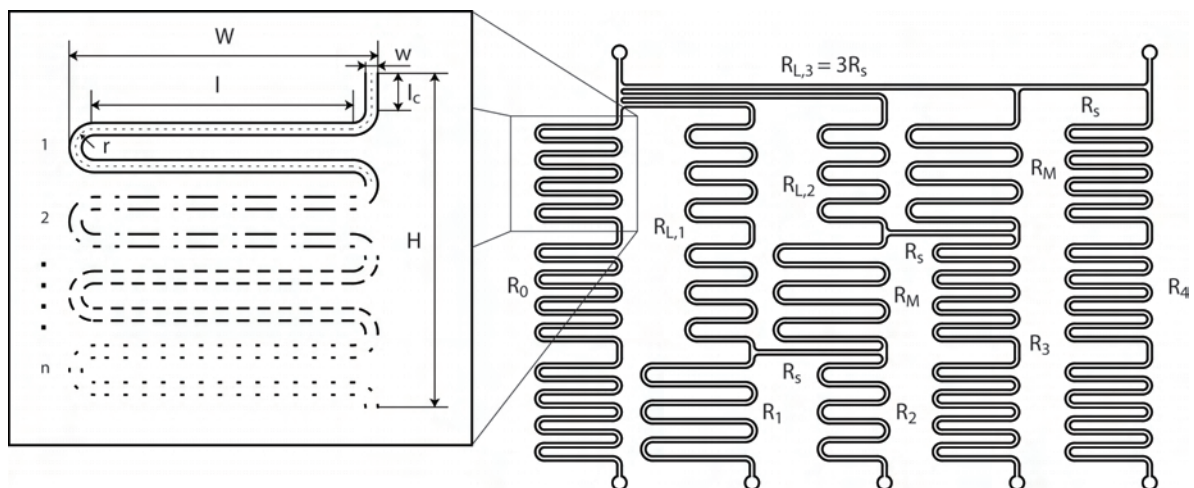


Figure 7.6.: Illustration of resistor network layout calculation.

This also leads to the total flow-rates entering the network from the buffer and compound inlet.

$$Q_B = Q_0 + \sum_{i=1}^{N-1} Q_{L,i} \quad (7.3)$$

$$Q_C = Q_N + Q_{R,N-1} \quad (7.4)$$

Using these values and *Kirchhoff's* voltage law the fluidic resistances can be calculated.

$$\left\{ \begin{array}{l} R_2 = R_S \frac{Q_{R,1}}{Q_2} + R_1 \frac{Q_1}{Q_2} \\ \dots \\ R_i = R_S \frac{Q_{R,i-1}}{Q_i} + R_M \frac{Q_{L,i-1} + Q_{R,i-1}}{Q_i} + R_{i-1} \frac{Q_{i-1}}{Q_i} \end{array} \right\} \quad (7.5)$$

$$\left\{ \begin{array}{l} R_{L,N-2} = R_{L,N-1} \frac{Q_{L,N-1}}{Q_{L,N-2}} + R_M \frac{Q_{L,N-1} + Q_{R,N-1}}{Q_{L,N-2}} + R_S \frac{Q_{R,N-2}}{Q_{L,N-2}} \\ \dots \\ R_{L,i} = R_{L,i+1} \frac{Q_{L,i+1}}{Q_{L,i}} + R_M \frac{Q_{L,i+1} + Q_{R,i+1}}{Q_{L,i}} + R_S \frac{Q_{R,i}}{Q_{L,i}} \\ \dots \\ R_{L,0} = R_{L,1} \frac{Q_{L,1}}{Q_0} + R_1 \frac{Q_1}{Q_0} \end{array} \right\} \quad (7.6)$$

$$\text{where } R_{L,N-1} = (N-1)R_S$$

Consequently, if the cross-sections ($w \times h$) of all channels in the circuit are identical the fluidic resistance is proportional to the channel length L , meaning that each value of R can be interpreted as a length. Nevertheless, it is still necessary to calculate how exactly these channel lengths can be integrated into a design layout as shown in figure 7.6. Each resistor is a serpentine channel with a certain cycle number n , loop length l , radius of every turn r and the length of the connection channel to the next resistor l_c . Depending on these numbers the resistor has a total height H , width W and length L , which have to fit into the design.

$$H = n4r + l_c \quad (7.7)$$

$$W = l + 2r + w \quad (7.8)$$

$$L \propto R = 2n(\pi r + l) + l_c \quad (7.9)$$

For simplicity an equal resistor height H is favorable to avoid accounting for connection channel lengths. Consequently the radius r needs to be adjusted, depending on the number of cycles n . The resistor with the highest number of cycles is naturally also the highest and the radii of all the other ones have to be adjusted in order to reach the same height. Therefore, first, the maximum number of necessary resistor cycles n_{\max} needs to be determined. By using equation 7.8 and 7.9 and requiring

that no resistor is wider than the connection distance from one outlet arm to the other

$$W \leq R_S \quad (7.10)$$

the cycle number for every resistor would be

$$n = \text{roundup} \left(\frac{L - l_c}{2(\pi r + R_S - 2r - w)} \right), \quad (7.11)$$

leading the the cycle vectors \mathbf{n}_i for the $\mathbf{R}_i = \{R_0, R_1, R_2, \dots\}$ and $\mathbf{n}_{L,i}$ for the $\mathbf{R}_{L,i} = \{R_{L,1}, R_{L,2}, R_{L,3}, \dots\}$.

Before selecting the highest n within \mathbf{n}_i and $\mathbf{n}_{L,i}$ it is important to note that some resistors can be $\{2\times, 3\times, 4\times, \dots\}$ as high as others (as e. g. R_3 in figure 7.6 is $2\times$ as high as R_2). This means the values in \mathbf{n}_i and $\mathbf{n}_{L,i}$ need to be divided by these factors. For the R_i the factors follow the rule $\{N - 2, 1, 1, 2, 3, \dots\}$ and respectively for the $R_{L,i}$ they are $\{N - 2, N - 3, N - 4, \dots\}$. After this n -compensation the resistor with the highest n determines n_{\max} .

$$n_{\max} = \max(\mathbf{n}_i, \mathbf{n}_{L,i}) \quad (7.12)$$

With a predefined minimum radius r_{\min} this leads to the maximum resistor hight H_{\max} . Resistors with identical n have identical radii but those with lower numbers of n need a larger radius to compensate and still reach the same hight according to (7.7):

$$r_i = \frac{H_{\max} - l_c}{4} n_i^{-1} \quad (7.13)$$

$$r_{L,i} = \frac{H_{\max} - l_c}{4} n_{L,i}^{-1} \quad (7.14)$$

Finally the loop length for each resistor is a result from its radius, the compensated cycle number and (7.9):

$$l_i = \frac{R_i - l_c}{2} n_i^{-1} - \pi r_i \quad (7.15)$$

$$l_{L,i} = \frac{R_{L,i} - l_c - iR_S}{2} n_{L,i}^{-1} - \pi r_{L,i} \quad (7.16)$$

With these values the serpentine channels can be designed and form the resistor network as shown in figure 7.6.

7.2.3. Loading of the compounds

The compound libraries are usually stored in well plates and have to be loaded sequentially by a sampling robot into the tubing leading to the chip. In order to avoid mixing of these compounds they have to be spaced by either a second phase (e. g. oil or air) or by sufficient aqueous buffer. The oil thereby often led to problems within the dilution network, since oil droplets where able to block one of

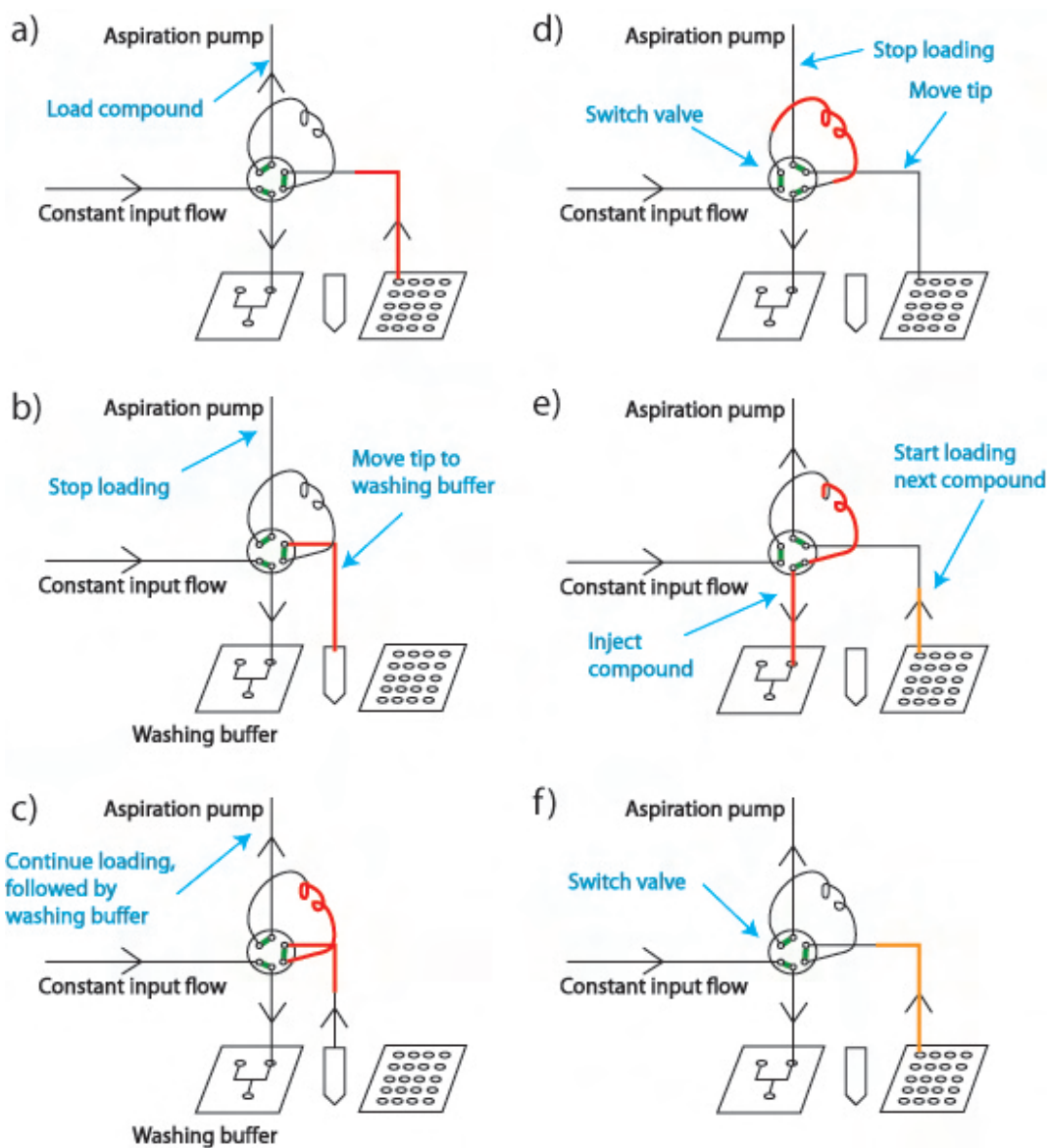


Figure 7.7.: Compound loading procedure. a) The aspiration pump pulls-in a small plug of compound. b) The aspiration pump stops while the tip moves to a washing buffer reservoir. c) The aspiration pump continues to withdraw and fill the sample loop. The sample is followed by washing buffer. d) The valve switches and the loop starts emptying towards the microfluidic chip. e) The constant input flow-rate empties the the loop while the aspiration pump can already start loading the next compound. f) The valve switches back and the cycle restarts.

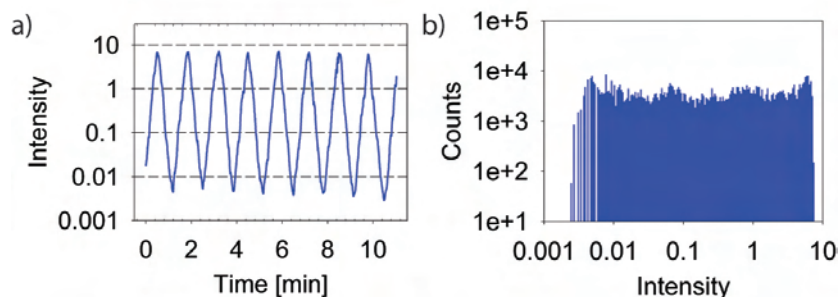


Figure 7.8.: Dilution module characterization with a $100\ \mu\text{M}$ Fluorescein solution. The withdraw pumps performed 38 linear steps to scan over the gradient. Since the gradient is composed of logarithmic dilution streams the response of this linear ramping is exponential. a) Timeline showing the dynamic of the ramping. b) Histogram showing the droplet counts for each concentration. The whole dilution range is covered homogeneously; no over- or under sampling is observed. At the lowest concentrations the signal reached the noise level leading to detection problems.

the parallel channels due to hydrophobic interactions with the channel walls. Therefore, buffer has to be utilized as a spacer, but it needs to be considered that the buffer-compound interface mix (diffusion and Taylor dispersion) within time and distance along the channel. In order to minimize this transition zone, the tubing has to be as short as possible, which requires either an autosampler directly next to the chip or it might be even favorable to built a sampling robot directly around the fluidic station to optimize for higher throughput.

A simple strategy envisioned is illustrated in figure 7.7. A traditional autosampler valve (Rheodyne) could be installed just above the chip, minimizing the distance from the valve to the chip. The well-plate could be installed directly next to the microfluidic chip with a sampling arm (a similar system is already in use at Raindance [102]). Furthermore it might be possible to avoid dispersion in the loading tube (leading to the valve) by aspirating small air plugs before and after each compound. These air plugs can then be removed to the waste during the valve operation (so only an aqueous phase will flow to the chip). By these measurements it should be possible to almost completely avoid dispersion within the loading phase, since the buffer and compound phase can only mix during the short time traveling from the valve to the chip.

7.3. Results

7.3.1. Dilution module characterization

In order to characterize and test the dilution device a solution of $100\ \mu\text{M}$ Fluorescein in PBS was used at the inhibitor inlet and the dilutions was ramped while recording the fluorescence at the outlet. The results are shown in figure 7.8. The timeline in figure 7.8a shows the dynamic response of the ramping and the reproducibility. The fastest ramps tested ran within $\sim 20\ \text{s}$ at 19 linear syringe pump steps. Figure 7.8b shows the recorded histogram. It can be seen that the system homogeneously covers the

whole dilution range without over- or under sampling certain regions, which is also an indicator for the stability and precision in adjusting the different dilutions. At the lowest concentrations the limit of the fluorescence detection system was reached, which led to the detection noise to the left in the histogram.

These tests suggest that this dilution module fulfills all the requirements demanded previously. It operates with only 4 syringe pumps, has constant input and output fluidic ports for good connectivity to other modules, the dilution range is further up- or down scalable, it is robust towards fluctuations and by scanning in linear syringe pump steps over the gradient, the response in dilution is exponential (see figure 7.8a).

7.3.2. Dose-response curve determination

An aqueous phase of 120 μM PETG (the inhibitor) and 100 μM sodium Fluorescein in PBS were injected into the 'compound' input of the microfluidic device (figure 7.4c) at a flow-rate of 111 $\mu\text{L h}^{-1}$. A second aqueous phase, PBS, was injected into the 'diluent' input at a flow-rate of 389 $\mu\text{L h}^{-1}$. The dilution network in the device split and mixed these flows to generate a laminar flow into the scanning chamber with five discrete concentrations of the inhibitor side-by-side: 120 μM , 12 μM , 1.2 μM , 0.12 μM and 0 μM . The flow-rate of each aspirating pump connected to the scanning chamber was ramped up and down between 20 and 430 $\mu\text{L h}^{-1}$ as a triangle wave with a 60 s period. The total aspirating flow-rate was always 450 $\mu\text{L h}^{-1}$, leaving an output stream of 50 $\mu\text{L h}^{-1}$ to the dilution channel. This stream was combined with two further aqueous streams: (i) the enzyme solution flowing at 30 $\mu\text{L h}^{-1}$ and (ii) the substrate solution flowing at 80 $\mu\text{L h}^{-1}$. The oil flowing at 400 $\mu\text{L h}^{-1}$ was used to compartmentalize the mixture and generate 90 pL aqueous droplets.

The droplets flowed through a 75 s incubation delay-line in the microfluidic device and then passed one at a time through the 488 and 532 nm laser spot. The amounts of fluorescent resorufin (liberated by β -galactosidase activity) and fluorescein (coding for the dilution) were determined for each droplet by measuring the fluorescence intensities. The values were plotted in an XY-graph with initial reaction rate (liberated resorufin by the assay) against inhibitor concentration (encoded by the fluorescein concentration), as shown in figure 7.9. A 4-parameter log-logistic curve was fitted to the points. The IC₅₀ of PETG in the described enzyme/substrate/inhibitor system was found to be 2.21 μM (95% confidence intervals: 2.20-2.22 μM) (see figure 7.10a). This value compares favorably to the value measured in a standard microplate assay: 1.43 μM (95% confidence intervals: 1.37-1.49 μM).

7.3.3. K_m determination

A similar experiment procedure as in section 7.3.2 was performed to determine the K_m of the same model enzyme/substrate system. The dilution network and chip was operated with the same values as described previously.

An aqueous phase of 520 μM RBG (the substrate), 100 μM sodium fluorescein, and 5 % (v/v) DMSO in PBS were injected into the 'compound' input of the microfluidic device (figure 7.4c). A

7.3. Results

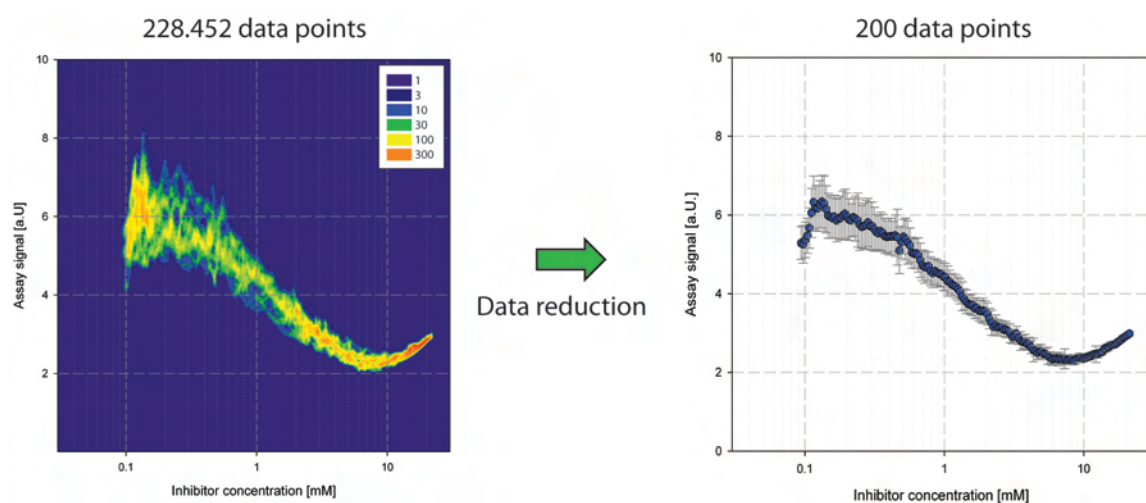


Figure 7.9.: A density plot of the assay signal against the PETG (the inhibitor) concentration. As the inhibitor concentration increases, the assay signal (reaction rate) decreases. Furthermore it is demonstrated how the data reduction algorithm reduces the data and extracts the essential information for curve fitting and long-term storage.

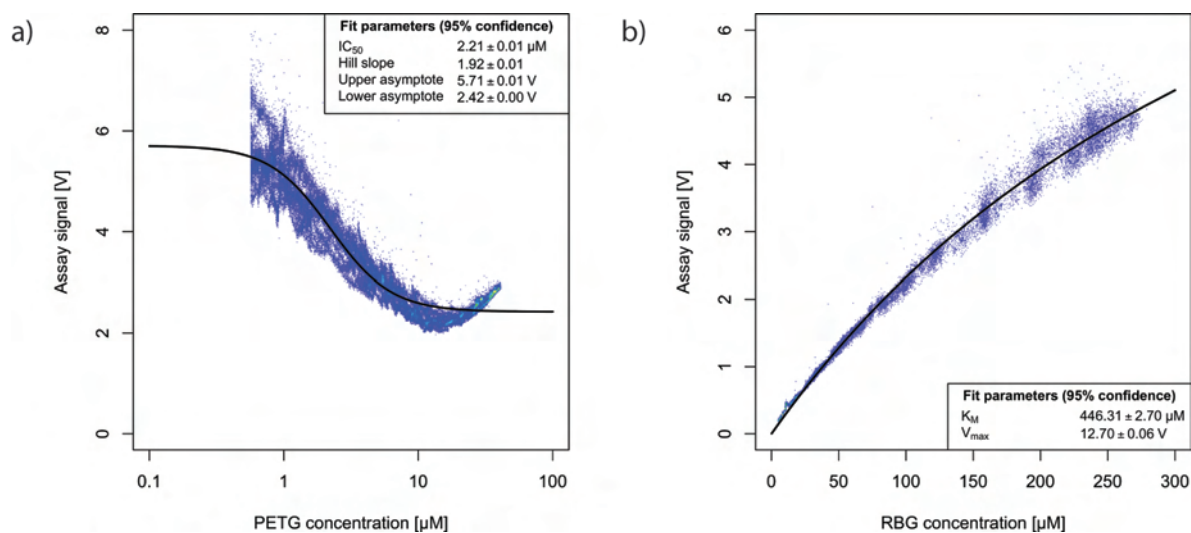


Figure 7.10.: Measured results and fits for the IC_{50} (a) and K_m (b) of the model enzyme/substrate/inhibitor or enzyme/substrate system.

second aqueous phase, 5 % (v/v) DMSO in PBS, was injected into the 'diluent' input. The output stream from the dilution module was then combined on-chip with the enzyme solution flowing at $80 \mu\text{L h}^{-1}$: 1 U mL^{-1} β -galactosidase and 2 g L^{-1} BSA in PBS and at the droplet nozzle the mixture was compartmentalized into droplets. The droplets flowed through the 75 s delay-line and then passed one at a time through the 488 and 532 nm laser spot. The amounts of fluorescent resorufin-liberated by β -galactosidase activity-and sodium fluorescein were determined for each droplet by measuring fluorescence intensity in the 590-625 and 500-520 nm channels, respectively. A Michaelis-Menten curve was fitted to the points. The K_m of RBG in the described enzyme/substrate system was found to be $446.31 \mu\text{M}$ (95% confidence intervals: 432.68 - $437.05 \mu\text{M}$) as shown in figure 7.10. This value is in the same order of magnitude as the value measured in a standard microplate assay: $115.6 \mu\text{M}$ (95% confidence intervals: 102.7 - $128.6 \mu\text{M}$).

7.4. Materials and methods

7.4.1. Microfluidic chip fabrication and operation

Soft-lithography in poly(dimethylsiloxane) (PDMS, Sylgard 184, Dow Corning) was used to prepare the devices [43]. The molds consisted of SU-8 (Microchem) with two different heights [33]. The dilution device and the delay-line in figure 7.4c are in the deeper region of $75 \mu\text{m}$ whereas the droplet nozzle and the fluorescent readout are in the lower channels of $25 \mu\text{m}$. After casting the mold in PDMS and binding it to a glass slide (after activation in an oxygen plasma) the channels were made hydrophobic using a commercial surface coating agent (Aquapel, PPG Industries). The flow-rates were controlled by syringe pumps (PHD2000; Harvard Apparatus).

The dilution module runs with a constant flow-rate of $111 \mu\text{L h}^{-1}$ for the compound inlet and $389 \mu\text{L h}^{-1}$ for the dilution buffer - $500 \mu\text{L h}^{-1}$ in total entering the gradient channel. The withdraw pumps run ramps of 10 or $20 \mu\text{L h}^{-1}$ steps every 200 ms between 20 - $430 \mu\text{L h}^{-1}$ (vice-versa) in order to maintain a constant flow-rate of $50 \mu\text{L h}^{-1}$ exiting the dilution module. The remaining flow-rates are: enzyme ($30 \mu\text{L h}^{-1}$), substrate ($80 \mu\text{L h}^{-1}$) and oil ($400 \mu\text{L h}^{-1}$). This combination leads to 53 - $55 \mu\text{m}$ droplets ($\sim 90 \text{ pL}$) at a $50 \mu\text{m}$ flow-focusing nozzle.

7.4.2. Reagents

The oil phase for all experiments consisted of HFE-7500 fluorinated oil (3M) with 1% (w/w) 'EA' surfactant (Raindance Technologies, Inc.). The buffer was always $1\times$ phosphate-buffered saline (PBS; Sigma-Aldrich Co.) and during the characterization experiments $100 \mu\text{M}$ Fluorescein were added to this buffer at the compound inlet.

The model systems comprised an enzyme, a substrate, and an inhibitor for IC_{50} measurements and an enzyme and substrate alone for K_m measurements. In all cases the enzyme was β -galactosidase (Sigma-Aldrich Co.), the substrate was resorufin β -D-galactopyranoside (RBG; Invitrogen Corporation), and the inhibitor was phenylethyl β -D-thiogalactopyranoside (PETG; Invitrogen Corporation).

Other components in the model systems were bovine serum albumin (BSA; Sigma-Aldrich Co.) and dimethyl sulfoxide (DMSO; Sigma-Aldrich Co.). During the dose response experiments following concentrations were used: (i) Enzyme: 2.67 U mL^{-1} β -galactosidase and 5.3 g L^{-1} BSA in PBS and (ii) Substrate: $520 \text{ }\mu\text{M}$ RBG and 5% (v/v) DMSO in PBS

7.5. Chapter summary and conclusion

In summary it was possible to prove that these methods described here are capable of leading to a novel drug-screening platform exceeding any current technology in terms of qHTS throughput, amount of data (statistics) and most likely also cost savings. Nevertheless, it is still a project being worked on by several other researchers within the lab and amongst our collaborators at Raindance Inc. and Sanofi-Aventis, R&D. It still needs to be shown that it is actually possible to screen an entire well-plate reliably and questions need to be investigated of whether the methods can be applied to any kind of libraries.

Appendix A.

Co-authored work

The following pages include the publications led by other colleagues within our laboratory, to which contributions have been made.

Droplet-Based Microfluidic Platforms for the Encapsulation and Screening of Mammalian Cells and Multicellular Organisms

Jenifer Clausell-Tormos,^{1,2,4} Diana Lieber,^{1,2,4} Jean-Christophe Baret,^{1,2} Abdeslam El-Harrak,^{1,2} Oliver J. Miller,^{1,2} Lucas Frenz,^{1,2} Joshua Blouwoff,^{1,2,3} Katherine J. Humphry,³ Sarah Köster,³ Honey Duan,³ Christian Holtze,³ David A. Weitz,³ Andrew D. Griffiths,^{1,2,*} and Christoph A. Merten^{1,2,*}

¹Institut de Science et d'Ingénierie Supramoléculaires, Université Louis Pasteur

²CNRS UMR 7006

8 allée Gaspard Monge, 67083 Strasbourg Cedex, France

³School of Engineering and Applied Sciences/Department of Physics, Harvard University, Cambridge, MA 02138, USA

⁴These authors contributed equally to this work.

*Correspondence: cmerten@isis.u-strasbg.fr (C.A.M.), griffiths@isis.u-strasbg.fr (A.D.G.)

DOI 10.1016/j.chembiol.2008.04.004

SUMMARY

High-throughput, cell-based assays require small sample volumes to reduce assay costs and to allow for rapid sample manipulation. However, further miniaturization of conventional microtiter plate technology is problematic due to evaporation and capillary action. To overcome these limitations, we describe droplet-based microfluidic platforms in which cells are grown in aqueous microcompartments separated by an inert perfluorocarbon carrier oil. Synthesis of biocompatible surfactants and identification of gas-permeable storage systems allowed human cells, and even a multicellular organism (*C. elegans*), to survive and proliferate within the microcompartments for several days. Microcompartments containing single cells could be reinjected into a microfluidic device after incubation to measure expression of a reporter gene. This should open the way for high-throughput, cell-based screening that can use >1000-fold smaller assay volumes and has ~500× higher throughput than conventional microtiter plate assays.

INTRODUCTION

Miniaturization has been the feature that has enabled many of the most dramatic technological developments in recent decades. In electronics, the number of transistors per integrated circuit has roughly doubled every 2 yr since their invention in 1961. Miniaturization in biology and chemistry, although important, has been much less dramatic. Reaction volumes have typically been reduced from a few milliliters (in test tubes) to a few microliters (in microtiter plates)—a reduction of only 1000-fold. Nevertheless, today, high-throughput screening (HTS) programs can process up to 100,000 compounds per d (~1 s⁻¹). Unfortunately, there is little scope for further miniaturization of microtiter-plate technology due to evaporation and capillary action causing “wicking” and bridging of liquid between wells (Dove, 1999).

A promising approach to overcome these limitations is to use microfluidic systems, which consist of networks of channels of typically 10–100 μm diameter. Small quantities of reagents can be brought together in a specific sequence, mixed, and allowed to react for a specified time in a controlled region of the channel network by using electrokinetic and/or hydrodynamic pumping (Li and Harrison, 1997; Lin et al., 2001). They are being developed for use in several areas, allowing, for example, protein purification, DNA separation, and PCR on a drastically decreased scale (Hawtin et al., 2005; Wang, 2002). The ability to rapidly fabricate microfluidic devices in poly(dimethylsiloxane) (PDMS) by using soft lithography (Squires and Quake, 2005) has greatly stimulated the development of microfluidic systems. It has even enabled sophisticated microfluidic arrays containing thousands of compartments separated by valves (Thorsen et al., 2002).

Even though commercial microfluidic lab-on-a-chip systems already represent a serious competing technology for 1536-well plates for certain types of screen, the laminar flow in microfluidic devices creates two problems (Song et al., 2003). First, mixing is slow; second, the concentration of reagents changes continuously in the microchannels due to diffusion and the parabolic flow profile. Additionally, crosscontamination can create serious problems. These problems can be overcome by using systems in which the individual assays are compartmentalized in aqueous microdroplets, separated by immiscible oil. Non-microfluidic systems based on the compartmentalization of reactions in aqueous microdroplets of water-in-oil (w/o) emulsions were originally developed for directed evolution and have since been applied in a number of areas (Tawfik and Griffiths, 1998; Kelly et al., 2007; Griffiths and Tawfik, 2006), including ultra-high-throughput sequencing (Margulies et al., 2005; Shendure et al., 2005). However, making and manipulating droplets in two-phase (droplet-based) microfluidic systems allows for a level of control of picoliter scale biochemical assays that was hitherto impossible. Highly monodisperse (<3% polydispersity) w/o drops can be generated at frequencies greater than 10 kHz (Umbanhowar et al., 2000; Thorsen et al., 2001; Anna et al., 2003). Furthermore, the aqueous microdroplets can be fused or subdivided (Link et al., 2004, 2006; Ahn et al., 2006), the contents of microdroplets can be mixed rapidly, and sorting

modules allow for the specific enrichment of microdroplets (Song et al., 2003; Link et al., 2006; Ahn et al., 2006). Droplet-based microfluidic systems based on the formation of arrays of plugs (droplets that fill the microfluidic channels) have also been developed (Chen and Ismagilov, 2006). Each aqueous sample plug is stored in a holding component (e.g., a piece of tubing or a capillary) and is spaced by a second immiscible liquid or gas. In this way, microcompartments can be generated and stably separated without the use of any surfactant.

Droplet-based microfluidic systems have been used for a range of different applications, including single-molecule PCR, proteome analysis, clinical diagnosis on human physiological fluids, protein crystallization, and titration of anticoagulants (Beer et al., 2007; Wheeler et al., 2005; Srinivasan et al., 2004; Chen and Ismagilov, 2006; Song et al., 2006). They have also been used to encapsulate prokaryotic and eukaryotic cells (Martin et al., 2003; Grodrian et al., 2004; Sakai et al., 2005; He et al., 2005; Oh et al., 2006; Huebner et al., 2007), and even the embryos of multicellular organisms (Funfak et al., 2007). However, neither the incubation and/or recovery of viable mammalian cells nor a full life cycle of an encapsulated multicellular organism was demonstrated. Furthermore, none of those systems allowed for an automated analysis of individual compartments subsequent to an incubation period as required for high-throughput, cell-based assays.

We present here two complementary droplet-based microfluidic platforms that allow fully viable human cells to be recovered with high yield after several days in microcompartments. The volume of each microcompartment can be over 1,000-fold smaller than the smallest volumes utilizable in microtiter-plate-based assays, and single or multiple human cells, as well as multicellular organisms such as *C. elegans*, can be compartmentalized and can replicate in these systems. To prove the utility of this approach for cell-based assays, we also demonstrate automated fluorescence-based analysis of single cells in individual compartments after 16 hr of incubation.

RESULTS

Emulsion-Based Encapsulation

The ultimate goal of this study was to set up microfluidic platforms for high-throughput, cell-based assays. Hence, the technology should allow for (1) Encapsulation of a predefined number of cells per microcompartment (with the option of encapsulating single cells being highly desirable), (2) storage of the compartmentalized samples within a CO₂ incubator, and (3) recovery of the cells from the compartments in a way that does not abolish cell viability.

The encapsulation step (Figures 1A and 1B; Movie S1, see the Supplemental Data available with this article online) was performed on a PDMS chip in which 660 pl drops (corresponding to a spherical diameter of 100 μm ± 1.7%) were created from a continuous aqueous phase by "flow focusing" with a perfluorinated carrier oil (Anna et al., 2003). Perfluorocarbon oils are perfectly suited for this purpose, since they are compatible with PDMS devices, immiscible with water, transparent (allowing for optical readout procedures), and have been shown to facilitate respiratory gas delivery to both prokaryotic and eukaryotic cells in culture (Lowe et al., 1998). The number of cells per

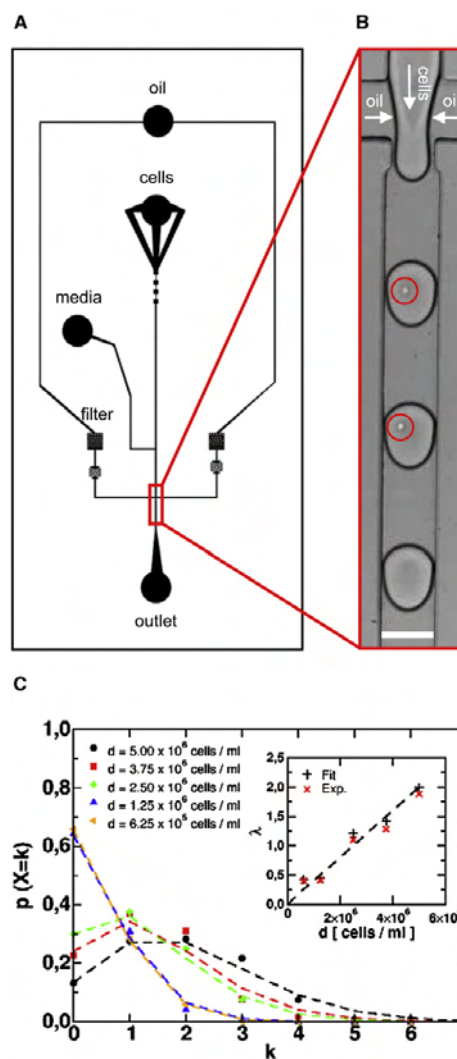


Figure 1. Encapsulation of Jurkat Cells into Aqueous Microdrops of a Water-in-Oil Emulsion

(A) Design of the microfluidic chip (main channels were 75 μm deep and 100 μm wide). The red rectangle indicates the section shown in (B), in which the drops are generated by flow focusing.

(B) Encapsulation of single Jurkat cells (highlighted by red circles) into 660 pl droplets at a frequency of 800 Hz. White bar, 100 μm.

(C) On-chip dilution of the cell-suspension allows for the controlled encapsulation of single cells (here: Jurkat cells). The experimentally determined probability (p , y axis) for the number of cells per drop (k , x axis) is in good agreement with a Poisson distribution (dashed lines) for various cell densities (resulting from on-chip dilution). Inset: the average number of cells per drop (λ) plotted against the cell density for the experimental data (Exp.) and the Poisson distribution (Fit). The dashed line is the theoretical number of cells per drop according to the cell density only (homogeneously distributed).

Chemistry & Biology

Cells in Drops

droplet was controlled by using on-chip dilution of the cells to regulate the cell density (Figure 1C): a culture of Jurkat cells, with an initial density of 5×10^6 cells/ml, was brought together with a stream of sterile medium by co-flow immediately before drop formation, and the relative flow rates of the cell suspension and the medium were changed, whereas the sum of the two flow rates was kept constant. The number of cells per drop (k) was always in good agreement with a Poisson distribution, and high cell densities at the nozzle ($\geq 2.5 \times 10^6$ cells/ml) made the encapsulation of multiple cells per drop highly likely ($p > 30\%$). In contrast, cell densities of 1.25×10^6 cells/ml and below resulted in low probabilities ($p \leq 7\%$) for the encapsulation of more than one cell per drop (while increasing the probability of finding drops without any cells inside). At the same time, the average number of cells per drop (λ) decreased from approximately 2 (at 5×10^6 cells/ml) to far below 1 (at $\leq 1.25 \times 10^6$ cells/ml). Hence, the number of cells per drop can easily be regulated, even allowing for the compartmentalization of single cells.

The generation of stable drops requires the use of a surfactant that decreases the surface tension and, which for the encapsulation of cells, also has to be biocompatible. For this reason, we synthesized several perfluoropolyether-derived surfactants (PFPE surfactants) and tested their effect on long-term cell survival (Figure 2). The surfactants differed solely in their hydrophilic head groups, which should be the only part of the molecule in contact with the encapsulated cells. The common perfluorinated tail should be dissolved in the carrier oil and thus be oriented away from the cells. To analyze the biocompatibility, we seeded HEK293T cells on top of a perfluorocarbon oil layer in the presence (0.5% w/w) and absence of different surfactants. In the absence of any surfactant, the cells retained an intact morphology and even proliferated, whereas the ammonium salt of carboxy-PFPE (Johnston et al., 1996) and poly-L-lysine-PFPE (PLL-PFPE) mediated cell lysis. However, polyethyleneglycol-PFPE (PEG-PFPE) and dimorpholinophosphate-PFPE (DMP-PFPE) showed good biocompatibility, did not affect the integrity of the cellular membrane, and even allowed for cell proliferation. Since DMP-PFPE generated more stable emulsions than PEG-PFPE (data not shown), it was used for all further experiments.

As the next step, procedures allowing for the recovery of encapsulated cells had to be established. Addition of 15% (v/v) Emulsion Destabilizer A104 (RainDance Technologies) to the emulsions mediated reliable breaking without an obvious impact on cell viability. This allowed for the determination of the survival rates of suspension (Jurkat) and adherent (HEK293T) cells for different incubation times within drops. For this purpose, we encapsulated cells at a density corresponding to an average of less than 1 cell per 660 pl drop (1.25×10^6 cells/ml at the nozzle, resulting in a λ value of ~ 0.55 and single cells in $\sim 31.7\%$ of all drops) and collected the resulting emulsions in 15 ml centrifugation tubes. After different incubation times at 37°C within a CO_2 incubator, the emulsions were broken and the cells were treated with a live/dead stain to determine the survival rate and the total number (live and dead) of recovered cells (Figures 3A and 3C). During the first 4 d, the fraction of recovered viable Jurkat cells did not change significantly and was always in excess of 79%. Then, the percentage of live cells decreased from 71% after 5 d to 32% after 6 d and finally to 1% after 14 d of encapsulation. The total number of recovered cells divided by the number of

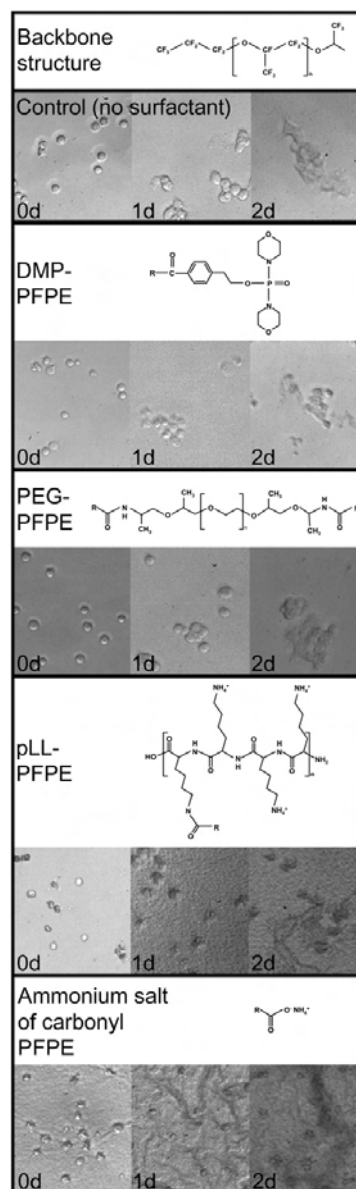


Figure 2. Surfactants Used to Generate the Emulsions

For each surfactant, the chemical structure and the results of the biocompatibility assay (microscopical bright-field images) are shown. For the assay, HEK293T cells were incubated for 48 hr on a layer of perfluorinated FC40 oil in the presence or absence (control) of the indicated surfactant (0.5% w/w).

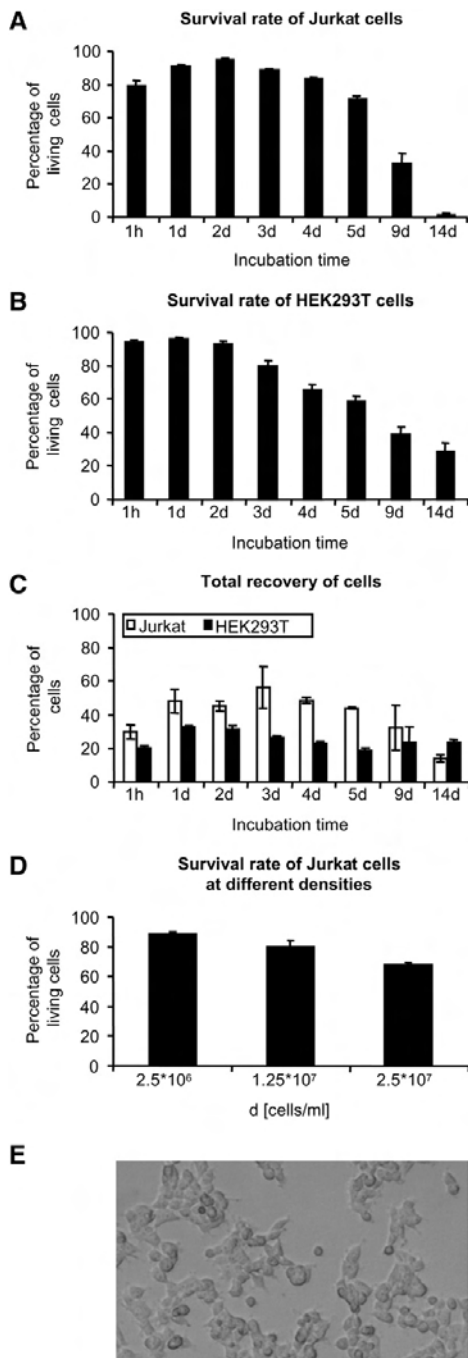


Figure 3. Cell Viability, Recovery, and Recultivation of Cells Encapsulated in 660 μ l Drops

(A and B) The percentage of viable (A) Jurkat and (B) HEK293T cells recovered from emulsions at the indicated time points.

(C) The total number of recovered Jurkat and HEK293T cells (live and dead) relative to the number of initially encapsulated cells.

(D) The percentage of viable Jurkat cells encapsulated at different densities after 3 d.

(E) Recultivation of HEK293T cells recovered after 48 hr of encapsulation.

Error bars show the standard deviation of three independent experiments.

initially encapsulated cells (equal to the aqueous flow rate multiplied by the injection time multiplied by the cell density at the nozzle) was defined as the recovery rate and increased from 29% after 1 hr to more than 55% after 2 d. This indicates some degree of proliferation within the drops, which is also supported by the fact that after 24 hr the percentage of dead cells was lower than after 1 hr. During further incubation within drops, the recovery rates slowly decreased to just 14% after 14 d. This decrease can be explained by the fact that dead cells ultimately disintegrate (after several days) and thus cannot be stained anymore. This effect is well known and has been analyzed in detail for bacterial cells (Villarino et al., 2000). However, early time points and the live stain are not affected by this phenomenon. When repeating the experiments with adherent HEK293T cells, similar results were obtained (Figures 3B and 3C). During the first 2 d, the fraction of recovered viable cells remained constant at more than 90% before slowly decreasing to 58% after 5 d and 39% after 9 d. Finally, after 14 d of encapsulation, 28% of the recovered cells were still alive. The total recovery rate increased slightly from 20% after 1 hr to more than 32% after 2 d. During further incubation within drops, the recovery rates slowly decreased to 23% after 14 d. The longer cell survival compared to Jurkat cells is most likely explained by slower proliferation, resulting in slower consumption of the available nutrition. Recovered cells could also be recultivated (instead of stained) after incubation for 2 d within droplets, resulting in normally proliferating cells (Figure 3E).

In an additional experiment, we assessed the effect of the cell density on the survival rates. For this purpose, we used 5- and 10-fold higher densities of Jurkat cells than used initially. Comparison of the cell survival after 3 d showed that the cell density inversely correlated with the survival rate (Figure 3D). Whereas almost 90% of viable cells were recovered by using the initial cell density, only 80% and 68%, respectively, survived for the 5- and 10-fold increased cell density. Insufficient gas exchange can be ruled out, since equally dense cultures in ordinary tissue-culture flasks did not survive longer: using a density equal to 1 cell in a 660 μ l drop ($\sim 1.5 \times 10^6$ cells/ml), the number of viable Jurkat cells remained above 87% for the first 2 d, before decreasing to 51% after 4 d and 0% after 9 d (data not shown). Therefore, we conclude that the encapsulated cells most likely die due to the lack of nutrition or the accumulation of toxic metabolites, not because of compartmentalization-specific factors such as the oil and surfactant.

Plug-Based Encapsulation

In parallel to encapsulating cells into aqueous drops of a w/o emulsion, we established a system in which aqueous plugs spaced by immiscible oil within a piece of tubing serve as

Chemistry & Biology

Cells in Drops

a culture vessel. This approach allows for the generation of aqueous microcompartments big enough to host small cell populations and even multicellular organisms. This cannot be achieved by simply increasing the drop size of a given emulsion. First, the maximum size of a drop generated on a microfluidic chip is limited by the channel dimensions. Second, as the size of the drops increases, they become less stable, resulting in uncontrolled sample coalescence. These problems can be circumvented by alternately aspirating aqueous plugs and immiscible oil into a holding cartridge (e.g., a capillary or a piece of tubing) (Chen and Ismagilov, 2006). We used this approach to encapsulate several thousand cells into single microcompartments.

First, we assessed holding cartridges made of different materials for their suitability to host living cells. For this purpose, we generated 660 nl plugs hosting 3300 Jurkat cells each. While gas-permeable PTFE tubing allowed for cell survival for several days, the use of glass capillaries and vinyl tubing (all with an inner diameter of ~0.5 mm) resulted in cell death within 24 hr (data not shown). Live/dead stains revealed that, when using PTFE tubing, the survival rate of Jurkat cells remained at ~90% for the first 2 d, before decreasing gradually from 69% after 3 d, to 38% after 5 d, and finally to 6% after 14 d (Figure 4A). The total number of recovered cells increased from 69% after 1 hr to 194% after 5 d, indicating roughly 1–2 cell divisions (Figure 4C). When repeating the experiments with adherent HEK293T cells, slightly different results were obtained (Figures 4B and 4C). Here, the fraction of viable cells remained above 80% for the first 4 d, before slowly decreasing to 31% after 14 d. The recovery rate increased during the first 5 d from 83% to ~147%. Recultivation experiments demonstrated the recovery of fully viable and normally proliferating HEK293T cells after 2 d of encapsulation (Figure 4E).

To assess the influence of the cell density on cell survival, we also performed experiments with five and ten times more Jurkat cells per plug. Once again, we obtained an inverse correlation between cell density and survival. Whereas ~69% viable Jurkat cells were recovered after 3 d when using the initial cell density, only 52% and less than 1% survived when encapsulating five and ten times more cells per plug, respectively (Figure 4D). This massive decrease in cell survival is probably due to the fact that higher cell densities directly resulted in more cells per plug (even at the lowest density, all plugs were occupied), whereas, when encapsulating single cells into drops, the proportion of occupied drops was increased first (with a single cell in a drop still experiencing the same cell density).

In addition, we analyzed if the plugs were subjected to any evaporation during the incubation period. For this purpose, we determined the mean length of the plugs over time by measuring the size of 30 plugs for each time point by using a digital slide gauge and multiplying the mean value by the inner tube diameter to obtain the corresponding plug volumes. No significant decrease in size was observable (Figure 4F), most likely due to the fact that we performed the incubation step in a water-saturated atmosphere (at 37°C, 5% CO₂).

We also investigated the possibility of encapsulating multicellular organisms. Starting with eggs of the nematode *C. elegans*, we analyzed the plugs under the microscope at different time points (Figure 5). Whereas after 2 d hatched worms had already reached the L2–L3 larvae stage, 4 d of encapsulation resulted in the growth of adult worms and the birth of the next generation

(L1 larvae). Longer encapsulation resulted in plugs hosting up to 20 (Movie S2) worms, which finally died after 6–9 d. The passing of individual worms into adjacent microcompartments was never observed, even at high flow rates (up to 1000 µl/hr).

On-Chip Postincubation Analysis of Individual Compartments

High-throughput, cell-based assays require the readout of individual samples after the incubation step (e.g., to screen the phenotype of individual cells within a heterogeneous population). For this purpose, microcompartments stored in a piece of tubing or a reservoir have to be reinjected into an on-chip readout module after the incubation period. To prove the feasibility of this approach, we encapsulated HEK293T cells within 660 pl drops, collected the resulting emulsions, and incubated the samples for 2 and 14 d. Subsequently, the emulsions were reinjected into a chip (same design as for the encapsulation step) and were analyzed microscopically. During reinjection of the emulsion after 2 d of incubation, hardly any coalescence of individual samples was detectable (Figure 6A; Movie S3). After 14 d of incubation, some degree of coalescence was observable; however, the majority of drops (>90%) remained intact. Microscopical comparison of the drops at the time of incubation and reinjection revealed no obvious reduction of the drop size (Figure 6B). This indicates that the drops are not subjected to significant evaporation during the incubation period (within a water-saturated atmosphere).

To demonstrate that the drops can be analyzed individually after reinjection, we encapsulated a population of HEK293T cells that, 2 wk before the experiment, had been incubated in bulk with viral particles (murine leukemia virus pseudotyped with the G protein of the vesicular stomatitis virus) having packaged the *lacZ* gene. The fraction of cells stably expressing the corresponding gene product (β -galactosidase) was ~13.9%, as determined in an X-Gal assay (Stitz et al., 2001). During the drop production, a fluorogenic substrate (1.7 mM fluorescein di- β -D-galactopyranoside, FDG) for β -galactosidase was co-encapsulated into the drops, and a laser beam (488 nm wavelength) was focused onto the channel (downstream of the nozzle). The emitted light was collected in a photomultiplier (Figure 6D) to record the fluorescence signal at t_0 . This measurement was performed with the initial population of transduced HEK293T cells and a sample that had been diluted 1:9 with nontransduced HEK293T cells. At the time of encapsulation, no difference in the fluorescence signals was observable, and even drops without any cell showed the same signal intensity (data not shown). After an incubation time of 16 hr at 37°C, the emulsions were reinjected into the chip together with additional fluorinated oil (separately injected into the oil inlet to space out the drops) to repeat the fluorescence measurement (at t_1 ; analyzing 500 drops/s). Plotting the maximum fluorescence intensity of the drops against the peak width (which corresponds to the drop size and therefore is a good indicator of coalescence) revealed different distinct populations (Figure 6F). Analysis of the peak width proved that even though populations with 2-fold and 3-fold higher volumes were observable, the majority of drops did not coalesce (>93%). In terms of the fluorescence, two main populations with an ~35-fold difference in their intensity were obtained, as also confirmed by fluorescence microscopy

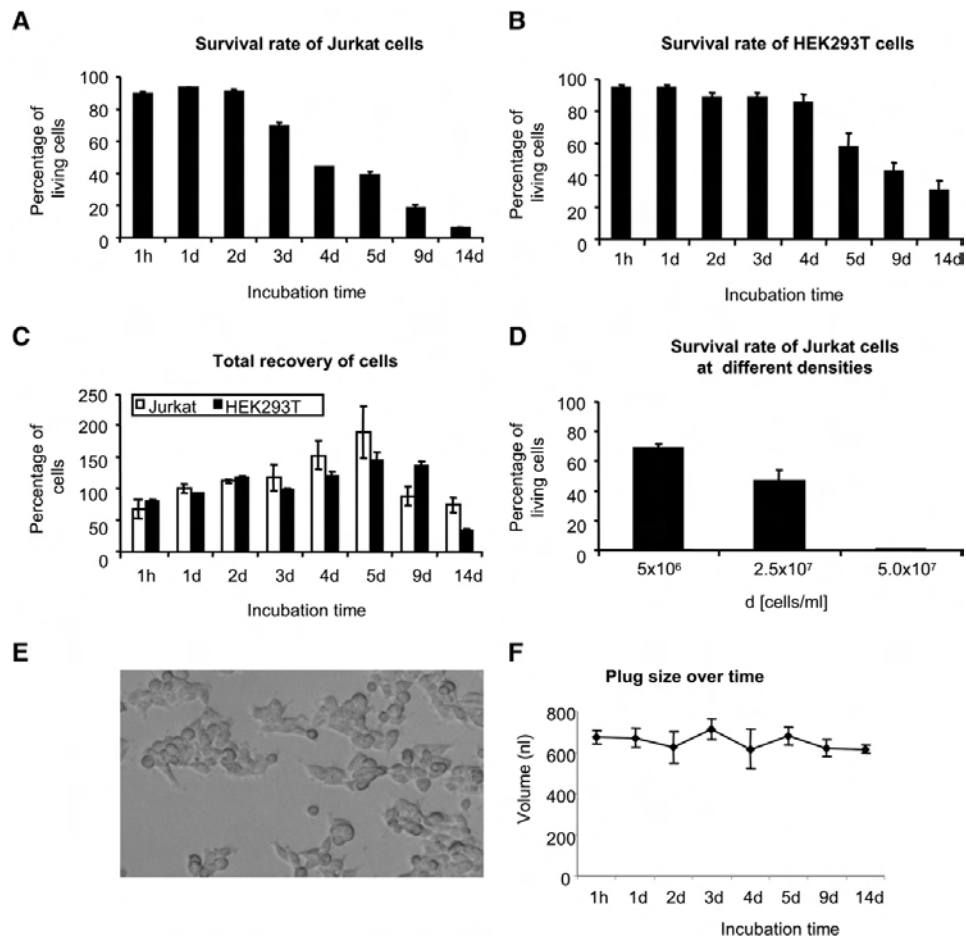


Figure 4. Cell Viability, Recovery, and Recultivation of Cells Encapsulated in 660 nl Plugs

(A and B) The percentage of viable (A) Jurkat and (B) HEK293T cells recovered from plugs at the indicated time points.
 (C) The total number of recovered Jurkat and HEK293T cells (live and dead) relative to the number of initially encapsulated cells.
 (D) The percentage of viable Jurkat cells encapsulated at different densities after 3 d.
 (E) Recultivation of HEK293T cells recovered after 48 hr of encapsulation.
 (F) Mean size of plugs harboring HEK293T cells plotted against the incubation time.
 Error bars show the standard deviation of three independent experiments.

in which the drops appeared to be either highly fluorescent or nonfluorescent (Figure 6C). Based on these observations, we set gates for the quantitative interpretation of the data (as routinely done in FACS analysis). Gates were set to solely analyze those drops that had not coalesced (corresponding to the populations with the lowest peak width). Based on the way the peak width was defined, fluorescence-positive drops appeared to be bigger (see Figure 6E). Nonetheless, plotting the fluorescence against the peak width enabled noncoalesced drops to be clearly distinguished from coalesced drops for both species (positives and negatives). The use of gating leads to the conclu-

sion that ~5.08% of all noncoalesced drops were fluorescence positive in the sample with nondiluted transduced cells. This number corresponds to ~12.7% of the corresponding cell population when taking into account that only 40.0% of the drops were occupied (as determined by microscopical analysis of the drops during the encapsulation step). This value is in the same range as the fraction of positive cells determined in bulk (~13.9%), by using a conventional X-Gal assay. For the diluted sample, we obtained 0.63% positive drops, corresponding to 1.8% of the cells (34.8% of the drops were occupied). Compared to the nondiluted sample, the negative population showed

Chemistry & Biology

Cells in Drops



Figure 5. Growth of the Nematode *C. elegans* within Aqueous 660 nl Plugs

Eggs (black arrow) were encapsulated at room temperature, and bright-field microscopical images were taken after 0, 2, or 4 d. White arrows show larvae of the second generation of encapsulated worms. White bar, 100 μm .

a lower fluorescence intensity. This is most likely due to the fact that all drops (even the ones without cells) contain traces of soluble β -galactosidase, resulting from the few dead cells within the syringe (during the encapsulation step). Since the diluted sample contains less enzyme in total, a lower background can be expected, too. Another possible explanation would be the exchange of fluorescein between the drops. However, this seems to be unlikely, since for incubation periods of up to 24 hr we never observed any significant exchange of fluorescein for any surfactants tested (including the ammonium salt of carboxy-PFPE and PEG-PFPE; data not shown). The resulting 7.1-fold difference in terms of positive cells between the samples is in good agreement with the initial 1:9 dilution (assuming an accuracy of $\pm 10\%$ when counting the cultures in a Neubauer chamber before mixing leads to the conclusion that the effective ratio might have been as low as 1:7.4). In summary, these results clearly demonstrate the possibility of quantitatively analyzing individual drops in a high-throughput fashion (we analyzed the drops at a frequency of 500 Hz).

DISCUSSION

We have used droplet-based microfluidic systems to create miniaturized reaction vessels in which both adherent and nonadherent cells can survive for several days. Even though we generated microcompartments with volumes of 660 μl and 660 nl only, in principle almost any volume can be generated by changing the channel sizes and flow rates, or by splitting relatively large microcompartments through a T-junction into smaller units (Adamson et al., 2006). Thus, microcompartments tailored for the encapsulation of small objects like single cells can be generated as well as compartments big enough to host multicellular organisms like *C. elegans*. Furthermore, the size can be adjusted according to the assay duration. Cell density was found to inversely correlate with the survival time of encapsulated cells. Larger compartments are hence preferential for long-term assays, especially since encapsulated cells proliferate within the microcompartments. Consequently, even proliferation assays (e.g., for screening cytostatic drugs) should be possible as long as the chosen volume is big enough to guarantee sufficient supply of nutrition. On the other hand, small volumes might be advantageous for other applications, for example to minimize reagent costs or to rapidly obtain high concentrations of secreted cellular factors. Besides the volume, additional factors, notably the biocompati-

bility of the surfactants and the gas permeability of the storage system, have a major impact on cell survival. Both of the nonionic surfactants described here allowed for cell survival and proliferation, whereas the two ionic surfactants mediated cell lysis. Even though there is no direct proof of correlation, it seemed quite striking that poly-L-lysine, a compound widely used to improve cell attachment to surfaces (Budd et al., 1989), mediated membrane disruption when used as a head group of an ionic surfactant. Long-term incubation also requires sufficient gas exchange. This can be ensured either by using open reservoirs or channels or tubing made of gas-permeable materials such as fluorinated polymers. Efficient gas exchange is also helped by the fact that perfluorocarbon carrier fluids can dissolve more than 20 times the amount of O_2 , and 3 times the amount of CO_2 , than water and have been shown to facilitate respiratory gas delivery to both prokaryotic and eukaryotic cells in culture (Lowe et al., 1998).

The possibility of reinjecting microcompartments into a chip after the incubation step opens the way for integrated droplet-based microfluidic systems for cell-based HTS. As we have shown here, a fluorescence-based readout of the expression of a cellular reporter gene can be performed in individual compartments at frequencies of 500 Hz. Hence, a wide range of commercially available fluorescence-based assays (Gonzalez and Negulescu, 1998; Sundberg, 2000) can potentially be performed in a high-throughput fashion. The fact that possible coalescence of individual drops does not necessarily bias the readout is noteworthy. As shown here, coalesced drops with higher volumes can easily be identified and excluded from the data analysis. In theory, the use of gates also allows for the analysis of only those compartments hosting a specific number of (fluorescent) cells. In contrast to conventional FACS analysis, the assay readout does not have to be based on fluorophores that remain in, or on the surface of, the cells (e.g., GFP or fluorescent antibodies). Using compartmentalization, we have been able to measure the activity of an intracellular reporter enzyme (β -galactosidase) by using a fluorescent product that is highly membrane permeable (fluorescein).

The integration of additional microfluidic modules into the microfluidic platforms shown here should allow the application range to be expanded. Integrating a microfluidic sorting module (based on dielectrophoresis or valves) (Ahn et al., 2006; Fu et al., 2002) could, for example, enable the screening of drug candidates. In the simplest case, the candidates could be genetically

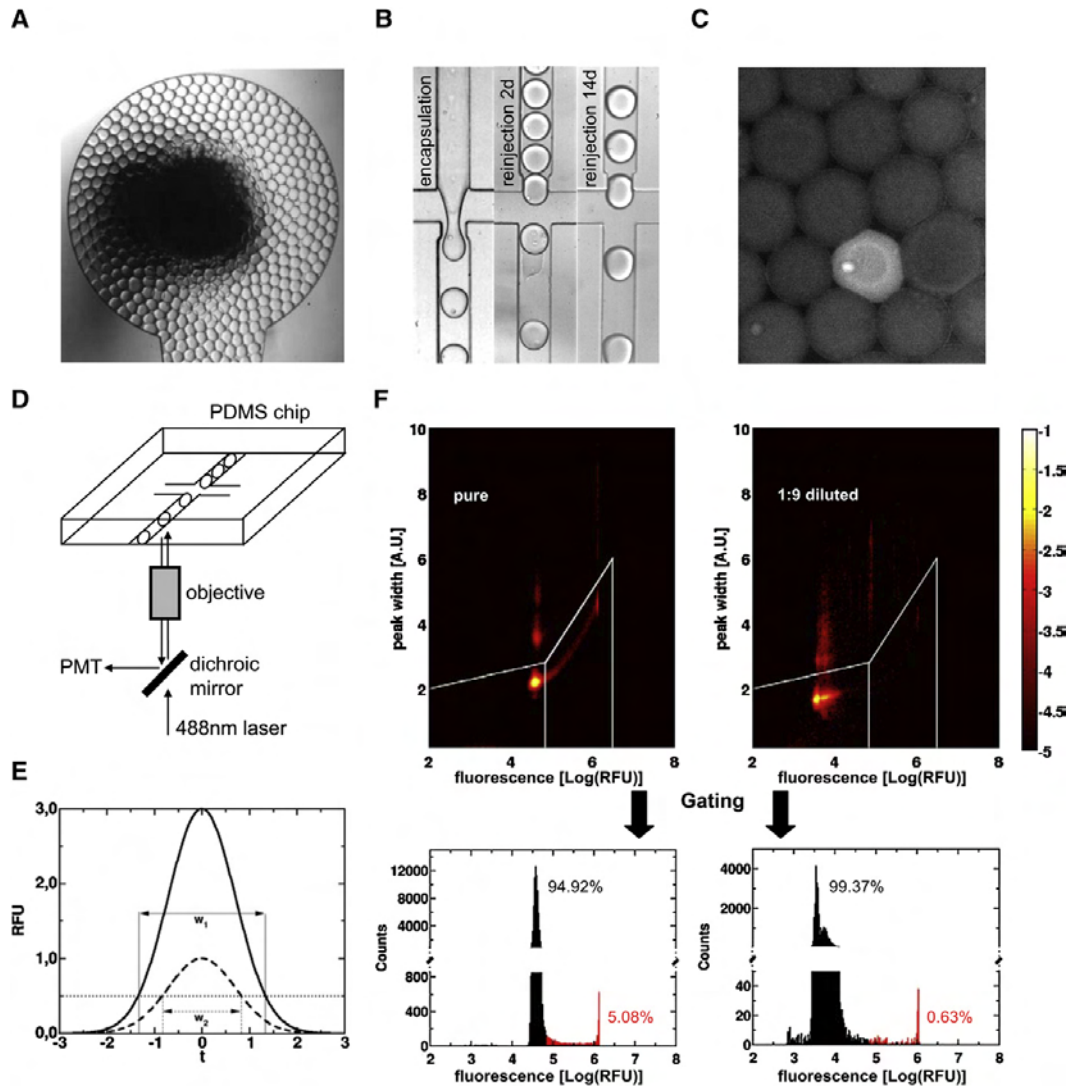


Figure 6. Reinjection and Analysis of Emulsions after Incubation

(A) Bright-field image of the inlet during reinjection of an emulsion (drops containing HEK293T cells) after 2 d of incubation.

(B) Bright-field images of individual drops during encapsulation and after reinjection (off-chip incubation for 2 and 14 d).

(C) Fluorescence-microscopic image of drops hosting *lacZ*-expressing HEK293T cells (converting the fluorogenic substrate FDG) after 16 hr of incubation.

(D) Optical setup for fluorescence measurements.

(E) Influence of the fluorescence intensity (y axis) on the peak width (w). The peak width is defined as the time (t , x axis) for which a fluorescent signal above a certain threshold (dotted, horizontal line) can be measured (due to a drop passing the laser beam). Different fluorescence intensities of the drops (continuous and dashed peaks) result in different apparent peak widths (w_1 and w_2).

(F) Fluorescence signals of drops after reinjection. Upper panels: fluorescence intensity (x axis) plotted against the peak width (y axis) for pure (left) and 1:9 diluted (right) transduced cells. The relative frequency of all events is color coded according to the bar on the right (numbers corresponding to the exponent of the frequency). White gates correspond to noncoalesced drops: left gate, drops considered as negatives; right gate, drops considered as positives. Lower panel: fluorescence intensity (x axis) plotted against the drop counts (y axis) of all events within the gates. Positive events are depicted in red, and negative events are depicted in black.

Chemistry & Biology

Cells in Drops

encoded by the encapsulated cells themselves (starting with a cell library); hence, the collection of sorted positive drops would allow for the identification of hits by DNA sequencing. Alternatively, the sorting module could be used to screen synthetic compounds fixed on beads (e.g., one-bead-one-compound libraries) coencapsulated in the drops. After the sorting step, beads that mediated the desired effect could be recovered from the drops for a subsequent decoding step (e.g., by mass spectroscopy). Using optical barcodes encoding the compound identity might even allow the decoding step to be performed in real time (without the need for a sorting module) (Battersby et al., 2002; Pregibon et al., 2007). For example, different fluorescence channels could be used for the assay and label readout. The fact that the optical barcode does not even have to be directly linked to the test compound when using droplet-based microfluidics is noteworthy: the label can simply be mixed with the test compound prior to the encapsulation step.

SIGNIFICANCE

Aqueous microcompartments can be used as miniaturized vessels for chemical and biological reactions (Tawfik and Griffiths, 1998; Kelly et al., 2007; Griffiths and Tawfik, 2006). We show here how this approach can also be utilized for cell-based applications. We demonstrate that human cells, and even a multicellular organism (*C. elegans*), can be compartmentalized and remain fully viable for several days in droplets. The microfluidic platforms described here allow the encapsulation step to occur at rates of more than 800 per sec. As the number of cells per drop follows a Poisson distribution, the optional encapsulation of single cells causes the generation of empty drops, thus decreasing the resulting encapsulation rate to ~ 300 per sec. We have demonstrated postincubation fluorescence readout of individual compartments at 500 Hz, and additional droplet manipulation procedures (such as fusion, splitting, and sorting) can be performed at similar rates (Link et al., 2004, 2006; Ahn et al., 2006). Consequently, the throughput of a single integrated, droplet-based microfluidic system for cell-based screening could potentially be 500 times higher than conventional robotic microtiter-plate-based HTS technologies that can perform a maximum of $\sim 100,000$ assays per d, or $\sim 1 \text{ s}^{-1}$. Using compartments as small as 660 pl, the volume of each assay, and hence the cost of reagents for screening, could be reduced by >1000 -fold relative to the smallest assay volumes in microtiter plates (1–2 μl). This may allow many high-throughput biochemical screens to be replaced by more physiologically relevant cell-based assays (Chapman, 2004; Johnston and Johnston, 2002), including assays with highly valuable cells, e.g., primary human cells, which are arguably the most physiologically relevant model systems, but which generally cannot be obtained on the scale required for HTS.

EXPERIMENTAL PROCEDURES

Fabrication of Microfluidic Chips

The microfluidic device (Figure 1A) was fabricated by patterning 75 μm deep channels into poly(dimethylsiloxane) (PDMS) by using soft lithography (Squires

and Quake, 2005). The PDMS was activated by incubation for 3 min in an oxygen plasma (Plasma Prep 2, Gala Instrumente) and was bound to a 50 mm \times 75 mm glass slide (Fisher Bioblock). Inlets and outlets were made by using 0.75 mm diameter biopsy punches (Harris Uni-Core). The channels were flushed with a commercial surface-coating agent (Aqualap, PPG Industries) and, subsequently, with N_2 prior to use.

Cells

HEK293T cells were grown and encapsulated in DMEM medium (GIBCO-BRL), and Jurkat cells were grown and encapsulated in RPMI medium (GIBCO-BRL). Both media were supplemented with 10% fetal bovine serum (GIBCO-BRL) and 1% penicillin/streptomycin (GIBCO-BRL). Cells were incubated at 37°C under a 5% CO_2 atmosphere saturated with water.

For fluorescence readouts, the *lacZ* gene was introduced into HEK293T cells by retroviral transduction as described elsewhere (Stitz et al., 2001). In brief, by transfecting HEK293T cells, we generated murine leukemia virus-derived particles (pseudotyped with the G protein of the vesicular stomatitis virus) that had packaged a vector encoding *lacZ*. Two days after transfection, the particles were harvested from the cell-culture supernatants and were used for transduction of fresh HEK293T cells during 1 hr of incubation. Subsequently, the cells were cultivated for 2 wk before encapsulating them together with 1.7 mM fluorescein di- β -D-galactopyranoside (FDG, Euromedex) in drops.

Synthesis of Surfactants

Detailed synthesis and characterization of fluorinated surfactants will be published elsewhere by A.E. and C.H. (unpublished data). In brief, surfactants (Figure 2) were synthesized as follows:

Carboxy-PFPE

To obtain the ammonium salt of carboxy-PFPE, Krytox FS(L) 2000 (DuPont) was reacted with NH_4OH as described (Johnston et al., 1996).

DMP-PFPE

Synthesis of the hydrophilic head group dimorpholinophosphate (DMP) was carried out by reaction of PhEtOH (Aldrich), POCl_3 (Fluka), and morpholine (Fluka) with $(\text{Et})_3\text{N}$ (Sigma-Aldrich) in THF (Fluka) on ice. Subsequently, DMP was coupled to water/cyclohexane/isopropanol-extracted Krytox FS(H) 4000 (DuPont) by Friedels-Craft-Acylation.

PEG-PFPE

Reaction of Krytox FS(H) 4000 (DuPont) with polyethyleneglycol (PEG) 900 (Sigma) resulted in a mixture of PEG molecules coupled to either one or two PFPE molecules.

Poly-L-Lysine-PFPE

Krytox FS(L) 2000 (DuPont) was reacted with poly-L-Lysine (15,000–30,000; Sigma).

Biocompatibility Test for Different Surfactants

A 100 μl suspension of HEK293T cells (1.5×10^6 cells/ml in fresh media) was seeded on top of a layer of perfluorocarbon oil (FC40, 3M) in the presence (0.5% w/w) and absence of the tested surfactants. After incubation at 37°C for 0 hr, 24 hr, and 48 hr, bright-light images were taken with a Leica DMIRB microscope.

Drop-Based Encapsulation, Cell Recovery, and Live/Dead Staining

Cells were adjusted to a density of 2.5×10^6 cells/ml (determined with a Neubauer counting chamber), stirred at 200 rpm by using an 8 mm magnetic stir-bar (Roth) in a 5 ml polyethylene syringe (Fisher Bioblock), and injected via PTFE tubing (0.56 mm \times 1.07 mm internal/external diameter, Fisher Bioblock) into the microfluidic device (Figure 1A) by using a syringe pump (PHD 2000, Harvard Apparatus) at a flow rate of 1000 $\mu\text{l/hr}$. The cell suspension was diluted on-chip (see below) by diluting it with sterile media (1000 $\mu\text{l/hr}$ if not otherwise stated), and drops were generated by flow focusing (Anna et al., 2003) of the resulting stream with perfluorinated oil (FC40, 3M), containing 0.5% (w/w) DMP-PFPE (4000 $\mu\text{l/hr}$). The drop volume was calculated by dividing the flow rate by the drop frequency (determined by using a Phantom V4.2 high-speed camera). Experimental variations in the drop frequency (at constant flow rates) were defined as the degree of polydispersity in terms of the volume (corresponding to the third power of the polydispersity in terms of the diameter when considering a perfect sphere). For each sample, 500 μl of the resulting emulsion was collected within a 15 ml centrifuge tube and

incubated at 37°C within a CO₂ incubator (5% CO₂, saturated with H₂O). After incubation, 250 µl of the emulsion was transferred into a new centrifuge tube and broken by the addition of 15% Emulsion Destabilizer A104 (RainDance Technologies; Guilford, CT) and 10 ml live/dead staining solution (LIVE/DEAD Viability/Cytotoxicity Kit for animal cells, Invitrogen Kit L-3224) and subsequent mixing. After incubation for 3 min (to allow sedimentation of the oil phase), the supernatant was transferred into a 25 cm² tissue-culture flask and incubated for 1 hr at room temperature.

On-Chip Dilution of Cells

Drops were generated and diluted on-chip by bringing together two channels containing the cell suspension and sterile media, respectively, and varying the relative flow rates while keeping the overall aqueous flow rate constant at 2000 µl/hr by using two syringe pumps. The number of cells per drop was determined by evaluating movies taken with a high-speed camera (Phantom V4.2) mounted on a microscope. For each dilution, 120 drops were analyzed to determine the number of cells per drop. Subsequently, the data were fitted to a Poisson distribution ($P_{k = n} = e^{-\lambda} \times \lambda^n / k!$) by using Xmgrace (<http://plasma-gate.weizmann.ac.il/Grace/>).

Reinjection of Emulsions and Fluorescence Readout of Individual Samples

The emulsions were collected in open syringes (without the plunger being inserted) and incubated within a water-saturated atmosphere (37°C, 5% CO₂). During the encapsulation step, a laser beam (488 nm wavelength) was focused onto the channel by using an objective with a 40-fold magnification (Figure 6D, downstream of the nozzle) to excite the fluorophore. Emitted light was diverted by a dichroic mirror (488 nm notch filter), filtered (510 nm ± 10 nm), and collected in a photomultiplier to record the first fluorescence measurement (t_0). After the desired incubation time, mineral oil was added to fill the syringe completely before inserting the plunger and reinjecting the emulsion together with 0.5% w/w DMP-PFPE surfactant in FC40 (injected into the oil inlet to space out the drops) into a chip with the same design as for the encapsulation step. To avoid fragmentation of the drops before the second fluorescence measurement (at t_1), the flow direction was reversed compared to the encapsulation step (the emulsion was injected into the outlet [Figure 1A] to avoid branching channels). All signals from the photomultiplier were recorded by using Labview (National Instruments) and by running an in-house program for the data analysis.

Plug-Based Encapsulation, Cell Recovery, and Live/Dead Staining

To prepare the plugs, 5×10^6 cells/ml (determined with a Neubauer counting chamber) were stirred at 510 rpm within a 1.8 ml cryotube (Nunc) by using an 8 mm magnetic stir-bar (Roth) and were kept at 4°C. Subsequently, 660 nl plugs of this cell suspension and perfluorinated oil (FC40, 3M) were aspirated (at 500 µl/hr) into PTFE tubing (0.56 µm × 1.07 mm internal/external diameter, Fisher Bioblock) in an alternating fashion by using a syringe pump (PHD 2000, Harvard Apparatus). For each sample, 30 plugs were loaded before the tubing was sealed (by clamping microtubes to both ends) and were incubated at 37°C within a CO₂ incubator (5% CO₂, saturated with H₂O). After incubation, the plugs were infused into a 25 cm² tissue-culture flask. Subsequently, 4 ml live/dead staining solution (LIVE/DEAD Viability/Cytotoxicity Kit for animal cells, Invitrogen Kit L-3224) was added, and the samples were incubated for 1 hr at room temperature. When using adherent cells, the staining solution was additionally supplemented with 0.25 g/l trypsin (GIBCO-BRL) to break up cell clumps.

Determination of the Survival Rates and Total Recovery

After staining, live and dead cells were counted manually by using a microscope (Leica DMIRB) with a UV-light source (LEJ ebq 100). For each sample within a 25 cm² tissue-culture flask, 30 fields of view (corresponding to ~4.2 mm²) were evaluated to calculate the total number of living (green stain) and dead (red stain) cells.

Encapsulation of *C. elegans*

Eggs were resuspended in M9 minimal media (Sigma) supplemented with *E. coli* OP50 (10% w/v of pelleted bacteria). Plugs of the resulting suspension were aspirated into PTFE tubing and incubated at room temperature.

Recultivation Experiments

For recultivation of cells recovered from drops or plugs, semiconditioned medium supplemented with 30% fetal bovine serum (GIBCO-BRL) was added to the cells instead of the staining solution. Cells were then incubated for 2 d at 37°C within a CO₂ incubator (5% CO₂, saturated with H₂O) before imaging with bright-field microscopy.

SUPPLEMENTAL DATA

Supplemental Data include movies of cell encapsulation, the incubation of *C. elegans* in aqueous plugs, and the reinjection of an emulsion and are available at <http://www.chembiol.com/cgi/content/full/15/5/427/DC1/>.

ACKNOWLEDGMENTS

The authors would like to thank Michael Samuels (Raindance Technologies) and Wolfgang Hinz (Rothberg Institute for Childhood Diseases) for their help with developing the emulsion-breaking protocol, Raindance Technologies for the kind gift of Emulsion Destabilizer A104, and Luis Briseño Roa for his introduction to the cultivation of nematodes. C.A.M. and D.L. were supported by a Liebig Grant of the Fonds der Chemischen Industrie, which is partially funded by the Bundesministerium fuer Bildung und Forschung (BMBF). J.-C.B. was supported by a European Molecular Biology Organization long-term fellowship, and A.E.-H. was supported by the European Commission Framework Programme 6 (EC FP6) MiFem Network. O.J.M. was supported by the Medical Research Council (UK) and the Ministry of Defense (UK). L.F. was supported by the EC FP6 Marie Curie Research Training Network, ProSA. S.K. was supported by a research grant of the Deutsche Forschungsgemeinschaft (DFG, KO 3572/1). This work was also supported by the Ministère de l'Enseignement Supérieur et de la Recherche, Centre National de la Recherche Scientifique, and Agence National de la Recherche. The Medical Research Council (MRC), Harvard University, and the Institut de Science et d'Ingénierie Supramoléculaires (ISIS) have filed patent applications that include some of the ideas described in this manuscript. Should these facilities receive revenues as a result of licensing these patents the authors are entitled to receive payments through the corresponding Inventor's Rewards Schemes.

Received: December 14, 2007

Revised: April 2, 2008

Accepted: April 8, 2008

Published: May 16, 2008

REFERENCES

- Adamson, D.N., Mustafi, D., Zhang, J.X.J., Zheng, B., and Ismagilov, R.F. (2006). Production of arrays of chemically distinct nanolitre plugs via repeated splitting in microfluidic devices. *Lab Chip* 6, 1178–1186.
- Ahn, K., Kerbage, C., Hunt, T.P., Westervelt, R.M., Link, D.R., and Weitz, D.A. (2006). Dielectrophoretic manipulation of drops for high-speed microfluidic sorting devices. *Appl. Phys. Lett.* 88, 24104.
- Anna, S.L., Bontoux, N., and Stone, H.A. (2003). Formation of dispersions using "flow focusing" in microchannels. *Appl. Phys. Lett.* 82, 364–366.
- Battersby, B.J., Lawrie, G.A., Johnston, A.P.R., and Trau, M. (2002). Optical barcoding of colloidal suspensions: applications in genomics, proteomics and drug discovery. *Chem. Commun. (Camb.)* 14, 1435–1441.
- Beer, N.R., Hindson, B., Wheeler, E., Hall, S., Rose, K., Kennedy, I., and Colston, B. (2007). On-chip, real-time, single-copy polymerase chain reaction in picoliter droplets. *Anal. Chem.* 79, 8471–8475.
- Budd, J.S., Bell, P.R., and James, R.F. (1989). Attachment of indium-111 labelled endothelial cells to pretreated polytetrafluoroethylene vascular grafts. *Br. J. Surg.* 76, 1259–1261.
- Chapman, T. (2004). Drug discovery: the leading edge. *Nature* 430, 109–115.
- Chen, D.L., and Ismagilov, R.F. (2006). Microfluidic cartridges preloaded with nanoliter plugs of reagents: an alternative to 96-well plates for screening. *Curr. Opin. Chem. Biol.* 10, 226–231.

Chemistry & Biology

Cells in Drops

- Dove, A. (1999). Drug screening—beyond the bottleneck. *Nat. Biotechnol.* **17**, 859–863.
- Fu, A.Y., Chou, H.-P., Spence, C., Arnold, F.H., and Quake, S.R. (2002). An integrated microfabricated cell sorter. *Anal. Chem.* **74**, 2451–2457.
- Funfak, A., Brösing, A., Brand, M., and Köhler, J.M. (2007). Micro fluid segment technique for screening and development studies on *Danio rerio* embryos. *Lab Chip* **7**, 1132–1138.
- Gonzalez, J.E., and Negulescu, P.A. (1998). Intracellular detection assays for high-throughput screening. *Curr. Opin. Biotechnol.* **9**, 624–631.
- Griffiths, A.D., and Tawfik, D.S. (2006). Miniaturising the laboratory in emulsion droplets. *Trends Biotechnol.* **24**, 395–402.
- Grodrian, A., Metzke, J., Henkel, T., Martin, K., Roth, M., and Köhler, J.M. (2004). Segmented flow generation by chip reactors for highly parallelized cell cultivation. *Biosens. Bioelectron.* **19**, 1421–1428.
- Hawtin, P., Hardern, I., Wittig, R., Mollenhauer, J., Poustka, A., Salowsky, R., Wulff, T., Rizzo, C., and Wilson, B. (2005). Utility of lab-on-a-chip technology for high-throughput nucleic acid and protein analysis. *Electrophoresis* **26**, 3674–3681.
- He, M., Edgar, J.S., Jeffries, G.D.M., Lorenz, R.M., Shelby, J.P., and Chiu, D.T. (2005). Selective encapsulation of single cells and subcellular organelles into picoliter- and femtoliter-volume droplets. *Anal. Chem.* **77**, 1539–1544.
- Huebner, A., Srisa-Art, M., Holt, D., Abell, C., Hollfelder, F., deMello, A.J., and Edel, J.B. (2007). Quantitative detection of protein expression in single cells using droplet microfluidics. *Chem. Commun. (Camb.) Mar* **28**, 1218–1220.
- Johnston, K.P., Harrison, K.L., Clarke, M.J., Howdle, S.M., Heitz, M.P., Bright, F.V., Carrier, C., and Randolph, T.W. (1996). Water-in-carbon dioxide microemulsions: an environment for hydrophiles including proteins. *Science* **271**, 624–626.
- Johnston, P.A., and Johnston, P.A. (2002). Cellular platforms for hts: three case studies. *Drug Discov. Today* **7**, 353–363.
- Kelly, B.T., Baret, J.-C., Taly, V., and Griffiths, A.D. (2007). Miniaturizing chemistry and biology in microdroplets. *Chem. Commun. (Camb.) May* **14**, 1773–1788.
- Li, P.C., and Harrison, D.J. (1997). Transport, manipulation, and reaction of biological cells on-chip using electrokinetic effects. *Anal. Chem.* **69**, 1564–1568.
- Lin, Y.H., Lee, G.B., Li, C.W., Huang, G.R., and Chen, S.H. (2001). Flow-through sampling for electrophoresis-based microfluidic chips using hydrodynamic pumping. *J. Chromatogr. A* **937**, 115–125.
- Link, D.R., Anna, S.L., Weitz, D.A., and Stone, H.A. (2004). Geometrically mediated breakup of drops in microfluidic devices. *Phys. Rev. Lett.* **92**, 054503.
- Link, D.R., Grasland-Mongrain, E., Duri, A., Sarrazin, F., Cheng, Z., Cristobal, G., Marquez, M., and Weitz, D.A. (2006). Electric control of droplets in microfluidic devices. *Angew. Chem. Int. Ed. Engl.* **45**, 2556–2560.
- Lowe, K.C., Davey, M.R., and Power, J.B. (1998). Perfluorochemicals: their applications and benefits to cell culture. *Trends Biotechnol.* **16**, 272–277.
- Margulies, M., Egholm, M., Altman, W.E., Attiya, S., Bader, J.S., Bembien, L.A., Berka, J., Braverman, M.S., Chen, Y.J., Chen, Z., Dewell, S.B., et al. (2005). Genome sequencing in microfabricated high-density picolitre reactors. *Nature* **437**, 376–380.
- Martin, K., Henkel, T., Baier, V., Grodrian, A., Schön, T., Roth, M., Köhler, J.M., and Metzke, J. (2003). Generation of larger numbers of separated microbial populations by cultivation in segmented-flow microdevices. *Lab Chip* **3**, 202–207.
- Oh, H.J., Kim, S.H., Baek, J.Y., Seong, G.H., and Lee, S.H. (2006). Hydrodynamic micro-encapsulation of aqueous fluids and cells via 'on the fly' photopolymerization. *J. Micromech. Microeng.* **16**, 285–291.
- Pregibon, D.C., Toner, M., and Doyle, P.S. (2007). Multifunctional encoded particles for high-throughput biomolecule analysis. *Science* **315**, 1393–1396.
- Sakai, S., Kawabata, K., Ono, T., Iijima, H., and Kawakami, K. (2005). Higher viscous solution induces smaller droplets for cell-enclosing capsules in a co-flowing stream. *Biotechnol. Prog.* **21**, 994–997.
- Shendure, J., Porreca, G.J., Reppas, N.B., Lin, X., McCutcheon, J.P., Rosenbaum, A.M., Wang, M.D., Zhang, K., Mitra, R.D., and Church, G.M. (2005). Accurate multiplex polony sequencing of an evolved bacterial genome. *Science* **309**, 1728–1732.
- Song, H., Tice, J.D., and Ismagilov, R.F. (2003). A microfluidic system for controlling reaction networks in time. *Angew. Chem. Int. Ed. Engl.* **42**, 768–772.
- Song, H., Li, H.-W., Munson, M.S., Ha, T.G.V., and Ismagilov, R.F. (2006). On-chip titration of an anticoagulant argatroban and determination of the clotting time within whole blood or plasma using a plug-based microfluidic system. *Anal. Chem.* **78**, 4839–4849.
- Squires, T.M., and Quake, S.R. (2005). Microfluidics: fluid physics at the nanoliter scale. *Rev. Mod. Phys.* **77**, 977–1026.
- Srinivasan, V., Pamula, V.K., and Fair, R.B. (2004). An integrated digital microfluidic lab-on-a-chip for clinical diagnostics on human physiological fluids. *Lab Chip* **4**, 310–315.
- Stitz, J., Mühlebach, M.D., Blömer, U., Scherr, M., Selbert, M., Wehner, P., Steidl, S., Schmitt, I., König, R., Schweizer, M., et al. (2001). A novel lentivirus vector derived from apathogenic simian immunodeficiency virus. *Virology* **291**, 191–197.
- Sundberg, S.A. (2000). High-throughput and ultra-high-throughput screening: solution- and cell-based approaches. *Curr. Opin. Biotechnol.* **11**, 47–53.
- Tawfik, D.S., and Griffiths, A.D. (1998). Man-made cell-like compartments for molecular evolution. *Nat. Biotechnol.* **16**, 652–656.
- Thorsen, T., Roberts, R.W., Arnold, F.H., and Quake, S.R. (2001). Dynamic pattern formation in a vesicle-generating microfluidic device. *Phys. Rev. Lett.* **86**, 4163–4166.
- Thorsen, T., Maerkl, S.J., and Quake, S.R. (2002). Microfluidic large-scale integration. *Science* **298**, 580–584.
- Umbanhowar, P.B., Prasad, V., and Weitz, D.A. (2000). Monodisperse emulsion generation via drop break off in a coflowing stream. *Langmuir* **16**, 347–351.
- Villarino, A., Bouvet, O.M., Regnault, B., Martin-Delautre, S., and Grimont, P.A.D. (2000). Exploring the frontier between life and death in *Escherichia coli*: evaluation of different viability markers in live and heat- or uv-killed cells. *Res. Microbiol.* **151**, 755–768.
- Wang, J. (2002). On-chip enzymatic assays. *Electrophoresis* **23**, 713–718.
- Wheeler, A.R., Moon, H., Bird, C.A., Loo, R.R.O., Kim, C.-J.C.J., Loo, J.A., and Garrell, R.L. (2005). Digital microfluidics with in-line sample purification for proteomics analyses with maldi-ms. *Anal. Chem.* **77**, 534–540.

Fluorescence-activated droplet sorting (FADS): efficient microfluidic cell sorting based on enzymatic activity†

Jean-Christophe Baret,^{‡,a} Oliver J. Miller,^{‡,a} Valerie Taly,^a Michaël Ryckelynck,^a Abdeslam El-Harrak,^a Lucas Frenz,^a Christian Rick,^a Michael L. Samuels,^b J. Brian Hutchison,^b Jeremy J. Agresti,^c Darren R. Link,^b David A. Weitz^c and Andrew D. Griffiths^{*,a}

Received 5th February 2009, Accepted 14th April 2009

First published as an Advance Article on the web 23rd April 2009

DOI: 10.1039/b902504a

We describe a highly efficient microfluidic fluorescence-activated droplet sorter (FADS) combining many of the advantages of microtitre-plate screening and traditional fluorescence-activated cell sorting (FACS). Single cells are compartmentalized in emulsion droplets, which can be sorted using dielectrophoresis in a fluorescence-activated manner (as in FACS) at rates up to 2000 droplets s^{-1} . To validate the system, mixtures of *E. coli* cells, expressing either the reporter enzyme β -galactosidase or an inactive variant, were compartmentalized with a fluorogenic substrate and sorted at rates of ~ 300 droplets s^{-1} . The false positive error rate of the sorter at this throughput was <1 in 10^4 droplets. Analysis of the sorted cells revealed that the primary limit to enrichment was the co-encapsulation of *E. coli* cells, not sorting errors: a theoretical model based on the Poisson distribution accurately predicted the observed enrichment values using the starting cell density (cells per droplet) and the ratio of active to inactive cells. When the cells were encapsulated at low density (~ 1 cell for every 50 droplets), sorting was very efficient and all of the recovered cells were the active strain. In addition, single active droplets were sorted and cells were successfully recovered.

Introduction

The compartmentalization of assays in wells makes microtitre-plates the most flexible and most widely used screening platform in use today. However, reducing assay volumes to below 1–2 μl is problematic¹ and the maximum throughput, even when using sophisticated (and expensive) robotic handling, is little more than 1 s^{-1} . In contrast, fluorescence-activated cell sorting (FACS) is capable of analyzing and sorting cells at a rate of up to 7×10^4 cells s^{-1} .² However, during FACS, cell fluorescence is detected in a continuous aqueous stream³ and the absence of compartmentalization limits the range of activities that can be screened: the fluorescent marker(s) must remain either inside or on the surface of the cells to be sorted. This makes detection of secreted enzymes using fluorogenic substrates impossible. Additionally, if the enzyme is intracellular, then the cell may be impermeable to the substrate or the product may freely diffuse out of the cell. Conventional FACS machines also require typically more than 10^5 cells in the starting population,³ are very expensive and generate aerosols with serious biosafety ramifications.⁴

Microfluidic flow sorting systems have the potential to offer solutions to these problems, enabling the handling of small

numbers of cells in inexpensive, sterile, aerosol-free, disposable devices.^{2,5} Several approaches have already been demonstrated, including devices that sort cells by dielectrophoretic actuation, electrokinetic actuation, hydrodynamic flow-switching and optical forces (listed by Perroud *et al.*).⁶ However, as with conventional FACS, the absence of assay compartmentalization limits their flexibility.

The versatility of conventional FACS can be increased by *in vitro* compartmentalization (IVC)⁷ of assays in emulsion droplets, allowing selection for enzymatic activity.^{8,9} However, the technique has three main limitations: complex double emulsions structures must be generated; the emulsions are highly polydisperse, limiting quantitative analysis; and the capacity to modify the contents of droplets after encapsulation is restricted.¹⁰ These limitations can, however, be overcome by using droplet-based microfluidic systems, which allow the generation of highly monodisperse emulsions¹¹ and the fusion^{12–14} and splitting^{12,15,16} of droplets. It has even been possible to separate or sort droplets by charging them and steering them with an electric field¹⁷ or by exploiting dielectrophoresis,¹⁸ electrocoalescence,¹⁹ localized heating,²⁰ or Rayleigh–Plateau instabilities.²¹ It has not, however, been possible to selectively enrich specific subpopulations of droplets according to their fluorescence until now.

This manuscript describes a highly efficient droplet-based microfluidic FACS, optimized to sort picolitre-range droplets by dielectrophoresis.^{17,18} This fluorescence-activated droplet sorting (FADS) system combines many of the advantages of microtitre-plate screening and fluorescence-activated cell sorting (FACS): assays are compartmentalized in emulsion droplets, which are the functional equivalent of microtitre-plate wells, but can be analyzed and sorted at high speed (as in FACS). Although several techniques for monitoring fluorescent reactions^{22,23} and

^aInstitut de Science et d'Ingénierie Supramoléculaires (ISIS), Université de Strasbourg, CNRS UMR 7006, 8 allée Gaspard Monge, BP 70028, F-67083 Strasbourg Cedex, France. E-mail: griffiths@isis.u-strasbg.fr

^bRainDance Technologies, Inc., 44 Hartwell Avenue, Lexington, MA, 02421, USA

^cDepartment of Physics and School of Engineering and Applied Sciences, Harvard University, Cambridge, USA

† Electronic supplementary information (ESI) available: Model for cellular enrichment by FADS, supplementary Fig. S1–8, Table 1 and Movies S1–6. See DOI: 10.1039/b902504a

‡ These two authors contributed to the work equally.

fluorescent cells²⁴ in droplets have already been described, we report the first system capable of actually sorting droplets according to their fluorescence. This microfluidic system is also the first to be capable of sorting cells according to enzymatic activity. This latter application involves the following steps: (i) encapsulating a mixed population of cells in the droplets of a biocompatible emulsion; (ii) storing the emulsion to allow time for the fluorogenic substrate in each droplet to be turned-over by a cellular enzyme (if present); (iii) sorting the droplets according to fluorescence intensity (substrate turn-over) in a microfluidic sorting device; and (iv) recovering the cells from the sorted droplets. Such facile enrichment of specific cells according to enzymatic activity should provide a boon to fields such as directed evolution, where large libraries are functionally screened.

Results and discussion

Factors affecting sorting

12 pL monodisperse droplets containing 250 μM fluorescein were generated by the microfluidic flow-focusing of an aqueous stream by twin streams of fluorinated oil containing a surfactant¹¹ (Fig. 1a and Movie S1 in the ESI).[†] The surfactant-stabilized droplets were collected in a reservoir (Fig. 1b) and subsequently injected into the microfluidic sorting device where they were spaced-out (Fig. 1c and Movie S2 in the ESI)[†] and sorted at an asymmetric Y-shaped junction (Fig. 1d). The fluorescence of each droplet was measured with a photomultiplier tube (PMT) as it passed through a 488 nm laser line (Fig. 2). Droplets flowed down the wider 'negative' arm of the sorting junction by default due to its lower hydraulic resistance (Fig. 1d). If a particular droplet was chosen for sorting then a pulse of high-voltage alternating current (AC) was applied across the electrodes adjacent to the sorting junction. The resulting electric field deflected the droplet of interest into the narrower 'positive' arm of the junction by dielectrophoresis (Fig. 1d).

The frequency of droplet reinjection was found to correlate with the flow rate of reinjection in a linear fashion, as expected

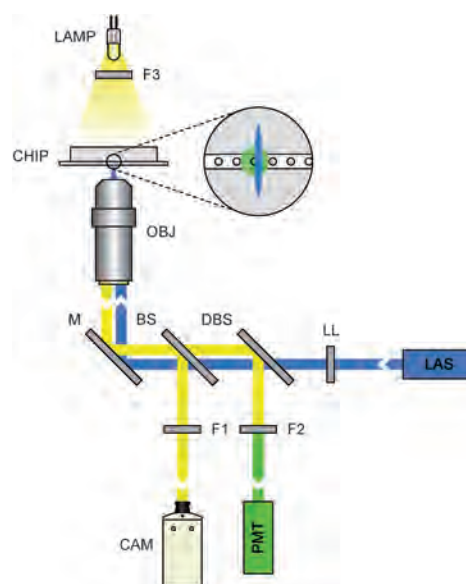


Fig. 2 Schematic representation of the optical setup. Laser light (488 nm) was emitted from the laser (LAS), shaped into a laser line (LL) and transmitted through a multi-edge dichroic beam splitter (DBS) to the microscope. Inside the microscope the laser light passed through a beam splitter (BS) and was reflected up into the objective (OBJ) by a conventional mirror (M). The shaped laser beam was focused to a $\sim 10 \times \sim 150 \mu\text{m}$ line across the sorting channel in the microfluidic chip (CHIP) where it excited droplets one at a time as they flowed past. The fluorescent emission from each droplet passed back along the path of the laser beam, but was reflected by the dichroic beam splitter (DBS) to the sensor of the photomultiplier tube (PMT) via a bandpass filter (F2). Filtered light from the microscope's halogen lamp (LAMP) illuminated the channels and droplets, allowing the trajectories of droplets to be monitored by the high-speed camera (CAM). The filter F3 removed wavelengths of light that were detected by the PMT to avoid a high background signal.

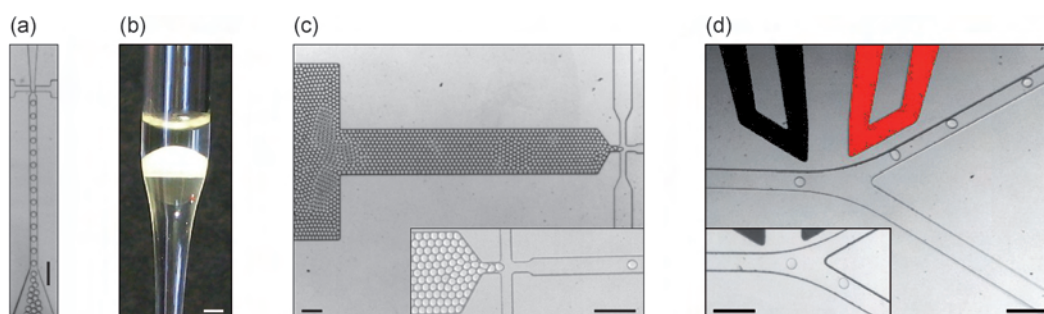


Fig. 1 Generating and sorting droplets triggered on droplet fluorescence. (a) Generation of a monodisperse emulsion by a microfluidic droplet production device. 12 pL aqueous droplets were generated in fluorinated oil containing surfactant by flow-focusing (Movie S1, ESI).[†] (b) Droplets being incubated in a Pasteur pipette. The droplets have floated up to the interface between the fluorinated oil and a layer of LB above. (c) Reinjection of a monodisperse emulsion into the sorting device (Movie S2, ESI).[†] The inset image shows the emulsion droplets being spaced-out with surfactant-free fluorinated oil. (d) Trajectories of droplets stream through the sorting junction. When an AC electric field was applied across the electrodes (1–1.4 kV_{P-P}), the droplets were deflected into the positive arm (Movie S3).[†] In the absence of a field, the droplets flowed into the negative arm owing to the lower hydraulic resistance (inset). The length of the scale-bar in each photograph is 100 μm , except in (b) where it is 1 mm.

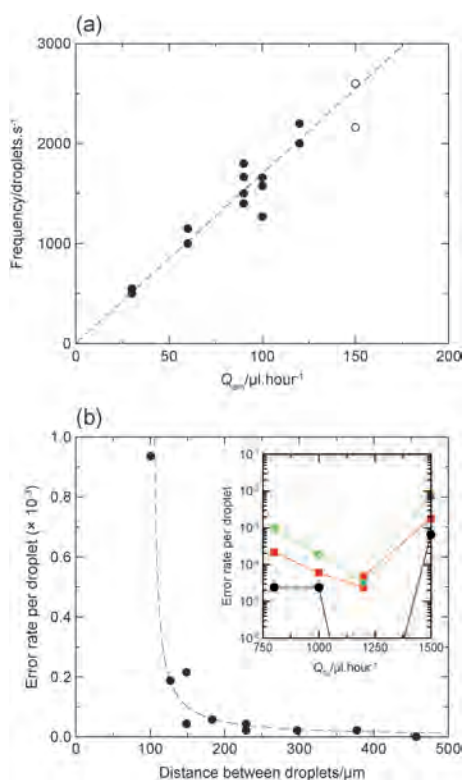


Fig. 3 Limits to the reinjection of 12 pl droplets. (a) The frequency of droplet reinjection was determined solely by the flow rate of the emulsion and was independent of the flow rate of the fluorinated oil. Open circles indicate data points where droplet-breakup was observed. (b) False positive error rate. The flow rate of the fluorinated oil determined the false positive error rate when the droplet reinjection rate was fixed. The lowest error rates were observed when the flow rate of the fluorinated oil was in the range 1–1.25 ml h⁻¹, with no errors at all observed over 1 min at a reinjection rate of ~500 droplets s⁻¹ (inset). The black circles correspond to an emulsion reinjection rate of 30 μl h⁻¹ (~500 droplets s⁻¹), the red squares to 60 μl h⁻¹ (~1000 droplets s⁻¹), the green diamonds to 90 μl h⁻¹ (~1500 droplets s⁻¹) and the blue triangle to 120 μl h⁻¹ (~2000 droplets s⁻¹). The fluorinated oil flow rate controlled the spacing of the droplets and sufficient droplet spacing (>200 μm) minimized the false positive error rate (main graph; the dashed line is a guide for the eye; data for all four reinjection rates are combined, excluding cases where droplet-breakup was observed).

(Fig. 3a). The maximum reinjection rate achieved was 2000 droplets s⁻¹: higher reinjection rates resulted in shearing of the droplets into smaller fragments.

The flow rate of the fluorinated oil did not influence the droplet reinjection frequency, but only the distance between two successive droplets with higher flow rates yielding a greater droplet spacing. Flow rates greater than 1.5 ml h⁻¹ caused the breakup of 12 pl droplets at the reinjection nozzle, creating pairs of droplets of different sizes. The spacing between droplets was found to be an important factor affecting sorting efficiency.

When too close, successive droplets impacted at the sorting junction, causing droplets to flow down the positive arm of the sorting junction in the absence of an electric field ('false positive errors'). False positive error rates were estimated by focusing the laser over the positive arm, counting the number of fluorescent droplets that passed along it over a period of 1 minute and dividing this figure by the number of droplets reinjected per minute. At a given droplet reinjection rate, the false positive error rate was observed to first decrease and then increase again with increasing fluorinated oil flow rate (Fig. 3b). The initial decrease was linked to the increase in droplet spacing, which reduced droplet impacts and favored the correct functioning of the sorter. When correctly spaced, the false positive error rate decreased to below 1 in 10⁴ droplets (1–1.25 ml h⁻¹ for the fluorinated oil flow rate and <60 μl h⁻¹ or <1000 droplets s⁻¹ for the emulsion reinjection rate). Increasing the fluorinated oil flow rate further resulted in an increase in the false positive error rate due to droplet breakup and, hence, emulsion polydispersity. However, it is worth noting that the false positive error rate was always less than 1 in 100 droplets under all conditions studied, even at a reinjection rate of 2000 droplets s⁻¹.

We were able to use electric actuation to deflect single droplets at throughputs up to 2000 droplets s⁻¹. Above this rate, it was not possible to reliably deflect every droplet. Two parameters were found to affect the deflection of droplets by dielectrophoresis: the intensity of the electric field and the time over which it was applied. We found that the field needed to be applied for at least 0.5 ms to successfully pull the droplet into the positive arm of the junction. This fact placed an upper limit on the rate of sorting of 2000 droplets s⁻¹ (1 s/0.5 ms = 2000). This limit could not be overridden by increasing the voltage across the electrodes; indeed, increasing the voltage above 1.8 kV_{p-p} caused tip-streaming of the droplets, resulting in depolarization and a much lower sorting efficiency. The optimum was found to be in the range 1.4–1.6 kV_{p-p}, which was effective at deflecting droplets at a reinjection rate of 2000 droplets s⁻¹ and at all rates below.

Measurement of sorting efficiency

The false positive and false negative error rates of the asymmetric sorting device (Fig. 1d) were accurately determined by image analysis of droplet trajectories during the sorting of a binary emulsion. False positive errors were defined as negative droplets wrongly entering the positive channel, while false negative errors were defined as positive droplets wrongly entering the negative channel.

A 'dual-emulsifier' device (Fig. S1b and Movie S4, ESI)† was used to generate two types of 12 pl droplet in parallel containing fluorescein at either 25 or 100 μM concentration. The binary emulsion was collected and then injected into the sorting device. Two distinct populations of droplets were observed differing in fluorescence by a factor of four, as expected (Fig. 4a and 4b). A minimum threshold for sorting was set between these two populations and the emulsion was sorted for several hours. High-speed movies recorded during this process were analyzed to determine the error rates of the device (Fig. 4c and 4d and Movie S3 in the ESI).† The false positive and false negative error rates while sorting at 300 droplets s⁻¹ were found to be <1 in 10⁴ droplets and ~1 in 1000 droplets, respectively.

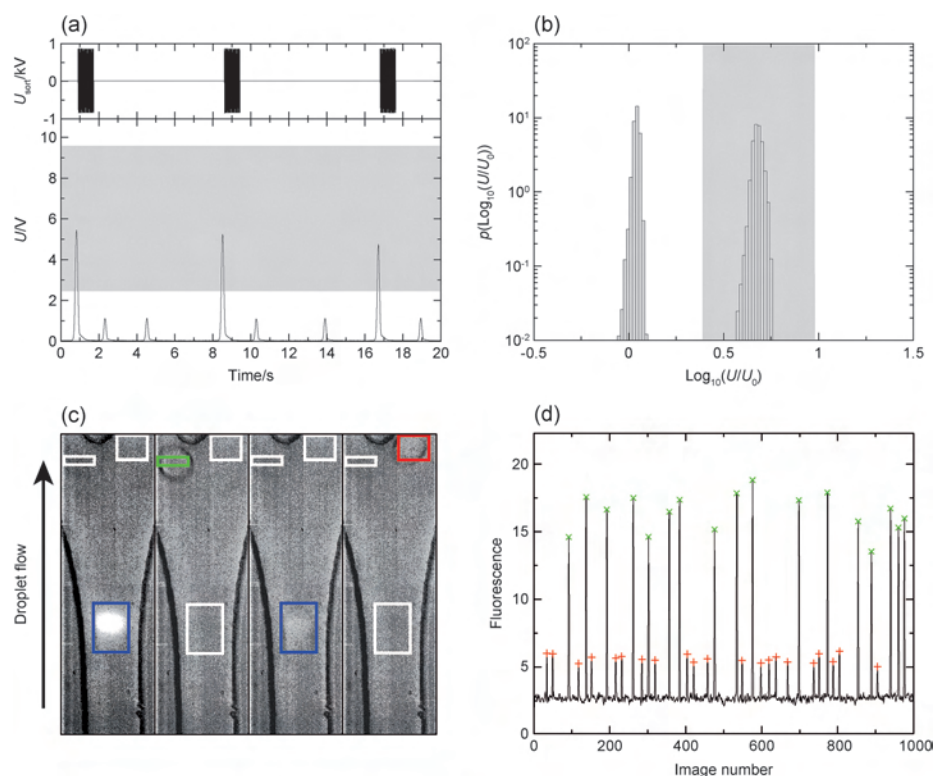


Fig. 4 Measurement of the sorting efficiency. (a) Time sequences of the PMT signal (U ; volts) and the AC pulses applied in response to sorting decisions (U_{sort} ; volts). The field was applied on the falling edge of fluorescent peaks that exceeded the threshold voltage (in gray). U_0 was a reference voltage (1 V). (b) Histograms of the fluorescent signals in a mixed emulsion containing droplets of 25 and 100 μM sodium fluorescein. The two populations of droplets were clearly separated, with the sorting gate (in gray) selecting only the high-fluorescence droplets. (c) Individual frames from the high-speed camera during sorting of the mixed emulsion, processed by MATLAB. In the first frame, the arrival of a highly fluorescent droplet (100 μM fluorescein) at the junction was observed and its fluorescence was determined (blue box). The trajectory of this droplet through the junction was monitored by examining pixel changes in the two arms (second frame). In this case, the droplet was correctly sorted into the positive arm (green box). In the third frame, a low fluorescence droplet (25 μM fluorescein) arrived at the junction and was registered (blue box). The droplet did not trigger the sorting mechanism and correctly flowed down the negative arm of the junction (red box in fourth frame). (d) A plot of the pixel intensity (fluorescence) at the junction entrance over a period of 20 ms (1000 camera frames collected at a frequency of 5 kHz). To verify sorting events, droplets were classified as containing either 25 or 100 μM fluorescein by virtue of their fluorescence at the mouth of the sorting junction. The subsequent trajectory of each droplet through the junction was tracked: droplets ending up in the positive and negative arms of the junction are depicted in the plot with green and red markers, respectively. Comparing the identity of each droplet with its subsequent trajectory allowed the false positive and the false negative error rates for the sorting device to be determined. In total, 1.3×10^5 images (40 gigabytes) were analyzed, corresponding to 10^4 droplets.

Sorting cells in droplets based on enzymatic activity

To determine the efficiency of the sorting device when sorting cells, we used two strains of *E. coli*: one strain expressing the classic reporter gene *lacZ* (encoding β -galactosidase) and the other expressing an inactive, frameshifted variant, ΔlacZ . Mixtures of these cells were emulsified with a fluorogenic β -galactosidase substrate (fluorescein-di- β -D-galactopyranoside; FDG) in 12 pL droplets using a microfluidic device. The emulsions were incubated at 20 $^\circ\text{C}$ for 14 hours (Fig. 1b) to allow time for cell growth and substrate hydrolysis by the enzyme. Following incubation, droplets containing *lacZ* cells were 100-fold more fluorescent than either empty droplets or those

containing ΔlacZ cells (Fig. 5). We sorted the high fluorescence droplets from each emulsion at a rate of 300 droplets s^{-1} (Movie S5, ESI)† and recovered and grew the cells to determine enrichment values.

FACS of live *E. coli* cells is normally precluded by their impermeability to FDG: the integrity of their membranes needs to be compromised for the substrate to come into contact with the cytoplasmic β -galactosidase.²⁵ However, when *E. coli* cells are compartmentalized in droplets, as here, they can be lysed *in situ*, for example using polymyxin B.²⁶ The released β -galactosidase and the fluorescent product (fluorescein) remain in the droplet, allowing identification and, potentially, sorting (Fig. S2, ESI).† Such an approach, however, prevents the recovery of

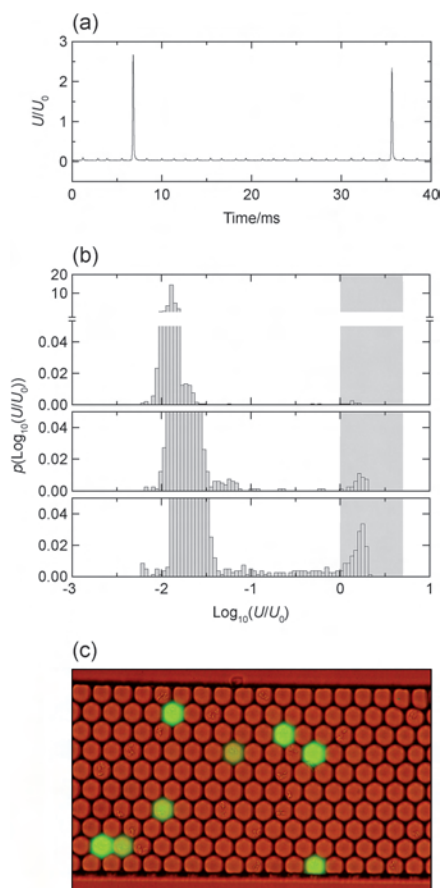


Fig. 5 Detection of β -galactosidase activity in cells in droplets. (a) Time sequence of the fluorescence analysis. Droplets could be analyzed at very high-throughput: up to 10^4 per second. (b) Histograms of the fluorescent signals of droplets in an emulsion containing both *lacZ* and $\Delta lacZ$ bacteria: ϵ_0 was 0.1 and λ was either 0.016 (upper graph), 0.16 (middle graph) or 1.6 (lower graph). In each case the two populations of droplets were separated, with the sorting gate (in gray) selecting only the high-fluorescence (*lacZ*) droplets. U was the signal from the PMT (volts) and U_0 was a reference voltage (1 V). (c) Fluorescence micrograph of droplets containing *lacZ* bacteria in the channel of a microfluidic device. Each droplet functioned as an independent microreactor with 10%–20% of the occupied droplets converting the non-fluorescent substrate FDG to fluorescent fluorescein.

viable cells after sorting and necessitates DNA amplification and retransformation steps. To avoid these steps and, thus, simplify the characterization of the sorting device, we used an alternative strategy. We observed, while examining emulsions containing only *lacZ* bacteria, that even in the absence of a lytic agent 10–20% of the occupied droplets were fluorescent (Fig. 5c and Fig. S2a in the ESI),[†] indicating the presence of one or more lyzed cells in each fluorescent droplet. This allowed us to sort viable *E. coli* based on β -galactosidase activity in a similar

manner to Nir *et al.*, who used FACS to sort small colonies of *E. coli* in agarose microbeads in which only a fraction of the cells were lyzed to catalyze FDG cleavage.²⁵ In both cases, it was the presence of a small clonal population of bacteria in each droplet/microbead that allowed sorting of viable cells: a minority of the population lyzed to expose β -galactosidase activity and the majority remained intact, facilitating recovery (Movie S6, ESI).[†] Approximately 50 viable cells were recovered per droplet, regardless of the fluorescence.

With the low error rate of the sorting device, the main factor expected to affect enrichment was the co-compartmentalization of $\Delta lacZ$ cells with *lacZ* cells. We expected the distribution of cells between droplets during encapsulation to follow the Poisson distribution.^{22,27,28} A model for enrichment was developed based upon the Poisson distribution (ESI).[†] In summary, the theoretical enrichment (η_m) is given by the equation:

$$\eta_m = \frac{1}{1 - e^{\epsilon_0 \lambda / (1 + \epsilon_0)}}$$

where ϵ_0 is the initial ratio of active to inactive cells and λ is the initial mean number of cells per droplet. The enrichment (η) is defined as the ratio of ϵ after sorting (ϵ_1) to ϵ before sorting (ϵ_0) (ESI).[†]

The derivation of this model is fully described in the ESI[†] and a plot of η_m as a function of ϵ_0 and λ is shown in Fig. 6c. The observed value of η (η_{exp}) was predicted to match η_m and, therefore, increase with decreasing ϵ_0 or decreasing λ . It was not expected that η_{exp} would be significantly affected by sorting errors when η_m was less than 10^4 because of the low false positive error rate of the sorting device (<1 in 10^4 droplets).

To test the model, we performed a series of sorts with mixed populations of *lacZ* and $\Delta lacZ$ cells, where we varied both ϵ_0 (0.01–1) and λ (0.016–1.6). For each sort, ϵ_0 was verified and ϵ_1 was determined by plating-out cell suspensions on agar medium containing X-gal and counting blue (*lacZ*) and white ($\Delta lacZ$) colonies (Fig. 6a and Table S1, ESI).[†] Bright-field microscopy was used to measure the proportion of droplets occupied by bacterial colonies and, by extension, λ . The results of the sorts are shown in Fig. 6b and compared to the theoretical enrichments in Fig. 6c. As predicted, η_{exp} was observed to increase with decreasing ϵ_0 or decreasing λ . At low λ (0.021 and 0.016), all the recovered cells were positive (*lacZ*). η_{exp} was found to be always within 5-fold of the predicted η_m value, suggesting that the model was accurate and that the Poisson distribution was indeed the dominant factor in determining enrichment. It is noteworthy that we also succeeded in recovering cells from a single sorted droplet (Fig. S3, ESI).[†]

Conclusions

We have demonstrated a highly efficient microfluidic sorting system that actively sorts droplets based on their fluorescence and used it to sort cells according to the presence or absence of an enzymatic activity. To allow more precise ‘binning’ of bacteria with specific activities, it would be necessary to eliminate membrane impermeability as a factor. For intracellular enzymes, such as β -galactosidase, this could be achieved by lyzing the cells while they are compartmentalized (Fig. S2, ESI);[†] alternatively, the enzyme could be secreted or displayed on the cell surface.

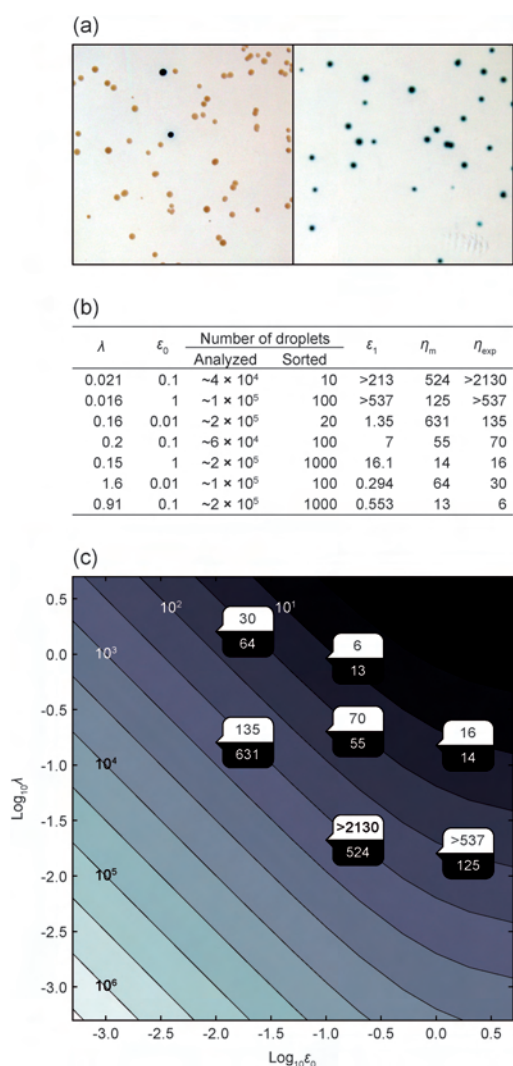


Fig. 6 Enrichment of cells by FADS based on β -galactosidase activity. (a) Photographs of *E. coli* colonies before (left photograph) and after sorting (right photograph) at $\epsilon_0 \approx 0.1$, $\lambda \approx 0.01$ emulsion. The colonies grew on LB agar containing ampicillin, IPTG and X-gal for blue/white screening. The *lacZ* bacteria (blue colonies) were completely purified from the $\Delta lacZ$ bacteria (white colonies) during sorting, resulting in only *lacZ* colonies growing on the agar. (b) Predicted (η_m) and experimentally obtained (η_{exp}) enrichment values after one round of sorting as a function of λ and the starting ratio of active (*lacZ*) to inactive ($\Delta lacZ$) cells (ϵ_0). For 7 combinations of λ and ϵ_0 , sorts were performed and highly fluorescent (*lacZ*) droplets were collected. The initial (ϵ_0) and final (ϵ_1) values for ϵ were determined by blue/white colony screening. (c) A plot of the same data. A split box with a pointed projection at the relevant coordinates is shown for each combination of λ and ϵ_0 . The relevant experimental value for η is shown (upper value; white background) along with the value predicted using the model (lower value; black background).

Indeed, FADS has already been used to sort *Bacillus subtilis* according to the activity of a secreted enzyme (Samuels *et al.*, unpublished) and to sort libraries of horseradish peroxidase displayed on *Sacharomyces cerevisiae* (Agresti *et al.*, unpublished). Beyond bacterial or yeast cells, FADS could be used to sort mammalian cells (which survive in droplets),^{22,28} viruses or even single genes expressed *in vitro*.²³

FADS has several other merits: setup time is short (<10 minutes per sample), reagent volumes are minimal (12 μ l of aqueous phase generates 10^6 droplets), aerosols are not generated and very small numbers of cells (≥ 3000) can be handled (Fig. S3, ESI).[†] The inverse correlation observed between error rate and throughput suggests that the system can be operated in different modes (as in FACS). When a high λ is used, co-compartmentalization events are frequent (26.4% when $\lambda = 1$), so a false positive error rate of 1 in 100 droplets is acceptable and high throughputs can be used (~ 2000 droplets s^{-1} or ~ 2000 cells s^{-1}): sorting errors would not significantly affect enrichment until $\epsilon_0 \leq 0.01$, at which point enrichment would plateau at ~ 100 -fold (Fig. 6c). In contrast to this ‘enrichment’ mode, FADS can also be performed in ‘purification’ mode by using lower λ values and lower throughputs, thereby reducing error rates and allowing cells to be sorted to high purities. Theoretically, enrichment values at any speed could be improved by rejecting droplets containing co-compartmentalized negative cells while sorting (as in FACS) or by exploiting self-organizational behavior of cells during compartmentalization to eliminate the Poisson distribution itself.²⁹

It is worth noting that by integrating the sorting device with modules for droplet splitting^{12,15,16} and/or fusion^{12–14} within the same chip, it should be possible to perform sophisticated assays involving high-speed manipulations that are currently impossible with existing technologies. Such tools would be enormously useful to fields such as directed evolution and proteomics.

Experimental

Materials

All materials were obtained from Sigma-Aldrich Co. unless otherwise stated.

Microfluidic devices

Each microfluidic device was prepared from poly-(dimethylsiloxane) (PDMS) by standard soft-lithography techniques.³⁰ A mould of SU-8 resist (MicroChem Corp.) was fabricated on a silicon wafer (Siltronix) by UV exposure (MJB3 contact mask aligner; SUSS MicroTec) through a photolithography mask (Fig. S1; Selba SA) and subsequent development (SU-8 developer; MicroChem Corp.). A curing agent was added to the PDMS base (Sylgard 184 silicone elastomer kit; Dow Corning Corporation) to a final concentration of 10% (w/w), mixed and poured over the mould to a depth of 5 mm. Following degassing for several minutes and cross-linking at 65 °C for several hours, the PDMS was peeled off the mould and the input and output ports were punched with a 0.75 mm-diameter Harris Uni-Core biopsy punch (Electron Microscopy Sciences). Particles of PDMS were cleared from the ports using pressurized nitrogen gas. The structured side of the PDMS slab was bonded

to a $76 \times 26 \times 1$ mm glass microscope slide (Paul Marienfeld GmbH & Co. KG) by exposing both parts to an oxygen plasma (PlasmaPrep 2 plasma oven; GaLa Instrumente GmbH) and pressing them together. Finally, an additional hydrophobic surface coating was applied to the microfluidic channel walls by injecting the completed device with Aquapel glass treatment (PPG Industries) and then purging the liquid with nitrogen gas.

If necessary, electrodes were included in the microfluidic device as additional microfluidic channels, which were filled with metal: the device was heated to 85°C and a 51In/32.5Bi/16.5Sn low-temperature solder (Indium Corporation) was melted inside the electrode channels.³¹ Electrical connections with the solder electrodes were made with short pieces of electrical wire (Radiospares).

The FADS system itself was composed of several modules. Firstly, an emulsification device was used to generate the droplets by flow-focusing an aqueous stream with two streams of fluorinated oil containing a surfactant¹¹ (Fig. 1a). Emulsification devices for generating a single type of droplet ('single emulsifiers') (Fig. S1a, ESI)[†] were fabricated with a channel depth of 25 μm microns and devices for generating two emulsions simultaneously ('dual emulsifiers') (Fig. S1b, ESI)[†] were fabricated with a channel depth of 21 μm . Single emulsifiers were used to emulsify bacterial cells while dual emulsifiers were used to generate mixed emulsions for analyzing sorting efficiency. The second device was a droplet reservoir consisting of either a syringe (no gas-exchange) or an open-topped Pasteur pipette (for gas exchange) (Fig. 1b). The final module was a sorting device (Fig. S1c, ESI)[†] in which droplets were reloaded, spaced-out with fluorinated oil at a flow-focusing junction (Fig. 1c) and finally sorted at a Y-junction, triggering on droplet fluorescence (Fig. 1d). Sorting devices were fabricated with a channel depth of 21 μm .

Optical setup, data acquisition and control system

The optical setup (Fig. 2) consisted of an Axiovert 200 inverted microscope (Carl Zeiss SAS) mounted on a vibration-dampening platform (Thorlabs GmbH). A 20 mW, 488 nm solid-state laser (LAS; Newport-Spectraphysics) was mounted on the platform *via* a heatsink (Newport-Spectraphysics). The laser beam was shaped into a $\sim 10 \times \sim 150$ μm line by a combination of a 25 mm-diameter cylindrical lens (effective focal length: -50 mm; Thorlabs GmbH) and a 25 mm-diameter plano-convex lens (effective focal length: 25 mm; Thorlabs GmbH) with a 5 cm distance between them (LL). The shaped beam was guided to the side camera port of the microscope *via* a series of periscope assemblies (Thorlabs GmbH). Inside the microscope, the laser light was reflected up into a LD Plan Neofluar $40\times/0.6$ microscope objective (OBJ; Carl Zeiss SAS) and focused across a channel within the microfluidic device (CHIP). A Phantom v4.2 high-speed digital camera (CAM; Vision Research) was mounted on the top camera port of the microscope to capture digital images during droplet production and sorting. A 488 nm notch filter (F1; Semrock Inc.) positioned in front of the camera protected the camera's sensor from reflected laser light. Light emitted from fluorescing droplets was captured by the objective and channeled back along the path of the laser into the system of periscope assemblies. The emitted light was separated from the laser beam

by a 488/532/638 nm-wavelength transmitting dichroic beam splitter (DBS; Semrock Inc.), passed through a 510 nm bandpass filter (F2; 20 nm bandwidth; Semrock Inc.) and collected in an H5784-20 photomultiplier tube (PMT; Hamamatsu Photonics KK). Data acquisition (DAQ) and control was performed by a PCI-7831R Multifunction Intelligent DAQ card (National Instruments Corporation) executing a program written in LabView 8.2 (National Instruments Corporation). The data acquisition rate for the system was 100 kHz. To sort a particular droplet, the DAQ card provided a signal to a Model 623B high-voltage amplifier (Trek Inc.), connected to the electrodes of the microfluidic device. Liquids were pumped into the microfluidic device using standard-pressure infusion-only PHD 22/2000 syringe pumps (Harvard Apparatus Inc.). Syringes were connected to the microfluidic device using 0.6×25 mm Neolus needles (Terumo Corporation) and PTFE tubing with an internal diameter of 0.56 mm and an external diameter of 1.07 mm (Fisher Bioblock Scientific).

Factors affecting sorting

A solution of 250 μM sodium fluorescein was prepared in a 50 mM Tris-HCl buffer pH 7. The solution was loaded into an Omnifix-F 1 ml disposable syringe (B. Braun Medical AG) and pumped into a single-emulsifier microfluidic device (Fig. S1a, ESI)[†] at a rate of $200 \mu\text{l h}^{-1}$. The fluorinated oil FC-40 (3M), containing 2.5% (w/w) Krytox-DMP surfactant,²² was pumped into the device from a 5 ml Injekt disposable syringe (B. Braun Medical AG) at a rate of 1 ml h^{-1} . The stream of fluorescein was flow-focused between two streams of fluorinated oil/surfactant mixture, yielding droplets of 12 pl (28 μm in diameter when spherical) at a rate of ~ 4000 droplets s^{-1} (Movie S1, ESI)[†]. Approximately 500 μl of emulsion were collected in an Omnifix-F 1 ml syringe with its plunger in place.

Next, the collected droplets were injected into the sorting device (Fig. S1c, ESI)[†] spaced-out with surfactant-free fluorinated oil (Movie S2, ESI)[†] and analyzed by the optical setup as they flowed into the sorting junction. Individual droplets were sorted by applying a square-wave pulse to the high-voltage amplifier, which amplified the voltage 1000-fold.

The following factors were observed to affect sorting: Q_{em} , the flow rate of the reinjected emulsion; Q_{flu} , the flow rate of the fluorinated oil for spacing-out the droplets; τ_{sort} , the duration of the sorting pulse; and U_{sort} , the peak-to-peak voltage applied across the electrodes.

Measurement of sorting efficiency

Image analysis was used to accurately define the error rates of the device when sorting droplets at the throughput chosen for sorting cells (300 droplets s^{-1}).

Two solutions of sodium fluorescein were prepared in a 50 mM Tris-HCl buffer pH 7: 25 and 100 μM . 12 pl droplets of each solution were generated simultaneously using a dual-emulsifier microfluidic device (Fig. S1b, ESI)[†].

The droplets in the mixed emulsion were injected into the device (300 droplet s^{-1}) and sorted as a function of fluorescence to select only those droplets containing 100 μM sodium fluorescein. The parameters for sorting were: $Q_{\text{em}} = 15\text{--}50 \mu\text{l h}^{-1}$,

$Q_{\text{flu}} = 0.8\text{--}1.2\text{ ml h}^{-1}$, F (the frequency of the sorting pulse) = 30 kHz, $\tau_{\text{sort}} = 0.4\text{--}1\text{ ms}$ and $U_{\text{sort}} = 1\text{--}1.4\text{ kV}_{\text{p-p}}$. These parameters were fine-tuned before each sort to ensure that droplets were correctly sorted and that no droplets flowed down the ‘positive’ arm of the sorting junction when the electric field was not applied. This fine-tuning was required because of slight variations in channel depth between devices, the distance of the electrodes from the sorting channel, the average droplet volume in the emulsion and unintended variations in the pumping rates from the syringe pumps.

The high-speed camera was triggered after sorting each droplet, allowing the operator to ensure that sorted droplets were being directed down the correct arm of the sorting junction. $\Delta\tau_{\text{cam}}$, the delay between the falling edge of the peak in fluorescence and the trigger pulse sent to the high-speed camera, was $\sim 800\text{ }\mu\text{s}$.

To determine the efficiency of sorting a MATLAB script (The MathWorks Inc.) was used to analyze individual frames from the high-speed camera. The principle of the analysis was to first determine the light intensity of the laser line as a droplet flowed past: this intensity correlated with the concentration of fluorescein in the droplet. Subsequent frames followed the trajectory of the droplet through the sorting junction as it was either sorted or not. By measuring the pixel intensities in each arm of the sorter, it was possible to determine whether the droplet ended up in the correct arm of the sorter. This method enabled us to analyze the sorting of $\sim 10^4$ droplets.

E. coli strains and preparation of cell suspensions

Standard molecular biology protocols were used to transform *E. coli* T7 Express cells (New England Biolabs Inc.) with the plasmids pVEX2.2EM-*lacZ* (encoding β -galactosidase) and pVEX2.2EM- Δ *lacZ* (encoding a frameshifted, inactive mutant of β -galactosidase).⁹ 5 ml aliquots of LB containing $100\text{ }\mu\text{g ml}^{-1}$ ampicillin were inoculated with single colonies of the resulting strains. These aliquots were grown for 14 hours at $37\text{ }^\circ\text{C}$ with a 230 rpm shaking. The following day, fresh 5 ml aliquots of LB containing ampicillin were inoculated with $50\text{ }\mu\text{l}$ of each overnight culture and grown under the same conditions to mid-log phase (an OD_{600} of 0.3–0.4). The growing cultures were rediluted 100-fold into LB containing ampicillin and 1 mM isopropyl β -D-1-thiogalactopyranoside (IPTG) to induce expression of either β -galactosidase or the inactive variant. After 3 hours, the cells in each induction culture were harvested (at an OD_{600} of 0.5–0.6) by centrifuging at $3000 \times g$ for 5 minutes at $4\text{ }^\circ\text{C}$. The supernatant was removed and the cell pellet was resuspended with 5 ml of ice-cold LB containing ampicillin. This washing step was repeated two further times to remove free enzyme from the cultures and, thus, lower the amount of background activity. The optical density of each resuspended culture was adjusted to an OD_{600} of 0.45. The cell suspensions were mixed together in the appropriate ratio for each experiment and diluted if necessary. The ratio was confirmed for each experiment by diluting an aliquot of the suspension to an OD_{600} of 4.5×10^{-5} and plating $50\text{--}100\text{ }\mu\text{l}$ on an imMedia Blue Amp agar plate (Invitrogen Corporation), containing ampicillin, IPTG and 5-bromo-4-chloro-3-indolyl- β -D-galactopyranoside (X-gal). Plates were incubated at $37\text{ }^\circ\text{C}$ for 14 hours, $4\text{ }^\circ\text{C}$ for 24 hours (to develop the color of the blue colonies) and digitally imaged.

Emulsification of cell suspensions on-chip

Each cell suspension was emulsified in HFE-7500 fluorinated oil (3M, St. Paul, Minnesota, USA) containing 2% (w/w) EA surfactant (RainDance Technologies, Lexington, MA, USA), which is a PEG–PFPE amphiphilic block copolymer.³² The cell suspension was loaded into a $250\text{ }\mu\text{l}$ gas-tight syringe (Hamilton Company) and pumped into the emulsification device (Fig. S1a, ESI)† at a rate of $100\text{ }\mu\text{l h}^{-1}$. A solution of LB containing ampicillin, $100\text{ }\mu\text{M}$ FDG (Euromedex) and $1\text{ }\mu\text{M}$ sodium fluorescein, was loaded into another syringe and pumped in at the same rate. These streams combined just before the nozzle of the device and were flow-focused by two streams of the fluorinated oil/surfactant mixture flowing at $1\text{--}1.15\text{ ml h}^{-1}$ from a 1 ml gas-tight syringe. The aqueous stream broke up into a series of 12 pl droplets at a rate of $\sim 4600\text{ droplets s}^{-1}$. The generated emulsion flowed off-chip through a 20 cm-length of Intramedic poly(ethylene terephthalate) (PET) PE 20 tubing (Becton, Dickinson and Company) to a glass Pasteur pipette containing $100\text{ }\mu\text{l}$ of LB with ampicillin (Fig. 1b). The emulsion was collected underneath the less-dense LB for 12 minutes, yielding a total volume of $40\text{ }\mu\text{l}$. The PET tubing was sealed and the pipette was incubated at $20\text{ }^\circ\text{C}$ for 12 hours. The layer of LB above the emulsion was necessary to prevent evaporation and coalescence, but still allow gas exchange with the atmosphere. Gas exchange was essential for the proliferation of cells in each droplet and the subsequent detection of β -galactosidase activity.

λ was determined for each emulsion following incubation by bright-field microscopy. The cells inside occupied droplets proliferated into small clonal populations (‘colonies’) overnight, which could be counted (Movie S6, ESI).† λ was found using the equation:

$$\lambda = -\ln(1 - k)$$

where k is the fraction of droplets occupied by colonies.

Sorting cells in droplets based on enzymatic activity

Excess fluorinated oil beneath the emulsion was drained and discarded. A 40 cm-length of Intramedic PET tubing was connected with a $0.4 \times 16\text{ mm}$ Neolus needle (Terumo Corporation) to a Omnifix-F 1 ml syringe previously filled with ddH_2O . The tubing was primed with the ddH_2O and connected to the Pasteur pipette using a PDMS connector block. A standard-pressure infuse/withdraw PHD 22/2000 syringe pump (Harvard Apparatus Inc.) was used to displace the plunger in the syringe and load the emulsion into the tubing at a rate of $200\text{ }\mu\text{l h}^{-1}$. After loading, the direction of flow was reversed and adjusted to $100\text{ }\mu\text{l h}^{-1}$. The tubing was connected to the sorting device (Fig. S1c, ESI).† Surfactant-free fluorinated oil was pumped into the device at a rate of 1 ml h^{-1} to space out the droplets in the sorting channel. When the system had stabilized, the flow rate of the reinjected emulsion was reduced to $20\text{ }\mu\text{l h}^{-1}$. The droplets were analyzed by the optical setup and highly fluorescent droplets were sorted (Movie S5, ESI).† Sorted droplets were collected in a ‘collection loop’ consisting of a coiled 25 cm length of PTFE tubing. Owing to the lower density of the droplets compared to the surrounding fluorinated oil, the droplets accumulated at the highest point in the loop. It was possible to trap even single droplets by this approach (Fig. S3, ESI).†

Recovery of cells from sorted droplets

Following a sort, droplets were recovered from the collection loop by sealing the end of the loop, severing it at about 2 cm distance from the chip and draining it into a 1.5 ml microcentrifuge tube (Axygen Inc.). To dislodge any droplets remaining in the loop, it was flushed with a 30 μ l plug of Droplet Destabilizer (RainDance Technologies, Lexington, MA, USA) followed by 200 μ l of LB containing ampicillin (using a syringe). The emulsion was completely broken by vortexing the microcentrifuge tube in a vigorous manner for 30 s. The broken emulsion was then briefly centrifuged ($1000 \times g$ for 3 s) and 150 μ l of the supernatant—consisting of LB and *E. coli* cells in suspension—were transferred to a new microcentrifuge tube. A fraction of this suspension was plated on imMedia Amp Blue agar plates, equivalent to 10 droplets (resulting in ~500 colonies). This procedure was not modified when recovering single droplets.

Acknowledgements

J.-C. B. was supported by a European Molecular Biology Organization long-term fellowship. O. J. M. was supported by the Medical Research Council (UK), the Ministry of Defence (UK) and the Human Frontier Science Program (HFSP). AE-H was supported by the European Commission Framework Programme 6 (EC FP6) MiFem Network. L. F. was supported by the EC FP6 Marie Curie Research Training Network, ProSA. J. J. A. and D. A. W. were supported by the NSF (DMR-0602684 and DBI-0649865) and the Harvard MRSEC (DMR-0820484). This work was also supported by the Ministère de l'Enseignement Supérieur et de la Recherche, Centre National de la Recherche Scientifique (CNRS), Agence National de la Recherche (ANR) (ANR-05-BLAN-0397) and the Fondation d'entreprise EADS.

References

- 1 L. M. Mayr and P. Fuerst, The future of high-throughput screening, *J. Biomol. Screen.*, 2008, **13**, 443–448.
- 2 M. Eisenstein, Cell sorting: divide and conquer, *Nature*, 2006, **441**, 1179–1185.
- 3 H. M. Shapiro, *Practical flow cytometry*. Wiley–Liss, New York, 2003.
- 4 I. Schmid, C. Lambert, D. Ambrozak, G. E. Marti, D. M. Moss and S. P. Peretto, International society for analytical cytology biosafety standard for sorting of unfixed cells, *Cytometry A*, 2007, **7**, 414–437.
- 5 V. Kiermer, FACS-on-a-chip, *Nat. Methods*, 2005, **2**, 91.
- 6 T. D. Perroud, J. N. Kaiser, J. C. Sy, T. W. Lane, C. S. Branda, A. K. Singh and K. D. Patel, Microfluidic-based cell sorting of *Francisella tularensis* infected macrophages using optical forces, *Anal. Chem.*, 2008, **80**, 6365–6372.
- 7 D. S. Tawfik and A. D. Griffiths, Man-made cell-like compartments for molecular evolution, *Nat. Biotechnol.*, 1998, **16**, 652–656.
- 8 A. Aharoni, G. Amitai, K. Bernath, S. Magdassi and D. S. Tawfik, High-throughput screening of enzyme libraries: thiolactonases evolved by fluorescence-activated sorting of single cells in emulsion compartments, *Chem. Biol.*, 2005, **12**, 1281–1289.
- 9 E. Mastrobattista, V. Taly, E. Chanudet, P. Treacy, B. T. Kelly and A. D. Griffiths, High-throughput screening of enzyme libraries: in vitro evolution of a beta-galactosidase by fluorescence-activated sorting of double emulsions, *Chem. Biol.*, 2005, **12**, 1291–1300.
- 10 A. D. Griffiths and D. S. Tawfik, Miniaturising the laboratory in emulsion droplets, *Trends Biotechnol.*, 2006, **24**, 395–402.
- 11 S. Anna, N. Bontoux and H. Stone, Formation of dispersions using “flow focusing” in microchannels, *Appl. Phys. Lett.*, 2003, **82**, 364–366.
- 12 H. Song, J. Tice and R. Ismagilov, A microfluidic system for controlling reaction networks in time, *Angew. Chem., Int. Ed.*, 2003, **42**, 768–772.
- 13 K. Ahn, J. Agresti, H. Chong, M. Marquez and D. Weitz, Electrocoalescence of drops synchronized by size-dependent flow in microfluidic channels, *Appl. Phys. Lett.*, 2006, **88**, 264105.
- 14 C. Priest, S. Herminghaus and R. Seemann, Controlled electrocoalescence in microfluidics: Targeting a single lamella, *Appl. Phys. Lett.*, 2006, **89**, 134101.
- 15 D. Link, S. Anna, D. Weitz and H. Stone, Geometrically mediated breakup of drops in microfluidic devices, *Phys. Rev. Lett.*, 2004, **92**, 054503.
- 16 L. Ménétrier-Deremble and P. Tabeling, Droplet breakup in microfluidic junctions of arbitrary angles, *Phys. Rev. E Stat. Nonlin. Soft Matter Phys.*, 2006, **74**, 035303.
- 17 D. R. Link, E. Grasland-Mongrain, A. Duri, F. Sarrazin, Z. Cheng, G. Cristobal, M. Marquez and D. A. Weitz, Electric control of droplets in microfluidic devices, *Angew. Chem., Int. Ed.*, 2006, **45**, 2556–2560.
- 18 K. Ahn, C. Kerbage, T. Hunt, R. Westervelt, D. Link and D. Weitz, Dielectrophoretic manipulation of drops for high-speed microfluidic sorting devices, *Appl. Phys. Lett.*, 2006, **88**, 024104.
- 19 L. M. Fidalgo, G. Whyte, D. Bratton, C. F. Kaminski, F. Clemens, C. Abell and W. T. S. Huck, From microdroplets to microfluidics: selective emulsion separation in microfluidic devices, *Angew. Chem., Int. Ed.*, 2008, **47**, 2042–2045.
- 20 C. N. Baroud, J.-P. Delville, F. Gallaire and R. Wunenburger, Thermocapillaryvalve for droplet production and sorting, *Phys. Rev. E Stat. Nonlin. Soft Matter Phys.*, 2007, **75**, 046302.
- 21 M. Chabert and J.-L. Viovy, Microfluidic high-throughput encapsulation and hydrodynamic self-sorting of single cells, *Proc. Natl. Acad. Sci. U. S. A.*, 2008, **105**, 3191–3196.
- 22 J. Clausell-Tormos, D. Lieber, J. C. Baret, A. El-Harrak, O. J. Miller, L. Frenz, J. Blouwolf, K. J. Humphry, S. Köster, H. Duan, C. Holtze, D. A. Weitz, A. D. Griffiths and C. A. Merten, Droplet-based microfluidic platforms for the encapsulation and screening of mammalian cells and multicellular organisms, *Chem. Biol.*, 2008, **15**, 427–437.
- 23 F. Courtois, L. F. Olguin, G. Whyte, D. Bratton, W. T. S. Huck, C. Abell and F. Hollfelder, An integrated device for monitoring time-dependent in vitro expression from single genes in picolitre droplets, *Chembiochem.*, 2008, **9**, 439–446.
- 24 A. Huebner, M. Srisa-Art, D. Holt, C. Abell, F. Hollfelder, A. J. deMello and J. B. Edel, Quantitative detection of protein expression in single cells using droplet microfluidics, *Chem. Commun.*, 2007, 1218–1220.
- 25 R. Nir, Y. Yisraeli, R. Lamed and E. Sahar, Flow cytometry sorting of viable bacteria and yeasts according to beta-galactosidase activity, *Appl. Environ. Microbiol.*, 1990, **56**, 3861–3866.
- 26 D. R. Storm, K. S. Rosenthal and P. E. Swanson, Polymyxin and related peptide antibiotics, *Annu. Rev. Biochem.*, 1977, **46**, 723–763.
- 27 R. G. Ashcroft and P. A. Lopez, Commercial high speed machines open new opportunities in high throughput flow cytometry (htfc), *J. Immunol. Methods*, 2000, **243**, 13–24.
- 28 S. Köster, F. E. Angilè, H. Duan, J. J. Agresti, A. Wintner, C. Schmitz, A. C. Rowat, C. A. Merten, D. Pisignano, A. D. Griffiths and D. A. Weitz, Drop-based microfluidic devices for encapsulation of single cells, *Lab Chip*, 2008, **8**, 1110–1115.
- 29 J. F. Edd, D. Di Carlo, K. J. Humphry, S. Köster, D. Irimia, D. A. Weitz and M. Toner, Controlled encapsulation of single-cells into monodisperse picolitre drops, *Lab Chip*, 2008, **8**, 1262–1264.
- 30 D. C. Duffy, J. C. McDonald, O. J. A. Schueller and G. M. Whitesides, Rapid prototyping of microfluidic systems in poly(dimethylsiloxane), *Anal. Chem.*, 1998, **70**, 4974–4984.
- 31 A. C. Siegel, D. A. Bruzewicz, D. B. Weibel and G. M. Whitesides, Microsolidics: Fabrication of three-dimensional metallic microstructures in poly(dimethylsiloxane), *Adv. Mater.*, 2007, **19**, 727–733.
- 32 C. Holtze, A. C. Rowat, J. J. Agresti, J. B. Hutchison, F. E. Angilè, C. H. J. Schmitz, S. Köster, H. Duan, K. J. Humphry, R. A. Scanga, J. S. Johnson, D. Pisignano and D. A. Weitz, Biocompatible surfactants for water-in-fluorocarbon emulsions, *Lab Chip*, 2008, **8**, 1632–1639.

Anal. Chem. **2009**, *81*, 4813–4821

Droplet-Based Microfluidic Systems for High-Throughput Single DNA Molecule Isothermal Amplification and Analysis

Linaz Mazutis,[†] Ali Fallah Araghi,[†] Oliver J. Miller,[†] Jean-Christophe Baret,[†] Lucas Frenz,[†] Agnes Janoshazi,^{†,‡} Valérie Taly,[†] Benjamin J. Miller,[‡] J. Brian Hutchison,[‡] Darren Link,[‡] Andrew D. Griffiths,^{†,*} and Michael Ryckelynck^{†,*}

Institut de Science et d'Ingénierie Supramoléculaire (ISIS), Université de Strasbourg, CNRS UMR 7006, 8 allée Gaspard Monge, 67083 Strasbourg Cedex, France, RainDance Technologies, Inc., 44 Hartwell Avenue, Lexington, Massachusetts 02421, Institut de Génétique et de Biologie Moléculaire et Cellulaire (IGBMC), Université de Strasbourg, CNRS UMR 7104, 1 rue Laurent Fries, 67404 Illkirch Cedex, France

We have developed a method for high-throughput isothermal amplification of single DNA molecules in a droplet-based microfluidic system. DNA amplification in droplets was analyzed using an intercalating fluorochrome, allowing fast and accurate “digital” quantification of the template DNA based on the Poisson distribution of DNA molecules in droplets. The clonal amplified DNA in each 2 pL droplet was further analyzed by measuring the enzymatic activity of the encoded proteins after fusion with a 15 pL droplet containing an *in vitro* translation system.

Digital PCR is based on the Poisson distribution of DNA molecules in microtiter plate wells (eq 1; in which $P(X = k)$ is the probability to have k DNA molecules per well, and λ is the mean number of DNA molecules per well).

$$P(X = k) = \frac{e^{-\lambda} \lambda^k}{k!} \quad (1)$$

At low λ (<0.3), the vast majority of wells contain no more than a single DNA molecule, and fitting the number of PCR competent wells to eq 1 allows the DNA concentration to be calculated. Digital PCR is used, for example, to detect low concentrations of mutations associated with colorectal cancer for diagnosis.¹ However, the large number of reactions required results in high reagent costs. Reaction volumes have been reduced by ~1000-fold (down to tens of nanolitres) using microfluidic systems by performing PCRs separated spatially in continuous flow^{2,3} or within compartments defined by elastomeric valves.⁴ However, single

DNA molecules can also be compartmentalized in microdroplets in water-in-oil emulsions,⁵ which act as microreactors with volumes down to 1 fL.⁶ Digital PCR in emulsions (emulsion PCR) is already used to quantify rare mutations using BEAMing⁷ and to prepare the template for two commercialized “next-generation” DNA sequencing systems.⁸

Direct, quantitative screening using emulsion PCR is, however, compromised by the polydispersity of bulk emulsions. Furthermore, it is difficult to add reagents to droplets after they are formed,⁶ which limits the range of assays that can be performed on the amplified DNA. However, both of these problems can potentially be overcome using droplet-based microfluidic systems that allow the production of highly monodisperse droplets⁹ and pairwise droplet electrocoalescence.^{10–14}

Digital PCR has previously been used to quantify DNA in droplets in microfluidic systems.^{15–18} This manuscript, however, describes the digital quantification of DNA using a droplet-based microfluidic system and isothermal “hyperbranched rolling circle

* To whom correspondence should be addressed. (A.D.G.) Phone: +33 (0)390 245 171. Fax: +33 (0)390 245 115. E-mail: griffiths@isis.u-strasbg.fr. (M.R.) Phone: +33 (0)390 245 217. Fax: +33 (0)390 245 115. m.ryckelynck@isis.u-strasbg.fr.

[†] Institut de Science et d'Ingénierie Supramoléculaire.

[‡] RainDance Technologies.

[‡] Institut de Génétique et de Biologie Moléculaire et Cellulaire.

(1) Vogelstein, B.; Kinzler, K. W. *Proc. Natl. Acad. Sci. U.S.A.* **1999**, *96*, 9236–9241.

(2) Li, H.; Xue, G.; Yeung, E. S. *Anal. Chem.* **2001**, *73*, 1537–1543.

(3) Dettloff, R.; Yang, E.; Rulison, A.; Chow, A.; Farinas, J. *Anal. Chem.* **2008**, *80*, 4208–4213.

(4) Ottesen, E. A.; Hong, J. W.; Quake, S. R.; Leadbetter, J. R. *Science* **2006**, *314*, 1464–1467.

(5) Tawfik, D. S.; Griffiths, A. D. *Nat. Biotechnol.* **1998**, *16*, 652–656.

(6) Griffiths, A. D.; Tawfik, D. S. *Trends Biotechnol.* **2006**, *24*, 395–402.

(7) Dressman, D.; Yan, H.; Traverso, G.; Kinzler, K. W.; Vogelstein, B. *Proc. Natl. Acad. Sci. U.S.A.* **2003**, *100*, 8817–8822.

(8) Mardis, E. R. *Annu. Rev. Genomics Hum. Genet.* **2008**, *9*, 387–402.

(9) Christopher, G. F.; Anna, S. L. *J. Phys. D: Appl. Phys.* **2007**, *40*, R319–R336.

(10) Chabert, M.; Dorfman, K. D.; Viovy, J. L. *Electrophoresis* **2005**, *26*, 3706–3715.

(11) Ahn, K.; Agresti, J.; Chong, H.; Marquez, M.; Weitz, D. A. *Appl. Phys. Lett.* **2006**, *88*, 264105.

(12) Link, D.; Grasland-Mongrain, E.; Duri, A.; Sarrazin, F.; Cheng, Z.; Cristobal, G.; Marquez, M.; Weitz, D. *Angew. Chem., Int. Ed.* **2006**, *45*, 2556–2560.

(13) Priest, C.; Herminghaus, S.; Seemann, R. *Appl. Phys. Lett.* **2006**, *89*, 134101.

(14) Frenz, L.; El Harrak, A.; Pauly, M.; Begin-Colin, S.; Griffiths, A.; Baret, J. C. *Angew. Chem., Int. Ed.* **2008**, *47*, 6817–6820.

(15) Beer, N. R.; Hindson, B. J.; Wheeler, E. K.; Hall, S. B.; Rose, K. A.; Kennedy, I. M.; Colston, B. W. *Anal. Chem.* **2007**, *79*, 8471–8475.

(16) Beer, N. R.; Wheeler, E. K.; Lee-Houghton, L.; Watkins, N.; Nasarabadi, S.; Hebert, N.; Leung, P.; Arnold, D. W.; Bailey, C. G.; Colston, B. W. *Anal. Chem.* **2008**, *80*, 1854–1858.

(17) Kiss, M. M.; Ortoleva-Donnelly, L.; Beer, N. R.; Warner, J.; Bailey, C. G.; Colston, B. W.; Rothberg, J. M.; Link, D. R.; Leamon, J. H. *Anal. Chem.* **2008**, *80*, 8975–8981.

(18) Schaeferli, Y.; Wootton, R. C.; Robinson, T.; Stein, V.; Dunsby, C.; Neil, M. A.; French, P. M.; Demello, A. J.; Abell, C.; Hollfelder, F. *Anal. Chem.* **2009**, *81*, 302–306.

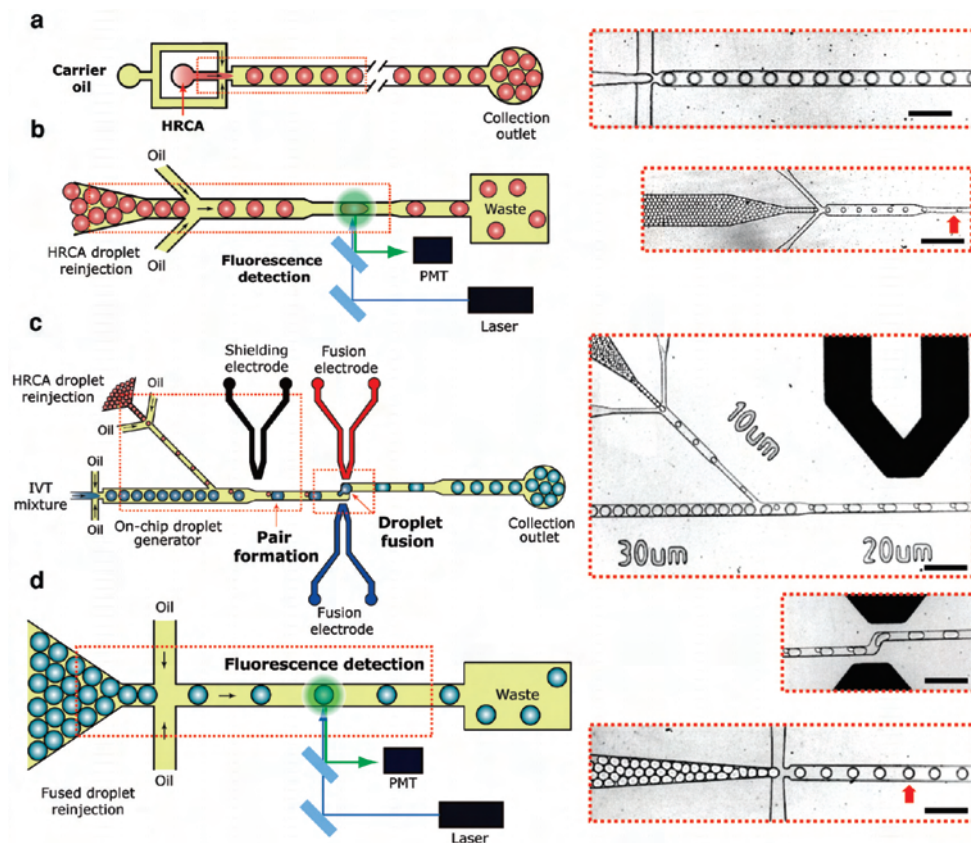


Figure 1. The microfluidic devices. (a) HRCA droplet generation device. An HRCA system containing the plasmid DNA was emulsified using HFE-7500 fluorinated oil with 2% (w/w) EA surfactant. (b) HRCA droplet analysis device. After incubation off-chip, HRCA droplets were reloaded into the device and spaced with HFE-7500 fluorinated oil, and their fluorescence was monitored using PMTs. (c) Droplet fusion device. HRCA droplets were reloaded, spaced by HFE-7500 fluorinated oil containing 2% (w/w) EA surfactant, and paired with IVT droplets generated on-chip. Droplet pairs were electrocoalesced between two electrodes (red and blue) by application of an AC field (30 kHz, 600 V) while shielding electrodes (black) prevented unwanted electrocoalescence. (d) Fused droplet analysis device. Fused droplets were reloaded and spaced with HFE-7500 fluorinated oil, and their fluorescence was monitored. Devices were fabricated in PDMS using soft lithography. The scale bar is 100 μm , and red arrows show the detection points. The corresponding movies can be found as Supporting Information.

amplification" (HRCA).¹⁹ In addition, the clonal amplified DNA in each droplet was further analyzed by measuring the activity of the encoded enzymes after fusion with a droplet containing an in vitro translation (IVT) system.

EXPERIMENTAL SECTION

Microfluidic Devices. Microfluidic devices were fabricated by patterning 10- μm -deep channels for the HRCA droplets generator device (Figures 1a and S-1 (Supporting Information)), 15- μm -deep channels for HRCA analysis device (Figures 1b and S-2 (Supporting Information)), or 20- μm -deep channels for the fusion and IVT analysis devices (Figure c and d and Figures S-3 and S-4 (Supporting Information)) into poly(dimethylsiloxane) (PDMS) using soft lithography.²⁰ Briefly, a mold of SU-8 resist (MicroChem

Corp., Newton, MA) was fabricated on a silicon wafer (Siltronix, Archamp, France) by UV exposure (MJB3 contact mask aligner; SUSS MicroTec, Garching, Germany) through a photolithography mask (Selba SA, Versoix, Switzerland) and subsequent development (SU-8 developer; MicroChem Corp.). Curing agent was added to PDMS base (Sylgard 184 silicone elastomer kit; Dow Corning Corp., Lyon, France) to a final concentration of 10% (v/v), mixed, and poured over the mold to a depth of 5 mm. Following cross-linking at 65 $^{\circ}\text{C}$ for \sim 12 h, the PDMS was peeled off the mold, and the input and output ports were punched with a 0.75-mm-diameter Harris Uni-Core biopsy punch (Electron Microscopy Sciences, Hatfield, PA). Particles of PDMS were cleared from the ports using pressurized nitrogen gas. The structured side of the PDMS slab was bonded to a 76 \times 26 \times 1 mm glass microscope slide (Paul Marienfeld GmbH & Co. KG, Lauda-Königshofen, Germany) by exposing both parts to an oxygen plasma (PlasmaPrep 2 plasma oven; GaLa Instrumente GmbH, Bad Schwalbach, Germany) and pressing them together. For the droplet

(19) Lizardi, P. M.; Huang, X.; Zhu, Z.; Bray-Ward, P.; Thomas, D. C.; Ward, D. C. *Nat. Genet.* **1998**, *19*, 225-232.

(20) Duffy, D.; McDonald, J.; Schueller, O.; Whitesides, G. *Anal. Chem.* **1998**, *70*, 4974-4984.

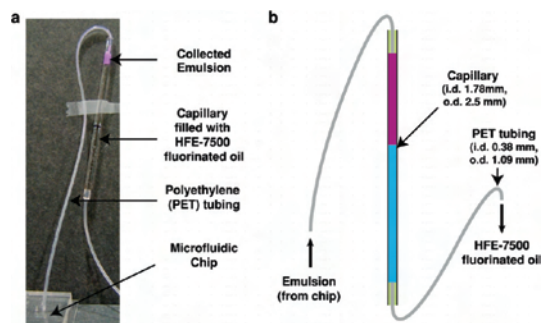


Figure 2. Capillary-based emulsion collecting system. (a) Photograph of the capillary-based system connected to a microfluidic chip. A glass capillary is interfaced with the chip by polyethylene tubing. (b) Schematic representation of the capillary-based collecting system. The capillary is represented in the collecting configuration with the syringe disconnected. The emulsion (purple) coming from the chip enters into the capillary filled with HFE-7500 fluorinated oil (blue) and pushes it out. PDMS adapters are shown in green, and polyethylene (PET) tubing, in gray.

fusion device, indium tin oxide (ITO)-coated glass slides were used (Delta Technologies, Stillwater, MN). Finally, the devices were coated with a commercial hydrophobic surface coating agent (Aqualap, PPG Industries, Pittsburgh, PA) and subsequently flushed with N_2 . Electrodes used for fusion were fabricated in close proximity to the microfluidic channels, as described previously.²¹ The patterned electrodes were filled with metal. The device was heated to 85 °C and $^{51}\text{In}/^{32.5}\text{Bi}/^{16.5}\text{Sn}$ low-temperature solder (Indium Corporation, Singapore) was melted inside the electrode channels. Electrical connections with the solder electrodes were made with short pieces of electrical wire (Radiospares, Beauvais, France). Dimensions of the microchannels are described in Figures S-1–4 (Supporting Information).

Liquids were pumped into microfluidic devices using standard-pressure infuse/withdraw PHD 22/2000 syringe pumps (Harvard Apparatus Inc., Holliston, MA). Syringes were connected to the microfluidic device using 0.6 × 25 mm Neolus needles (Terumo Corporation, La Chaussée St. Victor, France) and PTFE tubing with an internal diameter of 0.56 mm and an external diameter of 1.07 mm (Fisher Bioblock Scientific, Illkirch, France).

Fabrication of Capillary-Based Emulsion Collecting Systems. The capillary-based emulsion collecting system is shown in Figure 2. A disposable 200 μL glass capillary of internal diameter of 1.78 mm and an external diameter of 2.5 mm (Duran, Fisher Scientific, Illkirch, France) was assembled with PDMS connectors cast at both ends with 0.8-mm-diameter holes to permit the connection of thin (internal diameter of 0.38 mm and an external diameter of 1.09 mm) polyethylene (PET) tubing PE-20 (Intramedic, Becton Dickinson, Franklin Lakes, NJ). The capillary was connected to a syringe containing HFE-7500 fluorinated oil (3-ethoxy-1,1,1,2,3,4,4,5,5,6,6,6-dodecafluoro-2-(trifluoromethyl) hexane; 3M, St. Paul, MN) using a length of PET tubing. A second, shorter (10 cm) length of PET tubing was connected to the other

end of the capillary, and the whole assembly was primed with HFE-7500 fluorinated oil from the syringe.

DNA Preparation. The plasmid pVEX2.2EM-*lacZ*²² was replicated in *Escherichia coli* XL-1 blue cells (Stratagene, La Jolla, CA), purified using a Midiprep kit (Qiagen, Germantown, MD), and its concentration was estimated both on an agarose gel and by measuring the absorbance at 260 nm using a Nanodrop ND-1000 spectrophotometer (Thermo Scientific, Wilmington, DE). DNA dilutions were performed in 20 ng/ μL of carrier tRNA (Ambion, Foster City, CA).

Rolling Circle Amplification. HRCA amplifications were performed using the commercial “Illustra GenomiPhi V2 DNA Amplification Kit” (GE Healthcare, Saclay, France). Bulk amplifications were performed according to the manufacturer’s instruction for 4 h at 30 °C.

When HRCA reactions were performed in emulsions, the amplification mixture was further supplemented with 1 $\mu\text{g}/\mu\text{L}$ of purified BSA (New England Biolabs, Ipswich, MA), 2.3 $\mu\text{g}/\text{mL}$ of ds-DNA intercalating dye (RDT-D1, RainDance Technologies, Lexington, MA), and 1 mg/ μL 70 000 kDa dextran-Texas Red conjugate (Invitrogen, San Diego, CA). The aqueous phase was loaded into PTFE tubing (0.56 × 1.07 mm internal/external diameter, Fisher Bioblock Scientific) kept on ice throughout the emulsification process, and the tubing was connected to a syringe filled with 98% decane (Fluka, Sigma-Aldrich, Lyon, France). The HRCA mixture was injected into the droplet generator microfluidic device (Figures 1a and S-1 (Supporting Information)) using a syringe pump (PHD 2000, Harvard Apparatus, Holliston, MA) at a flow rate of 100 $\mu\text{L}/\text{h}$. Droplets were generated by flow focusing of the resulting stream with HFE-7500 fluorinated oil containing 2% (w/w) EA surfactant (RainDance Technologies, Lexington, MA), which is a PEG–PFPE amphiphilic block copolymer,²³ at a flow rate of 250 $\mu\text{L}/\text{h}$. The rate of droplet production was ~14 kHz. The droplet volume was calculated by dividing the flow rate of the aqueous phase by the droplet production frequency (determined by using a Phantom V4.2 high-speed camera).

When the HRCA reactions were analyzed by agarose gel electrophoresis, the emulsions were collected in a microtube under mineral oil to prevent evaporation. After incubation, the mineral oil was drained out, and 1/10 volume of Emulsion Destabilizer (RainDance Technologies, Lexington, MA) was added to 1 volume of emulsion. After a quick vortexing and centrifugation, the aqueous phase was transferred to a new tube, and the Phi29 polymerase was inactivated by heating the mixture for 20 min at 65 °C. HRCA products were then monomerized by incubating 20 μL of HRCA mixture with 10 U of *EcoRI* (Fermentas, GmbH, St Leon-Rot, Germany) overnight at 37 °C. Digested products were analyzed on a 1% agarose gel stained with ethidium bromide.

When the HRCA reactions were analyzed by monitoring droplet fluorescence, the emulsions were collected in capillaries filled with HFE-7500 fluorinated oil and incubated 4 h at 30 °C. Droplet fluorescence analyses were carried out by reinjecting HRCA emulsions from capillaries into the HRCA droplet analysis

(21) Siegel, A. C.; Bruzewicz, D. A.; Weibel, D. B.; Whitesides, G. M. *Adv. Mater.* **2007**, *19*, 727–733.

(22) Mastrobattista, E.; Taly, V.; Chanudet, E.; Treacy, P.; Kelly, B. T.; Griffiths, A. D. *Chem. Biol.* **2005**, *12*, 1291–1300.

(23) Holtze, C.; Rowat, A. C.; Agresti, J. J.; Hutchison, J. B.; Angile, F. E.; Schmitz, C. H.; Köster, S.; Duan, H.; Humphry, K. J.; Scanga, R. A.; Johnson, J. S.; Pitsignano, D.; Weitz, D. A. *Lab Chip* **2008**, *8*, 1632–1639.

device (Figures 1b and S-2 (Supporting Information)) at a flow rate of 10 $\mu\text{L}/\text{h}$. To allow data acquisition on isolated droplets, the droplets were spaced with surfactant-free HFE-7500 fluorinated oil at a flow rate of 150 $\mu\text{L}/\text{h}$, and droplet fluorescence was monitored using the optical setup shown in Figure S-5 (Supporting Information) by focusing the 488 nm laser beam in the middle of a 10- μm -wide and 15- μm -deep channel of the device. Fluorescence was measured using PMTs, and the signal output from the PMTs was analyzed using a PCI-7831R Multifunction Intelligent DAQ card (National Instruments Corporation, Austin, TX) executing a program written in LabView 8.2 (FPGA module, National Instruments Corporation). The data acquisition rate for the system was 100 kHz.

Enzymatic Assay of the in Vitro Translated *lacZ* in Droplets. The *lacZ* gene carried by the purified pIVEX2.2EM-*lacZ* plasmid,²² or the amplified plasmid was expressed, respectively, by directly mixing plasmid DNA with the IVT system or by fusing HRCA product-containing droplets with droplets containing the IVT system. The IVT system contained 0.7 volume of *E. coli* extract (EcoProT7 kit, Novagen, Merck, Darmstadt, Germany), 300 μM of methionine, 100 μM fluorescein di- β -D-galactopyranoside (Euromedex, Souffelweyersheim, France), 1 μM fluorescein, and 0.1 mg/ μL 70 000 kDa dextran-Texas Red conjugate (Invitrogen, San Diego, CA). The mixture was loaded in PTFE tubing kept on ice throughout the emulsification process, and the tubing was connected to a syringe filled with 98% decane (Fluka, Sigma-Aldrich, Lyon, France).

After *lacZ* gene HRCA amplification (4 h at 30 $^{\circ}\text{C}$), the emulsion was reinjected from the capillary into a droplet fusion device (Figures 1c and S-3 (Supporting Information)) at 20 $\mu\text{L}/\text{h}$ and spaced with HFE-7500 fluorinated oil containing 2% w/w EA surfactant at 120 $\mu\text{L}/\text{h}$ (~ 1.7 kHz). On-chip droplets (15 pL volume) were generated on the droplet generation module at ~ 1.85 kHz using the flow rates at 100 $\mu\text{L}/\text{h}$ for IVT mixture and 100 $\mu\text{L}/\text{h}$ for HFE-7500 fluorinated oil containing 2% (w/v) EA-surfactant. To obtain the highest frequency ($\sim 95\%$) of one-to-one fusion events, the flow rate of HFE-7500 fluorinated oil used to space reinjected HRCA droplets was adjusted to match the frequencies of reinjected droplets and droplets produced on-chip. Electrocoalescence of droplets^{10–14} was performed for 30 min at a rate of ~ 2000 fusion events/s by applying an electric field of 600 V AC at 30 kHz across electrodes using a Model 623b high-voltage amplifier (Trek, Inc.; BF: OPTILAS SAS, Evry, France). After droplet electrocoalescence, over 10^6 fused droplets were collected into a single glass capillary connected to the chip. The glass capillary was then transferred to a 37 $^{\circ}\text{C}$ air thermostat and incubated for 2 h to allow transcription and translation to occur in the droplets. Fused droplets were then reloaded into a fused droplet detection device (Figures 1d and S-4 (Supporting Information)) at 40 $\mu\text{L}/\text{h}$ and spaced by HFE-7500 fluorinated oil (without surfactant) at 120 $\mu\text{L}/\text{h}$, resulting in a reinjection frequency of ~ 0.9 kHz. The 488 and 532 nm laser beams (Figure S-5 (Supporting Information)) were focused in the middle of the 40- μm -wide and 20- μm -deep reinjection channel (~ 250 μm beyond the flow focusing junction). This allowed the measurement of both β -galactosidase activity (green) and Texas

Red (orange) in the droplets. Fluorescence-emitted light from $\sim 10^5$ droplets was recorded using two photomultiplier tubes (PMTs).

Confocal Microscopy Imaging. Droplets were placed between two 0.17-mm-thick microscope coverslips, and images were acquired with a Zeiss (Jena, Germany) LSM510 laser-scanning confocal microscope equipped with C-Apochromat 20 \times (n.a. 0.8) or 40 \times (n.a.1.1) water immersion objectives in multitrack mode. RDT-D1 was excited at 488 nm using an argon laser, and emission spectra were recorded from 505 to 550 nm. Texas Red fluorescence was excited at 543 nm using a helium–neon 543 nm laser, and emission spectra were recorded at wavelengths higher than 585 nm. Images were processed with the Zeiss LSM Image Browser, version 2.50.0929, software.

Estimation of Ribosome Content of the IVT System. Total RNA was extracted by mixing 1 volume of IVT mixture (35 μL of bacterial extract and 15 μL of water) with 1 volume of phenol/chloroform/isoamyl alcohol (25/24/1). Different dilutions of the recovered aqueous phase were run on an 8% denaturing acrylamid gel, together with 7–500 ng of a standard RNA of the same size. The intensity of the 120-bp band (5S RNA) was measured (Gel Logic 200 Imaging System, Kodak; Carestream Health Corp., New York, NY) and compared to those of the standard.

Measures to Minimize Contamination. To minimize contamination by exogenous DNA, the components of the HRCA kit were aliquoted upon arrival and stored at -80 $^{\circ}\text{C}$. A new aliquot was used for each set of experiments. Dilutions were performed in DNase-, RNase-free, DEPC-treated water (MP Biomedicals, Illkirch, France), and all DNA manipulations prior to amplification were performed in a UV-treated environment (Biocap DNA/RNA hood, Fisher Bioblock Scientific). A new device was used for each set of experiments, going from the more diluted to the more concentrated DNA sample to limit carry-over effects. In addition, all the experiments were carried out using certified DNA-free, sterilized, filtered pipet tips.

RESULTS AND DISCUSSION

In this study, we used a microfluidic system composed of separate devices (chips) (Figure 1) for droplet generation, fusion, and detection, allowing isothermal amplification and analysis of the 6 kb pIVEX2.2EM-*lacZ* plasmid²² encoding β -galactosidase.

A Hyperbranched Rolling Circle Amplification (HRCA) system (Illustra GenomiPhi V2; G.E Healthcare, Saclay, France) was first tested in bulk assays using as template the pIVEX2.2EM-*lacZ* plasmid at concentrations ranging from 35 to 0.07 pg/ μL . After incubation and polymerase inactivation, the amplification products were monomerized by *EcoRI* digestion and analyzed by agarose gel electrophoresis (Figure 3). Efficient amplification was observed at DNA concentrations down to 0.07 pg/ μL , confirming the high sensitivity of HRCA.²⁴ Because the HRCA system uses random hexamer primers, it can potentially amplify any DNA in a nonspecific manner. Consequently, we followed the procedure described in the Experimental Section to minimize the contamination by exogenous DNA molecules. For applications in which avoiding contamination is of paramount importance (e.g., diagnosis

(24) Li, F.; Zhao, C.; Zhang, W.; Cui, S.; Meng, J.; Wu, J.; Zhang, D. Y. *J. Clin. Microbiol.* **2005**, *43*, 6086–6090.

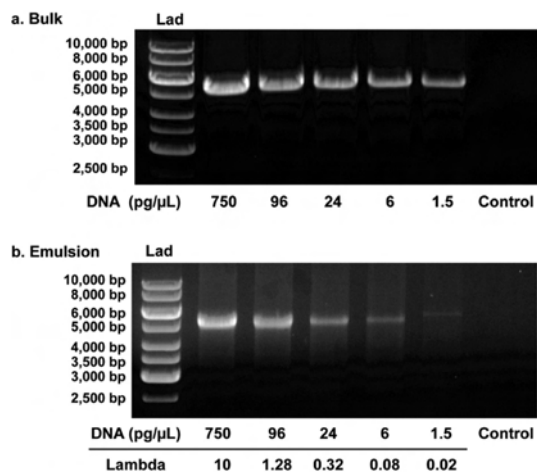


Figure 3. Gel analysis of bulk and emulsified HRCA reactions. Amplifications of the plasmid pIVEX 2.2EM-*lacZ* were performed in bulk (a), or in droplets (b). After incubation, the polymerase was inactivated, and the amplification products monomerized and analyzed on 1% agarose gel stained with ethidium bromide. The GeneRuler 1kb DNA Ladder (Fermentas) was used as standard (Lad), and the size of each band is given. The DNA concentration used to initiate the amplification is indicated under each picture, and theoretical λ values are given for emulsified reactions. Control lanes correspond to reactions performed with a DNA concentration corresponding to $\lambda = 10$ but for which Phi29 polymerase was omitted.

or library screening), a more thorough approach, similar to the one recently described for single-cell DNA sequencing methods,²⁵ could be used.

The same set of experiments was then carried out in an emulsion. HRCA mixtures supplemented with 1% BSA were dispersed in HFE-7500 fluorinated oil containing 2% (w/w) EA surfactant using a microfluidic flow-focusing device with a 10 μm nozzle (Figures 1a and S-1 (Supporting Information)) to produce a highly monodisperse emulsion of 2 pL droplets at 14 kHz. The emulsion was collected in a microtube under mineral oil to prevent evaporation and incubated 4 h at 30 °C. The emulsion was then broken with Emulsion Destabilizer (RainDance Technologies), the aqueous phase was recovered, the polymerase was inactivated, and the HRCA products were monomerized. Gel analysis revealed that the yield of amplified DNA was almost identical in droplets and in bulk at DNA concentrations corresponding to an average starting number of plasmid molecules per droplet (λ) >1 (Figure 3). The yield of DNA is limited by the available dNTPs, primers, or both, in both cases. However, at $\lambda < 1$, as expected, the yield of amplified DNA in droplets decreases rapidly in droplets compared to in bulk due to the presence of droplets that contained no plasmid DNA, which reduces the quantity of available dNTPs and primers. The yield of amplified DNA from emulsions in which all ($\lambda = 10$) or the majority ($\lambda = 1.28$) of droplets were initially occupied was quantified by agarose gel electrophoresis. We estimated that at both $\lambda = 10$ and $\lambda = 1.28$, each droplet

contained $\sim 30\,000$ HRCA monomerized products, indicating that a single encapsulated plasmid was amplified by $\sim 30\,000$ -fold.

The content of each droplet was then individually monitored by further supplementing the HRCA system with a ds-DNA intercalating dye (RDT-D1, RainDance Technologies), which becomes highly green fluorescent when intercalated into double-stranded DNA, to identify droplets where amplification occurred and with a dextran–Texas Red conjugate as an internal standard. A 2-step strategy was used (Figure 4a): (i) As above, the HRCA mixtures were compartmentalized in 2 pL droplets, but were collected this time in a glass capillary (Figure 2) and placed for 4 h at 30 °C. Droplet order is not strictly maintained in the capillary; however, the creaming and packing of droplets means that there is a tendency for the last droplets in to be the first out. However, droplet production and reinjection was fast enough (less than 10 min for 10^7 droplets) to make the difference in incubation times between the droplets insignificant. For applications in which larger numbers of droplets have to be collected, the capillary can be connected to a Peltier-based temperature control device (CP-031, TE-technology, Traverse City, MI), allowing the synchronization of reactions in droplets by collecting them at 4 °C and activating the reactions by switching the temperature to 30 °C (for HRCA) or 37 °C (for IVT). (ii) After incubation, the capillary was connected to the analysis chip (Figures 1b and S-2 (Supporting Information)), the droplets were reinjected at 4–8 kHz and spaced using HFE-7500 fluorinated oil, and the fluorescence intensity of the droplets was monitored using an optical setup comprising a 488 nm laser and PMTs measuring epifluorescence at 525 nm (green) and 585 nm (orange) to detect amplified DNA and dextran–Texas Red, respectively. As expected, this analysis revealed single major peaks, corresponding to either all-green fluorescent or all-nonfluorescent droplets with 35 $\text{pg}/\mu\text{L}$ DNA ($\lambda = 10$) or the control experiment in which the polymerase was omitted (Figure 4b and e), respectively. When using DNA concentrations from 0.07 to 4.5 $\text{pg}/\mu\text{L}$ ($\lambda = 0.02$ –1.28), two discrete populations corresponding to nonfluorescent (~ 25 RFUs) and green-fluorescent droplets (200–320 RFUs) were distinguishable (Figures 4c, d and S-6 (Supporting Information)). The small population between the peaks may result from abortive amplification of damaged plasmids. Consequently, only droplets in the positive peak were used to determine droplet occupancies. These occupancies were further confirmed by confocal microscopy (Figures 4 and S-6 (Supporting Information)). The mean fluorescence intensity of positive droplets decreased as DNA concentration and droplet occupancy increased (Figure 4f) due to passive transfer of RDT-D1 between the droplets and its uptake by the amplified DNA in occupied droplets. The occupancy was a Poisson distribution controlled by DNA concentration, and the experimental λ values closely fitted the theoretical ones calculated from the template DNA concentration ($R^2 = 0.903$) (Figure 4g). Hence, the technique allows accurate “digital” quantification of the template DNA.

The amplified DNA was then further characterized by expressing the *lacZ* gene carried on the plasmid. We first tested

(25) Zhang, K.; Martiny, A. C.; Reppas, N. B.; Barry, K. W.; Malek, J.; Chisholm, S. W.; Church, G. M. *Nat. Biotechnol.* **2006**, *24*, 680–686.

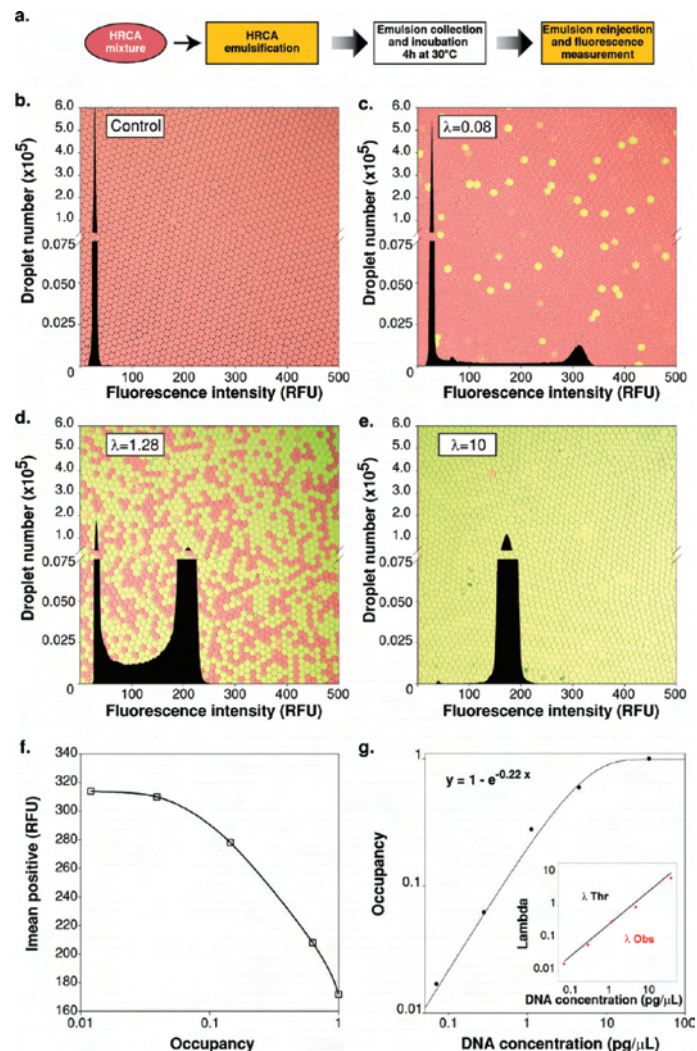


Figure 4. Characterization of digital HRCA reactions. (a) Overview of operations. (b–e) Histograms of green fluorescence, normalized by the orange fluorescence of the internal standard (dextran–Texas Red), of 10^6 droplets. Theoretical λ values are indicated, and confocal images of emulsions are shown (backgrounds). The control reaction was performed at $\lambda = 10$ but without polymerase. (f) The mean intensities (\bar{I}_{mean}) of the positive droplets versus droplet occupancies. (g) A curve described by the Poisson equation (occupancy = $1 - e^{-\lambda}$) was fitted to experimental data using SigmaPlot (Systat Software GmbH, Erkrath, Germany). Inset: λ values derived from experimental data (red dots) and theoretical λ values (black line) plotted versus DNA concentration.

the activity of compartmentalized IVT reactions by coencapsulating purified plasmid DNA with a coupled in vitro transcription/translation (IVT) system (EcoPro T7, Novagen), a fluorogenic β -galactosidase substrate (fluorescein-di- β -D-galactopyranoside; FDG) and dextran–Texas Red conjugate. A DNA concentration corresponding to that of an amplified DNA (i.e., $\lambda = 20\,000$) was used to produce 1.3 million 15 μL droplets (20 μL of aqueous phase) that were collected on ice and transferred to a microtiter plate. The production of fluorescein (due to β -galactosidase activity) was monitored for 2 h at 37 $^\circ\text{C}$ in a spectrophotometer. An equivalent volume (20 μL) of bulk

reaction was monitored in parallel and, as shown in Figure 5a, the rate of appearance of β -galactosidase activity was identical for both bulk and emulsified IVT at $\lambda = 20\,000$, demonstrating that IVT was not affected by the confinement in droplets. Interestingly, the same experiments performed with a DNA concentration equivalent to that prior to amplification (i.e., $\lambda = 2$, where 87% of the droplets contained at least one DNA molecule) gave no detectable β -galactosidase activity (in bulk or in emulsion). This observation was further confirmed by an experiment in which the fluorescence of each droplet was measured (Figure 5b) by reinjecting droplets into the device

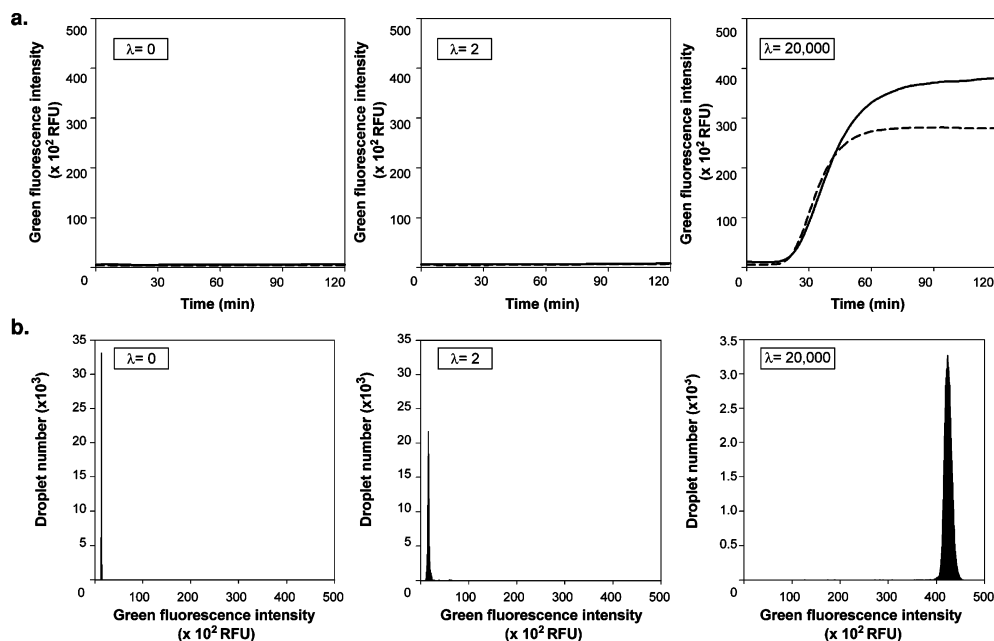


Figure 5. In vitro transcription/translation of *lacZ* genes carried by the plasmid pIVEX2.2EM-*lacZ* in droplets. (a) Kinetic monitoring of in vitro transcription/translation of *lacZ* genes. IVT systems containing FDG, dextran–Texas Red conjugate, and different plasmid concentrations corresponding to λ values of 0, 2, or 20 000 were either encapsulated in 20 pL droplets (solid lines) or kept in a bulk format (dashed lines), and the green fluorescence was monitored for 2 h at 37 °C in microtiter plate wells. (b) Different plasmid concentrations corresponding to λ values of 0, 2, or 20 000 were encapsulated in 20 pL droplets containing the IVT system, FDG, and dextran–Texas Red conjugate. After 2 h at 37 °C, the droplets were reinjected into the microfluidics device (Figures 1d and S-4 (Supporting Information)), and the green fluorescence intensity was measured.

shown in Figures 1d and S-4 (Supporting Information). Altogether, these results demonstrate that a successful amplification ($\lambda = 20\,000$) is necessary to observe β -galactosidase activity whereas without amplification ($\lambda = 2$), a single *lacZ* gene does not lead to efficient production of β -galactosidase. We calculated, on the basis of catalytic activity, that the yield of β -galactosidase reached a plateau at a DNA concentration equivalent to $\lambda = 2500$, corresponding to ~ 1700 molecules of β -galactosidase per gene (Supporting Information, and Figure S-5). This yield is close to that expected from the EcoPro T7 IVT system (~ 300 proteins/gene [28 μg of β -galactosidase produced from 2 μg of gene] quoted by the supplier²⁶). However, at lower DNA concentrations, the yield of active β -galactosidase dropped more rapidly than the decrease in DNA concentration (a 2800-fold drop in activity from $\lambda = 500$ to $\lambda = 5$), most likely due to the inefficient assembly of tetrameric β -galactosidase at low subunit concentrations. A yield of 1700 β -galactosidase molecules per gene is low compared to 30 000 green fluorescent protein (GFP) molecules expressed from single genes in droplets reported recently.²⁷ However, this difference can most likely be attributed to the fact that β -galactosidase is a large tetrameric protein of (4×116 kDa), whereas GFP is a 27 kDa monomeric protein, and hence, the yield of protein per gene by mass is almost identical for

(26) Ambuel, Y.; Handley, M.; Hayes, S. *in* *Innovations* 2003, 16, 3–6.

(27) Courtois, F.; Olguin, L. F.; Whyte, G.; Bratton, D.; Huck, W. T. S.; Abell, C.; Hollfelder, F. *ChemBioChem* 2008, 9, 439–446.

β -galactosidase and GFP (mass β -galactosidase per gene/mass GFP per gene = 0.97). The low yield of active β -galactosidase at low λ led us to perform fusion experiments between HRCA droplets with droplets containing an IVT system.

We used plasmid DNA at $\lambda = 0.25$ to minimize encapsulation of more than 1 plasmid/droplet ($P_{(\lambda>1)} = 0.026$). An emulsion in which the polymerase was omitted was used as the control. The procedure involved three steps (Figure 6a): (i) HRCA systems supplemented with 1% BSA and dextran–Texas Red were encapsulated in 2 pL droplets at 14 kHz using the device shown in Figures 1a and S-1 (Supporting Information), collected in glass capillaries (Figure 2), and incubated 4 h at 30 °C. (ii) These droplets were reinjected into the droplet fusion device at ~ 1.7 kHz (Figures 1c and S-3 (Supporting Information)). In parallel, the IVT system supplemented with FDG was encapsulated in 15 pL droplets on the same device (~ 1.85 kHz). Pairs of HRCA and IVT droplets were fused by electrocoalescence,^{10–14} collected in a glass capillary, and incubated 2 h at 37 °C. Model experiments using fluorescent dyes demonstrated that the device was highly efficient (see the Supporting Information, Figure S-7): with an 11% excess of on-chip droplets, 95% of the reinjected droplets were fused one-to-one with a droplet generated on-chip (Figure 6b). (iii) Finally, fused droplets were reinjected into the fused droplet detection device, and the fluorescence intensity of each droplet was monitored using the device shown in Figures 1d and S-4 (Supporting Information).

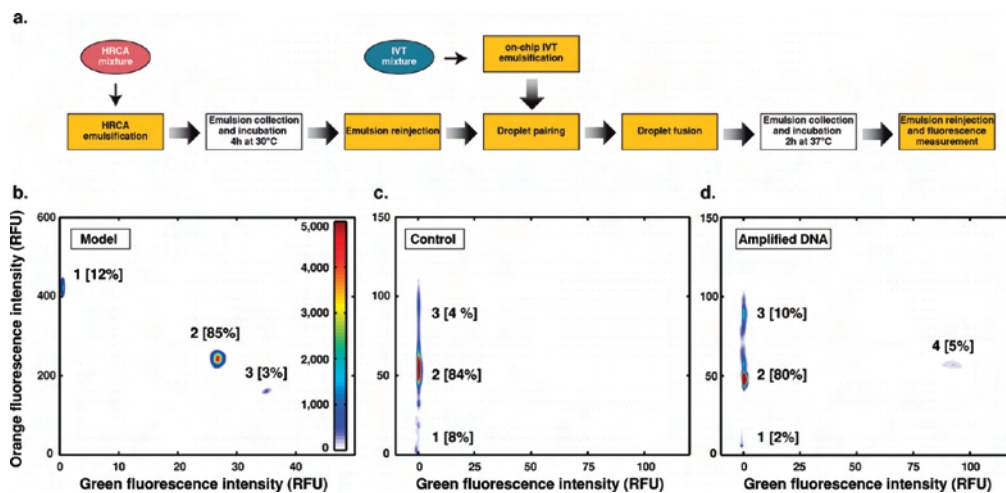


Figure 6. β -Galactosidase expression in fused droplets. (a) Overview of operations. (b) Model experiment. Reinjected droplets (2 pL) containing 10 μ M fluorescein (green fluorescence) and 50 mM methylene blue were fused with 10 pL droplets generated on-chip containing 100 μ M resorufin (orange fluorescence). The lower orange fluorescence in fused droplets was due to absorbance by the methylene blue. (c–d) HRCA reactions, containing Texas Red (orange fluorescence), were performed in 2 pL droplets at $\lambda = 0.25$ in the absence (c) or presence (d) of DNA polymerase. After *lacZ* gene amplification, these droplets were fused with 15 pL droplets containing an IVT system and FDG (which is transformed into fluorescein (green fluorescent) by β -galactosidase) and incubated, and the fluorescence of 150 000 droplets was analyzed. Unfused IVT droplets (population 1) and droplets fused one-HRCA-to-one-IVT (populations 2 and 4) and two-HRCA-to-one-IVT (population 3) are identified, and the percentage of the total population is indicated.

The orange fluorescence due to Texas Red in the HRCA droplets allowed pairwise-fused IVT droplets (1 HRCA/1 IVT) to be distinguished from nonfused and double-fused (2 HRCA/1 IVT) droplets. The green fluorescence resulting from FDG hydrolysis allowed droplets containing in vitro translated β -galactosidase to be identified. Fluorescein (1 μ M) was added to the IVT, allowing for the detection of nonfused IVT droplets (population 1 in Figure 6c and d). Without prior plasmid DNA amplification (Figure 6c) or when plasmids were directly emulsified in IVT mixture at $\lambda = 2$, no activity was observed (see above). The similar behavior of reactions in bulk and in emulsion ruled out an inhibitory effect of compartmentalization on IVT. However, when plasmid DNA was amplified, a green-fluorescent droplet population appeared (Figure 6d), indicating the presence of active β -galactosidase. Hence, single molecules of DNA compartmentalized in droplets can be amplified and the enzymatic activity of the encoded protein measured.

Six percent of pairwise-fused droplets (85% of the total droplets) contained active β -galactosidase, rather than 22%, as expected from the direct measurement of DNA amplification in droplets (Figure 4g). This effect cannot be due to stochastic variations in the number of ribosomes in droplets, since gel quantification of 5S rRNA content of the IVT system indicated that each droplet contains, on average, 10^6 ribosomes (data not shown). The origin of this effect is still under investigation.

CONCLUSIONS

This is the first time that such a high-throughput, on-chip analysis (up to 8 kHz) was achieved for clonal DNA amplification using microsystems. The use of an isothermal amplification system (HRCA) avoids many complications linked to the

thermocycling of PCRs. Furthermore, the ability not simply to measure DNA amplification but also to measure the activity of the encoded enzymes after IVT greatly increases the range of potential applications. IVT is widely used for the rapid identification of gene products (proteomics), localization of mutations causing truncated gene products, protein folding studies, and incorporation of modified amino acids.²⁸ Many of these applications could potentially be implemented in droplet-based microfluidic systems, with massive reagent cost savings: 10^6 IVT reactions in 20 pL droplets costs only \$4.50, as compared to \$1 137 500 for 10^6 5 μ L IVT reactions in microtiter plates (see Supporting Data).

In the future, by integrating further microfluidic modules, even greater functionality could be achieved. For example, droplets can be sorted or triggered on fluorescence using dielectrophoresis,^{29,30} which would allow the development of a completely in vitro system for directed evolution. The preamplification of genes before translation is likely to be important for such applications because, although the translation of single GFP genes in droplets in microfluidic systems has been reported,²⁷ we were unable to detect the expression of single *lacZ* genes, despite the fact that β -galactosidase is a highly active enzyme ($k_{\text{cat}} = 187 \text{ s}^{-1}$, $K_M = 150 \mu\text{M}$) which is efficiently translated in vitro.^{31–33}

(28) Katzen, F.; Chang, G.; Kudlicki, W. *Trends Biotechnol.* **2005**, *23*, 150–156.
(29) Ahn, K.; Kerbage, C.; Hunt, T. P.; Westervelt, R. M.; Link, D. R.; Weitz, D. A. *Appl. Phys. Lett.* **2006**, *88*, 024104.

(30) Baret, J. C.; Miller, O. J.; Taly, V.; Ryckelynck, M.; El-Harrak, A.; Frenz, L.; Rick, C.; Samuels, M. L.; Hutchison, J. B.; Agresti, J. J.; Link, D. R.; Weitz, D. A.; Griffiths, A. D. *Lab Chip*, DOI: 10.1039/b902504a.

(31) Lederman, M.; Zubay, G. *Biochem. Biophys. Res. Commun.* **1968**, *32*, 710–714.

ACKNOWLEDGMENT

We thank J. H. Leamon for helpful discussions and P. Nauny and G. Diss for help with microfluidic device preparation. This work was supported by the Ministère de l'Enseignement Supérieur et de la Recherche, Centre National de la Recherche Scientifique (CNRS), Agence National de la Recherche (ANR) (ANR-05-BLAN-0397), the Fondation d'Entreprise EADS, the Conseil Scientifique de l'Université Louis Pasteur, the Medical Research Council (U.K.), the Ministry of Defence (U.K.), the EC FP6 Marie Curie Research Training Network, ProSA, and the Human Frontier

(32) Zubay, G. *Annu. Rev. Genet.* **1973**, *7*, 267–287.

(33) Mierendorf, R.; Van Oosbree, T. R. U.S. Patent PCT/US1995014310,1995.

Science Program (HFSP). J.C.B. was supported by an EMBO long-term fellowship [ALTF 915–2006]. L.M. and A.F.A. contributed equally to this work.

SUPPORTING INFORMATION AVAILABLE

Additional information as noted in text. This material is available free of charge via the Internet at <http://pubs.acs.org>.

Received for review February 23, 2009. Accepted April 19, 2009.

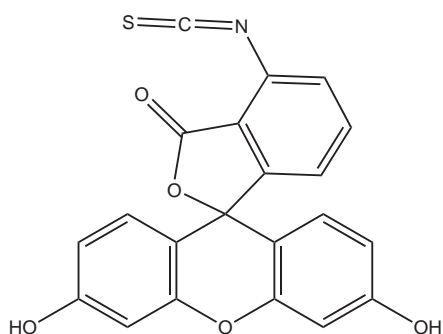
AC900403Z

Appendix B.

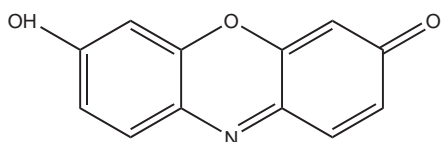
Compounds and chemicals structures

B.0.4. Fluorophores

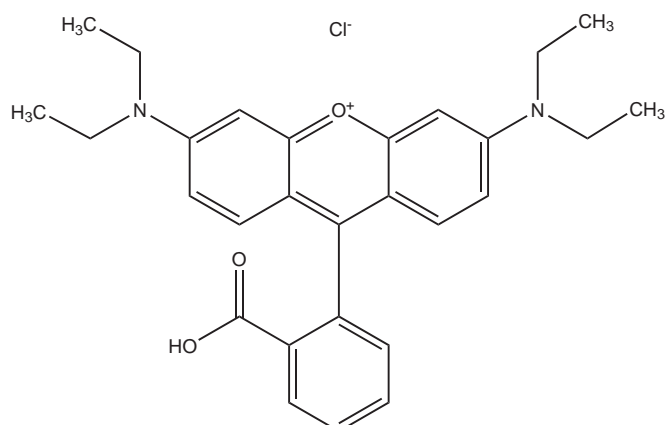
1. **Fluorescein isothiocyanate (FITC)** is a derivative of fluorescein used in wide-ranging applications including flow cytometry. FITC is the original fluorescein molecule functionalized with an isothiocyanate reactive group ($-N=C=S$), replacing a hydrogen atom on the bottom ring of the structure. This derivative is reactive towards nucleophiles including amine and sulfhydryl groups on proteins. It has an absorption maximum at 495 nm and emission maximum of 521 nm.



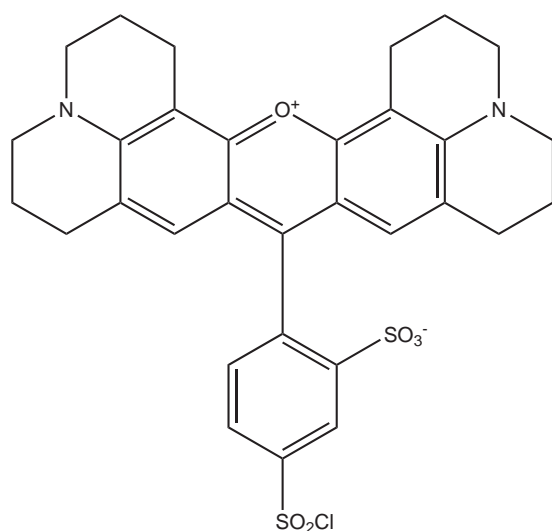
2. **Resorufin** has an absorption maximum at 572 nm and emission maximum of 583 nm.



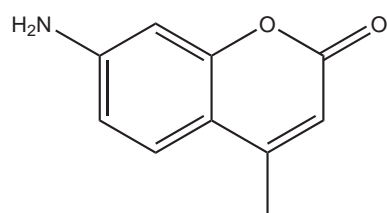
3. **Rhodamine** is a family of related chemical compounds, fluorone dyes. Examples are Rhodamine 6G and Rhodamine B. Rhodamine dyes are used extensively in biotechnology applications such as fluorescence microscopy, flow cytometry, fluorescence correlation spectroscopy and ELISA. The fluorescence yield is temperature dependent.



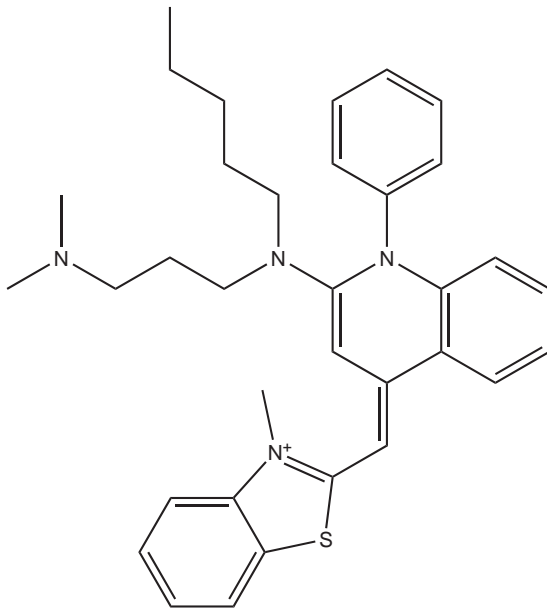
4. **Texas Red** (Sulforhodamin 101 Sulfonylechlorid) is a red fluorescent dye used in histology for staining cell specimens, for sorting cells with fluorescent-activated cell sorting machines, in fluorescence microscopy applications, and in immunohistochemistry. Texas Red, attached to a strand of DNA or RNA, can be used as a molecular beacon for highlighting specific sequences of DNA. Texas Red can be linked with another fluorophore. A tandem conjugate of Texas Red with R-phycoerythrin (PE-Texas Red) is often used. Texas Red fluoresces at about 615 nm (making it more purple than red), and the peak of its absorption spectrum is at 589 nm.



5. **Coumarin (Aminomethylcoumarin)** has an absorption maximum at 360 nm and emission maximum of 448 nm.

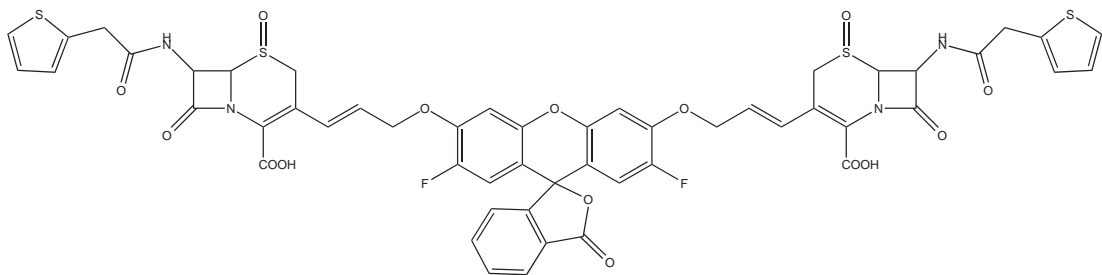


6. **SYBR Green I (SG)** is an asymmetrical cyanine dye used as a nucleic acid stain in molecular biology. SYBR Green I binds to double-stranded DNA. The resulting DNA-dye-complex absorbs blue light (max = 488 nm) and emits green light (max = 522 nm).

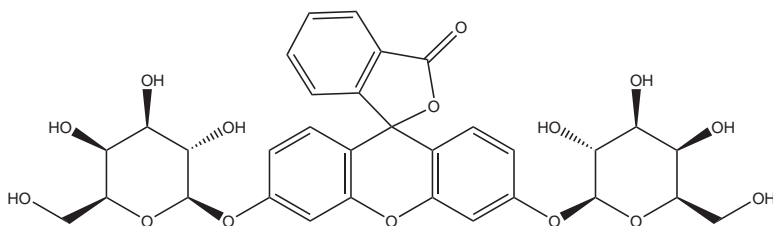


B.0.5. Substrates

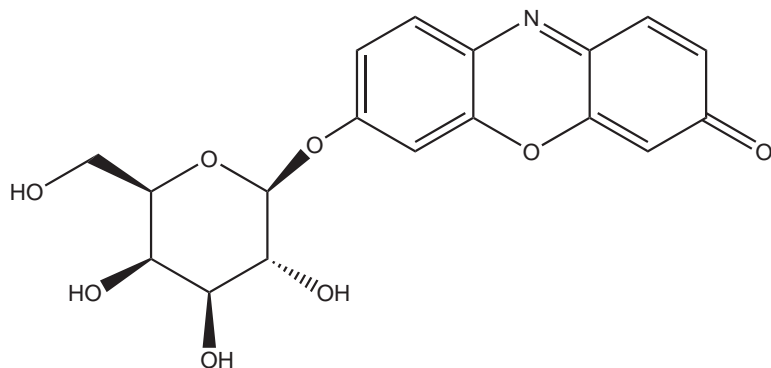
1. Fluorocillin_{495/525nm}: β -lactamase substrate: Fluorogenic substrate releasing a fluorescent dye upon hydrolysis that can be detected at 495/525 nm



2. FDG (fluorescein di- β -D-galactopyranoside): β -galactosidase substrate: Fluorogenic substrate releasing a fluorescent dye upon hydrolysis that can be detected at 488/512nm



3. RBG (resorufin β -D-galactopyranoside): β -galactosidase substrate: Fluorogenic substrate releasing a fluorescent dye upon hydrolysis that can be detected at 572/583nm

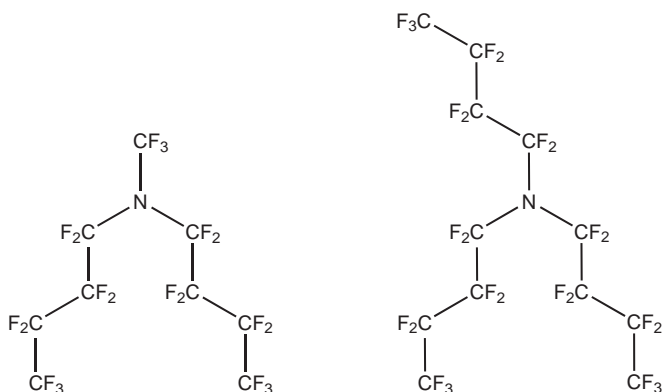


B.0.6. Oils

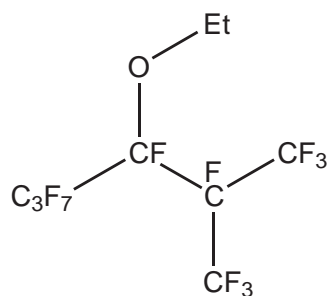
1. Mineral oil (Decane)



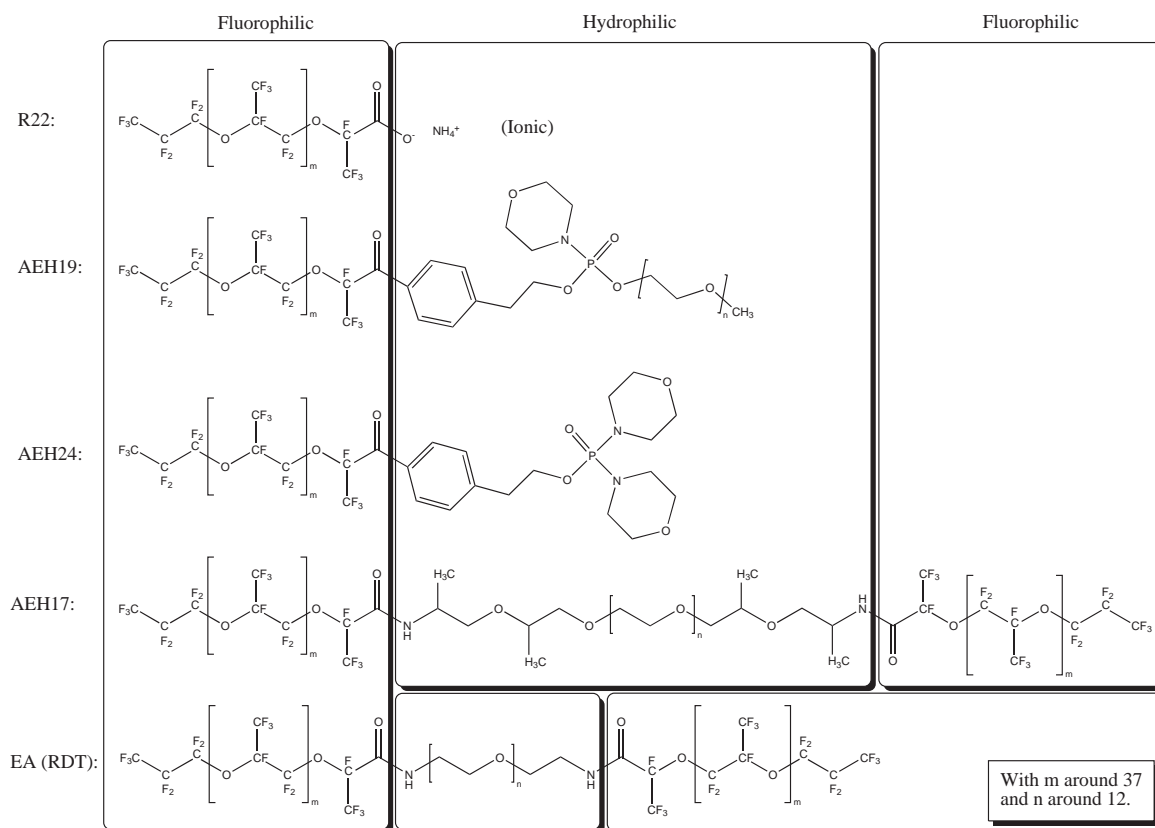
2. FC40



3. HFE-7500 (3-ethoxy-1,1,1,2,3,4,4,5,5,6,6,6-dodecafluoro-2-(trifluoromethyl) hexane)



B.0.7. Surfactants



Appendix C.

Instrumentation

Especially the optics are crucial for detection and interfacing the reactions on chip to the outside world (computer). Figure C.1 shows an illustration of the most complex optical setup used so far. It is an extension of the basic version in section 1.3.2 and is capable to excite and detect three different wavelengths as well as fluorescent polarization. Furthermore, it contains elements used in confocal microscopy, allowing to increase the sensitivity for small signals.

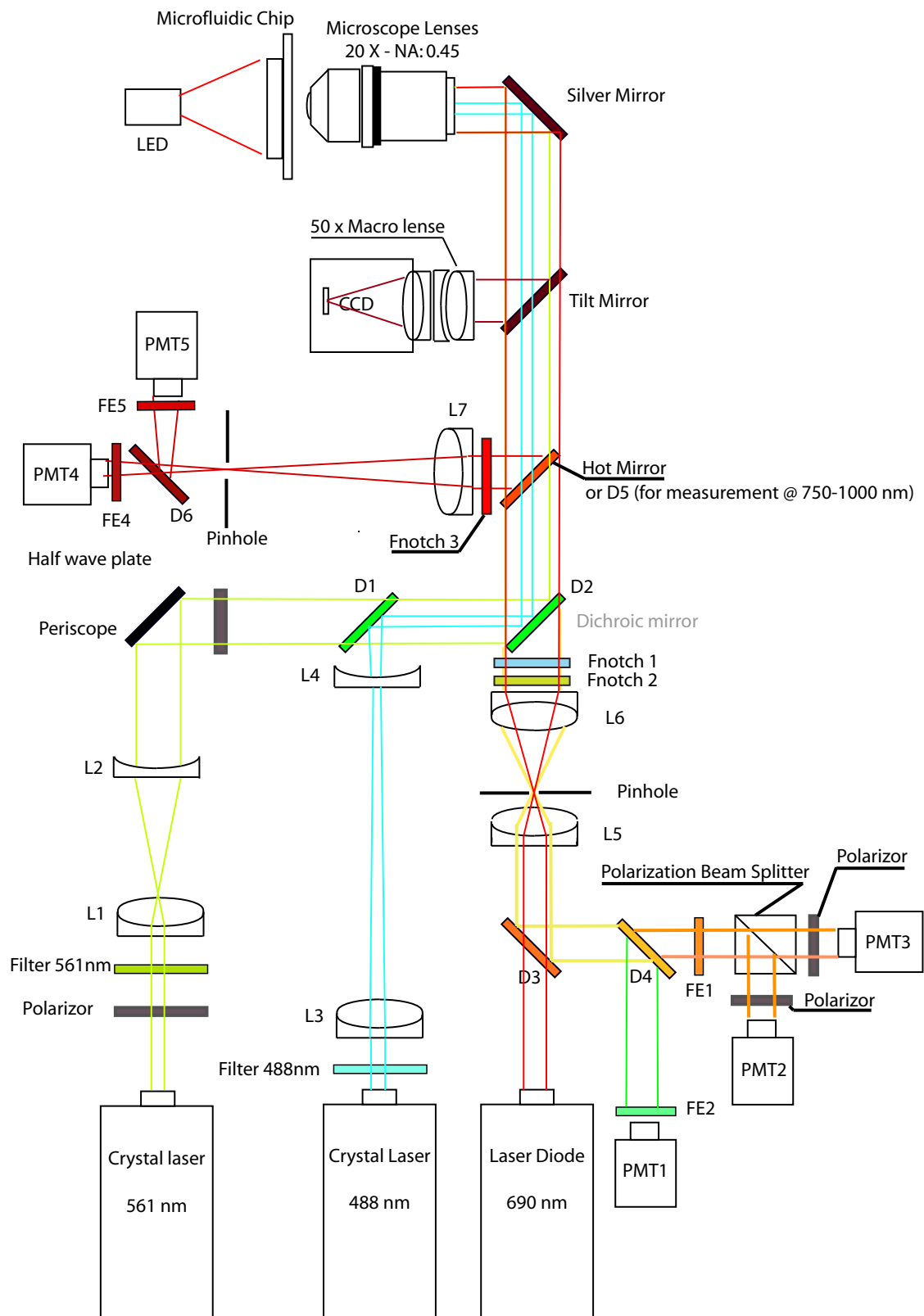


Figure C.1.: Detailed illustration for the most complex optical setup used so far. The system is utilizing three different lasers to excite the fluorophores, and is capable to detect three distinct wavelengths as well as fluorescent polarization.

References

- [1] J. Clayton, "Go with the microflow," *Nat. Methods*, vol. 2, pp. 621–627, Aug. 2005.
- [2] G. Whitesides, D. Janasek, J. Franzke, A. Manz, D. Psaltis, S. R. Quake, C. Yang, H. Craighead, A. deMello, J. El-Ali, P. Sorger, K. Jensen, P. Yager, T. Edwards, E. Fu, K. Helton, K. Nelson, M. Tam, and B. Weigl, "Lab on a chip," *Nature*, vol. 442, pp. 368–418, July 2006.
- [3] T. M. Squires and S. R. Quake, "Microfluidics: Fluid physics at the nanoliter scale," *Rev. Mod. Phys.*, vol. 77, pp. 977–1026, July 2005.
- [4] J. Atencia and D. J. Beebe, "Controlled microfluidic interfaces," *Nature*, vol. 437, pp. 648–655, Sept. 2005.
- [5] P. S. Dittrich, K. Tachikawa, and A. Manz, "Micro total analysis systems. latest advancements and trends," *Anal. Chem.*, vol. 78, pp. 3887–3907, June 2006.
- [6] C. Haber, "Microfluidics in commercial applications; an industry perspective," *Lab Chip*, vol. 6, no. 9, pp. 1118–1121, 2006.
- [7] J. Melin and S. R. Quake, "Microfluidic large-scale integration: the evolution of design rules for biological automation.," *Annu. Rev. Biophys. Biomol. Struct.*, vol. 36, pp. 213–231, 2007.
- [8] F. K. Balagaddé, L. You, C. L. Hansen, F. H. Arnold, and S. R. Quake, "Long-term monitoring of bacteria undergoing programmed population control in a microchemostat.," *Science*, vol. 309, pp. 137–140, Jul 2005.
- [9] P. Yager, T. Edwards, E. Fu, K. Helton, K. Nelson, M. R. Tam, and B. H. Weigl, "Microfluidic diagnostic technologies for global public health.," *Nature*, vol. 442, pp. 412–418, Jul 2006.
- [10] A. W. Martinez, S. T. Phillips, and G. M. Whitesides, "Three-dimensional microfluidic devices fabricated in layered paper and tape.," *Proc. Nat. Acad. Sci. U.S.A.*, vol. 105, pp. 19606–19611, Dec 2008.
- [11] H. Song, D. L. Chen, and R. F. Ismagilov, "Reactions in droplets in microfluidic channels.," *Angew. Chem. Int. Ed.*, vol. 45, pp. 7336–7356, Nov 2006.
- [12] A. D. Griffiths and D. S. Tawfik, "Miniaturising the laboratory in emulsion droplets.," *Trends Biotechnol.*, vol. 24, pp. 395–402, Sep 2006.
- [13] A. Huebner, S. Sharma, M. Srisa-Art, F. Hollfelder, J. B. Edel, and A. J. Demello, "Microdroplets: a sea of applications?," *Lab Chip*, vol. 8, pp. 1244–1254, Aug 2008.
- [14] S.-Y. Teh, R. Lin, L.-H. Hung, and A. P. Lee, "Droplet microfluidics.," *Lab Chip*, vol. 8, pp. 198–220, Feb 2008.

- [15] D. S. Tawfik and A. D. Griffiths, "Man-made cell-like compartments for molecular evolution.," *Nat. Biotechnol.*, vol. 16, pp. 652–656, Jul 1998.
- [16] G. F. Christopher and S. L. Anna, "Microfluidic methods for generating continuous droplet streams," *J. Phys. D: Appl. Phys.*, vol. 40, pp. R319–R336, Oct. 2007.
- [17] H. Song, J. D. Tice, and R. F. Ismagilov, "A microfluidic system for controlling reaction networks in time.," *Angew. Chem. Int. Ed.*, vol. 42, pp. 768–772, Feb 2003.
- [18] K. Ahn, J. Agresti, H. Chong, M. Marquez, and D. A. Weitz, "Electrocoalescence of drops synchronized by size-dependent flow in microfluidic channels," *Appl. Phys. Lett.*, vol. 88, p. 264105, June 2006.
- [19] D. R. Link, S. L. Anna, D. A. Weitz, and H. A. Stone, "Geometrically mediated breakup of drops in microfluidic devices.," *Phys. Rev. Lett.*, vol. 92, p. 054503, Feb 2004.
- [20] D. R. Link, E. Grasland-Mongrain, A. Duri, F. Sarrazin, Z. D. Cheng, G. Cristobal, M. Marquez, and D. A. Weitz, "Electric control of droplets in microfluidic devices," *Angew. Chem. Int. Ed.*, vol. 45, no. 16, pp. 2556–2560, 2006.
- [21] K. Ahn, C. Kerbage, T. P. Hunt, R. M. Westervelt, D. R. Link, and D. A. Weitz, "Dielectrophoretic manipulation of drops for high-speed microfluidic sorting devices," *Appl. Phys. Lett.*, vol. 88, p. 024104, Jan. 2006.
- [22] J.-C. Baret, O. J. Miller, V. Taly, M. Ryckelynck, A. El Harrak, L. Frenz, C. Rick, M. L. Samuels, J. B. Hutchison, J. J. Agresti, D. R. Link, D. A. Weitz, and A. D. Griffiths, "Fluorescence-activated droplet sorting (FADS): efficient microfluidic cell sorting based on enzymatic activity.," *Lab Chip*, vol. 9, pp. 1850–1858, 2009.
- [23] C. Holtze, A. C. Rowat, J. J. Agresti, J. B. Hutchison, F. E. Angilè, C. H. J. Schmitz, S. Köster, H. Duan, K. J. Humphry, R. A. Scanga, J. S. Johnson, D. Pisignano, and D. A. Weitz, "Biocompatible surfactants for water-in-fluorocarbon emulsions.," *Lab Chip*, vol. 8, pp. 1632–1639, Oct 2008.
- [24] F. Courtois, L. F. Olguin, G. Whyte, D. Bratton, W. T. S. Huck, C. Abell, and F. Hollfelder, "An integrated device for monitoring time-dependent in vitro expression from single genes in picolitre droplets.," *Chembiochem*, vol. 9, pp. 439–446, Feb 2008.
- [25] F. Courtois, L. F. Olguin, G. Whyte, A. B. Theberge, W. T. S. Huck, F. Hollfelder, and C. Abell, "Controlling the retention of small molecules in emulsion microdroplets for use in cell-based assays," *Anal. Chem.*, vol. 81, no. 0, pp. 3008–3016, 2009.
- [26] H. Song and R. F. Ismagilov, "Millisecond kinetics on a microfluidic chip using nanoliters of reagents.," *J. Am. Chem. Soc.*, vol. 125, pp. 14613–14619, Nov 2003.
- [27] D. R. Link, E. Grasland-Mongrain, A. Duri, F. Sarrazin, Z. Cheng, G. Cristobal, M. Marquez, and D. A. Weitz, "Electric control of droplets in microfluidic devices," *Angew. Chem.*, vol. 118, no. 16, pp. 2618–2622, 2006.
- [28] B. Zheng, J. D. Tice, and R. F. Ismagilov, "Formation of droplets of in microfluidic channels alternating composition and applications to indexing of concentrations in droplet-based assays," *Anal. Chem.*, vol. 76, pp. 4977–4982, Sept. 2004.

- [29] L. H. Hung, K. M. Choi, W. Y. Tseng, Y. C. Tan, K. J. Shea, and A. P. Lee, "Alternating droplet generation and controlled dynamic droplet fusion in microfluidic device for cds nanoparticle synthesis," *Lab Chip*, vol. 6, pp. 174–178, Feb. 2006.
- [30] L. Frenz, A. E. Harrak, M. Pauly, S. Bégin-Colin, A. D. Griffiths, and J.-C. Baret, "Droplet-based microreactors for the synthesis of magnetic iron oxide nanoparticles.," *Angew. Chem. Int. Ed.*, vol. 47, pp. 6817–6820, Jul 2008.
- [31] L. Frenz, J. Blouwolf, A. D. Griffiths, and J.-C. Baret, "Microfluidic production of droplet pairs.," *Langmuir*, vol. 24, pp. 12073–12076, Sep 2008.
- [32] G. I. Taylor, "Dispersion of soluble matter in solvent flowing slowly through a tube," *Proc. R. Soc. London, Ser. A*, vol. 219, pp. 186–203, 1953.
- [33] L. Frenz, K. Blank, E. Brouzes, and A. D. Griffiths, "Reliable microfluidic on-chip incubation of droplets in delay-lines," *Lab Chip*, vol. 9, pp. 1344–1348, 2009.
- [34] N. R. Beer, B. J. Hindson, E. K. Wheeler, S. B. Hall, K. A. Rose, I. M. Kennedy, and B. W. Colston, "On-chip, real-time, single-copy polymerase chain reaction in picoliter droplets.," *Anal. Chem.*, vol. 79, pp. 8471–8475, Nov 2007.
- [35] L. Mazutis, A. F. Araghi, O. J. Miller, J.-C. Baret, L. Frenz, A. Janoshazi, V. Taly, B. J. Miller, J. B. Hutchison, D. Link, A. D. Griffiths, and M. Ryckelynck, "Droplet-based microfluidic systems for high-throughput single dna molecule isothermal amplification and analysis.," *Anal. Chem.*, vol. 81, pp. 4813–4821, Jun 2009.
- [36] P. S. Dittrich and A. Manz, "Lab-on-a-chip: microfluidics in drug discovery," *Nat. Rev. Drug Discovery*, vol. 5, pp. 210–218, Mar. 2006.
- [37] J. Hong, J. B. Edel, and A. J. deMello, "Micro- and nanofluidic systems for high-throughput biological screening.," *Drug Discovery Today*, vol. 14, pp. 134–146, Feb 2009.
- [38] N. Malo, J. A. Hanley, S. Cerquozzi, J. Pelletier, and R. Nadon, "Statistical practice in high-throughput screening data analysis.," *Nat. Biotechnol.*, vol. 24, pp. 167–175, Feb 2006.
- [39] J. Inglese, D. S. Auld, A. Jadhav, R. L. Johnson, A. Simeonov, A. Yasgar, W. Zheng, and C. P. Austin, "Quantitative high-throughput screening: a titration-based approach that efficiently identifies biological activities in large chemical libraries.," *Proc. Nat. Acad. Sci. U.S.A.*, vol. 103, pp. 11473–11478, Aug 2006.
- [40] W. Menz, J. Mohr, and O. Paul, *Microsystem Technology*. Wiley-VCH, 2001.
- [41] H. Lorenz, M. Despont, N. Fahrni, J. Brugger, P. Vettiger, and P. Renaud, "High-aspect-ratio, ultrathick, negative-tone near-uv photoresist and its applications for mems," *Sens. Actuators, A*, vol. 64, no. 1, pp. 33–39, 1998.
- [42] B. Xu, F. Arias, S. T. Brittain, X.-M. Zhao, B. Grzybowski, S. Torquato, and G. M. Whitesides, "Making negative poisson's ratio microstructures by soft lithography," *Adv. Mater.*, vol. 11, no. 14, pp. 1186–1189, 1999.

- [43] Y. N. Xia and G. M. Whitesides, "Soft lithography," *Annu. Rev. Mater. Sci.*, vol. 28, pp. 153–184, 1998.
- [44] M. Eddings, M. Johnson, and B. Gale, "Determining the optimal pdms-pdms bonding technique for microfluidic devices," *J. Micromech Microeng.*, vol. 18, p. 067001, 2008.
- [45] G. M. Whitesides, E. Ostuni, S. Takayama, X. Jiang, and D. E. Ingber, "Soft lithography in biology and biochemistry," *Annu. Rev. Biomed. Eng.*, vol. 3, pp. 335–373, 2001.
- [46] A. C. Siegel, S. S. Shevkoplyas, D. B. Weibel, D. A. Bruzewicz, A. W. Martinez, and G. M. Whitesides, "Cofabrication of electromagnets and microfluidic systems in poly(dimethylsiloxane).," *Angew. Chem. Int. Ed.*, vol. 45, pp. 6877–6882, Oct 2006.
- [47] A. R. Abate, D. Lee, T. Do, C. Holtze, and D. A. Weitz, "Glass coating for pdms microfluidic channels by sol-gel methods.," *Lab Chip*, vol. 8, pp. 516–518, Apr 2008.
- [48] R. W. Johnson, *The Handbook of Fluid Dynamics*. Crc Press, 1998.
- [49] P. A. Tipler and G. P. Mosca, *Physics for Scientists and Engineers*. Palgrave Macmillan, 2007.
- [50] L. M. Fidalgo, G. Whyte, D. Bratton, C. F. Kaminski, C. Abell, and W. T. S. Huck, "From microdroplets to microfluidics: Selective emulsion separation in microfluidic devices.," *Angew. Chem. Int. Ed.*, vol. 47, pp. 2042–2045, Feb 2008.
- [51] C. H. J. Schmitz, A. C. Rowat, S. Köster, and D. A. Weitz, "Dropspots: a picoliter array in a microfluidic device," *Lab Chip*, vol. 9, pp. 44–49, 2009.
- [52] L. M. Fidalgo, G. Whyte, B. T. Ruotolo, J. L. P. Benesch, F. Stengel, C. Abell, C. V. Robinson, and W. T. S. Huck, "Coupling microdroplet microreactors with mass spectrometry: reading the contents of single droplets online.," *Angew Chem Int Ed Engl*, vol. 48, no. 20, pp. 3665–3668, 2009.
- [53] M. J. Fuerstman, P. Garstecki, and G. M. Whitesides, "Coding/decoding and reversibility of droplet trains in microfluidic networks.," *Science*, vol. 315, pp. 828–832, Feb 2007.
- [54] M. Prakash and N. Gershenfeld, "Microfluidic bubble logic.," *Science*, vol. 315, pp. 832–835, Feb 2007.
- [55] Y.-C. Tan, J. S. Fisher, A. I. Lee, V. Cristini, and A. P. Lee, "Design of microfluidic channel geometries for the control of droplet volume, chemical concentration, and sorting.," *Lab Chip*, vol. 4, pp. 292–298, Aug 2004.
- [56] A. Huebner, D. Bratton, G. Whyte, M. Yang, A. J. Demello, C. Abell, and F. Hollfelder, "Static microdroplet arrays: a microfluidic device for droplet trapping, incubation and release for enzymatic and cell-based assays.," *Lab Chip*, vol. 9, pp. 692–698, Mar 2009.
- [57] H. Boukellal, S. Selimovic, Y. Jia, G. Cristobal, and S. Fraden, "Simple, robust storage of drops and fluids in a microfluidic device," *Lab Chip*, vol. 9, pp. 331–338, 2008.
- [58] N. Damean, L. F. Olguin, F. Hollfelder, C. Abell, and W. T. S. Huck, "Simultaneous measurement of reactions in microdroplets filled by concentration gradients.," *Lab Chip*, vol. 9, pp. 1707–1713, Jun 2009.

- [59] A. R. Abate, M. B. Romanowsky, J. J. Agresti, and D. A. Weitz, "Valve-based flow focusing for drop formation," *Appl. Phys. Lett.*, vol. 94, no. 2, p. 023503, 2009.
- [60] A. R. Abate and D. A. Weitz, "Single-layer membrane valves for elastomeric microfluidic devices," *Appl. Phys. Lett.*, vol. 92, no. 24, p. 243509, 2008.
- [61] J. S. Edgar, G. Milne, Y. Zhao, C. P. Pabbati, D. S. W. Lim, and D. T. Chiu, "Compartmentalization of chemically separated components into droplets," *Angew. Chem. Int. Ed.*, vol. 48, no. 15, pp. 2719–2722, 2009.
- [62] T. Thorsen, R. W. Roberts, F. H. Arnold, and S. R. Quake, "Dynamic pattern formation in a vesicle-generating microfluidic device," *Phys. Rev. Lett.*, vol. 86, pp. 4163–4166, Apr. 2001.
- [63] A. M. Gañán-Calvo and J. M. Gordillo, "Perfectly monodisperse microbubbling by capillary flow focusing," *Phys. Rev. Lett.*, vol. 87, pp. 274501–, Dec. 2001.
- [64] P. Garstecki, M. J. Fuerstman, H. A. Stone, and G. M. Whitesides, "Formation of droplets and bubbles in a microfluidic t-junction-scaling and mechanism of break-up," *Lab Chip*, vol. 6, pp. 437–446, Mar 2006.
- [65] S. L. Anna, N. Bontoux, and H. A. Stone, "Formation of dispersions using "flow focusing" in microchannels," *Appl. Phys. Lett.*, vol. 82, pp. 364–366, Jan. 2003.
- [66] V. Mengeaud, J. Josserand, and H. H. Girault, "Mixing processes in a zigzag microchannel: finite element simulations and optical study," *Anal. Chem.*, vol. 74, pp. 4279–4286, Aug 2002.
- [67] R. H. Liu, M. A. Stremler, K. V. Sharp, M. G. Olsen, J. G. Santiago, R. J. Adrian, H. Aref, and D. J. Beebe, "Passive mixing in a three-dimensional serpentine microchannel," *J. Microelectromech. Syst.*, vol. 9, pp. 190–197, 2000.
- [68] A. D. Stroock, S. K. W. Dertinger, A. Ajdari, I. Mezic, H. A. Stone, and G. M. Whitesides, "Chaotic mixer for microchannels," *Science*, vol. 295, pp. 647–651, Jan 2002.
- [69] A. J. DeMello, "Control and detection of chemical reactions in microfluidic systems," *Nature*, vol. 442, pp. 394–402, Jul 2006.
- [70] H. Song, M. R. Bringer, J. D. Tice, C. J. Gerdt, and R. F. Ismagilov, "Experimental test of scaling of mixing by chaotic advection in droplets moving through microfluidic channels," *Appl. Phys. Lett.*, vol. 83, pp. 4664–4666, Dec 2003.
- [71] F. Sarrazin, L. Prat, N. Di Miceli, G. Cristobal, D. R. Link, and D. A. Weitz, "Mixing characterization inside microdroplets engineered on a microcoalescer," *Chem. Eng. J.*, vol. 62, pp. 1042–1048, Feb. 2007.
- [72] K. Handique and M. A. Burns, "Mathematical modeling of drop mixing in a slit-type microchannel," *J. Micromech. Microeng.*, vol. 11, pp. 548–554, Sept. 2001.
- [73] J. D. Tice, H. Song, A. D. Lyon, and R. F. Ismagilov, "Formation of droplets and mixing in multiphase microfluidics at low values of the reynolds and the capillary numbers," *Langmuir*, vol. 19, pp. 9127–9133, 2003.

- [74] D. L. Chen, C. J. Gerdts, and R. F. Ismagilov, "Using microfluidics to observe the effect of mixing on nucleation of protein crystals.," *J. Am. Chem. Soc.*, vol. 127, pp. 9672–9673, Jul 2005.
- [75] H. Small and M. A. Langhorst, "Hydrodynamic chromatography," *Anal. Chem.*, vol. 54, pp. 892A–898A, 1982.
- [76] L. M. Fidalgo, C. Abell, and W. T. S. Huck, "Surface-induced droplet fusion in microfluidic devices.," *Lab Chip*, vol. 7, pp. 984–986, Aug 2007.
- [77] J. S. Eow and M. Ghadiri, "Drop-drop coalescence in an electric field: the effects of applied electric field and electrode geometry," *Colloids Surf., A*, vol. 219, pp. 253–279, 2003.
- [78] S. N. Cohen, A. C. Chang, H. W. Boyer, and R. B. Helling, "Construction of biologically functional bacterial plasmids in vitro.," *Proc. Nat. Acad. Sci. U.S.A.*, vol. 70, pp. 3240–3244, Nov 1973.
- [79] R. K. Saiki, S. Scharf, F. Faloona, K. B. Mullis, G. T. Horn, H. A. Erlich, and N. Arnheim, "Enzymatic amplification of beta-globin genomic sequences and restriction site analysis for diagnosis of sickle cell anemia.," *Science*, vol. 230, pp. 1350–1354, Dec 1985.
- [80] D. Dressman, H. Yan, G. Traverso, K. W. Kinzler, and B. Vogelstein, "Transforming single dna molecules into fluorescent magnetic particles for detection and enumeration of genetic variations.," *Proc. Nat. Acad. Sci. U.S.A.*, vol. 100, pp. 8817–8822, Jul 2003.
- [81] R. Williams, S. G. Peisajovich, O. J. Miller, S. Magdassi, D. S. Tawfik, and A. D. Griffiths, "Amplification of complex gene libraries by emulsion pcr.," *Nat. Methods*, vol. 3, pp. 545–550, Jul 2006.
- [82] E. R. Mardis, "Next-generation dna sequencing methods.," *Annu. Rev. Genomics Hum. Genet.*, vol. 9, pp. 387–402, Jun 2008.
- [83] F. Diehl, M. Li, Y. He, K. W. Kinzler, B. Vogelstein, and D. Dressman, "Beaming: single-molecule pcr on microparticles in water-in-oil emulsions.," *Nat. Methods*, vol. 3, pp. 551–559, Jul 2006.
- [84] M. Li, F. Diehl, D. Dressman, B. Vogelstein, and K. W. Kinzler, "Beaming up for detection and quantification of rare sequence variants.," *Nat. Methods*, vol. 3, pp. 95–97, Feb 2006.
- [85] F. Diehl, M. Li, D. Dressman, Y. He, D. Shen, S. Szabo, L. A. Diaz, S. N. Goodman, K. A. David, H. Juhl, K. W. Kinzler, and B. Vogelstein, "Detection and quantification of mutations in the plasma of patients with colorectal tumors.," *Proc. Nat. Acad. Sci. U.S.A.*, vol. 102, pp. 16368–16373, Nov 2005.
- [86] T. Kojima, Y. Takei, M. Ohtsuka, Y. Kawarasaki, T. Yamane, and H. Nakano, "Pcr amplification from single dna molecules on magnetic beads in emulsion: application for high-throughput screening of transcription factor targets.," *Nucleic Acids Res.*, vol. 33, no. 17, p. e150, 2005.
- [87] F. J. Ghadessy, J. L. Ong, and P. Holliger, "Directed evolution of polymerase function by compartmentalized self-replication.," *Proc. Nat. Acad. Sci. U.S.A.*, vol. 98, pp. 4552–4557, Apr 2001.
- [88] F. J. Ghadessy, N. Ramsay, F. Boudsocq, D. Loakes, A. Brown, S. Iwai, A. Vaisman, R. Woodgate, and P. Holliger, "Generic expansion of the substrate spectrum of a dna polymerase by directed evolution.," *Nat. Biotechnol.*, vol. 22, pp. 755–759, Jun 2004.

- [89] M. Nakano, N. Nakai, H. Kurita, J. Komatsu, K. Takashima, S. Katsura, and A. Mizuno, "Single-molecule reverse transcription polymerase chain reaction using water-in-oil emulsion.," *J. Biosci. Bioeng.*, vol. 99, pp. 293–295, Mar 2005.
- [90] J. G. Wetmur, M. Kumar, L. Zhang, C. Palomeque, S. Wallenstein, and J. Chen, "Molecular haplotyping by linking emulsion pcr: analysis of paraoxonase 1 haplotypes and phenotypes.," *Nucleic Acids Res.*, vol. 33, no. 8, pp. 2615–2619, 2005.
- [91] P. Kumaresan, C. J. Yang, S. A. Cronier, R. G. Blazej, and R. A. Mathies, "High-throughput single copy dna amplification and cell analysis in engineered nanoliter droplets.," *Anal. Chem.*, vol. 80, pp. 3522–3529, May 2008.
- [92] M. Chabert, K. D. Dorfman, P. de Cremoux, J. Roeraade, and J. L. Viovy, "Automated microdroplet platform for sample manipulation and polymerase chain reaction.," *Anal. Chem.*, vol. 78, pp. 7722–7728, Nov. 2006.
- [93] N. R. Beer, E. K. Wheeler, L. Lee-Houghton, N. Watkins, S. Nasarabadi, N. Hebert, P. Leung, D. W. Arnold, C. G. Bailey, and B. W. Colston, "On-chip single-copy real-time reverse-transcription pcr in isolated picoliter droplets.," *Anal. Chem.*, vol. 80, pp. 1854–1858, Mar. 2008.
- [94] M. M. Kiss, L. Ortoleva-Donnelly, N. R. Beer, J. Warner, C. G. Bailey, B. W. Colston, J. M. Rothberg, D. R. Link, and J. H. Leamon, "High-throughput quantitative polymerase chain reaction in picoliter droplets.," *Anal. Chem.*, vol. 80, pp. 8975–8981, Dec 2008.
- [95] Y. Schaeferli, R. C. Wootton, T. Robinson, V. Stein, C. Dunsby, M. A. A. Neil, P. M. W. French, A. J. Demello, C. Abell, and F. Hollfelder, "Continuous-flow polymerase chain reaction of single-copy dna in microfluidic microdroplets.," *Anal. Chem.*, vol. 81, pp. 302–306, Jan 2009.
- [96] B. Vogelstein and K. W. Kinzler, "Digital pcr.," *Proc. Nat. Acad. Sci. U.S.A.*, vol. 96, pp. 9236–9241, Aug 1999.
- [97] E. A. Ottesen, J. W. Hong, S. R. Quake, and J. R. Leadbetter, "Microfluidic digital pcr enables multigene analysis of individual environmental bacteria.," *Science*, vol. 314, pp. 1464–1467, Dec 2006.
- [98] P. Gill and A. Ghaemi, "Nucleic acid isothermal amplification technologies: a review.," *Nucleosides Nucleotides Nucleic Acids*, vol. 27, pp. 224–243, Mar 2008.
- [99] M. Margulies, M. Egholm, W. E. Altman, S. Attiya, J. S. Bader, L. A. Bemben, J. Berka, M. S. Braverman, Y.-J. Chen, Z. Chen, S. B. Dewell, L. Du, J. M. Fierro, X. V. Gomes, B. C. Godwin, W. He, S. Helgesen, C. H. Ho, C. H. Ho, G. P. Irzyk, S. C. Jando, M. L. I. Alenquer, T. P. Jarvie, K. B. Jirage, J.-B. Kim, J. R. Knight, J. R. Lanza, J. H. Leamon, S. M. Lefkowitz, M. Lei, J. Li, K. L. Lohman, H. Lu, V. B. Makhijani, K. E. McDade, M. P. McKenna, E. W. Myers, E. Nickerson, J. R. Nobile, R. Plant, B. P. Puc, M. T. Ronan, G. T. Roth, G. J. Sarkis, J. F. Simons, J. W. Simpson, M. Srinivasan, K. R. Tartaro, A. Tomasz, K. A. Vogt, G. A. Volkmer, S. H. Wang, Y. Wang, M. P. Weiner, P. Yu, R. F. Begley, and J. M. Rothberg, "Genome sequencing in microfabricated high-density picolitre reactors.," *Nature*, vol. 437, pp. 376–380, Sep 2005.

- [100] J. Shendure, G. J. Porreca, N. B. Reppas, X. Lin, J. P. McCutcheon, A. M. Rosenbaum, M. D. Wang, K. Zhang, R. D. Mitra, and G. M. Church, "Accurate multiplex polony sequencing of an evolved bacterial genome.," *Science*, vol. 309, pp. 1728–1732, Sep 2005.
- [101] J. Shendure and H. Ji, "Next-generation dna sequencing.," *Nat. Biotechnol.*, vol. 26, pp. 1135–1145, Oct 2008.
- [102] <http://www.raindancetechnologies.com>.
- [103] V. Stein, I. Sielaff, K. Johnsson, and F. Hollfelder, "A covalent chemical genotype-phenotype linkage for in vitro protein evolution.," *Chembiochem*, vol. 8, pp. 2191–2194, Dec 2007.
- [104] H. Leemhuis, V. Stein, A. D. Griffiths, and F. Hollfelder, "New genotype-phenotype linkages for directed evolution of functional proteins.," *Curr. Opin. Struct. Biol.*, vol. 15, pp. 472–478, Aug 2005.
- [105] H. Lin and V. W. Cornish, "Screening and selection methods for large-scale analysis of protein function.," *Angew. Chem. Int. Ed.*, vol. 41, pp. 4402–4425, Dec 2002.
- [106] S. Becker, H.-U. Schmoldt, T. M. Adams, S. Wilhelm, and H. Kolmar, "Ultra-high-throughput screening based on cell-surface display and fluorescence-activated cell sorting for the identification of novel biocatalysts.," *Curr. Opin. Biotechnol.*, vol. 15, pp. 323–329, Aug 2004.
- [107] H. R. Hoogenboom, "Overview of antibody phage-display technology and its applications.," *Methods Mol. Biol.*, vol. 178, pp. 1–37, 2002.
- [108] S. S. Sidhu, H. B. Lowman, B. C. Cunningham, and J. A. Wells, "Phage display for selection of novel binding peptides.," *Methods Enzymol.*, vol. 328, pp. 333–363, 2000.
- [109] A. Aharoni, A. D. Griffiths, and D. S. Tawfik, "High-throughput screens and selections of enzyme-encoding genes.," *Curr. Opin. Chem. Biol.*, vol. 9, pp. 210–216, Apr 2005.
- [110] J. Hanes, L. Jermutus, and A. Plückthun, "Selecting and evolving functional proteins in vitro by ribosome display.," *Methods Enzymol.*, vol. 328, pp. 404–430, 2000.
- [111] F. Katzen, G. Chang, and W. Kudlicki, "The past, present and future of cell-free protein synthesis.," *Trends Biotechnol.*, vol. 23, pp. 150–156, Mar 2005.
- [112] A. C. Forster, V. W. Cornish, and S. C. Blacklow, "Pure translation display.," *Anal. Biochem.*, vol. 333, pp. 358–364, Oct 2004.
- [113] R. translation system on World Wide Web URL: <http://www.roche-applied-science.com/sis/proteinexpression/>.
- [114] D. H. Davies, X. Liang, J. E. Hernandez, A. Randall, S. Hirst, Y. Mu, K. M. Romero, T. T. Nguyen, M. Kalantari-Dehaghi, S. Crotty, P. Baldi, L. P. Villarreal, and P. L. Felgner, "Profiling the humoral immune response to infection by using proteome microarrays: high-throughput vaccine and diagnostic antigen discovery.," *Proc. Nat. Acad. Sci. U.S.A.*, vol. 102, pp. 547–552, Jan 2005.
- [115] B. T. Kelly, J.-C. Baret, V. Taly, and A. D. Griffiths, "Miniaturizing chemistry and biology in microdroplets.," *Chem. Commun.*, pp. 1773–1788, May 2007.

- [116] V. Taly, B. T. Kelly, and A. D. Griffiths, "Droplets as microreactors for high-throughput biology.," *Chem-biochem*, vol. 8, pp. 263–272, Jan 2007.
- [117] M. d'Abbadie, M. Hofreiter, A. Vaisman, D. Loakes, D. Gasparutto, J. Cadet, R. Woodgate, S. Pääbo, and P. Holliger, "Molecular breeding of polymerases for amplification of ancient dna.," *Nat. Biotechnol.*, vol. 25, pp. 939–943, Aug 2007.
- [118] J. J. Agresti, B. T. Kelly, A. Jäschke, and A. D. Griffiths, "Selection of ribozymes that catalyse multiple-turnover diels-alder cycloadditions by using in vitro compartmentalization.," *Proc. Nat. Acad. Sci. U.S.A.*, vol. 102, pp. 16170–16175, Nov 2005.
- [119] N. Doi and H. Yanagawa, "Stable: protein-dna fusion system for screening of combinatorial protein libraries in vitro.," *FEBS Lett.*, vol. 457, pp. 227–230, Aug 1999.
- [120] J. Bertschinger and D. Neri, "Covalent dna display as a novel tool for directed evolution of proteins in vitro.," *Protein Eng. Des. Sel.*, vol. 17, pp. 699–707, Sep 2004.
- [121] K. Bernath, M. Hai, E. Mastrobattista, A. D. Griffiths, S. Magdassi, and D. S. Tawfik, "In vitro compartmentalization by double emulsions: sorting and gene enrichment by fluorescence activated cell sorting.," *Anal. Biochem.*, vol. 325, pp. 151–157, Feb 2004.
- [122] E. Mastrobattista, V. Taly, E. Chanudet, P. Treacy, B. T. Kelly, and A. D. Griffiths, "High-throughput screening of enzyme libraries: in vitro evolution of a beta-galactosidase by fluorescence-activated sorting of double emulsions.," *Chem. Biol.*, vol. 12, pp. 1291–1300, Dec 2005.
- [123] A. Aharoni, G. Amitai, K. Bernath, S. Magdassi, and D. S. Tawfik, "High-throughput screening of enzyme libraries: thiolactonases evolved by fluorescence-activated sorting of single cells in emulsion compartments.," *Chem. Biol.*, vol. 12, pp. 1281–1289, Dec 2005.
- [124] A. Sepp, D. S. Tawfik, and A. D. Griffiths, "Microbead display by in vitro compartmentalisation: selection for binding using flow cytometry.," *FEBS Lett.*, vol. 532, pp. 455–458, Dec 2002.
- [125] A. D. Griffiths and D. S. Tawfik, "Directed evolution of an extremely fast phosphotriesterase by in vitro compartmentalization.," *EMBO J.*, vol. 22, pp. 24–35, Jan 2003.
- [126] R. Gan, Y. Yamanaka, T. Kojima, and H. Nakano, "Microbeads display of proteins using emulsion pcr and cell-free protein synthesis.," *Biotechnol. Progr.*, vol. 24, no. 5, pp. 1107–1114, 2008.
- [127] J. J. Agresti, E. Antipov, A. Abate, K. Ahn, A. Rowat, J.-C. Baret, M. Marquez, A. D. Klivanov, A. D. Griffiths, and D. A. Weitz, "Ultra-high-throughput screening in droplet-based microfluidics for directed evolution of peroxidases.," p. Submitted, 2009.
- [128] H. N. Joensson, M. L. Samuels, E. R. Brouzes, M. Medkova, M. Uhlén, D. R. Link, and H. Andersson-Svahn, "Detection and analysis of low-abundance cell-surface biomarkers using enzymatic amplification in microfluidic droplets.," *Angew. Chem. Int. Ed.*, vol. 48, no. 14, pp. 2518–2521, 2009.
- [129] M. Toner and D. Irimia, "Blood-on-a-chip.," *Annu. Rev. Biomed. Eng.*, vol. 7, pp. 77–103, 2005.

- [130] A. W. Martinez, S. T. Phillips, E. Carrilho, S. W. Thomas, H. Sindi, and G. M. Whitesides, "Simple telemedicine for developing regions: camera phones and paper-based microfluidic devices for real-time, off-site diagnosis.," *Anal. Chem.*, vol. 80, pp. 3699–3707, May 2008.
- [131] E. Carrilho, S. T. Phillips, S. J. Vella, A. W. Martinez, and G. M. Whitesides, "Paper microzone plates.," *Anal. Chem.*, vol. 81, pp. 5990–5998, Jul 2009.
- [132] A. K. Ellerbee, S. T. Phillips, A. C. Siegel, K. A. Mirica, A. W. Martinez, P. Striehl, N. Jain, M. Prentiss, and G. M. Whitesides, "Quantifying colorimetric assays in paper-based microfluidic devices by measuring the transmission of light through paper.," *Anal. Chem.*, Sep 2009.
- [133] S. Haerberle, R. Zengerle, and J. Ducree, "Centrifugal generation and manipulation of droplet emulsions.," *Microfluid. Nanofluid.*, vol. 3, pp. 65–75, 2006.
- [134] Y. Zhang, V. Bailey, C. M. Puleo, H. Easwaran, E. Griffiths, J. G. Herman, S. B. Baylin, and T.-H. Wang, "Dna methylation analysis on a droplet-in-oil pcr array.," *Lab Chip*, vol. 9, pp. 1059–1064, Apr 2009.
- [135] M. Chabert and J.-L. Viovy, "Microfluidic high-throughput encapsulation and hydrodynamic self-sorting of single cells.," *Proc. Nat. Acad. Sci. U.S.A.*, vol. 105, no. 9, pp. 3191–3196, 2008.
- [136] J. Q. Boedicker, L. Li, T. R. Kline, and R. F. Ismagilov, "Detecting bacteria and determining their susceptibility to antibiotics by stochastic confinement in nanoliter droplets using plug-based microfluidics.," *Lab Chip*, vol. 8, pp. 1265–1272, Aug 2008.
- [137] J. Clausell-Tormos, D. Lieber, J.-C. Baret, A. El-Harrak, O. J. Miller, L. Frenz, J. Blouwolff, K. J. Humphry, S. Köster, H. Duan, C. Holtze, D. A. Weitz, A. D. Griffiths, and C. A. Merten, "Droplet-based microfluidic platforms for the encapsulation and screening of mammalian cells and multicellular organisms.," *Chem. Biol.*, vol. 15, pp. 427–437, May 2008.
- [138] E. Brouzes, M. Medkova, N. Savenelli, D. Marran, M. Twardowski, J. B. Hutchison, J. M. Rothberg, D. R. Link, N. Perrimon, and M. L. Samuels, "Droplet microfluidic technology for single-cell high-throughput screening.," *Proc. Nat. Acad. Sci. U.S.A.*, 2009.
- [139] J. F. Edd, D. D. Carlo, K. J. Humphry, S. Koster, D. Irimia, D. A. Weitz, and M. Toner, "Controlled encapsulation of single-cells into monodisperse picolitre drops.," *Lab Chip*, vol. 8, pp. 1262–1264, 2008.
- [140] T. Beatus, T. Tlusty, and R. Bar-Ziv, "Phonons in a one-dimensional microfluidic crystal," *Nat. Phys.*, vol. 2, pp. 743–748, Nov. 2006.
- [141] M. Srisa-Art, D.-K. Kang, J. Hong, H. Park, R. J. Leatherbarrow, J. B. Edel, S.-I. Chang, and A. J. deMello, "Analysis of protein-protein interactions by using droplet-based microfluidics.," *Chembiochem*, vol. 10, pp. 1605–1611, Jul 2009.
- [142] S. Fields and O. Song, "A novel genetic system to detect protein-protein interactions.," *Nature*, vol. 340, pp. 245–246, Jul 1989.
- [143] G. Rigaut, A. Shevchenko, B. Rutz, M. Wilm, M. Mann, and B. Séraphin, "A generic protein purification method for protein complex characterization and proteome exploration.," *Nat. Biotechnol.*, vol. 17, pp. 1030–1032, Oct 1999.

References

- [144] P. Mathonet, "Compartmentalised selection of protein-protein interactions using a split-protein sensor," final report, University of Cambridge, 2006.
- [145] M. L. Bulyk, E. Gentalen, D. J. Lockhart, and G. M. Church, "Quantifying dna-protein interactions by double-stranded dna arrays.," *Nat. Biotechnol.*, vol. 17, pp. 573–577, Jun 1999.
- [146] G. MacBeath, A. N. Koehler, and S. L. Schreiber, "Printing small molecules as microarrays and detecting protein-ligand interactions en masse," *J. Am. Chem. Soc.*, vol. 121, pp. 7967–7968, 1999.
- [147] U. B. Nielsen, M. H. Cardone, A. J. Sinskey, G. MacBeath, and P. K. Sorger, "Profiling receptor tyrosine kinase activation by using ab microarrays.," *Proc. Nat. Acad. Sci. U.S.A.*, vol. 100, pp. 9330–9335, Aug 2003.
- [148] H. Zhu, J. F. Klemic, S. Chang, P. Bertone, A. Casamayor, K. G. Klemic, D. Smith, M. Gerstein, M. A. Reed, and M. Snyder, "Analysis of yeast protein kinases using protein chips.," *Nat. Genet.*, vol. 26, pp. 283–289, Nov 2000.
- [149] H. Zhu, M. Bilgin, R. Bangham, D. Hall, A. Casamayor, P. Bertone, N. Lan, R. Jansen, S. Bidlingmaier, T. Houfek, T. Mitchell, P. Miller, R. A. Dean, M. Gerstein, and M. Snyder, "Global analysis of protein activities using proteome chips.," *Science*, vol. 293, pp. 2101–2105, Sep 2001.
- [150] J. Ziauddin and D. M. Sabatini, "Microarrays of cells expressing defined cdnas.," *Nature*, vol. 411, pp. 107–110, May 2001.
- [151] M. F. Templin, D. Stoll, M. Schrenk, P. C. Traub, C. F. Vöhringer, and T. O. Joos, "Protein microarray technology.," *Trends Biotechnol.*, vol. 20, pp. 160–166, Apr 2002.
- [152] M. Srisa-Art, E. C. Dyson, A. J. deMello, and J. B. Edel, "Monitoring of real-time streptavidin-biotin binding kinetics using droplet microfluidics.," *Anal. Chem.*, vol. 80, pp. 7063–7067, Sep 2008.
- [153] J. R. Porter, C. I. Stains, B. W. Jester, and I. Ghosh, "A general and rapid cell-free approach for the interrogation of protein-protein, protein-dna, and protein-rna interactions and their antagonists utilizing split-protein reporters.," *J. Am. Chem. Soc.*, vol. 130, pp. 6488–6497, May 2008.
- [154] S. W. Michnick, "Protein fragment complementation strategies for biochemical network mapping.," *Curr. Opin. Biotechnol.*, vol. 14, pp. 610–617, Dec 2003.
- [155] N. Johnsson and K. Johnsson, "A fusion of disciplines: chemical approaches to exploit fusion proteins for functional genomics.," *Chembiochem*, vol. 4, pp. 803–810, Sep 2003.
- [156] F. Rossi, C. A. Charlton, and H. M. Blau, "Monitoring protein-protein interactions in intact eukaryotic cells by beta-galactosidase complementation.," *Proc. Nat. Acad. Sci. U.S.A.*, vol. 94, pp. 8405–8410, Aug 1997.
- [157] I. Remy and S. W. Michnick, "Clonal selection and in vivo quantitation of protein interactions with protein-fragment complementation assays.," *Proc. Nat. Acad. Sci. U.S.A.*, vol. 96, pp. 5394–5399, May 1999.

- [158] A. Galarneau, M. Primeau, L.-E. Trudeau, and S. W. Michnick, "Beta-lactamase protein fragment complementation assays as in vivo and in vitro sensors of protein protein interactions.," *Nat. Biotechnol.*, vol. 20, pp. 619–622, Jun 2002.
- [159] T. Wehrman, B. Kleaveland, J.-H. Her, R. F. Balint, and H. M. Blau, "Protein-protein interactions monitored in mammalian cells via complementation of beta -lactamase enzyme fragments.," *Proc. Nat. Acad. Sci. U.S.A.*, vol. 99, pp. 3469–3474, Mar 2002.
- [160] C.-D. Hu, Y. Chinenov, and T. K. Kerppola, "Visualization of interactions among bzip and rel family proteins in living cells using bimolecular fluorescence complementation.," *Mol. Cell*, vol. 9, pp. 789–798, 2002.
- [161] I. Remy and S. W. Michnick, "A cDNA library functional screening strategy based on fluorescent protein complementation assays to identify novel components of signaling pathways.," *Methods*, vol. 32, pp. 381–388, Apr 2004.
- [162] Y. C. Tan and A. P. Lee, "Microfluidic separation of satellite droplets as the basis of a monodispersed micron and submicron emulsification system," *Lab Chip*, vol. 5, no. 10, pp. 1178–1183, 2005.
- [163] Y. C. Tan, Y. L. Ho, and A. P. Lee, "Microfluidic sorting of droplets by size," *Microfluid. Nanofluid.*, vol. 4, pp. 343–348, Apr. 2008.
- [164] M. Yamada, M. Nakashima, and M. Seki, "Pinched flow fractionation: Continuous size separation of particles utilizing a laminar flow profile in a pinched microchannel," *Anal. Chem.*, vol. 76, pp. 5465–5471, Sept. 2004.
- [165] J. Takagi, M. Yamada, M. Yasuda, and M. Seki, "Continuous particle separation in a microchannel having asymmetrically arranged multiple branches," *Lab Chip*, vol. 5, no. 7, pp. 778–784, 2005.
- [166] Y. Sai, M. Yamada, M. Yasuda, and M. Seki, "Continuous separation of particles using a microfluidic device equipped with flow rate control valves," *J. Chromatogr. A*, vol. 1127, pp. 214–220, Sept. 2006.
- [167] H. Maenaka, M. Yamada, M. Yasuda, and M. Seki, "Continuous and size-dependent sorting of emulsion droplets using hydrodynamics in pinched microchannels.," *Langmuir*, vol. 24, pp. 4405–4410, Apr 2008.
- [168] S. Krishnadasan, R. J. C. Brown, A. J. Demello, and J. C. Demello, "Intelligent routes to the controlled synthesis of nanoparticles.," *Lab Chip*, vol. 7, pp. 1434–1441, Nov 2007.
- [169] L. H. Hung and A. P. Lee, "Microfluidic devices for the synthesis of nanoparticles and biomaterials," *J. Med. Biol. Eng.*, vol. 27, no. 1, pp. 1–6, 2007.
- [170] A. A. Hassan, O. Sandre, V. Cabuil, and P. Tabeling, "Synthesis of iron oxide nanoparticles in a microfluidic device: preliminary results in a coaxial flow millichannel.," *Chem. Commun.*, pp. 1783–1785, Apr 2008.
- [171] G. Reiss and A. Hutten, "Magnetic nanoparticles - applications beyond data storage," *Nat. Mater.*, vol. 4, pp. 725–726, Oct. 2005.
- [172] S. Mornet, S. Vasseur, F. Grasset, and E. Duguet, "Magnetic nanoparticle design for medical diagnosis and therapy," *J. Mater. Chem.*, vol. 14, no. 14, pp. 2161–2175, 2004.

- [173] A.-H. Lu, E. Salabas, and F. Schüth, "Magnetic nanoparticles: Synthesis, protection, functionalization, and application," *Angew. Chem.*, vol. 119, pp. 1242–1266; *Angew. Chem. Int. Ed.* **2007**, *46*, 1222–1244 (and References therein), 2007.
- [174] T. J. Daou, G. Pourroy, S. Begin-Colin, J. M. Greneche, C. Ulhaq-Bouillet, P. Legare, P. Bernhardt, C. Leuvrey, and G. Rogez, "Hydrothermal synthesis of monodisperse magnetite nanoparticles," *Chem. Mater.*, vol. 18, pp. 4399–4404, Sept. 2006.
- [175] H. Song, J. D. Tice, and R. F. Ismagilov, "A microfluidic system for controlling reaction networks in time," *Angew. Chem.*, vol. 115, no. 7, pp. 792–796, 2003.
- [176] H. Song, D. L. Chen, and R. F. Ismagilov, "Reaktionen in mikrofluidiktröpfchen," *Angew. Chem.*, vol. 118, no. 44, pp. 7494–7516, 2006.
- [177] E. Rio, A. Daerr, B. Andreotti, and L. Limat, "Boundary conditions in the vicinity of a dynamic contact line: experimental investigation of viscous drops sliding down an inclined plane.," *Phys. Rev. Lett.*, vol. 94, p. 024503, Jan 2005.
- [178] N. Brémond, A. Thiam, and J. Bibette, "Decompressing emulsion droplets favors coalescence," *Phys. Rev. Lett.*, vol. 100, no. 2, p. 024501, 2008.
- [179] I. Shestopalov, J. D. Tice, and R. F. Ismagilov, "Multi-step synthesis of nanoparticles performed on millisecond time scale in a microfluidic droplet-based system.," *Lab Chip*, vol. 4, pp. 316–321, Aug 2004.
- [180] A. C. Siegel, S. S. Shevkoplyas, D. B. Weibel, D. A. Bruzewicz, A. W. Martinez, and G. M. Whitesides, "Cofabrication of electromagnets and microfluidic systems in poly(dimethylsiloxane)," *Angew. Chem.*, vol. 118, no. 41, pp. 7031–7036, 2006.
- [181] K. P. Johnston, K. Harrison, M. Clarke, S. Howdle, M. Heitz, F. Bright, C. Carlier, and T. W. Randolph, "Water in carbon dioxide micro-emulsions: an environment for hydrophiles including proteins," *Science*, vol. 271, p. 624, 1996.
- [182] F. X. Gu, R. Karnik, A. Z. Wang, F. Alexis, E. Levy-Nissenbaum, S. Hong, R. S. Langer, and O. C. Farokhzad, "Targeted nanoparticles for cancer therapy," *Nano Today*, vol. 2, pp. 14–21, June 2007.
- [183] P. Garstecki, H. A. Stone, and G. M. Whitesides, "Mechanism for flow-rate controlled breakup in confined geometries: a route to monodisperse emulsions.," *Phys. Rev. Lett.*, vol. 94, p. 164501, Apr 2005.
- [184] C. Priest, S. Herminghaus, and R. Seemann, "Controlled electrocoalescence in microfluidics: Targeting a single lamella," *Appl. Phys. Lett.*, vol. 89, p. 134101, 2006.
- [185] T. Nisisako and T. Torii, "Microfluidic large-scale integration on a chip for mass production of monodisperse droplets and particles.," *Lab Chip*, vol. 8, pp. 287–293, Feb 2008.
- [186] D. Weaire and W. Drenckhan, "Structure and dynamics of confined foams: a review of recent progress.," *Adv. Colloid Interface Sci.*, vol. 137, pp. 20–26, Feb 2008.
- [187] M. Chabert, K. D. Dorfman, and J. L. Viovy, "Droplet fusion by alternating current (ac) field electrocoalescence in microchannels," *Electrophoresis*, vol. 26, pp. 3706–3715, Oct. 2005.

- [188] T. Henkel, T. Bermig, M. Kielpinski, A. Grodrian, J. Metze, and J. M. Kohler, "Chip modules for generation and manipulation of fluid segments for micro serial flow processes," *Chem. Eng. J.*, vol. 101, pp. 439–445, Aug. 2004.
- [189] V. Barbier, H. Willaime, P. Tabeling, and F. Jousse, "Producing droplets in parallel microfluidic systems," *Phys. Rev. E*, vol. 74, p. 046306, Oct. 2006.
- [190] M. J. Fuerstman, A. Lai, M. E. Thurlow, S. S. Shevkoplyas, H. A. Stone, and G. M. Whitesides, "The pressure drop along rectangular microchannels containing bubbles.," *Lab Chip*, vol. 7, pp. 1479–1489, Nov 2007.
- [191] M. T. Sullivan and H. A. Stone, "The role of feedback in microfluidic flow-focusing devices.," *Philos Transact A: Math Phys Eng Sci*, vol. 366, pp. 2131–2143, Jun 2008.
- [192] B. Zheng, L. S. Roach, and R. F. Ismagilov, "Screening of protein crystallization conditions on a microfluidic chip using nanoliter-size droplets.," *J. Am. Chem. Soc.*, vol. 125, pp. 11170–11171, Sep 2003.
- [193] S. Köster, F. E. Angilè, H. Duan, J. J. Agresti, A. Wintner, C. Schmitz, A. C. Rowat, C. A. Merten, D. Pisignano, A. D. Griffiths, and D. A. Weitz, "Drop-based microfluidic devices for encapsulation of single cells.," *Lab Chip*, vol. 8, pp. 1110–1115, Jul 2008.
- [194] S. Xu, Z. Nie, M. Seo, P. Lewis, E. Kumacheva, H. A. Stone, P. Garstecki, D. B. Weibel, I. Gitlin, and G. M. Whitesides, "Generation of monodisperse particles by using microfluidics: control over size, shape, and composition.," *Angew. Chem. Int. Ed.*, vol. 44, pp. 724–728, Jan 2005.
- [195] T. Hatakeyama, D. L. Chen, and R. F. Ismagilov, "Microgram-scale testing of reaction conditions in solution using nanoliter plugs in microfluidics with detection by maldi-ms.," *J. Am. Chem. Soc.*, vol. 128, pp. 2518–2519, Mar 2006.
- [196] Z. T. Cygan, J. T. Cabral, K. L. Beers, and E. J. Amis, "Microfluidic platform for the generation of organic-phase microreactors.," *Langmuir*, vol. 21, pp. 3629–3634, Apr 2005.
- [197] A. Huebner, L. F. Olguin, D. Bratton, G. Whyte, W. T. S. Huck, A. J. de Mello, J. B. Edel, C. Abell, and F. Hollfelder, "Development of quantitative cell-based enzyme assays in microdroplets.," *Anal. Chem.*, vol. 80, pp. 3890–3896, May 2008.
- [198] J. R. Anderson, D. T. Chiu, R. J. Jackman, O. Cherniavskaya, J. C. McDonald, H. Wu, S. H. Whitesides, and G. M. Whitesides, "Fabrication of topologically complex three-dimensional microfluidic systems in pdms by rapid prototyping.," *Anal. Chem.*, vol. 72, pp. 3158–3164, Jul 2000.
- [199] A. Krebber, S. Bornhauser, J. Burmester, A. Honegger, J. Willuda, H. R. Bosshard, and A. Plückthun, "Reliable cloning of functional antibody variable domains from hybridomas and spleen cell repertoires employing a reengineered phage display system.," *J. Immunol. Methods*, vol. 201, pp. 35–55, Feb 1997.
- [200] M. Hashimoto, J. Feng, R. L. York, A. K. Ellerbee, G. Morrison, S. W. Thomas, L. Mahadevan, and G. M. Whitesides, "Infochemistry: encoding information as optical pulses using droplets in a microfluidic device.," *J Am Chem Soc*, vol. 131, pp. 12420–12429, Sep 2009.
- [201] A. Dove, "Drug screening—beyond the bottleneck.," *Nat. Biotechnol.*, vol. 17, pp. 859–863, Sep 1999.

References

- [202] A. V. Hill, "The possible effects of the aggregation of the molecules of haemoglobin on its dissociation curves.," *J. Physiol. (London)*, vol. 40, pp. 4–7, 1910.
- [203] A. Yasgar, P. Shinn, A. Jadhav, D. Auld, S. Michael, W. Zheng, C. P. Austin, J. Inglese, and A. Simeonov, "Compound management for quantitative high-throughput screening.," *JALA*, vol. 13, pp. 79–89, Apr 2008.
- [204] K. Lee, C. Kim, B. Ahn, R. Panchapakesan, A. R. Full, L. Nordee, J. Y. Kang, and K. W. Oh, "Generalized serial dilution module for monotonic and arbitrary microfluidic gradient generators," *Lab Chip*, vol. 9, pp. 709–717, 2009.
- [205] K. Hattori, S. Sugiura, and T. Kanamori, "Generation of arbitrary monotonic concentration profiles by a serial dilution microfluidic network composed of microchannels with a high fluidic-resistance ratio," *Lab Chip*, p. online, 2009.

Acknowledgement

First of all I would like to thank all of the people who helped me during the past 3 years - of course I am very thankful for all the scientific help, but especially I would like to acknowledge those who helped making life as a PhD student, still an enjoyable life.

Very special thanks in this sense go to Andrew Griffiths. You were a great supervisor, gave me so many opportunities and helped throughout the whole time. I appreciate that you always welcomed people to come and see you in your office, even though the group got so large by now and work was probably overwhelming - well, probably not only your desk. I really learned a lot and thank you for always being so patient and helpful with me.

I acknowledge the receipt of the Marie Curie Research Training Network 'ProSA' fellowship. It allowed me to get a feeling for things happening outside the lab and Strasbourg. It broadened my view in any sense. The meetings with the other network members were always extremely instructional and I greatly acknowledge the generous funding allowing me to meet and interact with so many people on conferences and other meetings.

Thank you also to Prof. Whitesides and his group to host me for half a year and giving me the opportunity for a very special time in Boston.

Then I am very grateful for Isabelle and before that Sylvie, our secretaries. It is amazing how much work and time you spend to help everyone in the lab. During the entire time, I think, I never heard a "no, I won't/can't help you with this". I am truly thankful for everything and even talking French wasn't always that bad.

Furthermore, I would like to thank the people working most closely with me. Kerstin, I still think the project we did together, was the one I enjoyed most during this entire time, and it was great how perfect we interacted here. But of course also thanks for all the other discussions, the advices and the many gossip!! Abdes, I also want to thank you for your help and the effort in the nanoparticle time, but also for just always knowing everything what people could possibly ask you. Michael, your knowledge and enthusiasm for the biology and especially your crazy RNA world is quite fascinating - one day we will also find a solution to your circle problem. Thank you also for all the help with the thesis and the biological discussions. Many thanks also to Oli. It was always inspiring talking to you

and I still believe we somehow have a very similar way of thinking and logic. Also very important were people as JC, Agnes, Christoph, Thomas M., Eric, Josh, Matthias P. and Sylvie Bégin-Colin - thank you for the help on the different projects.

Many thanks also to all the other members of the lab. I don't want to talk so much about the science any more, instead I would like to emphasize the many nice things we had also next to work (of course I have to mention and thank Lucia in this context). Thanks for the lunches we had, the many BBQs, the restaurant evenings, the Europapark, the marché Noël, all the little trips and events and of course I also have to mention our 'secret' counter-strike evenings in the microfluidics. Too bad some of the most eager slaves had to leave in the end. Thanks to all of you: Ali, Antoine, Bashir, Christian, Christoph, Diana, Dave, Deniz, Estelle, Felix, Francois, Jenny, Linas, Lucia, Majdi, Philippe, Shigeyoshi, Thomas B., Valerie, Victoire, Yousr.

I would also like to thank some other important friends from other labs: Corinna, Barbara, Adi, Ashleigh and Gabrielle. I'll just prepare some hand-grounded coffee and 'German'-carbonara to express my gratitude you for all the good times we had.

A big thank you also to the helpers, who read and corrected parts of this thesis: Ashleigh, Chris, Christen, Lais, Michelle, Sam, Sumeet and Tom. I am sorry if you don't want to hear the word droplet ever again. . . It was really great of you doing this. And another great contribution is of course also the cover picture which has been designed by my brother Tobias and everyone can tell you did a great job here.

Last, but not any less important than anyone else here, I would like to thank my family, my parents and brothers. You have been always there for me, have brought me to this point in life and no matter if things were good or bad, I could always rely on you. Thank you!